Stallebrass, S.E. (1990). Modelling the effect of recent stress history on the deformation of overconsolidated soils. (Unpublished Doctoral thesis, City University London)

CITY UNIVERSITY
LONDON

EST 1894

Original citation: Stallebrass, S.E. (1990). Modelling the effect of recent stress history on the deformation of overconsolidated soils. (Unpublished Doctoral thesis, City University London)

Permanent City Research Online URL: http://openaccess.city.ac.uk/7666/

MODELLING THE EFFECT OF RECENT STRESS HISTORY ON THE DEFORMATION OF OVERCONSOLIDATED SOILS

by

Sarah Elizabeth Stallebrass

A Thesis submitted for the Degree of
Doctor of Philosphy

THE CITY UNIVERSITY
Civil Engineering Department

September 1990

CONTENTS

LIST OF TABLES

LIST OF FIGURES

ACKNOWLEDGEMENTS

The three years that I have spent at City University have been rewarding, interesting and above all great fun. I would like to thank my supervisor Prof. J. H. Atkinson for first persuading me that I would be interested in postgraduate research and then giving me so much support and encouragement during the project.

The research was supported by SERC and carried out in collaboration with Ove Arup and Partners represented by Dr B. Simpson. Dr Simpson provided several valuable opportunities for me to benefit from both his experience in the field and that of his colleagues. I am also very grateful for the interest Mr M. Gunn has shown in the project and the comments made by Dr W. Powrie on the draft thesis.

Working at City University has been so enjoyable because of the contribution of all the other members of the research group. I would particularly like to thank Dr R. N. Taylor for all his advice and help, Dr Lewin and Mr K O'Connor for carrying out the extra experimental work that was necessary for the thesis, all the technicians but in particular Mr K. Osborne and Mr L. Martyka and, finally Dr M. Allman, Mr R. Boese, Mr K. O'Connor and Miss G. Viggiani for their helpful comments on the thesis and their friendship and assistance during the past year.

In conclusion, many thanks to my family for their constant support, especially, my sister who has always provided much needed encouragement and my mother who together with Miss R. Pearce typed the majority of this thesis.

DECLARATION

I grant powers of discretion to the University Librarian to allow this thesis to be copied in whole or in part without further reference to me. This permission covers only single copies made for study purposes, subject to normal conditions of acknowledgement.

ABSTRACT

The aim of the research was to study the behaviour of overconsolidated soils subjected to small changes of strain or stress appropriate to the investigation of ground movements around excavations, retaining walls or foundations, and to develop a constitutive soil model that can predict such behaviour.

The principal feature of soil behaviour investigated was the effect of recent stress history, defined by θ the angle of rotation between the previous and current stress path directions. Stress path triaxial tests were carried out on both reconstituted and undisturbed samples of speswhite kaolin and London clay. The tests, which followed on from previous work by Richardson (1988), examined details of the influence of recent stress history, which was found to have a significant influence on the stress-strain response of the soil for the current loading path.

The data from the tests together with a re-evaluation of the existing experimental data and a limited investigation of the effect of recent stress history in 3D stress space, enabled the main features of the soil behaviour to be identified. The stress-strain response of the soil was found to be highly non-linear, inelastic and dependent on recent stress history; if the stress path rotation was 180°, i.e. a complete reversal, the soil stiffness was at a maximum and was at a minimum for no rotation. As the loading path continued the influence of the recent stress history gradually diminished until it was no longer evident. Recent stress history also affects strain paths and effective stress paths measured during drained and undrained loading respectively. The significance of mean effective pressure and overconsolidation ratio was also investigated.

Soil models which can predict this behaviour need to include at least one kinematic yield surface which allows plastic straining inside the state boundary surface. A two-surface yield model of this type, formulated by Al Tabbaa (1987) was evaluated. The predictions of this model did not compare well with several important aspects of the experimental observations and it was shown that an additional kinematic surface is necessary to model non-linearity, inelasticity and the recent stress history effect. A new three-surface model based on the two-surface model was developed, within the framework of Critical State soil mechanics, which successfully predicts all the main features of the soil behaviour. It is described by eight parameters which are all soil properties and, with one exception, all have a clear physical meaning.

LIST OF SYMBOLS

b	scalar measure of degree of approach of yield surface to bounding surface - two-surface model
b_1	scalar measure of degree of approach of history surface to bounding surface - three-surface model
b_2	scalar measure of degree of approach of yield surface to history surface - three-surface model
b_{max}	maximum value of b
b_{1max}	maximum value of b_1
b_{2max}	maximum value of b_2
e	void ratio
e_λ	current value of $(e + \lambda \ln p)$
h_o	hardening function when the current stress state lies on the bounding surface - two-surface and three-surface model
n	overconsolidation ratio - general
$\underline{n}$	normal to the yield surface at the current stress state- two-surface model
$\underline{n}_h$	normal to the history surface at the conjugate stress point- three-surface model
$\underline{n}_y$	normal to the yield surface at the current stress point- three-surface model
p'	mean effective pressure
p'_a	mean effective pressure at the centre of the history surface
p'_b	mean effective pressure at the centre of the yield curface
p'_e	equivalent pressure: value of p' at the point on the normal compression line at the same specific volume
p'_i	mean effective pressure at the start of the common path
p'_m	the maximum mean effective pressure to which the soil has been loaded
$2p'_o$	mean effective pressure at the intersection of the current swelling line with the normal compression line
p'_s	mean effective pressure at the conjugate stress point- three-surface model

p'_α	the mean effective pressure at the centre of the yield surface - two-surface model
$\dot{p}'$	rate of change of mean effective stress
q'	deviatoric stress
q'_a	deviatoric stress at the centre of the history surface-three-surface model
q'_b	deviatoric stress at the centre of the yield surface - three surface model
q'_i	deviatoric stress at the start of the common path
q'_s	deviatoric stress at the conjugate stress point - three surface model
q'_α	deviatoric stress at the centre of the yield surface - two-surface model
t_{100}	time for 100% consolidation
v	specific volume
v_κ	specific volume of isotropically overconsolidated soil swelled to $p' = 1$kPa
w	moisture content of the soil
x, y, z	cartesian coordinate axes
B	Skempton's pore pressure parameter indicating the degree of saturation of the soil
Cu	undrained shear strength
E'	Young's modulus
E'_h	horizontal Young's modulus for a cross-anisotropic soil
E_u	Young's modulus for undrained loading
E'_v	vertical Young's modulus for a cross-anisotropic soil
G'	shear modulus
G^*	shear modulus in stiffness matrix derived by Graham and Houlsby (1983) for a transverse isotropic elastic soil
G'_e	elastic shear modulus - three-surface model
G_s	specific gravity
G_u	shear modulus for undrained loading
H	hardening function - two-surface model

H_1, H_2	hardening functions - three-surface model
J'	modulus coupling shear and volumetric strains
J	modulus coupling shear and volumetric strains in stiffness matrix derived by Graham and Houlsby (1983) as above
K'	bulk modulus
K^*	bulk modulus in stiffness matrix derived by Graham and Houlsby (1983)
K_o	coefficient of lateral earth pressure at rest
K_{onc}	K_o during one-dimensional normal consolidation
OCR	overconsolidation ratio defined as the maximum previous vertical effective stress divided by the current vertical effective stress
R	ratio of size of yield surface to bounding surface - two-surface model
R_o	overconsolidation ratio defined as p'/p'_m
S	ratio of the size of the yield surface to the history surface -three-surface model
T	ratio of the size of the history surface to the bounding surface
β	for the two surface model, the vector joining the conjugate points on the yield and bounding surfaces; for the three-surface model the vector joining the conjugate points on the history and bounding surfaces
γ	the vector joining the conjugate points on the yield and history surfaces - three-surface model
ϵ	strain
ϵ_a	axial strain
ϵ_n	natural strain
ϵ_r	radial strain
ϵ_s	shear strain
ϵ_v	volumetric strain
ϵ_s^e	elastic shear strain
ϵ_v^e	elastic volumetric strain
ϵ_s^p	plastic shear strain
ϵ_v^p	plastic volumetric strain

η	stress ratio, q'/p'
θ	angle of stress path rotation
$-\kappa$	gradient of a swelling line in lnv : lnp′ space
$-\kappa_0$	gradient of the second section of a swelling line in v : lnp′ space as defined by Richardson (1988)
$-\kappa_1$	gradient of the initial section of a swelling line in v : lnp′ space as defined by Richardson (1988)
$-\lambda$	gradient of the normal compression line in lnv : lnp′ space
ν, ν'	Poisson's ratio
ν'_{vv}, ν'_{vh}	Poisson's ratio in cross-anisotropic soils
σ'	effective stress
σ'_a	axial effective stress
σ'_r	radial effective stress
ψ	exponent in the hardening modulus for both two-surface and three-surface models
Γ	specific volume of soil at critical state when $p' = 1$kPa
N	specific volume of isotropically normally consolidated soil when $p' = 1$kPa
M	critical state friction coefficient
$\Delta\sigma'_R$	change of stress at which the influence of recent stress history is no longer evident.

CHAPTER 1 INTRODUCTION

1.1 Background to the Project

The research described in this thesis investigates the behaviour of overconsolidated soils at small strains or small changes of stress, when the soil is far from failure. An understanding of the stress-strain response of overconsolidated soils at these stress or strain levels is critical in the calculation of ground movements around excavations, retaining walls and foundations. Both Simpson et al (1979) and Jardine et al (1986) showed that the majority of the soil around structures such as these undergoes strains of less than approximately 0.2%. The development of more accurate testing techniques enabled the highly non-linear stress-strain response of the soil at these strain levels to be measured, Jardine et al (1984). Only when the behaviour of the soil at these strains is properly investigated can appropriate models be developed to predict ground movement profiles accurately.

Existing models which incorporate this non-linearity and have been used in finite element programs to predict ground movements include the largely empirical model proposed by Jardine et al (1986) and the non-linear model for London Clay described by Simpson et al (1979). The non-linear analysis carried out by Simpson et al (1979) predicted profiles of ground movements which were substantially closer to those measured in the field than predictions using linear elastic theory, thus illustrating the importance of modelling small strain stiffness correctly. Unfortunately, neither of these models incorporate all the characteristics of the behaviour of soils at small strains or changes of stress, which have been observed in laboratory tests.

The stress-strain response of soil is not only highly non-linear, but depends on current state, overconsolidation ratio and additionally on the recent stress history of the soil (Atkinson, 1973, Richardson, 1988 and Som, 1968). The recent stress history may be described either by a sudden change in direction of stress path or a period of rest at a particular stress state. If more realistic predictions of ground movements are to be made stress-strain relationships should be derived that predict the effect not only of state and overconsolidation ratio, but also of recent stress history. This is particularly important for civil engineering works where the recent stress history of the soil changes significantly across the construction site due to geological variations or nearby construction.

In this thesis the term recent stress history refers only to changes in direction of stress path, time effects are considered separately. The research builds on previous work at City University, primarily that described by Richardson (1988). The latter investigated the general characteristics of the recent stress history effect, for a variety of soils, through an extensive series of stress path tests on reconstituted samples.

The aims of the research reported in this thesis are as follows:

(i) To investigate recent stress history effects in more detail and hence to define the effect more clearly.

(ii) To derive and evaluate a new constitutive soil model that takes account of the influence of recent stress history.

(iii) To demonstrate that the principal features of the effect observed in reconstituted samples (Richardson, 1988) also exist in undisturbed samples.

1.2 Basic Framework

1.2.1 Basic Methodology of the Research

The general form of a constitutive equation for soil is

$$\{\delta\epsilon\} = [C]\{\delta\sigma'\} \qquad (1.2.1)$$

where in general stress space [C] is a 6×6 compliance matrix defining the relationship between increments of stress and strain. The 36 components of this matrix may be functions of soil properties, state or history of the soil. In this thesis both the experimental work and the numerical models will be confined to the triaxial plane. For these triaxial conditions the state of the soil will be described by the stress parameters, p', q' and the specific volume, v (Schofield and Wroth, 1968), where $p' = 1/3(\sigma'_a + 2\sigma'_r)$, $q' = \sigma'_a - \sigma'_r$ and v, the specific volume, is the volume in space occupied by unit volume of soil grains. Corresponding strain parameters are $\epsilon_v = \epsilon_a + 2\epsilon_r$ and $\epsilon_s = 2/3(\epsilon_a - \epsilon_r)$. These parameters will be calculated using natural strains which are more appropriate for analyses and models based on incremental relationships as they are computed from current dimensions. The expression, $\epsilon_n = -\ln(1 - \epsilon)$, relates natural strains to ordinary strains.

For axial symmetry, i.e. stress states in the triaxial plane, and using the stress and strain parameters given above, following Graham and Houlsby (1983) the general constitutive equation becomes.

$$\begin{bmatrix} \delta\epsilon_v \\ \delta\epsilon_s \end{bmatrix} = \begin{bmatrix} 1/K' & 1/J' \\ 1/J' & 1/3G' \end{bmatrix} \begin{bmatrix} \delta p' \\ \delta q' \end{bmatrix} \qquad (1.2.2)$$

For the particular case of a cross-anisotropic soil, J', which models the cross coupling of shear and volumetric effects, could be written in terms of standard anisotropic elastic parameters as follows.

$$J' = \frac{3E'_v E'_h}{2(E'_h(1 - \nu'_{vv}) - E'_v(1 - \nu'_{vh}))} \qquad (1.2.3)$$

However, the coefficients of the compliance matrix in equation 1.2.2 are not necessarily elastic moduli. To develop a model which will predict the stress-strain response of the soil it is necessary to determine the functions of the soil properties, state and history which are represented by K', 3G' and J' in this equation. These functions must be consistent with the values of K', 3G' and J' calculated, as shown in section 1.2.3, from the stress-strain response measured experimentally.

There are two possible approaches to deriving these functions: first, empirically by fitting a numerical expression to appropriate stress-strain data. In this method, K', 3G' and J' are functions of the shape of the stress-strain or stiffness-strain curve obtained for a given loading path, state and history. If the loading path, state or history of the soil changes then tests should be carried out to obtain a new stress-strain curve and hence derive new values of K', 3G' and J'. This method has been used by Duncan and Chang (1970), who approximated the stress-strain curves to hyperbolae, and by Jardine et al (1986) to model the small strain behaviour of soils. The alternative method is to propose a conceptual model which incorporates all aspects of the soil behaviour and from which functions for K', 3G' and J' can be determined. These will be direct functions of soil properties, the stress state and model parameters which define the history of the soil, such as p'_o in the Cam-clay model. The model would only require basic soil properties to be determined experimentally. Typical models of this type have been proposed by Al Tabbaa (1987), Mröz et al (1979) and Hashiguchi (1985).

The latter approach to modelling the behaviour of overconsolidated soils has been adopted in this thesis. The only independent variables in the new constitutive model described in Chapter 5 are soil properties. The effect of state, overconsolidation ratio and recent stress history are all included in the definition of the model. This type of model was used because, if it is installed in a finite element program, it will be possible to calculate the integrated effect of any number of different elements of soil loaded along different stress paths and with different states and recent stress histories all using one set of soil parameters. Depending on the complexity of the site, finite element calculations using empirical models would require considerably more sets of stress-strain data.

1.2.2 Theoretical Framework

The description and analysis of the experimental data presented in this thesis will be based on the following assumptions. Firstly, that the state of the soil, described by the stress parameters p', q' and v (Schofield and Wroth, 1968) always lies within or on the state boundary surface defined by the Modified Cam-clay soil model (Roscoe and Burland, 1968). Secondly, that when the state lies on the state boundary surface the soil deforms elasto-plastically and the plastic strains can be calculated using a version of the Modified Cam-clay constitutive equations and, finally, that all soils ultimately reach a critical state, as defined by Schofield and Wroth (1968).

The version of the Modified Cam-clay model which has been used as the basic framework for the new model has also been used by Houlsby et al (1982) and Al Tabbaa (1987) and incorporates the natural compression law proposed by Butterfield (1979) such that the isotropic normal compression line is given by the equation.

$$\ln v = N - \lambda \ln p' \tag{1.2.4}$$

where N is the value of lnv when $p' = 1$ and λ is the gradient of the line in lnv:lnp' space, as shown in Figure 1.2.1(b). This figure also shows the idealised isotropic elastic swelling line defined by

$$\ln v = v_\kappa - \kappa \ln p' \tag{1.2.5}$$

This equation not only defines the elastic volumetric strains that occur in the Modified Cam-clay model, but also any purely elastic, volumetric strain that occur in any other model proposed in this thesis. The parameter κ is not used to describe the varying gradient of experimental swelling curves. These are usually characterised by the variation of the bulk modulus, K'. The critical state line is defined in lnv:lnp' and q':p' space respectively by the equations.

$$\ln v = \Gamma - \lambda \ln p' \tag{1.2.6}$$

and

$$q' = \pm Mp' \tag{1.2.7}$$

The critical state line is shown in lnv:lnp' space in Figure 1.2.1(b) and in q':p' space in Figure 1.2.1(a). States to the right of the critical state line are "wet" of critical and states to the left "dry" of critical, see Figure 1.2.1(b). This figure also shows the Modified Cam-clay yield locus, which is formed by the intersection of an elastic wall and the state boundary surface and is defined by

$$(p' - p_o')^2 + q'^2 / M^2 = p_o'^2 \tag{1.2.8}$$

where $2p_o'$ is the mean effective stress at the intersection of the current swelling line and the isotropic normal compression line, see Figure 1.2.1. This yield locus also acts as a plastic potential, i.e. the normality rule applies and the plastic strain increment vector is perpendicular to the yield surface and is given by

$$\frac{\delta \epsilon_v{}^p}{\delta \epsilon_s{}^p} = \frac{(p' - p_o')}{q'/ M^2} \tag{1.2.9}$$

An isotropic hardening law which links the expansion of the yield surface to plastic volumetric strain is given by.

$$\delta \epsilon_v{}^p = (\lambda - \kappa)\ \delta p_o'/ p_o' \tag{1.2.10}$$

The resulting constitutive equation for the plastic strains is:

$$\begin{bmatrix} \delta \epsilon_v^p \\ \\ \delta \epsilon_s^p \end{bmatrix} = \frac{(\lambda - \kappa)}{p_o' p' (p' - p_o')} \begin{bmatrix} (p' - p_o')^2 & (p' - p_o') \dfrac{q'}{M^2} \\ (p' - p_o') \dfrac{q'}{M^2} & \dfrac{q'^2}{M^4} \end{bmatrix} \begin{bmatrix} \delta p' \\ \\ \delta q' \end{bmatrix} \tag{1.2.11}$$

1.2.3 Interpretation of Data

The basic type of test used to investigate the effect of recent stress history is described in detail in section 3.6.2. The tests examine the stress-strain response along a fixed path such a OP, in Figure 1.2.2, where the starting point O is approached from different directions by loading along paths such as AO and BO. The recent stress history associated with a different 'approach' path is described by the angle through which the direction of loading has to rotate to follow the fixed path. This is the angle, θ, shown in Figure 1.2.2, which is defined as positive when the rotation is in a clockwise direction. The angle of rotation, θ, is not a measure of the rotation of the principal stress directions, which are fixed in a triaxial test. The initial state of the fixed or 'common path' is described by the stress coordinates, p_i', q_i'.

The majority of the test data comes from overconsolidated soils, for which the overconsolidation ratio is defined as $R_o = p_m'/p'$. For an isotropically compressed soil p_m' is the maximum mean effective pressure to which the soil has been loaded, see Figure 1.2.3(a). When the soil is loaded anisotropically p_m' is calculated using the Modified

Cam-clay yield locus as shown in Figure 1.2.3(b). The parameter, p'_m, is not equivalent to $2p'_o$, defined in section 1.2.2, since for models such as those proposed in Chapter 5, plastic strains may occur inside the state boundary surface and so, unlike p'_m, p'_o can decrease as well as increase.

The tests provide a series of different stress-strain curves all measured along the common path but corresponding to different approach paths. In order to obtain a clearer picture of the differences between these curves, stiffness parameters should be calculated. As noted in section 1.2.1 in the case of axial symmetry, increments of stress and strain can be related by a compliance matrix as shown below, (Atkinson and Richardson, 1985).

$$\begin{bmatrix} \delta\epsilon_v \\ \delta\epsilon_s \end{bmatrix} = \begin{bmatrix} 1/K' & 1/J' \\ 1/J' & 1/3G' \end{bmatrix} \begin{bmatrix} \delta p' \\ \delta q' \end{bmatrix} \tag{1.2.12}$$

where K' and G' are the bulk and shear moduli of the soil for the current increment. The modulus J' models the coupling of shear and volumetric effects (Graham and Houlsby, 1983). The majority of the stress probe tests investigating the effect of recent stress history used drained loading paths. To isolate the moduli K' and G' two particular types of loading were used as the common path: these were loading at constant p' and loading at constant q'. For constant p' loading paths, $\delta p' = 0$, so in the limit as the increment tends to zero

$$dq'/\, d\epsilon_s = 3G' \tag{1.2.13}$$

Hence 3G' can be defined as the gradient of a shear stress-shear strain curve obtained from constant p' loading. Similarly for constant q' loading paths $\delta q' = 0$ and hence

$$dp'/\, d\epsilon_v = K' \tag{1.2.14}$$

The modulus K' is defined as the gradient of the mean effective stress-volumetric strain curve for a constant q' loading path. Because of the coupling of shear and volumetric effects, K' and G' cannot be obtained uniquely from conventional triaxial compression tests. As part of the analysis of test data, the strain paths followed during loading were also examined. These paths provide information on the nature of the deformations as described in section 4.2.5. The gradient of these paths is the strain increment ratio, $d\epsilon_v/d\epsilon_s$, which is a measure of the anisotropy of the soil. For constant p' loading paths from equations (1.2.12)

$$d\epsilon_v/d\epsilon_s = 3G'/J' \qquad (1.2.15)$$

and for constant q' loading

$$d\epsilon_v/d\epsilon_s = J'/K' \qquad (1.2.16)$$

For a small number of the tests, an undrained compression stage was the common path. The cross coupling of shear and volumetric effects means that the gradient of the stress-strain curve obtained from undrained compression paths is not equal to 3G' as defined above. For undrained tests $\delta\epsilon_v = 0$, so inverting the matrix in equation 1.2.12, the value of undrained shear modulus, G_u, in terms of the stiffness moduli given in equation 1.2.12 is

$$dq'/d\epsilon_s = 3G_u = \frac{-3G'J'^2}{(3K'G' - J'^2)} \qquad (1.2.17)$$

The shape of the effective stress path obtained from an undrained compression test provides information on the nature of the deformations in the same way as the strain paths from drained tests. The variation in the anisotropy of the soil during the test can be measured from the gradient of the path, dp'/dq', as

$$dp'/dq' = -K'/J' \qquad (1.2.18)$$

The variation of stiffness parameters with R_o is mostly investigated by normalising the mean effective pressure p' by p'_m. In some cases, however, for the reasons given in section 4.2 the equivalent pressure p'_e is more appropriate. The equivalent pressure is the mean effective stress on the isotropic normal compression line at the current specific volume of the soil, see Figure 1.2.4.

CHAPTER 2 LITERATURE REVIEW

2.1 Introduction

This literature review examines work carried out in the three main areas of measurement, evaluation and modelling of recent stress history effects at small strains of changes of stress. In the sections covering the development of testing techniques, and the experimental investigation of small strain deformations and recent stress history effects, the majority of the work reviewed was carried out in the laboratory, mostly using triaxial testing apparatus. This review concentrates on laboratory experimentation and apparatus because it is in this field that most of the recent work has taken place and it is from this work that the current project continues.

The development of laboratory testing techniques for measuring soil stiffness at low strain and for small stress changes was undertaken primarily in an attempt to explain the differences between stiffness moduli measured in the laboratory and moduli back calculated from field measurements. The latter were observed to be between five and ten times those derived from laboratory tests and the differences were attributed not only to deficiencies in the experimental methods used to measure stiffness in the laboratory but also to the effect on the stress-strain response of the recent stress history of the soil (Simpson et al, 1979).

In order to investigate soil stiffness at small strains and low stress levels, and in particular the effect of recent stress history, it is necessary to follow a variety of stress paths. Stress path cells of the Bishop and Wesley (1975) design are ideally suited to this purpose. These cells are used extensively at City University and Imperial College where most of the work in this area has been concentrated.

2.2 Development of Experimental Techniques in Laboratory Testing

Experimental techniques used to investigate the small strain behaviour of overconsolidated soils should be able to measure stiffness moduli accurately for small changes of stress and especially at low strain levels subsequent to or during carefully selected stress paths. The major advances in laboratory test equipment and testing techniques which made these measurements possible were, firstly, the development of the hydraulic stress path cell (Bishop and Wesley, 1975) and secondly the design and use of devices to measure axial and radial strains on the sample inside the cell. In addition, equipment such as the resonant column apparatus has been used to measure stiffnesses at very small strains, less than 0.001%.

2.2.1 Developments in Hydraulic Stress Path Cells

The hydraulic stress path cell was developed by Bishop and Wesley (1975). The cell incorporates the feature employed by Atkinson (1973) of applying the axial load by hydraulic pressure using Bellofram rolling diaphragm seals. The sample sits on an axial ram, where it is loaded from below by fluid pressure in a chamber divided from the cell fluid by two Belloframs, one above and one below the ram. A sketch showing a cross-section of the cell is given in Figure 2.2.1. The standard Bishop and Wesley cell for 38mm diameter samples was developed into a cell which can accommodate samples in excess of 100mm in diameter by Atkinson et al. (1984).

The Bishop and Wesley cell was designed to test samples both in axial compression and axial extension following a wide variety of stress paths. In order to conduct these tests three controllable pressure sources are required and for strain controlled tests a constant rate of flow source. Bishop and Wesley (1975) recommended a relatively unwieldy system of self compensating mercury controllers and a screw control cylinder (Bishop and Henkel, 1962) as a method of controlling the cell. Various rather simpler methods of controlling the standard Bishop and Wesley cell have since been devised. Menzies et al (1977) described a system of motor driven closed rams with self contained feed-back control to regulate pressures. Atkinson, Evans and Scott

(1983) used continuous motors, automatically controlled by a microcomputer, to control manostat air pressure regulators. Two subsequent modifications to this system substituted, first electromanostats for the motor driven pressure regulators (Atkinson, 1985) and, secondly, analogue pressure converters, (Viggiani, 1990).

The hydraulic stress path cell was developed so that soil deformation parameters could be measured over a wide range of stress paths. Lewin and Burland (1970) and Davis and Poulos (1968), among others, recognised that stiffness measured directly from a triaxial test is dependent on the stress path followed by the soil. Therefore, appropriate deformation characteristics would only be obtained if the appropriate stress path was followed. To conduct stress path tests in conventional triaxial cells the axial load is applied by dead weights and can only be increased in steps. This means that it is almost impossible to follow any stress path other than conventional triaxial compression or extension. A Bishop and Wesley hydraulic stress path cell operated by any of the control systems described here will enable the appropriate stress history of the soil, such as K_0 compression or swelling, to be followed with reasonable accuracy.

2.2.2 Developments in Strain Measuring Techniques

There are three main areas in which strain measuring techniques have been improved and developed. Firstly, errors in externally made measurements have been eliminated using special procedures and relatively simple modifications to existing testing apparatus. Secondly, methods of measuring strains local to the sample have been developed, in particular internal strain transducers mounted on the sample. Thirdly, laboratory testing apparatus that can measure very small strains, less than 0.001%, have been developed.

Atkinson and Evans (1985) described several precautions that could be undertaken to improve the accuracy of external axial strain measurements. They recommended measuring the deflection of the load cell so that appropriate corrections could be applied to the data, connecting the top platen to the load cell to prevent tilting and compressing the sample in the cell before shearing stages so that the top platen beds into the sample. The accuracy of the axial strains measured in this way was estimated as ±0.01%.

A considerable number of different approaches to the problem of measuring local axial strains have been developed. A comprehensive review of the early work in this field is given by Costa Filho (1985). The different types of procedure that have been used include X-ray techniques to measure the movement of lead shot set in the sample (for example Balasubramaniam (1976)) and a pair of cathetometers sighting on inscribed drawing pins stuck into the sample below the membrane (Atkinson, 1973).

Initial attempts to measure local axial and radial strains by mounting transducers on the sample were made using miniature LVDTs (for example Brown and Snaith, 1974). Costa Filho (1985) continued with this system and described a set up using two miniature LVDTs to measure strains over a gauge length of approximately 25mm on samples of overconsolidated London Clay, see Figure 2.2.2. The accuracy of measurements made at low strains was estimated as ±0.005%.

Burland and Symes (1982) described the use of electrolevel displacement gauges for the measurement of axial strains on laboratory soil samples. These gauges were developed further and used extensively by Jardine et al. (1984). The geometry of the hinged mounting for the gauge, which converts the displacement between two footings on the sample to a tilting of the electrolevel capsule was improved. A sketch showing the construction of the gauges is given in Figure 2.2.3. The footings were glued to the membrane and relied on the radial stress, applied by the cell pressure, to ensure that there was no movement between the membrane and the sample. No relative movement of this kind was observed until large strains occurred. These gauges were able to measure strains accurate to ±0.002%. The gauges were substantially remodelled by Ackerly et al. (1987), who replaced the electrolevel capsule by a pendulum inclinometer (see Figure 2.2.4). This system did not require the sophisticated input signal control and output voltage conditioning that was needed to obtain satisfactory results from the electrolevel gauges. Using the pendulum inclinometer gauges axial strains could be resolved to around 0.0005%.

There are two further methods of measuring local strains which have been used recently. The first, designed by Clayton and Khatrush (1986) and Clayton et al. (1989), made use of Hall effect semiconductors which operate by detecting changes in magnetic flux. The device is in two halves: the semiconductor and its mounting are fixed to the sample at one end of the gauge length and the magnet causing the changes in magnetic flux is on an arm fixed to the other end of the gauge length. Figure 2.2.5 shows this configuration, which is used to measure axial strains, and also a radial strain measuring device based on a Bishop and Henkel (1962) lateral strain caliper. Clayton and Khatrush (1986) reported that the gauges were temperature and voltage stabilised and capable of measuring axial strains to 0.002%. The second technique for measuring local strains was described by Hird and Yung (1987) who used proximity transducers to measure local strains on 100mm diameter samples with an accuracy of 0.009% for strains less than 0.1%.

It is particularly important to measure strains with gauges attached to the sample when testing stiff overconsolidated clays. At low stress levels the strains are very small, often less than 0.1%, and so inaccuracies in measurements made using a transducer mounted outside the cell will be significant. Jardine et al. (1984) and Clayton et al. (1989) identified a number of errors in external measurements such as load cell deflection and bedding and tilting of the sample. A diagram of a typical sample in a triaxial cell showing the exact origin of the errors identified by Jardine et al. (1984) is given in Figure 2.2.6. Both this paper and the paper by Clayton et al. (1989) concluded that these errors were the primary cause of the observed difference between field and laboratory measured stiffness moduli. However, the errors can be largely eliminated using the procedures given by Atkinson and Evans (1985) who felt that the increased accuracy obtained by measuring axial strains locally compared with external strains measured following their guidelines, was principally due to the greater resolution of the equipment.

The effect of end restraint, which causes the sample to deform non-uniformly, will also generate a difference between strains measured locally and externally. Costa Filho (1985) compared the relative importance of end restraint and bedding errors and, for samples of undisturbed London clay, found that, although end restraint effects would cause the stiffness to be somewhat overestimated, bedding errors were more significant.

The equipment used most commonly to measure shear stiffness at strains of less than 0.001% in the laboratory is the resonant column apparatus. Three types of test can be carried out using the resonant column to obtain values of the shear modulus of the soil. These tests are the resonant column test, the free vibration decay test and the cyclic torsional shear test. The original resonant column test (Richart et al., 1970) loaded a cylindrical sample, or column, of soil dynamically in torsional shear at a given amplitude but varying frequency. The shear modulus of the soil was calculated by comparing the response of the soil when resonance occurred to a theoretical model. Current resonant column testing methods employ all three types of test in a multistep technique (Isenhower, 1979).

The main alternative method of measuring these very small strain stiffness moduli in the laboratory was described by Schulteiss (1987) The technique used piezoceramic crystals, known as bender elements, to send pulse shear waves through a triaxial sample which were picked up by a further bender element acting as a sensor at the top of the sample. The shear modulus of the sample was calculated from the velocity of the waves obtained by measuring the time for the wave to pass between the two sensors.

Dynamic testing methods appear to be the only means of resolving strains of 0.001% or less in the laboratory. Recent work by Rampello (1989) testing Todi clay indicates that, at equivalent shear strains, dynamic stiffness moduli obtained from resonant column tests and static stiffness moduli measured in triaxial tests using local axial strain gauges are comparable. However, it should be noted that the loading path and recent stress history of soil subjected to dynamic testing are always the same and are equivalent to a series of unload-reload loops.

The development of the Bishop and Wesley stress path cell allowed the stress-strain response of a soil to be measured over any stress path and the appropriate overall and recent stress history of the soil to be recreated. Improved techniques of measuring strains, especially the use of local axial strain gauges in triaxial cells, means that this stress-strain response can be determined for strains as low as 0.001%. The shear stiffness of the soil can be obtained at lower strain levels using apparatus such as the resonant column or bender elements but these moduli are only applicable to the limited stress path and recent stress history provided by dynamic loading.

2.3 Experimental Investigation of Deformations at Small Strains

As noted in the previous section, experimental techniques enabling stress-strain relationships for overconsolidated soils to be determined at low stress levels and small strains have only been developed relatively recently and this section will concentrate on the comparatively limited selection of data obtained using these procedures.

The work in this area falls into two main categories.

(i) Experimental work concentrating on the accurate measurement of the small strain stiffness of soils.

(ii) The experimental evaluation of the effect of recent stress history.

The results of work carried out to fulfill the first category also provided data on the effect of recent stress history on soil behaviour although the tests were not specifically designed for this purpose.

More comprehensive reviews of the wide variety of laboratory experimental data concerning the deformation characteristics of overconsolidated soils are given by Richardson (1988). Another important source of data on the stiffness of overconsolidated soils is from field observations. Data on ground movements around a number of different structures constructed in London Clay were reported by Burland et al (1979).

The non-linear stress-strain response of overconsolidated soils was reported by Costa Filho and Vaughan (1980) for London Clay and Jardine et al (1984) and Jardine (1985) for a variety of soils but predominantly London Clay and a low plasticity North Sea clay. Costa Filho and Vaughan (1980) described results from unconsolidated undrained and anisotropically consolidated undrained tests on samples of London clay. During the tests local axial strains were measured using the method given in Costa Filho (1985). The stress-strain response of the London Clay in both tests was highly non-linear. In addition the anisotropically consolidated undrained tests showed an initial stiffness which was greater than that observed in the undrained tests on unconsolidated samples, see Figure 2.3.1. Costa Filho and Vaughan (1980) and Costa Filho (1979) concluded that in comparing the stiffness of overconsolidated soils, such as London Clay, it is necessary to account for both the strain level and stress history of the soil.

Jardine (1985) reached similar conclusions from the results of an extensive series of tests on reconstituted samples of a low plasticity North Sea clay. All the tests were undrained but different stress histories and reconsolidation procedures were followed before the compression or extension shearing stage. Electrolevel internal strain gauges were used to measure the highly non-linear stress-strain response of the soil. This non-linear stress-strain response was characterised using an initial secant Young's modulus, when the axial strain was 0.01%, and a non-linearity index or a non-linearity function. For the one-dimensionally consolidated soil the non-linearity function was found to depend both on preshearing conditions, i.e. the stress history of the soil, and the length of time that the soil was held at the current stress state, and the loading direction.

Jardine (1985) concluded that the stress-strain behaviour of the soil was not strictly elastic and identified three main zones of behaviour during undrained shearing. At axial strains of less than 0.01% deformations were recoverable but non-linear, between 0.01% and 0.1% axial strain, there were plastic strains but no volumetric yield and at axial strains above 0.1% volumetric yield occurred and plastic strains predominated. Figure 2.3.2 shows the first two of these zones plotted on a set of typical stress paths. The previous stress history of the soil appeared to affect the size and shape of the zones.

The observation was also reported in Jardine et al (1984) and Hight et al. (1985). Hight et al. (1985) identified a region or zone bounded by strains of 0.01% in order to explain the behaviour of soil after different stress paths and histories during sampling. If the current stress path was a continuation of the previous path the zone was hardly traversed at all and the initial stiffness observed was lower. If there was a stress reversal the zone was traversed completely and there was an increase in stiffness. There was also some indication that the zone decreased in size as the soil swelled back from a normally consolidated state.

It should be noted that none of the results that have been reviewed above isolate the influence of recent stress history. Where differences in the stress-strain behaviour of the soil have been attributed to the influence of previous stress history, the stress history referred to is not necessarily only recent stress history as stress state and overconsolidation ratio have also been altered. Although the zones of different behaviour identified by different strain levels provide a useful method of monitoring the variation in stress-strain response of the soil, they cannot be used to explain this stress-strain behaviour which was itself used to define them.

Clinton (1987) carried out a series of stress probing tests on samples of Gault clay in order to determine anisotropic stiffness moduli. The results of the tests implied that the soil had different stiffness parameters for the same stress state and overconsolidation ratio when the probe was preceded by different recent stress histories. In this case the effect of recent stress history was isolated from the effect of state or overconsolidation ratio.

Jardine (1985) also performed three tests using a resonant column apparatus to investigate the dynamic shear modulus of the low plasticity North Sea clay. The general characteristics of the variation of the stiffness of the soil with change in strain obtained from these tests compared well with the results of the triaxial tests. Data from the tests implied that the soil had a constant shear modulus for shear strains of less than 0.001%. Rampello (1989) testing Todi clay also established from tests using a resonant column apparatus, similar to that used by Isenhower (1979), that the shear modulus is at a maximum and constant for strains less than 0.001%. Rampello (1989) used both undisturbed samples and samples which as part of their previous stress history had been swelled back to very low effective stresses. Both types of sample were tested at a number of different initial stress states. The results of these tests are shown in Figure 2.3.3 as shear modulus normalised by the initial maximum shear modulus against strain amplitude. The variation of the normalised shear modulus is approximately constant for all the tests. The general form of this curve is typical of many results of resonant column tests on clays (see Sun et al. (1988)).

Rampello (1989) also compared the moduli observed from the resonant column tests directly with corresponding moduli obtained by using electrolevel gauges to measure local axial strains during triaxial undrained shear tests. The data compare well as shown by Figure 2.3.4 which shows the data plotted as the variation of Young's modulus with axial stress.

These results clearly confirm the highly non-linear stress-strain behaviour of overconsolidated clays at strains greater than 0.001%. However it is difficult to draw any conclusions about the importance of recent stress history because the two tests impose different stress conditions on the sample and the recent stress history of the triaxial samples is not always clear.

There have been very few laboratory test programs specifically aimed at investigating the effect of recent stress history on the stress-strain behaviour of overconsolidated soils. However, Som (1968) testing London Clay reported that if a sample was held at a constant stress state in an oedometer for many days before a new load increment was applied, the stiffness for that load increment was increased provided that the increment was small. This illustrated the effect of rest period on the subsequent stiffness of soil.

Atkinson (1983) examined the effect of recent stress history on two pairs of samples of speswhite kaolin. All four samples were sheared in undrained compression from the same stress state and overconsolidation ratio. However, one pair had been anisotropically and the other isotropically consolidated and swelled. In addition, for both pairs one sample was swelled back past the initial state for the shearing stage and recompressed back. The other sample was only swelled to the initial state and sheared. Both the samples which had been subjected to a recompression cycle before shearing showed a much less stiff stress-strain response. The undrained effective stress path followed by these two samples was also affected by the recompression stage but the different overall stress histories, i.e. isotropic or anisotropic, of the soil appeared to have a more significant influence.

The most important series of tests used to study the effect of recent stress history on the stress-strain behaviour of overconsolidated soils was completed by Richardson (1988). A comprehensive program of drained stress path tests on reconstituted samples of speswhite kaolin, London clay, Cowden Till, Ware Till and slate dust was carried out. The stress probes followed during the tests isolated the effect of recent stress history for soils subjected to different overall stress histories such as one-dimensional consolidation and swelling. Various overconsolidation ratios and time effects were also investigated. Combinations of stress probes were frequently duplicated to ensure that the results were repeatable. Richardson (1988) found that the recent stress history of a soil has a significant effect on both the stiffness of a soil and its stress induced anisotropy. The results of this work form the basis of much of the work in this thesis and are reviewed in more detail in section 4.3. A selection of the data obtained from the tests on London Clay is described by Atkinson et al. (1990). A typical set of data obtained from an investigation of the effect of recent stress history on the stress-strain response of an overconsolidated sample of London clay for a constant p' loading is given in Figure 2.3.5.

The triaxial tests carried out by Richardson (1988) used hydraulic stress path cells to follow the required stress probes but all the strains were measured externally and hence axial strain measurements were only accurate to 0.01%. These results still clearly showed the non-linearity of the stress-strain response of the soil, as well as the dependence of stiffness on recent history, but only for strain levels greater than 0.01%. The results of the undrained tests by Jardine (1985) and the resonant column tests by Rampello (1989), among others, give a more extensive picture of the non-linear stress-strain behaviour and identify an elastic region of soil deformation at strains of less than 0.001%. Unfortunately it is not easy to quantify the effect of recent stress history on this behaviour from these latter tests.

2.4 Soil Models for the Stress-Strain Behaviour of Overconsolidated Soil

This section reviews existing continuum numerical models which have been formulated to predict the stress-strain behaviour of fine grained soils at states lying within the state boundary surface. The majority of the models reviewed in this section were originally defined in general stress space and then modified to model the specific case of soils tested in triaxial stress conditions. As most test data is obtained from triaxial tests it is simpler to evaluate the model in this form. The models can be divided into two groups.

(i) Models which assume all deformations inside the state boundary surface are elastic.

(ii) Models which allow plastic yielding to occur inside the state boundary surface.

2.4.1 Elastic Models

The basic elastic model governing soil behaviour before yielding is given by Hookes laws of elasticity, which were stated by Love (1942) in the form - each of six components of stress at any point of a body is a linear function of the six components of strain at that point. This general form of the laws can be simplified if the soil is assumed to be isotropic linear elastic when the relationship between the stresses and strains in a soil can be expressed using any two of the four isotropic elastic soil parameters, E', ν', G' and K'. E' is the Youngs modulus of the soil, ν' Poissons ratio, the shear modulus G' =

$E'/2(1+\upsilon')$, and the bulk modulus $K' = E'/3(1-2\upsilon')$. Using the stress and strain invariants p', q', ϵ_v and ϵ_s, the matrix equation relating increments of stress and strain for an isotropic elastic soil is;

$$\begin{bmatrix} \delta p' \\ \delta q' \end{bmatrix} = \begin{bmatrix} K' & 0 \\ 0 & 3G' \end{bmatrix} \begin{bmatrix} \delta \epsilon_v \\ \delta \epsilon_s \end{bmatrix} \tag{2.4.1}$$

The isotropic linear elastic stress-strain behaviour represented by this equation has been used extensively to predict ground movements around structures constructed in stiff clays, (e.g. Davis and Poulos, 1968).

A simple form of non-linear isotropic elasticity was incorporated in the Cam-clay critical state soil model formulated by Schofield and Wroth (1968). The model can undergo recoverable volumetric strains inside the state boundary surface but not recoverable shear strains. The state boundary surface for Cam-clay was derived by assuming a balanced energy equation. Introducing recoverable shear strain would alter the state boundary surface. The elastic volumetric strains were defined by the relationship $\delta\epsilon_v = -\delta v/v = \kappa\delta p'/vp'$. Hence the incremental bulk modulus, K' given in equation 2.4.1 is vp'/κ and G' is infinite. The Modified Cam-clay model (Roscoe and Burland, 1968) used the same definition of elastic stress-strain behaviour.

Atkinson and Bransby (1978) proposed that a more realistic model for the elastic deformation of soil would be obtained by assuming that G' was not infinite but varied with mean effective stress in the same way as K'. Thus $G' = K'[3(1-2\upsilon')/2(1+\upsilon')]$ where υ' is a constant. The state boundary surface derived in the Cam-clay model was not modified. Experimental evidence that G' is dependent on the mean effective pressure had previously been provided by Wroth (1971), who analysed data from tests on undisturbed samples of London clay carried out by Webb (1967). Wroth (1971) concluded that the parameters K' and G' in a model of the elastic stress-strain response of the soil should be determined primarily by p' and to a lesser degree by overconsolidation ratio. The overconsolidation ratio could be represented by the parameter e_λ where $e_\lambda = e + \lambda \ln p'$. These experimental data also confirmed the assumption that Poissons ratio was a constant.

Zytinski et al. (1978), examining the thermodynamic implications of an elastic model where G′ varied with p′ while Poissons ratio remained constant, found that it was not conservative which is a condition for elastic behaviour. However, the alternative assumption, that Poissons ratio varied and G′ was a constant, resulted in negative values for Poissons ratio, which were clearly unreasonable. The only remaining option was to abandon the idea of a purely elastic model for soil behaviour.

As reported above, in the critical state soil models elastic volumetric strains occurring during the swelling and recompression of the soil are modelled by assuming that the specific volume of the soil varies linearly with the logarithm of the mean effective stress. As an alternative Butterfield (1979) proposed that the logarithm of the specific volume should be related to the logarithm of the mean effective stress state. For overconsolidated soils the most significant advantage of this "natural compression law" is that natural volumetric strains, as defined in section 1.2.1 are linked directly to the logarithm of the stress change. For isotropic elastic behaviour, $\delta\epsilon_v = (\kappa'/p')\delta p'$, or $K' = \kappa'/p'$.

All the above models assume that soil can be modelled as isotropic elastic although for many natural soils it is more realistic to use an anisotropic elastic model. The most appropriate form of anisotropy assumes that the soil has a vertical axis of symmetry and is known as cross-anisotropy or transverse isotropy. Love (1942) established that five independent parameters were required to define the behaviour of a transversely isotropic soil and the various thermodynamic limits on the values of these five parameters were investigated by Pickering (1970) and Gibson (1974). Graham and Houlsby (1983) provided a matrix equation for a transverse isotropic elastic soil in terms of triaxial stress invariants.

$$\begin{bmatrix} \delta p' \\ \delta q' \end{bmatrix} = \begin{bmatrix} K^* & J \\ J & 3G^* \end{bmatrix} \begin{bmatrix} \delta\epsilon_v \\ \delta\epsilon_s \end{bmatrix} \qquad (2.4.2)$$

The three parameters K^*, G^* and J represent the three parameters that can be obtained from a triaxial test on a vertically cut sample of a transverse isotropic soil.

None of the models discussed so far would predict the highly non-linear stress-strain behaviour observed by Jardine et al (1984) and Jardine (1985) for undrained stress paths and by Richardson (1988) for constant p' loading paths. Non-linear isotropic elastic models which are able to represent non-linear behaviour, include the hyperbolic model formulated by Duncan and Chang (1970) and the periodic logarithmic functions used to characterise undrained stress-strain data by Jardine et al (1986) and Jardine and Potts (1988).

The empirical soil model used by Jardine et al (1986) and Jardine and Potts (1988) is the only one which has been derived directly from high quality test data obtained using the recently developed strain measuring techniques and stress path cells. In this model the relationship between the undrained secant Youngs modulus and the logarithm of the axial strain is represented by a periodic logarithmic function of the form.

$$E_u/Cu = A + B\cos\{\alpha[\log(\epsilon_a/C)]^{\gamma}\} \qquad (2.4.3)$$

where the constants are defined in Figure 2.4.1. An expression for the tangent modulus is obtained by differentiating and rearranging this function. Similar periodic logarithmic functions linking shear modulus with shear strain and bulk modulus with volumetric strain were presented by Jardine and Potts (1988). The functions were fitted to data from a stress path triaxial test on a reconstituted sample of a North Sea clay with an overconsolidation ratio, $n = 2$. The resulting relationship was used to model the small strain behaviour of the soil around the driven piles for the Hutton tension leg platform. The stress-strain response predicted by the non-linear relationship was assumed to be reversible when the soil was unloaded (Jardine et al. (1985)).

The only non-linear elastic model that predicts that the stress-strain response of the soil may be affected by its recent stress history is Model LC devised by Simpson et al. (1979). The main feature of this model, created specifically to predict the behaviour of London Clay, was the kinematic yield surface (KYS) which was defined as a sphere in strain space within which the stiffness of the model was ten times the stiffness in the intermediate strain range. The stiffness of the model dropped to the stiffness given by the standard anisotropic elastic parameters that defined deformations in the intermediate strain range when the soil had strained by a sufficient amount to reach the edge of the KYS and "drag" it along, see Figure 2.4.2. In this way the model predicted highly non-linear stress-strain curves which were affected by recent stress history if the stress path rotation exceeded 90°. A more detailed evaluation of this model is given in section 5.2.

2.4.2 Yielding Models

The majority of the soil models which predict that plastic deformations occur within the state boundary surface use the Modified Cam-clay state boundary surface formulated by Roscoe and Burland (1968). Of the models reviewed here the only exceptions are those devised by Nova (1982) and Pender (1978, 1982). A constant volume section through the Modified Cam-clay state boundary surface.projects as an ellipse in $q':p'$ space. If soil deformations inside the state boundary surface are elastic this ellipse also acts as a yield surface. Attempts to plot this yield surface experimentally by identifying yield points in stress-strain curves, (e.g Parry and Nadarajah, 1973) appear to indicate that the surface changes shape during K_0 consolidation. However, this method of locating the yield surface for a soil is unreliable because it is difficult to identify yield points clearly, (Pickles, 1989). Experimental investigations using careful normalization of data from appropriate stress paths (Pickles, 1989, Graham et al, 1988) have shown that the isotropic Modified Cam-clay state boundary surface is relevant not only for isotropically consolidated but also K_0 consolidated soils.

The models proposed by Nova (1982) and Pender (1978, 1982) were derived directly from observations of soil behaviour unlike the majority of yielding soil models which are adaptations of formulations designed initially to describe the plastic behaviour of metals. Pender (1978) developed a model in which all deformations were plastic and the shape of the undrained stress path was used to determine the hardening function of the soil. The stress-strain response of the soil was governed both by the position of the current stress point relative to critical state and the initial state of the stress path. Pender (1982) modified the model to include the effect of stress reversals by assuming that the initial stress conditions were reset every time there was a stress reversal.

The model formulated by Nova (1982) is essentially in two parts. The part concerning the modelling of the unloading and reloading behaviour employed a "paraelastic" model which was path independent between stress reversal points. Deformations were controlled by the loci which were created at stress reversals and the orientation of the current stress rate with respect to the stress increment.

Dafalias and Herrmann (1982) adapted the bounding surface theory, which was originally developed to model metal plasticity, and used it to predict soil behaviour. In this model the previous compression history of the soil determined a "bounding surface" which in its simplest form was defined as the Modified Cam-clay state boundary surface. The stress state of the soil always lay within or on the bounding surface. The deformation at overconsolidated stress states, within the bounding surface, occurred at a progressive rate which depended on the distance between the current stress point and its "image" on the bounding surface, see Figure 2.4.3. The loading-unloading direction was governed by the gradient of the bounding surface at the image point.

Many different forms of the kinematic hardening model, also originally developed for metal plasticity, have been used to predict soil behaviour. In addition to isotropic hardening, described by a consolidation surface, kinematic hardening occurs due to the presence of one or more kinematic yield surfaces which lie within the consolidation surface. Mröz et al. (1979) described one of the simplest forms of kinematic hardening soil model, a two surface model, which has one kinematic yield surface inside the consolidation surface. This yield surface enclosed a region in stress space where deformation was elastic. If the soil was loaded from this elastic state so that the stress point reached the yield surface, plastic deformations occurred and the surface was "dragged" along by the stress point as loading continued. The plastic hardening rule for the soil was determined by the distance between the stress point and a conjugate point on the consolidation surface. Figure 2.4.4 shows the configuration of the surfaces during a typical loading path.

The model described above is a simplification of a multi-surface model which used a series of nesting kinematic yield surfaces in order to define the hardening modulus of the soil more precisely (Mröz et al., 1981). A third class of kinematic yield model, with an infinite number of yield surfaces, was described by Mröz and Norris (1982). The yield surface expands with the stress point as the soil is loaded. When a stress reversal occurs the current yield surface becomes the "stress reversal surface" until it is superseded by a new surface expanding from the stress reversal point, see Figure 2.4.5.

A two-surface kinematic hardening model was also formulated by Hashiguchi (1985) which is similar to the model described by Mröz et al. (1979) except in its precise mathematical definition. In order to obtain a smooth elastic-plastic transition Hashiguchi modified this model by adding a third surface. The third surface is inside the kinematic yield surface and concentric with it, see Figure 2.4.6. The surface expands and contracts with the stress point and defines the plastic deformations which occur. Al Tabbaa (1987) and Al Tabbaa and Wood (1989) modified and developed the two-surface kinematic yield model within the Cam-clay framework such that for monotonic loading the model reduces to Modified Cam-clay. The result was a relatively straightforward set of constitutive equations defined in terms of the critical state invariants and only requiring two additional parameters.

The models proposed by Nova (1982), Pender (1979,1982) and Dafalias and Herrmann (1982) can distinguish between loading and unloading events. However, only the kinematic hardening models and Model LC, described by Simpson et al. (1979), will predict that the stress-strain response of a soil is determined by more general variations in the recent stress history of that soil. A more detailed evaluation of these models is given in section 5.2.

2.5 Summary

The first two sections of this literature review show that despite major advances in laboratory testing techniques, including the use of stress path cells and local strain measurement, there is only a restricted amount of reliable data illustrating the general behaviour of overconsolidated soils at small strains. The most important feature of the behaviour identified by these tests was the highly non-linear nature of the deformation, except at very small strains which can only be measured using dynamic techniques. Richardson (1988) carried out the only significant series of tests investigating the effect of recent stress history which was clearly recognisable even without local strain measurements.

The review of existing numerical models indicates that the non-linear stress-strain response can be modelled either by using an elastic model with an empirical expression to fit the stress-strain curve or by an elasto-plastic model where yielding occurs inside the state boundary surface. The only models that will link the changes in stress-strain response with changes in recent stress history are those which incorporate kinematic hardening, for example Mröz et al (1979) or Hashiguchi (1985), or Model LC devised by Simpson et al. (1979).

CHAPTER 3 EXPERIMENTAL WORK

3.1 Introduction

The experimental work undertaken as part of this research project consisted of a series of triaxial tests carried out using computer controlled stress path cells. The objectives of the experimentation were as follows.

(i) To investigate the influence of factors such as state and overall history on the recent stress history effect in overconsolidated soils.

(ii) To provide test data for the evaluation of numerical models which describe the effect, either analysed to give the soil parameters required for the models or for direct comparison with numerical predictions.

(iii) To investigate the effect of changes in recent stress history on the behaviour of undisturbed samples of heavily overconsolidated clay.

The first two objectives were achieved by performing a variety of tests on reconstituted 38mm diameter samples of both speswhite kaolin and London clay, as detailed in section 3.6.3. A number of tests on undisturbed samples of London clay, including one on a 100mm diameter sample, were carried out to satisfy the third objective.

The programme of tests on reconstituted soil samples was designed to provide data that would expand on the extensive series of tests carried out by Richardson (1988). Aspects of the recent stress history effect that were considered to have been comprehensively investigated by Richardson (1988) were not included in the tests. In addition, observations made by Richardson (1988) about the effect, in particular that a wide variety of soils all display the same characteristics, were used as a basis for this work. The testing programme mainly uses samples of speswhite kaolin.

The basic form of the stress probe tests used to investigate the behaviour was also derived from Richardson (1988), although the detailed procedure was devised specifically for these tests (see section 3.6). Standard triaxial testing techniques for using the computer controlled Bishop and Wesley hydraulic stress path cells are well documented, for example Clinton (1987), Lau (1988) and Pickles (1989). The sections describing the apparatus, sample preparation, basic setting up and saturation procedures concentrate on aspects of the equipment and testing methods particular to this project, especially the use of local axial strain measuring devices on some of the undisturbed London clay samples.

3.2 Apparatus

3.2.1 Stress Path Cells

Stress path tests on 38mm diameter soil samples were carried out using standard hydraulic stress path cells similar to those described by Bishop and Wesley (1975). Two types of computerised control and monitoring systems were used to operate the cells.

The "Spectra" system (Atkinson et al, 1983), which controlled several cells simultaneously, consisted of a Spectra-xb microcomputer and a separate Epson computer with a printer. The Spectra-xb controlled the cells by operating electric motors driving either Fairchild manostats to regulate mains air pressure and provide the required pressures, or a Bishop ram to control axial strains. The Spectra-xb also monitored cell instruments and was linked to the Epson computer, which was used to record the data both on disc and as a print-out. Figure 3.2.1 shows a schematic diagram of the system.

The "BBC" system used a BBC microcomputer and a Spectra Micro-ms analogue to digital (A-D) converter dedicated to a single stress path cell. In this system the computer controlled relays which operated incremental stepper motors driving the electromanostats and the Bishop ram. The computer also monitored and recorded data from the cell instruments. Details of the control program "Trilog3" and a more comprehensive description of the system are given by Pickles (1988) and Clinton (1987) respectively. The system is shown schematically in Figure 3.2.2.

The main advantage of the Spectra system was the higher resolution transducer output provided by the Spectra-xb microcomputer compared to the Spectra Micro-ms used in the BBC system. This was most apparent for axial and volumetric strain measurements made using standard resistance transducers. The resolution of axial strain measurements was 0.002% for the Spectra system and 0.02% for the BBC system. The resolution of both axial and volumetric strain measurements made using the BBC system was improved substantially by using high voltage output transducers. The BBC control system is more flexible than the Spectra system as it is easily adapted to monitor additional instruments and can control a wider variety of stress or strain paths.

A large sized hydraulic stress path cell as designed by Atkinson et al (1984) to accommodate soil samples up to 100mm diameter was used for the single test carried out using this size of sample. The control system for this cell was similar to that for the BBC system described above. The only difference was that an IBM-XT compatible personal computer fitted with a card that partly acted as an A-D converter was substituted for the BBC computer/Spectra Micro-ms combination. This system is shown in Figure 3.2.3.

3.2.2 Instrumentation

Conventional instrumentation for a Bishop and Wesley hydraulic stress path cell was used, mounted as shown in Figures 3.2.1 to 3.2.3. All the stress path cells were fitted with internal load cells which were either Imperial College type load cells or Wykeham Farrance load cells made to the Surrey University design. The Imperial College load cells have a capacity of 4.4kN and the Surrey University load cells 5kN. Cell and pore pressures were measured by Druck or Wykeham Farrance pressure transducers with a range of 0-980 kPa.

Standard resistance transducers were used to measure axial displacements on the cells controlled by the Spectra system. The BBC and IBM controlled cells required higher voltage output linear variable differential transformers (LVDTs) as discussed above. A limited number of tests on 38mm diameter samples and a test using a 100mm sample were carried out with Hall effect local axial strain transducers (Clayton et al., 1989) attached to the samples.

Volumetric strains were measured by 50cc and 100cc Imperial College volume gauges for tests on 38mm and 100mm diameter samples respectively. The same type of transducer that was used to measure axial strains was fitted to the appropriate volume gauge.

The instruments were recalibrated every 3-4 months using standard procedures which are described in detail by Lau (1988). Typical calibration curves for the axial and volumetric strain transducers are given in Figures 3.2.4 and 3.2.5. The Hall effect transducers were calibrated against a new micrometer device described in Stallebrass (1990a). A typical calibration curve for these transducers is shown in Figure 3.2.6.

3.2.3 Accuracy of Measurements

The accuracy of the measurements made by the various types of stress and strain transducer used during the experimental work is given in Tables 3.2.1(a) and (b). The overall accuracies are quoted as an absolute value below which measurements are unreliable, together with a percentage of the current transducer reading. The absolute error represents the noise in the output and the percentage error results from drift, hysteresis and non-linearity in the calibration of the transducers.

For both stress and strain transducers drift is due either to a deterioration in the transducer's performance, in which case the results of the test would probably be discarded, see section 4.2.1, or to changes in supply voltage and temperature. The voltage supply to the transducers was very stable, fluctuating by less than ±.04%, therefore the majority of the drift that occurred was due to temperature changes in the laboratory. The laboratory was temperature controlled to approximately ±1°C, but the local axial strain gauges and the volume gauges are particularly sensitive to temperature changes. Although the drift in the transducer output was monitored over seven days, the percentages given in the table were calculated by assuming that an average stage lasted for 24 hours during which the axial stress changed by approximately 100kPa and the strains by 1% or, 0.2% when undisturbed samples were tested using the local axial strain gauges. Additional factors which influence the accuracy of axial and volumetric strain measurements are given below.

(i) Volumetric strains

To obtain reliable volumetric strain measurements it was necessary both to carry out frequent leakage tests (Pickles, 1989 and Lau, 1988) and to maintain a constant back pressure during drained tests. Providing these conditions are fulfilled the accuracy of the measurements is as given in Table 3.2.1. As shown in the table errors due to hysteresis are negligible for the LVDTs. For the Spectra system the resolution of the transducer output did not affect the accuracy of the readings. The BBC system resolved strains to less than 0.001% when the transducer output was close to zero and in the most sensitive voltage range of the A-D converter. When the voltage output was higher, the resolution could be as low as 0.01%. Hence, to measure small strains the transducer was adjusted to give a very low voltage output.

(ii) Axial strains

Axial strain measurements made externally were always corrected to eliminate deflections caused by compliance of the load cell. The magnitude of these deflections was obtained by placing a steel dummy sample in the cell and observing the axial strains that occurred when the stress paths used in the test were applied to the dummy sample. Typical curves for Imperial College and Surrey University load cells are given in Figure 3.2.7. The reliability and repeatability of these data is discussed in detail in Section 4.2.1 with reference to particular series of tests. The two curves demonstrate an important difference between the two types of load cell. The compliance curve for the Imperial College load cell shows two significant jumps in measured deflection with changing deviator stress, which occur when the deviator stress is approximately zero and when it reaches a given negative stress. The compliance curve for the Surrey load cell is linear through zero because it uses a fixed beam arrangement rather than the loose fitting star diaphragm in the Imperial College load cell. The compliance curves are affected by both cell pressure and direction of loading and so loading paths were repeated precisely to obtain the appropriate data. The deflection at a high negative deviator stress is caused by the load cell moving in its mounting and can be eliminated using the simple restraining device illustrated in Figure 3.2.8. In addition to load cell compliance, axial strains measured in the 100mm diameter cells were also corrected for compliance caused by changes in cell pressure, approximately 0.03mm/100 kPa.

All samples were subjected to consolidation stages with the load cell attached rigidly to the sample and therefore errors due to seating, tilting and bedding of the sample were considered to be insignificant for reconstituted soil samples. The values of the accuracy of axial strain measurements given in Table 3.2.1 assume that reliable compliance measurements could be made, see Section 4.2.1.

As shown in Table 3.2.1 the Hall effect local axial strain transducers were more susceptible to inaccuracies caused by noise and temperature changes than the conventional axial strain transducers. The transducers were not used to measure strains greater than 0.2% because of the development of shear planes in the heavily overconsolidated soils being tested. The main advantage of local measurements was that they were not affected by errors either due to bedding of samples or unreliable compliance data. Figure 3.2.9 shows comparisons between local strain measurements and external measurements corrected for compliance. The local strains may be higher or lower than corrected external strain measurements depending on the magnitude of deflections caused by bedding errors relative to the disparity between the middle third and the overall sample strains caused by end effects. The axial strains in the middle third of the sample will be different to the overall strain (Costa Filho (1985) and Cherrill (1990)). More detailed comparisons are given in Stallebrass (1990a). Radial strains were not measured directly during any of the tests.

3.3 Soil used in the Experimental Work

Two types of soil were used, London Clay and speswhite kaolin. Both undisturbed and reconstituted samples of London clay were tested, but the majority of the tests using reconstituted soil were carried out on samples of speswhite kaolin. Speswhite kaolin has a considerably higher permeability than London Clay and hence a generally lower value of t_{100}, the time for 100% consolidation (see Table 3.3.1(a)). This allows the soil to be loaded at a faster rate without generating high excess pore pressures, Atkinson (1984). Typical critical state parameters for London Clay and speswhite kaolin are given in Table 3.3.1(b).

The undisturbed samples of London Clay were taken from three sites, but all except two were obtained from a single site in North East London using U100 sampling tubes of wall thickness 4mm. A typical soil profile for the site is given in Figure 3.3.1, together with porewater pressure and K_o profiles. The water table is approximately 2m below ground level, where the porewater pressure gradient is hydrostatic, although below a depth of 8m the porewater gradient drops to slightly below hydrostatic. The K_o profile was obtained from pressuremeter tests.

The estimated maximum previous mean effective stress, defined as in section 1.2, at the three different sites from which the soil samples were obtained are given in Table 3.3.2. On all of these sites there was evidence that the soil had been reloaded by deposition of river gravels or under-drainage of the London Clay following the anisotropic swelling caused by the erosion of the overburden. Hence, standard expressions linking overconsolidation ratio to the in situ value of K_o, which are based on monotonic unloading to the current stress state, are not valid. Additionally no specific data for the amount of overburden at these sites has been found in previous work, so typical values have been used: for central London a value of approximately 180m obtained by Skempton and Henkel (1957) and for north London a value of 50m derived from oedometer tests and geological data by Jardine (1985) for a site at Canons Park. The values of p'_m given in Table 3.3.2 were calculated from these estimates. No allowance has been made for the effects of secondary consolidation or creep which might increase the value of p_m'. This table also gives the in situ stress state and water content of the samples. Test No. LAS5 was carried out on soil taken from a thin-walled U100 sampling tube, wall thickness 2.5mm. The 100mm diameter sample required for Test No. DLC4 was a rotary cored sample, sealed with wax coated polythene film. Despite the wire line coring technique used to obtain the sample it appeared to have suffered from stress-relief during sampling.

3.4 Sample Preparation

3.4.1 Undisturbed Samples

To obtain 38mm samples, the soil was extruded directly from the U100 sampling tube into a 38mm diameter thin-walled brass tube of wall thickness 2mm, which is equivalent to an area ratio of approximately 18%. The 38mm diameter brass tube was clamped rigidly a few millimetres above the centre of the sampling tube. Excess soil was trimmed from around the brass tube as the U100 sample was extruded. The soil was then extruded from the 38mm diameter brass tube into a sample cradle where it was trimmed to a length of 76mm. Care was taken to ensure that the ends of the sample were plane, parallel and perpendicular to the axis of the sample. Offcuts were used to obtain an indication of the initial moisture content of the sample. After trimming, the sample dimensions were measured and the sample was placed in the cell.

100mm diameter samples were formed by first removing the wax and polythene which had been used to seal the soil. The sample was then placed in a cradle and carefully trimmed to a length of 200mm. The moisture content and dimensions of the sample were measured, as outlined above for 38mm diameter samples, before placing the sample in the cell.

During preparation of the undisturbed samples the time for which the sample was exposed to the air was kept to a minimum to prevent the surface of the sample drying out.

3.4.2 Reconstituted Samples

Reconstituted samples were obtained by mixing dry soil with de-aired distilled water to form a slurry which was then one-dimensionally consolidated in a consolidation press. This method of preparing reconstituted samples is frequently used at City University, with minor variations, and has been described in some detail by Richardson (1988) and Ho (1988). The method is outlined below.

The dry soil used in the slurry was in the form of a powder. To produce a powder from intact London Clay the soil was first broken into small pieces, oven-dried and then ground using a pestle and mortar. The powder was sieved to ensure that no particles greater than 0.3mm were used in the slurry. Speswhite kaolin is supplied as a powder.

The slurry was mixed to a water content of approximately 100% for the London Clay and 150% for the kaolin. A measured quantity of the slurry, sufficient to produce a sample of the required length, was then poured into a consolidation press. The floating ring consolidation press was a 38mm diameter thick-walled perspex tube with pistons at both ends, which had porous stones set into the end faces. A typical press is shown in Figure 3.4.1. The sample was loaded gradually using weights placed on a hanger to a total of 8kg. The separate ring at the base of the consolidation press was removed during loading so that the tube could "float" on the lower piston and thus allow uniform consolidation. After loading the sample was left for a minimum of 24 hours to allow excess pore pressures to dissipate. When the sample was required it was weighed and extruded directly onto the bottom platen of the stress path cell. Richardson (1988) observed that the variation in water content between the end and centre of the sample, at the end of consolidation, was between 0.75 and 1% of the mean water content of the sample for both London clay and speswhite kaolin. This variation was caused by friction along the length of the tube but will not be significant if the sample is compressed to high stresses in the cell.

3.5 Test Procedure

This section describes the setting up of the samples in the cell, saturation stages and any compression or swelling stages required to bring the sample to the stress state at the start of the main stress path probing test. Generally the standard procedures used at City University were followed, which have been described in some detail by other research workers such as Richardson (1988) and Pickles (1989). All the loading stages were automatically controlled and monitored by the computer system attached to the cell. Except for stages where one step consolidation or swelling occurred the loading paths were always applied as a smooth variation in stress or strain.

3.5.1 Setting up the Sample

(i) Undisturbed Samples

Samples were set up in the cell, as shown in Figure 3.5.1, using a standard procedure described in detail by several authors, including Lau (1988) and Ho (1988) for 38mm diameter samples, and Clinton (1987) for 100mm diameter samples. To prevent changes in the sample moisture content, top and bottom filter papers were dampened before use, as were the modified Bishop and Henkel (1962) type side drains. The modification, devised by Pickles (1989), requires a pattern of cuts to be made in the drains, see Figure 3.5.2, which ensures that they have little stiffness in extension. The all-round drainage allowed the samples to be tested at reasonable loading rates without generating large excess pore pressures, see Section 3.6.2. Non-uniformities caused by all-round drainage were negligible for the loading rates used in these tests, Atkinson et al (1985).

38mm diameter samples were enclosed in a single membrane sealed against the bottom pedestal and top platen using a film of silicon grease and two O-rings. Two membranes were required for the 100mm diameter sample in order to prevent the membrane splitting around the Hall effect transducer mountings as the sample deformed to failure. Silicon grease was used to seal the two membranes together.

If local axial strain measurements were required, two transducers were fitted to the sample at this stage in the procedure. The magnet arm mounting and the Hall effect sensor mounting were pinned and glued to the sample (see Figure 3.5.3) and the membrane was then resealed with vulcanising solution. When the vulcanising solution had set the sensor was inserted as shown in Figure 3.5.3 and positioned so that it provided an output within the linear range of the transducer. Further details of this procedure are given in Stallebrass (1990a).

The standard 38mm diameter cells used a suction cap screwed to the top platen to connect the load cell to the sample but the load cell was not connected until after the saturation stage. The load cell in the 100mm diameter cells was bolted rigidly to the top platen before the cell body was placed in position and filled with water. The axial and radial stresses were then increased at the same rate to reach the all-round stress required for the saturation stage.

(ii) Reconstituted Samples.

Reconstituted samples were set up as described above for the undisturbed soil samples, except that the sample dimensions were measured in the cell. Hall effect transducers were not used for any tests on reconstituted soil.

3.5.2 Saturation Stages

All samples were initially loaded isotropically under a constant cell pressure with the drainage valve closed until the pore pressure reached equilibrium. The drainage leads were then flushed through to remove any air trapped by the porous stone during setting up and the saturation or B value of the soil was measured. The minimum B value accepted was 0.97. At this stage most of the reconstituted soil samples had a B value close to one, demonstrating that the samples and the drainage connections were well saturated.

The undisturbed samples were often more difficult to saturate. If the procedure described above failed to saturate the sample this implied that there was air trapped, either between the membrane and the sample or in the soil, that would not dissolve under the pore pressure that it was possible to generate in the sample. In these cases the samples were swelled to the isotropic equivalent of their estimated in situ state by increasing the back pressure to the appropriate level with the drainage valve open. Any change in volume measured by the volume gauge during this process was assumed to be air dissolving.

If the sample became saturated without being swelled back to its in situ state, it was necessary to adjust the cell pressure, undrained until the pore pressure in the sample equalled the pre-set back pressure, either 100kPa or 200kPa. The 38mm diameter samples were then connected rigidly to the load cell by a rubber suction cap. The arrangement of the load cell, the rubber suction cap and the top platen of the sample is shown in Figure 3.5.1. The procedure for connecting the top platen to the load cell in this way was described by Lau (1988).

3.5.3 Initial Compression Stage

Most of the undisturbed soil samples were swelled or compressed directly to the stress state at which the stress path probing stages were to begin. The remainder followed stress paths similar to K_o swelling or recompression in order to recreate the recent stress history of the soil. Loading rates for these initial compression stages were on average $\dot{p}' = 4$kPa/hr for the 38mm diameter samples and $\dot{p}' = 8$kPa/hr for the 100mm sample.

The majority of the reconstituted speswhite kaolin samples were firstly isotropically compressed and then swelled back isotropically to the overconsolidated state required for the main loading stage. The rate of loading and unloading was 5kPa/hr, which was chosen to give an excess pore pressure of less than 1kPa calculated using the method outlined by Cherrill (1990) and Atkinson (1984). The sample was allowed to consolidate as the small excess pore pressures generated during the loading stages were equalised. The volumetric strain observed during this consolidation demonstrated that the excess pore pressures were generally less than 3kPa. Some special isotropic swelling and compression tests used different loading rates as described in section 3.6. All the reconstituted samples of London clay and some kaolin samples were compressed and swelled anisotropically. The loading rates for these tests were $\dot{p}'$ = 4.3kPa/hr for the London clay and $\dot{p}'$ = 4.3 - 5.7kPa/hr for the kaolin. Excess pore pressures estimated from the consolidation at the end of the swelling stages were approximately 6kPa and 2kPa respectively.

3.5.4 Main Loading Stages

The main loading stages were always carried out from an overconsolidated stress state and took the form of a series of stress probes. The stress probes followed a fixed pattern determined by the specific test being carried out (see section 3.6). Some samples were then recompressed to a point further down the normal compression line before being swelled back so that the test could be repeated at a different overconsolidation ratio. Loading rates for all the stages were calculated using the methods described by Atkinson (1984) and Cherrill (1990) so that excess pore pressures were minimised (see section 3.6).

3.5.5 Final Stages

Some of the samples were sheared undrained to failure from the stress state reached by the final stress probe. Finally, the samples were removed from the cells and a moisture content obtained.

3.6 Test Description

3.6.1 Objectives

The most important objective of the tests was to investigate the effects of a change in direction of the stress path on the subsequent stress-strain behaviour of the soil and to examine the additional effects of the current state and overall stress history. The tests followed on from work carried out by Richardson (1988) and used the same fundamental methods of testing, although a more restricted range of soils, loading paths and stress histories were considered. A basic description of the soil, sample type and the initial and final state for each test is given in Table 3.6.1.

3.6.2 Description of Basic Test

In the basic form of the test the stress-strain response of the soil was observed during loading along a fixed common stress path for each of a variety of different approach path directions, Richardson (1988). Figure 3.6.1 shows a typical pattern of loading stages to investigate the effect of recent stress history along a loading path OA with increasing q′ at constant p′. The start of the path is approached from directions such as BO, CO and DO, corresponding to stress path rotations of θ_B, θ_C, and θ_D where θ is as defined in section 1.2. The most frequently used common path was loading with increasing q′ and constant p′, although tests with q′ constant and p′ increasing or decreasing, and with undrained compression as the common path were also carried out. These particular stress paths are used for the reasons outlined in section 1.2.3.

The only significant variation on this basic form were tests which consisted of a series of purely isotropic swelling and recompression loading paths. These tests were primarily designed to provide data that would aid the determination of basic parameters required for the numerical models outlined in section 5.

In order to ensure that the objectives of the experimental work were fulfilled, detailed aspects of the test procedure such as the length of the loading paths, loading rates and the time allowed at the end of loading paths for dissipation of excess pore pressures were carefully chosen. These factors are discussed below together with the reasons for selecting the most commonly used pattern of stress path rotations.

(i) Stress path rotations.

As it was necessary to conduct the tests relatively slowly, following a number of paths, it was not possible to investigate the effect of a large number of stress path rotations for every common path or overall history. It was clear from the previous work by Richardson (1988) that the rotations which best characterised the different aspects of the recent stress history effect were 0°, ±90° and 180° (see section 4.3) and the majority of the tests carried out on reconstituted soil samples followed these rotations. A wider variety of stress path rotations was applied for the tests on undisturbed soil samples.

(ii) Length of loading paths

To prevent the build up of plastic strains during the tests it was important that the stress probes should not come too close to the state boundary surface, as defined by the preconsolidation pressure of the soil, p'_m, see section 1.2.3. This condition was met partly by keeping the loading paths as short as possible and partly by starting most of the tests from an isotropic state. If the loading paths are too short, however, the stress-strain response along the common path is affected not only by the approach path, for example CO in Figure 3.6.1, but also by the previous stress path, AC in this case. Richardson (1988) investigated the extent of the recent stress history effect using swelling and recompression tests and concluded that the effect ran out after a stress change equal to $0.35p'_i$, where p'_i is the mean effective pressure at O. Hence if the stress paths used in the tests are all longer than $0.35p'_i$ only the approach path influences the stress-strain response of the common path. All the stress paths used in these tests were longer than $0.35p'_i$. However, further experimental data obtained during the testing programme indicated that the overall stress history of the soil such as overconsolidation ratio may also influence the duration of the effect of a change in stress path direction, see section 4.2. This resulted in the use of longer stress paths where possible. Precise details of the approach path lengths used in the tests are given in Tables 3.6.2(a)-(c).

(iii) Loading rates

The loading rates used for the common stress path in the standard tests were chosen using the methods described by Cherrill (1990) to minimise excess pore pressures generated in the sample. Loading rates are most critical for constant q' paths (Atkinson (1984)) and the swelling and recompression tests were carried out at extremely low loading rates to ensure that excess pore pressures are negligible. The loading rates used in the tests are given in Tables 3.6.2(a)-(c). The loading rates used for the tests on reconstituted soil samples were very conservative as excess pore pressures were not measured directly using mid-point pore pressure probes. Data provided by Cherrill (1990), from tests on samples of speswhite kaolin where mid-point pore pressures were monitored, indicated that at these loading rates excess pore pressures would not exceed 0.1kPa. The immediate volumetric strains that resulted from the equalisation of excess pore pressures at the end of a stage did not exceed .03% and were usually negligible.

(iv) Rest period

At the end of the approach stress path, O in Figure 3.6.1, the sample was held for a time at a constant stress state to allow excess pore pressures to dissipate before beginning the common loading path: this time was called the rest period. Tests by Som (1968) and Richardson (1988) found that when a soil is held at a constant stress state in this way the subsequent stiffness of the soil is determined by the length of this rest period. Hence, in order to obtain consistent results which only illustrated the effect of stress path rotation on the stress-strain response of the soil, the rest period was fixed throughout a test and also for series of tests, see Tables 3.6.2(a)-(c).

3.6.3 Test Categories

This section describes the particular objectives and procedure applicable to the four different classes of tests that comprised the experimental work.

(i) Tests on undisturbed soil

Tests TT1-TT4, LAS5 and DLC4 (details in Table 3.6.2(a)) were all carried out on samples of undisturbed London Clay. The common loading paths were constant p' with q' increasing and constant q' with p' increasing. These were preceded by a variety of recent stress histories. Tests LAS5 and DLC4 were carried out with local axial strain gauges fitted to the samples.

(ii) Tests with an undrained common loading path

Tests ULC1, ULC2 and UK5-UK7 (details in Table 3.6.2(b)) were carried out on reconstituted samples of London clay and speswhite kaolin, compressed and swelled anisotropically in the cell. These tests investigated the effects of recent stress history on stiffness and, more importantly, the changing shape of the effective stress path during undrained compression.

(iii) Drained, constant p' and constant q' tests.

Tests DKP1, DKSR1 and DKSR3 (details in Table 3.6.2(c)) were carried out using reconstituted samples of speswhite kaolin. Test DKP1 and the second part of test DKSR3 consisted of series of probes to investigate the stress-strain response during constant p' compression paths at different values of p_i' and p_m'. These different stress states were attained by recompressing the sample to the normal compression line after each series of probes. Figure 3.6.2 shows a typical sequence of loading paths. Test DKSR1 and the first part of DKSR3 examined the behaviour of the soil during repeated stages of isotropic compression and swelling.

CHAPTER 4 THE EFFECT OF RECENT STRESS HISTORY ON SOIL BEHAVIOUR OBSERVED IN LABORATORY TESTS

4.1 Introduction

Data described in this chapter were obtained from three main sources.

(i) Tests carried out as part of this research project, described in section 3.6.3

(ii) Tests carried out by Richardson (1988).

(iii) Stress probe tests using a true triaxial cube apparatus, undertaken by Lewin (1990).

The programme of stress path triaxial tests, which was carried out as part of this research, was a continuation of work by Richardson (1988) which had already established the basic features of the effect of recent stress history. Figures 4.1.1 and 4.1.2 show typical results for a stress probe test on reconstituted Cowden till, taken from Richardson (1988). The stress-strain response of the soil was investigated along a constant p′ loading path, with q′ increasing. Similar results can be obtained for tests examining a constant q′ path, as shown in Figure 4.1.3. The characteristics of the stress-strain response of the soil, which can be observed from these graphs are:

(i) The stress-strain behaviour is highly non-linear. This is illustrated in Figures 4.1.1(a) and 4.1.2(a) by the graphs of q' versus ϵ_s and $dq'/vp'd\epsilon_s$ versus $\ln\eta$, i.e stress-strain curves and curves of stiffness against a measure of the progress of the test, both normalised.

(ii) The stress-strain behaviour varies with recent stress history described by θ, the angle of rotation of the stress path. At any stress level within the range of the effect of recent stress history, the stiffness of the soil is greatest for θ =

180°, a stress path reversal, and least for $\theta = 0°$, a continuous path.

(iii) Volumetric strains occur during the constant p′ loading producing the strain paths shown in Figure 4.1.1(b). These strain paths are characteristic for different values of θ. Corresponding curves which show the variation in shear strain with volumetric strain for a constant q′ path are given in Figure 4.1.3(b). The maximum variation in strain increment ratio is between $\theta = 90°$ and $\theta = -90°$.

(iv) The effect of the recent stress history gradually diminishes as the soil is loaded until after a certain stress change it is no longer evident. This is shown by the gradual convergence of the different curves of stiffness, $dq'/vp'd\epsilon_s$, versus $\ln\eta$ and strain increment ratio, $d\epsilon_v/d\epsilon_s$, versus $\ln\eta$.

This brief description of the effect of recent stress history, provides a background to the more detailed analysis undertaken later in this chapter.

The chapter begins with a section covering experimental results obtained during this research project. The aims of the programme of stress path tests were to investigate the behaviour of undisturbed soil samples, to examine the influence of state and overconsolidation ratio and to provide data for comparison with a theoretical soil model. Section 4.2 begins with an evaluation of the quality of these experimental data and a description of the way in which these data were analysed. Data from undisturbed soil samples are reviewed in section 4.2.3, followed by an analysis of results from reconstituted samples which show the effect of overall stress history and state. The section concludes with a discussion of the anisotropic behaviour of the soil illustrated by the variation in strain increment ratios during drained stress paths and the different effective stress paths followed during undrained compression.

Data on the effect of recent stress history obtained by Richardson (1988) are presented in section 4.3. Some of these data were reinterpreted for comparison with the results from section 4.2, because of the different method of analysis used by Richardson (1988). The results of the true triaxial cube tests are recorded in section 4.4. Finally, the important features of the effect of recent stress history on the stress-strain behaviour of overconsolidated soils are summarised, including a discussion of the evidence that the nature of the deformations is either elastic or elasto-plastic.

4.2 Experimental Data Obtained During Current Research Project

4.2.1 Quality of Data

This section examines the quality of data obtained from the stress path triaxial tests described in Chapter 3 and identifies the major causes of inaccuracies in the data with reference to particular series of tests. All external strain measurements presented have already been corrected to allow for compliance of the load cell (see section 3.2.3). None of these data have been smoothed or adjusted to remove inconsistent points because this would imply that the correct form of the data had already been established.

(i) Tests on undisturbed London clay

Tests TT1, TT2, TT3, and TT4 were carried out using Spectra controlled stress path cells. Figure 4.2.1 shows two stress-strain curves which illustrate the typical scatter in the results from both constant p' and constant q' tests. The scatter is largely due to the lack of accuracy of the incremental strain measurements. The average stress change between these readings is 5kPa. At low stress levels the stiffness of the soil will often exceed 100MPa. This is equivalent to a change in strain of 0.005% which cannot be measured accurately using this equipment (see Table 3.2.1). Unfortunately, this control system was only capable of taking data records at hourly intervals. If a large number of records are obtained it is possible to reduce the inaccuracies in the calculation of derived quantities such as stiffness by using a greater number of data points (see (iii)). This was not possible for these tests.

In addition, axial strain measurements at deviator stresses in the range +20kPa to -20kPa are unreliable. This is because over this stress range it was not possible to obtain a repeatable compliance curve for the Imperial College load cells that were used for these experiments. Figure 4.2.2 shows two compliance curves for a single load cell, subjected to a fixed constant p′ loading path. Imperial College load cells were used for all these tests.

Internal axial strain transducers were used in tests LAS5 and DLC4, which were carried out using BBC and IBM cells respectively. The use of these transducers eliminates uncertainties in axial strain measurements caused by both unreliable compliance data and end effects. A detailed comparison of the internal and external axial strain measurements made in these two tests is given in Stallebrass (1990a). This concludes that the relationship between internal and external strain measurements is mainly dependent on whether the compliance of the load cell can be determined accurately. If this is possible the difference in the internal and external measurements is due to the difference between the deformations measured in the middle third of the sample and those measured over the entire sample. For test DLC4 data records were obtained approximately every 15 minutes or 1kPa change in deviator stress. Figures 4.2.3 and 4.2.4 show comparisons between plots of shear stress against axial strain and shear stress against shear strain. For test LAS5 the shear stress against shear strain curves would be expected to show more scatter because the volumetric strain measurements, which were required to calculate the shear strains, are less accurate than the axial strains. In practice this effect appears to be negligible. In test DLC4, which uses a 100mm sample, this is not a problem. As noted in section 3.2.3, end effects mean that the overall axial strain of a sample will be different from the strain measured over the middle third of the sample (Cherrill (1990)). Therefore volumetric strains measured externally may not be comparable with internal axial strains.

(ii) Tests on reconstituted samples

The majority of tests on reconstituted samples were carried out in BBC controlled stress path cells fitted with high output voltage LVDT transducers and Surrey University designed internal load cells. The exceptions were the tests on London clay, tests ULC1 and ULC2, which used the same system as the set of tests on undisturbed London clay, TT1-TT4. Hence, the axial strain data obtained from tests ULC1 and ULC2 are subject to the same inaccuracies as outlined in (i) above. These errors are less significant for these tests where the main objective was to measure the shape of the undrained effective stress path.

The compliance curves for the Surrey University load cells are repeatable and linear through zero, see Figure 3.2.7, with a compliance of approximately 0.03mm/100kPa. Stress-strain data from three different tests are given in Figure 4.2.5. The data from test UK7 are also typical of tests UK5, UK6, and DKP1. During these tests data were only recorded at intervals of 5kPa deviator stress. The data for constant p′ and constant q′ paths shown in the second two graphs, which were recorded at intervals of approximately 1kPa, provide a much more complete picture of the stress-strain behaviour of the soil. These data are typical of tests DKSR1 and DKSR3.

Scatter in the constant q′ data may result from the extremely slow loading rate of 1kPa/hr. The load cell was only accurate to approximately 3kPa, and readings oscillated by ±1.5kPa. This caused the control system to adjust the load on the sample constantly in an attempt to maintain a constant loading rate. The soil never responded instantly to these changes, so that the recorded stress and strain levels were not necessarily an accurate picture of the state of the soil. The slight undulations in the plot of p′ versus ϵ_v may be caused by cycles of temperature change over the four days that the stage lasted. As noted in section 3.2.3 the volume gauge is especially sensitive to temperature changes. The duration of the loading stages in the swelling and recompression tests was an exception to the standard 12 to 24 hour period used in most tests.

The quality of data produced from these tests was also highly dependent on the reliability of the transducers, specifically, whether the zero voltage drifted substantially during the tests. This was a particular problem for tests such as DKP1, DKSR1 and DKSR3 which lasted for up to two months. Voltage drift in stress transducers was most critical because these were only zeroed once at the start of a test which was entirely stress controlled. The stress transducer readings were always checked at the end of a test, but at this stage it is almost impossible to establish at what point in the test the error ocurred. If the stress transducer zero reading were found to be significantly in error at the end of a test the data were not used.

(iii) Calculation and accuracy of tangent moduli

For all test results the stress-strain behaviour of the soil was characterised by the tangent to the stress-strain curve taken at a particular stress level. The reasons for using tangent moduli are explained in 4.2.2. This tangent modulus was calculated by fitting a straight line to data points either side of and including the point at which the modulus was required using a least squares method. The gradient of the line was taken as the tangent modulus of the soil at that point. The least squares calculation was carried out over a stress change of approximately 15kPa. The precision of the estimate of tangent modulus is improved by approximately the square root of the number of points in this stress range.

For stiff soils, when measuring small strains it is the absolute, not the percentage error that has the greatest influence on the calculation of stiffness data. This means that the reliability of these stiffness data is largely dependent on the magnitude of stiffness that the equipment is attempting to measure. Stiffness data are not quoted for stress state at the start of a loading stage where the transducers are just measuring noise.

(iv) Calculation of specific volume

The specific volume of the soil was calculated using volume change measurements made during the test together with the final specific volume of the sample, measured at the end of the test. The final specific volume was calculated using the equation $v = 1 + wG_s$, where w is the moisture content of the soil, and G_s the specific gravity of the soil grains. If the measurements used in this calculation are accurate, the results of all the isotropic normal compression stages for a given soil type should fall on a unique normal compression line. Data from the three tests on reconstituted samples of speswhite kaolin, DKP1, DKSR1 and DKSR3 are shown in Figure 4.2.6. Average values of λ and N obtained from these data are $\lambda = 0.073$ and $N = 1.144 \pm 0.007$, where N was calculated from the specific volume after consolidation at the end of the initial compression stages. These values correspond to the lnv : lnp' plots in Figure 4.2.6 and are different to the values usually quoted for speswhite kaolin which are calculated from v:lnp' plots. The scatter is caused by inaccuracies which build up during the test at large strains. Assuming that errors due to leakage and changing back pressure have been eliminated using the procedures described in section 3.3, the inaccuracies are mainly caused by incorrect sample dimensions, changes in water content of the filter paper and membrane, and gradual drift in the transducers (see Richardson (1988)). The calculated specific volumes of the soil in tests DKP1, DKSR1 and DKSR3 were adjusted so that the stress state of the soil fell on the average isotropic compression line at the end of the first compression stage in the test. This ensures that quantities such as p'_e, which are derived from these values are consistent between tests.

(v) Summary

Throughout the programme of experimental work the test equipment and experimental method were modified in an attempt to improve the accuracy and reliability of the measurements made in the tests. In particular, new types of external strain transducers were introduced and internal strain transducers were fitted to the cells. Because of this effort to try new techniques the success rate of the 22 tests carried out was relatively low. The data from 5 of the tests were discarded completely due to failure of stress transducers and parts of the computer control system. Many of the tests lasted for more than a month and some involved as many as thirty different loading stages.

Good quality data were obtained from the tests where external axial strain measurements were made in conjunction with Surrey University type load cells, or where internal axial strain measuring devices were used. The data quality is best for the less stiff reconstituted soil samples and when sufficient data records were obtained during the test. Even using internal axial strain transducers, the accuracy of the test equipment is only just adequate to measure the stiffness of heavily overconsolidated London Clay for small stress changes.

4.2.2 Analysis of Results

The analysis of the experimental results will be explained with reference to typical data taken from test DKSR3. These data are from a series of drained stress probes which resulted in four sets of stress and strain data, all for the same constant p′ loading path. Data are generally described by the common path that was followed and the current value of p'_m, where p'_m is defined as in section 1.2.1. In this case the common path was constant p′ with q′ increasing, where $p'_i = 300$kPa and $p'_m = 720$kPa.

The data are plotted in terms of the stress and strain parameters p′, q′, ϵ_v and ϵ_s. All the strains used are natural strains calculated from the ordinary strains recorded by the stress path control systems. Natural strains are preferred because they eliminate the errors in the values of shear and radial strain, calculated from original measurements, which can build up as the strains become large (Richardson (1988)). They are also incremental strains related to current dimensions and are therefore more appropriate for comparison with incremental constitutive soil models.

For a constant p′ path the stress-strain response of the soil is shown by the relationship between q′ and ϵ_s. The four curves of q′ against ϵ_s for this test are shown in Figure 4.2.7(a). Graphs of ϵ_v versus ϵ_s, Figure 4.2.7(b), provide information on the nature of the soil deformations, see section 4.2.5.

A clearer picture of the effect of recent stress history on the stress-strain response of the soil loaded along this constant p′ path is gained from graphs of tangent shear stiffness against stress change and stress increment ratio against stress change. As described in section 1.2, for a constant p′ path the tangent shear stiffness of the soil, or 3G′, is the gradient of the q′ versus ϵ_s curve. Similarly the stress increment ratio, $d\epsilon_v/d\epsilon_s$, is the gradient of the ϵ_v versus ϵ_s curve. Values of bulk stiffness, K′, and strain increment ratio, $d\epsilon_s/d\epsilon_v$, can be obtained in the same way from p′ versus ϵ_v and ϵ_s

versus ϵ_v graphs for constant q′ paths. Using tangent stiffness data rather than the more conventional secant stiffness data reduces the cumulative effect of any inaccuracies in the strain measurements at the start of the test. In addition tangent stiffness data are more appropriate for comparison with incremental soil models.

For all tests the variation in tangent stiffness and strain increment ratio is plotted against stress level rather than strain level. The data are presented in this way for several reasons. Firstly, as noted by Richardson (1988), if two different recent stress histories were applied to two otherwise identical soil samples before they were loaded to failure, the soil would fail at different strain levels but the same value of q′. The only unifying factor is the stress level in the soil. Secondly, for some loading paths the current strain level of the soil is not well defined, because of inaccuracies at the start of the loading, unlike the current stress state. Finally, the soil models described in sections 5.2 and 5.3, which have been developed to model the effect of recent stress history, are largely defined in stress space. Figures 4.2.8(a) and (b) show graphs of tangent shear stiffness and strain increment ratio respectively against stress , q′. The graph of tangent shear stiffness against stress level, Figure 4.2.8(a), shows a feature which is common to most of these stiffness data when they are derived from a large number of data points. The curve is not smooth but follows slight humps. This is probably caused by a combination of two effects. Firstly, momentary increases in the stiffness of the soil which result from poor control of stresses causing the soil to be unloaded and hence stiffer on reloading. Secondly, the stiffnesses are calculated from a large number of data points so that these sudden jumps in the stress-strain data affect a considerable section of the curve. It is difficult to avoid this problem if it is also necessary to reduce errors caused by random scatter. There is no experimental evidence, however, that the stress-strain response of a soil should form a smooth curve.

Richardson (1988) plotted all stiffness data as normalised stiffness, $dq'/vp'd\epsilon_s$, against the logarithm of stress change normalised by the current mean effective stress. These data are only normalised to illustrate a particular aspect of the soil behaviour, as in section 4.2.4. Plotting data against the logarithm of stress change exaggerates the initial part of the curve, in general the most inaccurate part.

The graphs in Figures 4.2.7 and 4.2.8, illustrating the effect of four different recent stress histories, clearly describe the same characteristics as those identified by Richardson (1988) and detailed in the introduction to this chapter. As explained in Chapter 3, for most of these tests only the recent stress histories represented by, $\theta = 0°$, $90°$, $-90°$ and $180°$, were investigated.

The tests for which undrained compression was the common path were analysed slightly differently. The tangent shear stiffness obtained from an undrained compression stage is not equal to 3G', unless the soil is isotropic and elastic, see section 1.2.3, and will be identified as $3G_u$. The variation in stiffness, G_u, obtained from these tests is only used in section 5.5.4, for comparison with model predictions. The undrained effective stress paths which result from the different recent stress histories are plotted in q':p' space, and the gradient of these stress paths dp'/dq' are plotted against stress level. Hence, the four basic graphs for the undrained tests are, q' versus ϵ_s, $3G_u$ versus q', the undrained effective stress path plotted in q':p' space and dp'/dq' versus q'.

4.2.3 Behaviour of Undisturbed Soil Samples

Six tests on undisturbed London clay were completed, of which four investigated the effect of three or more recent stress histories. These four tests TT3, TT4, LAS5 and DLC4 provide the four complete sets of data presented in this section.

(i) Stiffness

The shear stiffness data obtained from TT4, LAS5 and DLC4, for a common loading path at constant p' with q' increasing, are given in Figures 4.2.9 to 4.2.11. The poor quality of data obtained from test TT4, explained in section 4.2.1, is reflected in the stiffness plot shown in Figure 4.2.9. The higher stiffnesses could not be measured reliably and so for a given recent stress history the stiffness of the soil appears to be approximately constant. Data from tests LAS5 and

DLC4 show considerably more non-linearity. The stiffness curve for $\theta = 90°$ has been omitted from Figure 4.2.10. because the soil had been held at a constant state for too long before starting the constant p' loading.

In common with data for reconstituted samples, different curves are obtained when the recent stress history is altered. At a given stress level the stiffness is generally greatest for $\theta = 180°$, but the curves for rotations of greater than 90° are quite similar, as shown in Figure 4.2.11. The limit of the influence of recent stress history cannot be determined from these data. It is probable that the soil was not loaded along a sufficiently long path for the extent of the influence to be exceeded. Figure 4.2.12 shows curves of bulk stiffness, K', against change in stress for the constant q' loading path with p' decreasing, which was the common path for test TT3. These curves also show the variation in stress-strain response with θ more clearly, and the extent of the influence of the effect is also better defined.

(ii) Strain Paths and Strain Increment Ratios

Plots of ϵ_v versus ϵ_s and ϵ_s versus ϵ_v for the four main tests are shown in Figures 4.2.13 to 4.2.16. Allowing for the accuracy of the measurements these plots still show clear trends indicating that different values of θ lead to different strain paths, although the pattern of paths is not the same as the typical data obtained from reconstituted samples. For the reconstituted samples, for which p'_m is comparatively low, stress path rotations of $\theta = -90°$ and $\theta = 90°$ produce opposite types of strain paths (see section 4.2.5). Unfortunately, only two of the sets of data investigated here include both positive and negative rotations, and the data from them are not conclusive.

The strain increment ratio against stress change curves derived from the strain paths obtained in test DLC4, Figure 4.2.17, converge towards a positive value of strain increment ratio. This indicates that initially the soil is tending to compress rather than dilate as it is sheared. This is in contrast to the proposal in section 4.2.5, that soils dry of critical state should tend to dilate once outside the influence of recent stress history.

(iii) Normalised Stiffness Data

The estimated overall stress history and state of the six undisturbed samples of London clay at the start of the common path, is given in Table 4.2.1. As there are comparatively little data illustrating the effect of recent stress history on the stress-strain response during constant q′ loading, only the data for constant p′ paths were normalised, i.e. tests TT1, TT4, LAS5 and DLC4. These data have been normalised with respect to p′, in accordance with elastic theory. Figure 4.2.18 shows values of G′/p′ taken at the stress level $\Delta q'/p' = 0.2$, plotted against angle of stress path rotation. Arrows are used as well as points to indicate ranges of possible values of G′/p′. Figure 4.2.18 confirms the trend of decreasing stiffness with θ for a given stress level. Unfortunately, variations in the experimental method used to carry out the four tests and inaccuracies in the determination of these stiffness data, mean that comparing data from the different tests is not valid.

In summary, all the stiffness data obtained from these tests illustrate the difficulty of making the very small strain measurements which would enable the details of the stress-strain behaviour of the samples to be determined, even using internal strain gauges. Qualitatively, the stiffnesses and strain paths obtained by loading samples of heavily overconsolidated London clay are sensitive to recent stress history in the same way as for reconstituted samples.

4.2.4 Influence of State and Overconsolidation Ratio

This section examines how state and overconsolidation ratio affect the bulk and shear stiffness of an overconsolidated soil, both when the soil is loaded beyond the effect of recent stress history and when it is subject to that effect. In addition the section considers the factors which determine the magnitude of $\Delta\sigma'_R$, the point at which the curves of stiffness against stress change converge, which marks the limit of the influence of recent stress history, as defined in Figure

4.2.19. Stress-strain data from both constant p′ and constant q′ loading paths are analysed.

The Modified Cam-clay model (Roscoe and Burland, 1968) which provides a basic framework for all the analysis in this thesis, assumes that deformations within the state boundary surface are elastic. The version of this model defined in section 1.2.2 uses the natural compression law proposed by Butterfield (1979), which implies that both the bulk modulus, K′, and shear modulus, G′, are dependent only on p′. However, the data already presented in this chapter show that within the influence of recent stress history, G′ and K′ are heavily dependent on a combination of θ, the stress path rotation, and $\Delta\sigma'/\Delta\sigma'_R$, the stress level in the soil relative to $\Delta\sigma'_R$. To determine whether p′ is an additional parameter governing G′ and K′, and also, the importance of overconsolidation ratio, stiffness data from both constant p′ paths and constant q′ paths are normalised by p′ and plotted against p'/p'_m, the inverse of overconsolidation ratio.

Assuming that the stress change, $\Delta\sigma'_R$, which defines the range of the effect is not a constant, which has already been demonstrated by Richardson (1988), see section 4.3, it may depend on any of the following.

(a) The current mean effective pressure, p′.

(b) The overconsolidation ratio, R_o.

(c) A combination of p′ and R_o.

The test data for both constant p′ and constant q′ tests which illustrate the variation in $\Delta\sigma'_R$ are comparatively limited and $\Delta\sigma'_R$ is not always clearly defined. Therefore the data are normalised to investigate whether $\Delta\sigma'_R$ is solely determined by p′.

(i) Constant q′ tests

The stress probe tests DKSR1 and DKSR3 provided two types of constant q′ data. In Figure 4.2.20, the initial states of the constant q′ paths that were investigated during these tests are shown in lnv:lnp′

space. At A, B, C and D the bars indicate the changes in specific volume between the start of the first and second times that the soil was loaded in isotropic compression along the common paths. These changes are caused by irrecoverable volumetric strains during intermediate swelling and recompression stages.

During the tests the soil was also swelled back isotropically from normally consolidated states of 200, 300 and 400kPa, shown in Figure 4.2.20 as points W, X and Y. The loading path from Z starts at a slightly overconsolidated state as for this test p'_m is 720kPa. Figure 4.2.21 shows stiffness data from these isotropic swelling stages plotted as K' against p'. The initial parts of all these curves are affected by recent stress history, represented by a stress path rotation of 180°. In Figure 4.2.22 these data are plotted as normalised bulk stiffness, K'/p', against the inverse of overconsolidation ratio, or p'/p'_m. The figure shows that as the influence of recent stress history runs out the value of K'/p' becomes approximately constant and independent of overconsolidation ratio.

Stiffness data from the isotropic compression paths starting at A, B, C and D can now be added to Figure 4.2.22. These stiffness data are shown in Figures 4.2.23 and 4.2.24 plotted as K' against p'. There are two sets of data for each of these isotropic compression paths, one for $\theta = 0°$ and one for $\theta = 180°$. The data for the path starting at D when $\theta = 180°$ was obtained from a repeat test by O'Connor (1990). Both sets of stiffness data measured for the path starting at A correspond to a rest period of 48 hours, whereas the rest period for the other paths was 24 hours.

In order to isolate the effect of p' and R_0 on the stiffness data effected by recent stress history, values of K'/p' at two fixed stress levels $\Delta\sigma'/\Delta\sigma'_R = 0.5$ and 0.3 have been extracted from the stiffness data for $\theta = 180°$. Figure 4.2.25 combines these points and the data for $\theta = 0°$ with the swelling data first illustrated in Figure 4.2.22. When $\theta = 0°$ the whole loading path should have been outside the influence of recent stress history, but at the beginning of the compression stage the stress-strain response of the soil was affected by the rest period before loading commenced. Therefore, only the latter parts of the stiffness curves for these loading stages are free of any form of recent stress history, and only these parts of the curves were used in Figure 4.2.25.

Several further observations about the factors that influence the variation of the bulk stiffness of the soil can be made with reference to Figure 4.2.25. The addition of the data for $\theta = 0°$, well outside the influence of recent stress history, shows that the stress-strain response of the soil swelled back from a normally consolidated state was affected by recent stress history until approximately $p'/p'_m = 0.35$. The data for $\theta = 0°$ from the paths with initial states at A, B, C and D show that outside the influence of recent stress history K' is approximately proportional to p' and also that the value of K'/p' decreases very slightly with increasing p'/p'_m.

It is difficult to draw firm conclusions about the variation of bulk stiffness with p' and R_o within the influence of recent stress history from the small amount of stiffness data available for $\theta = 180°$, particularly as the data from the path beginning at A is not consistent with the other stiffness data for the reasons given earlier. Nevertheless, from the data shown in Figure 4.2.25 it appears that the bulk stiffness of the soil is dependent on overall stress history in a different way to the bulk stiffness of the soil when it is loaded beyond the influence of recent stress history.

All the data from paths identified by A, B, C and D demonstrate that within the state boundary surface the deformation of the soil during constant q' loading is not purely dependent on p', but also on R_o. The stiffness data are already normalised to account for changes in p', therefore along a constant q' path, changing stiffness with R_o must imply that p'_m is changing. This can only occur if the state of the soil is moving from one elastic wall to another during loading, ie the soil is deforming plastically.

In Figure 4.2.26 data from the loading paths starting at A, B and C are plotted as K'/p' versus $\Delta p'/p'$. Values for $\Delta\sigma'_R$ obtained by inspection from Figures 4.2.23 and 4.2.24 are marked on these curves and imply that p' is not the only parameter determining the range of the effect.

(ii) Constant p′ tests

There are three sets of constant p′ data taken from tests DKP1 and DKSR3. The initial states for the constant p′ loading paths for these data are shown in Figure 4.2.27, as points P, Q, and R. As in Figure 4.2.20 the bars indicate the change in specific volume of the sample during the test. Irrecoverable volumetric strains occurred during each series of probes but particularly in the case of path P where the soil was initially very lightly overconsolidated. The stress probes ended too close to the current yield surface and although the soil may initially have been at an overconsolidation ratio of 1.5 the final overconsolidation ratio of the soil was probably closer to 2.

The stiffness data, shown as curves of G′ against q′ in Figures 4.2.28 to 4.2.30, are normalised in a similar way to the constant q′ data. However, because of the significant change in specific volume during the tests the stress change during loading is normalised by p'_e not p'_m, where p'_e is defined in section 1.2.3. The normalising parameter p'_e should provide a more accurate measure of the current overconsolidation ratio of the soil. In addition there are two graphs, one showing values of G′/p′ for $\theta = 0°$, 90°, −90° and 180° at $\Delta\sigma'/\Delta\sigma'_R = 0.3$ plotted against p'/p'_e, Figure 4.2.31(a) and the second equivalent values of G′ (Figure 4.2.31(b)). For the path starting at R ranges of possible values of G′/p′ and G′ are given where appropriate. The stress levels corresponding to $\Delta\sigma'_R$ were again obtained by inspection and are shown in Figures 4.2.27 to 4.2.29.

Despite the limited data available, Figure 4.2.31(a) indicates that within the influence of recent stress history, $\theta = 180°$, −90° and 90°, G′ is not simply proportional to p′. Figure 4.2.31(b) indicates that there is also no clear pattern of variation with R_o. From Figures 4.2.31(a) and (b) the stiffness data for $\theta = 0°$, outside the influence of recent stress history, appear to correspond to similar data for bulk stiffness, K′.

The plots of G′/p′ against Δq′/p′ for $\theta = 0°$ and $\theta = 180°$ along paths P, Q and R, shown in Figure 4.2.32, demonstrate that p′ is a significant factor in determining the limit of the effect of recent stress history, but probably not the only factor.

(iii) Summary

The graphs of G'/p' versus p'/p'_e, Figure 4.2.30(a), and K'/p' versus p'/p'_m, Figure 4.2.25, demonstrate that outside the influence of recent stress history, K' and probably G' are proportional to p' and also to a lesser degree R_o, such that as R_o increases K' increases. Within the influence of recent stress history G' is not simply proportional to p'. The bulk stiffness data for states within the influence of recent stress history are inconclusive. For the range of stress paths and stress histories presented in this section $\Delta\sigma'_R$ is mainly, but not entirely, determined by p'.

4.2.5 Strain Increment Ratios, Undrained Effective Stress Paths

The shape of a strain path, plotted in $\epsilon_v:\epsilon_s$ space, resulting from a drained loading stage provides fundamental information on the nature of the strains that are occurring. The shape can be defined by the variation in the strain increment ratio during the loading stage. Similarly, the effective stress path followed by a soil during undrained loading also provides information on the nature of the deformations. This section begins by considering the implications of typical ϵ_v versus ϵ_s data from drained stress probes and then evaluates the stress paths observed in undrained tests. The characteristics of the strain and effective stress paths are examined in more detail by plotting the change in strain increment ratio and gradient of the effective stress path. Finally, the influence of R_o on the pattern of strain increment ratio versus change in stress curves is reviewed by comparing data for states "wet" and "dry" of critical.

(i) Drained tests

The strain paths and plots of $d\epsilon_v/d\epsilon_s$ versus q', shown in Figures 4.2.33 and 4.2.34, were measured along a drained constant p' stress path with increasing q', $p'_i = 300$kPa, $p'_m = 720$kPa, i.e. R in Figure 4.2.27. The data were taken from test DKSR3 on speswhite kaolin, see section 4.2.2. The deformations measured along this path can be compared with those expected from an isotropic elastic material, an anisotropic elastic material or an elasto-plastic material. During a constant p′ path, $d\epsilon_v/d\epsilon_s = 0$ for an isotropic elastic soil and if the soil is anisotropic elastic, $d\epsilon_v/d\epsilon_s = 3G'/J'$. If the degree of anisotropy of the soil is constant, then K′, G′ and J′ vary in the same way along a linear stress path and 3G′/J′ is constant, (Atkinson et al, 1990). If the soil is elasto-plastic, $d\epsilon_v/d\epsilon_s$ varies because the plastic component of the strain increment ratio is changed as different plastic potentials are crossed during the loading path.

The data in Figures 4.2.33 and 4.2.34 clearly show that within the influence of recent stress history the soil must be deforming elasto-plastically, as $d\epsilon_v/d\epsilon_s$ varies continuously with $\Delta q'$ for all θ. In Figure 4.2.35, the strains are assumed to be entirely plastic, and then plotted in q′:p′, $d\epsilon_s$:$d\epsilon_v$ space as vectors representing the strain increment at a given stress change. Vectors for the start of the loading stage are omitted due to scatter in the strain data. The pattern of these vectors is consistent with plastic potentials that are initially approximately normal to the direction of the approach path and are gradually re-orientated during loading along the new path, so that they become approximately normal to this new path, as the stress level approaches $\Delta\sigma'_R$.

(ii) Undrained tests

A number of tests incorporating an undrained compression stage were carried out on reconstituted samples of London clay and speswhite kaolin. The tests on London clay investigated the effective stress paths obtained during undrained compression after stress path rotations of $\theta = 90°$ and $\theta = -90°$. The tests on speswhite kaolin looked at the four standard rotations, 0°, 90°, −90° and 180°. All the samples were consolidated anisotropically to the same normally consolidated state, and swelled back to $p'_i = 200$kPa, $R_o \approx 3$.

For an undrained effective stress path $dp'/dq' = -K'/J'$ (equation 1.2.18) in comparison to $d\epsilon_v/d\epsilon_s = 3G'/J'$, for a constant p′ path, where K′, G′ and J′ are not necessarily elastic moduli. Within the state boundary surface, K′ and G′ will always be positive, and so the gradient of an undrained stress path, dp′/dq′, and the stress increment ratio, $d\epsilon_v/d\epsilon_s$, will always have opposite signs. Undrained effective stress paths from tests on speswhite kaolin are shown in Figure 4.2.36(a). These curves and plots of dp'/dq' versus q' (Figure 4.2.37(a)) can be compared with data from the drained constant p' path previously shown in Figures 4.2.33 and 4.2.34 and data from the loading path starting at Q (Figure 4.2.27) where $p_i' = 100$kPa, $p_m' = 400$kPa and which are shown in Figures 4.2.36(b) and 4.2.37(b). Figure 4.2.37, shows how the curves of dp'/dq' mirror the shape of the curves of $d\epsilon_v/d\epsilon_s$ against q'. As noted previously outside the influence of recent stress history the initially distinct curves of $d\epsilon_v/d\epsilon_s$ converge. Similar behaviour is observed for the dp'/dq' data. The loading paths for which data are plotted in this figure extend far enough for it to be clear that dp'/dq' does not reach a constant value after $\Delta\sigma_R'$.

The data for tests on London clay, shown in Figure 4.2.38 also demonstrates the influence of recent stress history. These data can be compared with plots of ϵ_v versus ϵ_s from tests by Richardson (1988), presented in section 4.3.

The continuously changing value of dp'/dq' and the different effective stress paths produced by following different recent stress histories, are further evidence of the elasto-plastic nature of the soil deformation.

(iii) "Wet" and "Dry" States

As noted in section 1.2, in terms of the Modified Cam-clay model, soils at states where $R_o > 2$ are "dry" of critical and states where $R_o < 2$ are "wet" of critical. For a drained constant p' path soils dry of critical will dilate as they reach the state boundary surface and yield towards critical state, $d\epsilon_v/d\epsilon_s < 0$, whilst soil sheared at constant p' from wet of critical will compress to reach critical state, $d\epsilon_v/d\epsilon_s > 0$. If the soil deformations within the state boundary surface are elasto-plastic then the strain increment ratio of the soil loaded beyond the influence of recent stress history should be affected by both q'/p' and R_o.

Most of the drained constant p' loading paths used as common paths during the tests were not continued long enough to provide data on strain paths outside the influence of recent stress history, except for data from the strain path for $\theta = 0°$. The stress increment ratios along the paths P, Q and R, for $\theta = 0°$, are plotted against q'/p' in Figure 4.2.39. At low values of q'/p', R_0 does not appear to influence the deformation as all the samples are compressing. R_0 becomes more significant as q'/p' increases. The curve for $R_0 = 1.5$ tends towards a positive strain increment ratio, unlike the strain increment ratio data for $R_0 = 4$ and 2.4, which as predicted above are tending towards zero or negative values.

(iv) Summary

Both the patterns of the the strain paths obtained from drained constant p' stress paths, and the different effective stress paths resulting from undrained loading, provide evidence that the deformation of the overconsolidated soil is elasto-plastic.

4.3 Evaluation of Data from Richardson (1988)

4.3.1 Data As Presented

Data presented by Richardson (1988) were obtained from stress path triaxial tests on reconstituted samples of five different soils. This review concentrates on the results of stress path tests designed to investigate the effect of recent stress history, using a method similar to that described in Chapter 3. The tests were all carried out using Spectra controlled stress path cells and the results should be evaluated with reference to the accuracies quoted in Table 3.2.1. In Richardson (1988) these tests are known as threshold effect tests, because the effect of recent stress history was then described as a stress path threshold effect. Data on the range of the effect were also obtained from the compression and swelling stages that were required to bring the reconstituted samples to an overconsolidated state. The main series of tests was carried out on all five types of soil; London Clay, slate dust, Ware till, speswhite kaolin and Cowden till. Only London Clay was used for the additional tests which investigated further aspects of the effect. Table 4.3.1 provides a summary of all the tests used to establish the effect of recent stress history. As described in the introduction to this chapter, where a typical set of data were presented, all the stiffness data were normalised with respect to the current specific volume and mean effective pressure. Normalised stiffness data were then plotted against the change in stress state normalised by current effective pressure. The range of stiffness, R, at any stress level is defined as

$$R = \frac{dq'/vp'd\epsilon_s \ (\theta = 180^\circ)}{dq'/vp'd\epsilon_s \ (\theta = 0^\circ)} \qquad (4.3.1)$$

(i) Compression and Swelling stages

Swelling and recompression curves plotted in v:lnp' space were characterised by two straight lines of slopes κ_1 and κ_0, see Figure 4.3.1, which also shows how the range of the effect was obtained from these plots. The difference in slope between κ_1 and κ_0 indicated that the stiffness of the soil changed by 5 to 10 times between the beginning and end of the constant q' path, depending on soil type. The estimates of the range of the effect obtained from these curves are only approximate because the idealisation of the curve using two straight lines is rather subjective.

(ii) Main test series

All the tests in the main test series investigated the stress-strain response of the soil on the same constant p' loading path, starting from p'= 200kPa, q' = 0, R_0 = 2, and with q' increasing. All five soils showed the same characteristics as the typical data shown in 4.1. Figure 4.3.2, a plot of dq'/vpdϵ_s versus θ for two different stress ratios, 0.05 and 0.4, illustrates the steady variation of stiffness with θ within the influence of recent stress history, at $\Delta q'/p' = 0.05$. At $\Delta q'/p' = 0.4$, the soil is outside the influence of recent stress history. Richardson (1988) noted that for a given value of θ the soil stiffness is lower for negative stress path rotations than positive rotations. Figure 4.3.2, which uses results from many tests on London clay, also illustrates the repeatability of the data. The characteristics of these results are common to all the soils tested, but plotting the range of stiffness, R, against plasticity index, Figure 4.3.3, Richardson (1988) found that recent stress history has a more significant effect as the plasticity of the soil increases.

As shown in section 4.1, the strain increment ratios obtained from these tests were non-unique. Richardson (1988) concluded that the behaviour was inelastic using the same arguments that were outlined in section 4.2.5. In order to establish the pattern of the data, the strain increment ratios at $\Delta q'/p' = 0.05$ were plotted against θ, Figure 4.3.4.

(iii) Different stress paths

The most complete set of data for different stress paths was obtained from tests on London Clay, using three paths all beginning at $p' = 200$kPa, $q' = 0$ and $R_0 = 2$. The paths were constant p', q' decreasing and constant q', p' increasing and decreasing. The same pattern of stress-strain behaviour was obtained from these tests; in particular the strain increment ratio data for the constant q' tests were also non-uniform. Figures 4.3.5 and 4.3.6 show plots of q' or p' versus ϵ_s or ϵ_v and ϵ_v versus ϵ_s for these tests plus a set of data for the standard constant p', q' increasing path. The graphs, taken from Atkinson et al (1990) clearly show the similarity in the results for the different paths.

(iv) Initial compression history

In these tests the London clay was compressed anisotropically, at q'/p' of 0.25 and 0.75, one-dimensionally ($q'/p' \approx 0.57$) and two-dimensionally ($q'/p' \approx -0.4$), to $p' = 400$kPa and then swelled back to $p' = 200$kPa. For these tests R_0, as defined in section 1.2.3, is different for each compression history, but the overconsolidation ratio as defined in Richardson (1988) is constant and equal to 2. The different overall stress histories also mean that the initial state of the constant p' path is not always isotropic.

Data from these tests fell into the same general pattern as data from isotropically compressed soil. In particular the extent of the influence of the effect was unaffected by the initial compression history and the general trend of the stress increment ratio graphs was the same for all the initial compression histories. Richardson (1988) noted that if the anisotropy of the soil was stress induced, the values of stress increment ratio would tend to increase for soil compressed to greater vertical effective stresses, which did not occur. Figure 4.3.7 shows the influence of initial compression history on stiffness and range of stiffness. Unfortunately it is not clear from these tests whether the stress-strain response of the soil is being affected by the anisotropic initial compression history or the anisotropy of the initial stress state for the constant p' path.

(v) Overconsolidation ratio

Richardson (1988) investigated the effect of overconsolidation ratio for both isotropically and one-dimensionally compressed samples, by compressing the soil to $p' = 400$kPa and then swelling back to different states. The soil was tested at nominal overconsolidation ratios of 8, 4, 2 and 1.5. The constant p' paths for these tests start at states which lie on the one-dimensional swelling line.

Again the usual pattern of data was obtained from both isotropically and one-dimensionally compressed samples at all overconsolidated states. The isotropically compressed data converged at a stress level of approximately $\Delta q'/p' = 0.35$, but the range of the effect is investigated in more detail in section 4.3.2. The anisotropically compressed samples converged at a stress level, $\Delta q'/p'$ which increased with overconsolidation ratio.

Figures 4.3.8 and 4.3.9 show plots of stiffness against overconsolidation ratio for both isotropic and one-dimensionally compressed samples. For the isotropically compressed samples the soil stiffness is generally highest at an overconsolidation ratio of eight. A wider range of strain increment ratios was observed at low stress levels as the overconsolidation ratio increased. The one-dimensionally compressed samples show approximately the same variation in stiffness and range of stiffness with overconsolidation ratio as the isotropically compressed samples. The data are re-plotted in section 4.3.2 to establish whether the slight differences that exist are caused by the definition of overconsolidation ratio. Richardson noted that for the one-dimensionally compressed samples, there was a trend of increasing positive values of $d\epsilon_v/d\epsilon_s$ as the overconsolidation ratio of the soil increased. This trend may be the result of the decreasing value of q'/p' at the start of the constant p' paths, as the soil is swelled back down the one-dimensional swelling line.

(vi) Approach path length - Range of effect

The results of the swelling and recompression stages indicated that the range of the effect was 18% to 35% of the current mean effective stress, depending on soil type, but regardless of the state of the sample. This compared with 30% to 35% from constant p' paths. To establish the range of the effect more carefully, a constant p' path test was carried out with θ constant at 90°, but with varying lengths of approach path. A stiffer response was observed for an approach path length of 45kPa. When the approach path length was as low as 22kPa the soil stiffness was equivalent to a complete reversal. The length of an approach path required to eliminate the influence of a previous change in stress path direction is equal to the range of the effect of recent stress history at that stress. Therefore, from this test the range of influence of recent stress history was 22.5% of p' = 200kPa.

(vii) Rest period

To investigate the effect of rest period on the stiffness of the soil, Richardson (1988), observed response of a sample along a constant p' path after a rest periods of 3 hours, 48 hours and 11 days for $\theta = 90°$ and 3 hours and 11 days for $\theta = 0°$ and 180°. Table 4.3.2 shows that the change in stiffness with rest period was approximately linear with the logarithm of time. Measurements of the volumetric strains that occurred during the rest period showed that they accumulated at a rate proportional to the logarithm of time elapsed, and therefore can be modelled by a typical creep rate equation. The stiffness data also show that the effects of time, or rest period, and recent stress history are additive.

(viii) Change in direction of total stress path

Two sets of tests were carried out. Firstly, tests with different total stress approach paths for which the pore-pressure was varied so that the effective stress path change was the same. The response of the soil was unchanged by changes in total stress approach path. The second set of tests had the same total stress approach path but different effective stress paths. The results of these tests showed the expected variation in response with θ. The conclusion from these tests was that the stress-strain response of overconsolidated soils is only influenced by recent effective stress history.

4.3.2 Re-interpretation of Data

Data from tests carried out by Richardson (1988) have been reinterpreted in two ways. The results of three tests on London clay isotropically compressed to $p' = 400$kPa and swelled to overconsolidation ratios of 1.5, 2 and 4, were completely re-analysed. Corrected stress-strain and strain path data were available for these tests and they have been re-processed using the methods described in section 4.2.2, to give graphs of G' versus q'. These were then normalised in the same way as the data presented in 4.2.4, to establish the dependence of both stiffness and $\Delta\sigma'_R$ on R_o and p'.

Strain data corrected for compliance of the load cell were not available for all the tests. Therefore, the comparison between one-dimensionally and isotropically compressed data was clarified by re-plotting the existing normalised stiffness data against p'/p'_m.

(i) Effect of p' and R_o

The data in Figures 4.3.10 to 4.3.12 are the G' versus Δq' plots for tests on reconstituted London clay, isotropically compressed and swelled to $R_o = 1.5$, 2 and 4 respectively. In the tests carried out by Richardson (1988) there was no rest period at the start of the common path, when $\theta = 0°$, thus the change in G' along this path must be caused by the changing stress ratio, q'/p'. A rest period does occur in the tests carried out as part of the present research project and reviewed in section 4.2, so this variation was not clear. Figure 4.3.13 shows values of G′ taken at $\Delta\sigma'/\Delta\sigma'_R = 0.3$ plotted against p'/p'_m for each value of θ, specific volume data were not available. The value of $\Delta\sigma'_R$ was a little difficult to estimate because the loading paths were too short. The estimated values are marked on Figures 4.3.10 to 4.3.12. The variation of G′ with p'/p'_m shown in Figure 4.3.13 follows the same pattern as the data from tests on speswhite kaolin shown in Figure 4.2.31 (b).

To investigate the influence of R_0 and p′ on the range of the effect, curves of G'/p' versus $\Delta q'/p'$ for $\theta = 0°$ and $\theta = 180°$, are compared in Figure 4.3.14. This figure confirms that p′ is the main influence on $\Delta\sigma'_R$.

(ii) Comparison of isotropically and one-dimensionally compressed samples

Values of $dq/vp'd\epsilon_s$ at $\Delta q'/p' = 0.05$ are plotted against p'/p'_m in Figure 4.3.15 for the eight tests carried out at nominal overconsolidation ratios of 1.5, 2, 4 and 8. The important difference in the one-dimensionally compressed samples is that the constant p′ paths begin at anisotropic stress states. Very few of the tests reviewed in this chapter use common paths which have an anisotropic initial stress state. Figure 4.3.15 shows that the stiffness of the one-dimensionally compressed samples is lower than the stiffness of the isotropically compressed samples by an amount which increases with θ.

4.4 Evaluation of Data from 'True Triaxial' Test

4.4.1 Introduction

To investigate the effect of recent stress history in three-dimensional stress space, a stress probe test was undertaken by Lewin (1990) using a hydraulic stress path cube apparatus. The apparatus allows all three principal stress or strain directions to be controlled and monitored. For the purposes of this review, the three principal stresses will be described as σ'_z, σ'_y and σ'_x where σ'_z is the vertical effective stress and σ_y' and σ_x' are the two horizontal effective stresses. The corresponding strains are ϵ_z, ϵ_y and ϵ_x.

4.4.2 Description of test

As far as possible the test procedure was the same as that used for the other tests carried out as part of this project. The soil sample consisted of a cube of reconstituted speswhite kaolin, which had been consolidated one-dimensionally from a slurry, following the method described in section 3.4.2. The floating ring consolidation press was similar to presses used for the conventional 38mm diameter triaxial samples, but it had a square cross-section of internal dimensions 60mm. The initial dimensions of the sample placed in the apparatus were 58.8mm (vertical) x 60mm x 60mm. The moisture content was approximately 51%.

The sample was compressed isotropically to $p' = 400$kPa and then swelled back to $p' = 200$kPa, $R_o = 2$. This was the stress state at the beginning of the constant p' loading path, with q' increasing, which was the common path for the subsequent series of probes. All the probes, common path and approach paths, were 100kPa in length, and the loading rate along these paths was 5kPa/hr. The rest period between the end of the approach paths and the start of the common path was 24 hours.

The test investigated the variation in stress-strain response along the common constant p' loading path, for three different recent stress histories represented by the three different approach paths described in Figure 4.4.1(a). Two of these approach paths lie in the triaxial plane, BO and CO, whereas DO which when projected on the triaxial plane appears to approach from the same direction as BO, actually lies outside the triaxial plane, the common path is shown as OA. The angles of rotation associated with these paths, defined in three-dimensional stress space, are 0° for BO and 45° for CO and DO. As shown in Figure 4.4.1(b) points C and D lie on a 90° cone with its apex at O and principal axis following a line of constant p'.

Stresses are applied to the sides of the cube sample using air pressure acting on membranes, which tend to bow under the strain.

Because the strains are recorded at the centre of each face, the sum of the three principal strains, which should have equalled the volume strain that occurred during the test was generally greater than the strain measured by the volume gauges. Sample dimensions calculated from the transducer measurements are in error by a maximum of 2%. Additional errors occur because the transducer measures the maximum strain for a stress applied over the whole surface for which the average strain may only be half the measured value. This causes an error of about 8% of the transducer strain reading. Apart from these additional sources of error, the accuracy of the strain measurements is approximately equivalent to the measurements made externally using the BBC control system and given in Table 3.2.1.

4.4.3 Results

Stress-strain curves are plotted as deviatoric stress, q', against shear strain, ϵ_s, where

$$q' = 1/\sqrt{2}[(\sigma_x' - \sigma_y')^2 + (\sigma_y' - \sigma_z')^2 + (\sigma_z' - \sigma_x')^2]^{1/2} \qquad (4.4.1)$$

and

$$\epsilon_s = \sqrt{2}/3[(\epsilon_x - \epsilon_y)^2 + (\epsilon_y - \epsilon_z)^2 + (\epsilon_z - \epsilon_x)^2]^{1/2} \qquad (4.4.2)$$

Stress-strain curves for each of the three different recent stress histories are plotted in Figure 4.4.2. Shear stiffness, G', defined as $dq'/3d\epsilon_s$ and calculated from stress-strain data using the method of analysis described in section 4.2.2 is plotted against deviator stress to give the curves shown in Figure 4.4.3.

All three recent stress histories produce a different stress-strain response from the soil. As would be expected, there is no similarity in the behaviour of the soil after paths BO and DO, which appear to be the same path in triaxial stress space. However, the soil is subject to the same change in stress path direction after paths DO and CO, so the difference in the stiffness curves for these paths indicates that recent stress history cannot be defined solely by θ, the angle of rotation of the stress path. The overall position of the approach path in stress space is also important. As observed in the tests carried out using conventional triaxial equipment, the stiffness curves converge as the effect of recent stress history gradually runs out.

4.5 Summary of Experimental Data

This review of experimental data describing the influence of recent stress history on the deformation of overconsolidated soils, shows that the basic characteristics of the effect are reasonably well defined by a large number of test results. Data clearly illustrating more detailed features of the effect or the way in which the basic features are modified by changes in stress state or overall history are more scarce.

The effect of recent stress history on the stress-strain response of a soil, which was loaded along a new stress path, was observed in all tests. As the soil was loaded further along the new path the influence of recent stress history decreased. The stress-strain behaviour of the soil was highly non-linear and all strains measurable by the triaxial equipment used for this research are inelastic. The evidence that the deformations are inelastic is as follows.

(a) The stress-strain response of the soil varies with θ, the recent stress history of the soil. This means that strains are not recoverable except for the special case of a loading cycle which includes two 180° rotations. Figure 4.5.1 shows the stress-strain response of a soil along three consecutive constant p' loading paths. The soil is loaded at constant p', following a stress path rotation of 90°, then unloaded and reloaded at constant p'. Strains are recovered on the last loop, which is the special case, but not for the initial loading and unloading cycle. As strains are not recoverable the deformations cannot be elastic.

(b) Further evidence of the inelastic nature of the deformations is provided by the strain paths and effective stress paths followed during drained and undrained loading respectively. Data are not consistent with the behaviour predicted by standard isotropic or transversely anisotropic elastic soil models, as demonstrated in section 4.2.5.

(c) Additionally, the pattern of the strain vectors plotted in section 4.2.5 indicate that the elasto-plastic deformations are controlled by a kinematic plastic potential.

The soil's memory of recent stress history, described by θ, the stress path rotation, affects both stiffness and the shape of the strain paths or effective stress paths that are obtained from drained or undrained loading. The effect has been observed on a variety of stress paths at a variety of stress states.

At a given state the initial stiffness of the soil is determined by θ, which lies in the range 0° to 180°. The initial stiffness of the soil is a maximum when $\theta = 180°$, decreasing to its minimum value for $\theta = 0°$. Data from Richardson (1988) covering a wide range of values for θ show that for stress paths in triaxial stress space the initial stiffness is approximately proportional to θ. The results of the "true triaxial" test indicate that outside the triaxial plane a different definition of recent stress history may be required.

The stiffness of the soil decreases smoothly with stress change as the influence of recent stress history decreases. The stress change required to move outside the influence of recent stress history is defined as $\Delta\sigma'_R$. Hence the stiffness of the soil after a certain stress change $\Delta\sigma'$ along the loading path is also dependent on $\Delta\sigma'/\Delta\sigma'_R$. Unfortunately $\Delta\sigma'_R$ is not always well defined and so the way in which it varies with state and overall history is uncertain. From data presented in section 4.2.4, $\Delta\sigma'_R$ is not solely dependent on p', the assumption made by Richardson (1988), but also on R_o. Swelling and recompression tests carried out by Richardson (1988) also show that $\Delta\sigma'_R$ varies with soil type. For speswhite kaolin and the tests carried out as part of the present research project $\Delta\sigma'_R$, for constant p' loading, lies in the range 39% to 41% of the current value of p' depending on R_o, but for constant q' loading the range is 19% to 27%.

Data from tests on speswhite kaolin and the re-interpreted data obtained from tests on London Clay, reviewed in sections 4.2.4 and

4.3, show that within the influence of recent stress history G' is not simply proportional to p' and not influenced by R_0 in any well defined manner. The variation of K' with p' and R_0 cannot be determined from the available data. Outside the influence of recent stress history K' and probably G' are proportional to p' and also decrease slightly as R_0 decreases.

The tests by Richardson (1988) provided no clear evidence that the initial compression history (i.e isotropic or anisotropic) of the soil significantly affects the subsequent stress-strain behaviour. The differences in the data from one-dimensionally and isotropically compressed samples, which were re-plotted in section 4.4.2, are probably caused by the initial anisotropic stress state of the constant p' paths, when the soil was one-dimensionally compressed. The undisturbed soil samples, from which reliable data were obtained, have a different compression history characterised by an extremely high preconsolidation pressure caused by the geological history of the soil. This may explain any differences between the effect of recent stress history observed in these undisturbed samples and the effects measured in reconstituted samples. Qualitatively the behaviour was comparable.

There is limited evidence from data presented in section 4.3.1 that the pattern of strain increment ratio against stress change curves observed for drained loading are altered by R_0. There is no evidence for stress induced anisotropy in anisotropically compressed samples. Strain increment ratios for loading paths following $\theta = 0°$, i.e. data from outside the influence of recent stress history, were plotted against q'/p' in section 4.2.5. These curves demonstrate that strain increment ratios are increasingly affected by R_0 as q'/p' increases and the loading paths approach the state boundary surface.

The detailed features of the effect described above were mainly identified from tests on London clay and speswhite kaolin. Richardson (1988) established that the basic behaviour could be observed during constant p' loading at $p_i' = 200$ kPa, $p_m' = 400$kPa for a wide variety of soils. The plasticity index of the soils is linked to the difference between the initial stiffness at $\theta = 180°$ and $\theta = 0°$, a measure of the sensitivity of the soil to the effect. The testing programme carried out as part of this research was based on the assumption that the detailed characteristics of the behaviour observed by testing a single type of soil, at a wider range of stress states and overall histories, are also present qualitatively in other soils.

It should be noted that the stiffness of the soil is also heavily dependent on rest period. A limited investigation of the mechanism of the effect was carried out by Richardson (1988), who concluded that during the rest period there was creep of the volumetric strain, so that stiffness increased with the logarithm of time. He found that the effects of rest period and stress path rotation were additive.

4.6 Implications for Numerical Modelling

4.6.1 Major characteristics to be modelled

The following list describes the aspects of the soil stress-strain response which best characterise the influence of recent stress history and which should be included in models for overconsolidated soil.

(a) A region of truly elastic deformation, explored in dynamic tests, see section 2.3, although, all the strains measured in the tests presented in this chapter are inelastic.

(b) Non-linear and inelastic deformations outside this elastic region.

(c) A memory of recent stress history, which determines the initial stiffness of the soil such that for $\theta = 180°$, the stiffness is at a maximum and a minimum for $\theta = 0°$.

(d) A gradual loss of memory with loading such that the initial stiffness decreases until a stress level $\Delta\sigma'_R$. Data obtained by Richardson (1988) indicated that at this stress level the stiffness for $\theta = 0°$ is approximately the same as the stiffness for $\theta = 180°$.

(e) A pattern of strain paths obtained from a drained loading path which is determined by θ and consistent with those shown in sections 4.2 and 4.3, implying plastic deformations governed by some form of plastic potential.

(f) Limited data indicate that the mean effective pressure p' may be an important factor in the determination of $\Delta\sigma'_R$.

(g) Within the influence of recent stress history, in addition to θ and $\Delta\sigma'/\Delta\sigma'_R$, G' should be affected by R_o and not solely dependent on p'. Outside the range of the effect K' should be heavily dependent on p' and slightly influenced by R_o.

The final two characteristics are not particularly well defined by the present experimental data and, in any case, are less important requirements for the proposed soil model.

4.6.2 Appropriate Models

With reference to section 2.3 the only existing soil models which could be used to predict the behaviour outlined above are those which include at least one kinematic yield surface within the state boundary surface. The stress-strain behaviour predicted by this type of model will be inelastic and non-linear. The models also incorporate a means of remembering previous stress paths through the kinematic yield surface.

Only models defined in triaxial stress space will be considered, because there are very little data on the influence of recent stress history in three-dimensional stress space.

CHAPTER 5 NUMERICAL MODELLING

5.1 Introduction

The previous chapter concluded by listing the major characteristics of the stress-strain behaviour of overconsolidated soils. The only existing soil models that can predict these characteristics are those which include plastic strains throughout most of the loading and which incorporate at least one kinematic yield surface. This chapter begins by looking in more detail at the models that fulfill this requirement. An appropriate model would have the potential to predict the behaviour discussed in Chapter 4. It should be defined by only a few parameters which, if possible, would have some physical meaning. In section 5.3 an existing model selected using these criteria is described and evaluated. In this way the shortcomings and advantages of the model are determined and the modifications which are necessary to derive an improved model are established. The new model is described in detail in section 5.4. In section 5.5 the success of this improved model in predicting the correct soil stress-strain response is assessed by examining how the model predicts the major characteristics of the experimental data described in section 4.6.

5.2 Evaluation of Existing Models

Models incorporating a kinematic yield surface are capable of predicting the effect of recent stress history because of the way the kinematic yield surface moves in stress or strain space as it follows the changing state of the soil. The position of the kinematic yield surface relative to the current state of the soil is different after different loading paths, see Figure 5.2.1. Thus the model predicts different stress-strain responses when the soil is subsequently loaded along the same loading path.

Various soil models incorporating one or more kinematic yield surfaces were described in section 2.3. Model LC, devised by Simpson et al. (1979), is the only model where the kinematic yield surface is not acting as a plastic potential defining the onset of yielding. In this model the "intermediate" strains that occur when the soil state reaches the kinematic yield surface are described by a set of anisotropic elastic parameters, although deformations are not necessarily recoverable. The kinematic yield surface is defined in strain space as a sphere of radius 0.02% strain. When the soil is unloaded, the strain path moves inside the kinematic surface and the stiffness of the soil is ten times the stiffness of the intermediate strains (see Figure 2.4.2). The size of the kinematic yield surface and the magnitude of the stiffness moduli within this region were chosen to fit field data and were also consistent with results of tests by Som (1968). When the surface is reached once more the stiffness reduces again.

An advantage of the model is that the principle is relatively simple but unfortunately the predictions do not fulfill some of the basic characteristics of the observed soil behaviour. Firstly, there is no difference in the stress-strain response predicted by the model for strain path rotations of ±90° to 0° and, as the anisotropic elastic parameters are constants, the stress-strain response is linear. For strain path rotations in the range ±90° to 180° the stiffness varies as a step function. In addition, the model will not predict the type of strain paths which were observed in the stress probe tests because the deformations are not modelled as associated plastic flow. Hence, although the model does predict a non-linear, or bi-linear, stress-strain response and the effect of recent stress history for some paths, the major details of the behaviour identified in Chapter 4 are not reproduced, in particular the plastic nature of the deformations.

All the other models use one or more kinematic yield surfaces which are defined in stress space and for which plastic flow is associated. As stated in the introduction to this chapter, it is important that the model used to predict the effect of recent stress history should be relatively simple and so only two-surface models will be considered at this stage. Later modifications to improve the model will be evaluated against the increased accuracy in predictions that they offer. Two-surface kinematic yielding models for soil have been formulated by Mröz et al (1979) and Mröz and Norris (1982), Hashiguchi (1985) and, most recently, Al Tabbaa (1987) and Al Tabbaa and Wood (1989).

All the models are very similar and are based on roughly equivalent theories which were originally used to model metal plasticity. The model described by Hashiguchi (1985) is formulated generally to fit any set of yield surfaces but those models presented by Mröz et al (1979) and Al Tabbaa (1987) are based within the framework of Critical State soil mechanics and use the Modified Cam-clay state boundary surface to define the outer surface. The kinematic yield surface used in these models is similar in shape to this surface. When the stress state lies on the kinematic yield surface the soil deforms elasto-plastically. The plastic deformations are governed by the location of the current stress state on the yield surface, i.e. plastic flow is associated, and also on the position of the surface relative to the state boundary surface. Thus the models should be capable of predicting the non-linearity of the response and the shape of the strain paths, as well as the effect of recent stress history.

The model derived by Al Tabbaa (1987) is an adaptation of the model formulated by Hashiguchi (1985) and was originally used to model the results of cyclic stress path tests on speswhite kaolin. The two-surface "bubble" model derived by Al Tabbaa (1987) incorporates most of the more important aspects of all the other two-surface models but in a considerably more approachable format. In the following section the model is described and evaluated against data from Chapter 4 in order to establish whether two-surface kinematic yield models are, in general, capable of predicting the observed soil behaviour.

5.3 Two-surface "Bubble" Model - Al Tabbaa (1987) and Al Tabbaa and Wood (1989)

5.3.1 Description of Model

A detailed description of the derivation of this model is given in Al Tabbaa (1987). The methods used to derive this model are largely the same as those subsequently used to formulate the three-surface model described in section 5.4. In this section only the principal features of the model will be described together with the equations which define the model.

(i) Basic Framework

The model is based within the framework of Critical State soil mechanics and reduces to the Modified Cam-clay soil model for monotonic loading when yielding continuously. The Modified Cam-clay model was further modified by incorporating the natural compression law proposed by Butterfield (1979), as defined in section 1.2.2. The yield locus formed by the intersection of the Modified Cam clay state boundary surface and an elastic wall is given by:

$$(p' - p'_o)^2 + q'^2/M^2 = p'^2_o \tag{5.3.1}$$

where $2p'_o$ is the mean effective pressure at the intersection of the current swelling line with the normal compression line. In the two-surface model this was no longer a yield surface and was described as the "bounding" surface by Al Tabbaa (1987). The inner kinematic yield surface enclosing the truly elastic region was of similar shape, with a size ratio denoted by R and centre coordinates (p'_α, q'_α), see Figure 5.3.1. The equation of this yield surface was:

$$(p' - p'_\alpha)^2 + \frac{(q' - q'_\alpha)^2}{M^2} = R^2 p'^2_o \tag{5.3.2}$$

For states inside the yield surface the strains were assumed to be elastic and isotropic such that:

$$\begin{bmatrix} \delta\epsilon^e_v \\ \delta\epsilon^e_s \end{bmatrix} = \begin{bmatrix} \kappa/p' & 0 \\ 0 & \gamma/p' \end{bmatrix} \begin{bmatrix} \delta p' \\ \delta q' \end{bmatrix} \tag{5.3.3}$$

where $\gamma = 2\kappa(1 + \nu)/9(1 - 2\nu)$.

R was a constant so that when the bounding surface expanded the kinematic yield surface also expanded. This surface "dragged" by the current stress state translated according to a translation rule, described later, which ensured that the surfaces met at a common tangent and never intersected. Plastic flow on the kinematic yield surface was associated and so the relative magnitudes of shear and volumetric strain were governed by the normality rule. The absolute magnitude of these plastic strains was controlled by a hardening rule, also given later.

(ii) Translation of the Kinematic Yield Surface

The translation rule was devised to make certain that the surfaces would not intersect and, furthermore, that at any point of contact the outward normal was the same for both surfaces. Thus when the surfaces were in contact the plastic strains calculated using the kinematic yield surface would equal the strains calculated from the Modified Cam-clay state boundary surface. This condition was achieved by associating each point, C, on the kinematic yield surface with a conjugate point, D, on the bounding surface which had the same outward normal, see Figure 5.3.2 and ensuring that the translation of the kinematic yield surface was always along β, the vector joining C and D. The translation rule was divided into two components:

(a) The contraction and expansion of the kinematic yield surface due to changes in p_o' as plastic volumetric strains occur. This was calculated for $\beta = 0$.

(b) The change in position of the kinematic yield surface as it is "dragged" by the current stress state,and translates along β.

The resulting translation rule controlled the movement of p_α' and q_α' as follows:

$$\begin{bmatrix} \delta p_\alpha' \\ \\ \delta q_\alpha' \end{bmatrix} = \frac{\delta p_o'}{p_o'} \begin{bmatrix} p_\alpha' \\ \\ q_\alpha' \end{bmatrix} + S \begin{bmatrix} \dfrac{p' - p_\alpha'}{R} - (p' - p_o') \\ \dfrac{q' - q_\alpha'}{R} - q' \end{bmatrix} \tag{5.3.4}$$

where the final term in [] is the vector β. The second half of the equation covered the translation along β and S was calculated using the consistency equation for the kinematic yield surface as:

$$S = \frac{(p' - p'_\alpha)\left[\delta p' - \frac{\delta p'_o}{p'_o}p'\right] + \frac{(q' - q'_\alpha)}{M^2}\left[\delta q' - \frac{\delta p'_o}{p'_o}q'\right]}{(p' - p'_\alpha)\left[\frac{p' - p'_\alpha}{R} - (p' - p'_o)\right] + \frac{(q' - q'_\alpha)}{M^2}\left[\frac{q' - q'_\alpha}{R} - q'\right]} \qquad (5.3.5)$$

The first part of this translation rule, given in equation 5.3.4, was oversimplified as it assumed that when the surfaces were in contact, loading was always in the direction of the outward normal at the point of contact. The new translation rule used in the three-surface model described in section 5.4 is more general.

(iii) Hardening Rule

The hardening rule was initially formulated for the special case where the bounding surface and kinematic yield surface were in contact and then modified to accommodate a more general case. As noted previously the vector of plastic strain increment was assumed to be normal to both the yield surfaces, and the Modified Cam-clay hardening rule applied so that,

$$\delta p'_o = \frac{p'_o}{(\lambda - \kappa)} \quad \delta\epsilon^p_v \qquad (5.3.6)$$

This linked the change in size of both surfaces with the component of plastic volumetric strain. The definitions of λ and κ are given in section 1.2.2. When the surfaces were in contact the equation defining the increments of plastic volumetric and shear strain on the kinematic yield surface was:

$$\begin{bmatrix} \delta\epsilon^p_v \\ \\ \delta\epsilon^p_s \end{bmatrix} = \frac{1}{h_o}\begin{bmatrix} (p' - p'_\alpha)^2 & (p' - p'_\alpha)\frac{(q' - q'_\alpha)}{M^2} \\ (p' - p'_\alpha)\frac{(q' - q'_\alpha)}{M^2} & \left[\frac{(q' - q'_\alpha)}{M^2}\right]^2 \end{bmatrix}\begin{bmatrix} \delta p' \\ \\ \delta q' \end{bmatrix} \qquad (5.3.7)$$

where $h_o = \frac{(p' - p'_\alpha)}{(\lambda - \kappa)}\left\{ p'(p' - p'_\alpha) + q'\frac{(q' - q'_\alpha)}{M^2} \right\}$

Al Tabbaa (1987) assumed a more general expression for the hardening modulus, $h = h_0 + H$, and observed that for $H = 0$ there were four singularity points on the kinematic yield surface which defined two regions of instability, as shown in Figure 5.3.3. The exact positions of points g_3 and g_4 in the diagram depends on the position of the kinematic yield surface in stress space. Figure 5.3.3 shows one example. There were a number of constraints on the values that h_0 and H could take. Where instability had not been observed for $H = 0$, i.e. $\eta < M$, the function $h_0 + H$ should be greater than zero. When the two surfaces were in contact each should predict the same plastic strains so H should reduce to zero. Finally $H \geq 0$ so that the plastic strain increments on the kinematic yield surface were always less than or equal to those on the bounding surface. Hence H was defined as a function of b, which is a measure of how close the yield surface is to the bounding surface. The parameter b was the scalar product of the vector $\underline{\beta}$ and the normal to the yield surface at the current stress state, $\underline{n}$, see Figure 5.3.4, divided by a measure of the size of the yield locus. The vector $\underline{n}$ was defined as

$$\underline{n} = \begin{bmatrix} (p' - p'_\alpha) \\ \dfrac{(q' - q'_\alpha)}{M^2} \end{bmatrix} \tag{5.3.8}$$

Hence the magnitude of b was

$$b = \frac{1}{Rp'_0}\left[(p' - p'_\alpha)\left[\frac{(p' - p'_\alpha)}{R} - (p' - p'_0)\right] + \frac{(q' - q'_\alpha)}{M^2}\left[\frac{q' - q'_\alpha}{R} - q'\right]\right] . \tag{5.3.9}$$

For $M<1$ the maximum value of b, $b_{max} = 2p'_0(1 - R)$, occurs for the configuration of surfaces shown in Figure 5.3.4(b). The component of the hardening modulus H was defined by a function of b as

$$H = \left(\frac{b}{b_{max}}\right)^{\psi} \frac{1}{\lambda - \kappa} \; p_0'^{\,3} \tag{5.3.10}$$

This choice of function for H was not unique and introduced an extra parameter ψ. The resulting hardening modulus was:

$$h = \frac{1}{(\lambda - \kappa)} \left[(p' - p'_\alpha) \left\{ p'(p' - p'_\alpha) + q' \frac{(q' - q'_\alpha)}{M^2} \right\} + \left\{ \frac{b}{b_{max}} \right\}^{\psi} p_o'^{3} \right] \tag{5.3.11}$$

5.3.2 Calculation of Model Parameters

The seven parameters required to define the model are as follows:

M - critical state friction coefficient

λ - gradient of the isotropic normal compression line in lnv : lnp' space

κ - gradient of the isotropic swelling line in lnv : lnp' space, immediately after a stress path reversal, when deformations should be elastic.

R - extent of this elastic region

ν - Poissons ratio in the elastic region

ψ - exponent in the hardening function

A point on the isotropic compression line to fix the model in lnv : lnp' space.

Al Tabbaa (1987) noted that these parameters could be obtained from a single multistage test, as shown in Figure 5.3.5. An isotropic normal compression stage would allow λ to be calculated and κ and R could be obtained from the initial part of the subsequent swelling curve. The latter part of this curve would define ψ. If the soil was then sheared from this overconsolidated state, the stress state at failure would provide a value for M. Any point on the isotropic compression line fixes the model in lnv : lnp' space.

In this section model parameters will be derived for speswhite kaolin using the detailed experimental data presented in section 4.2. The parameters λ, M and a point on the isotropic compression line can be obtained relatively simply using the method recommended by Al Tabbaa (1987). Values of R, κ, ν and ψ are more difficult to derive because the model does not fit some aspects of the data.

(i) Isotropic Compression and Critical State

In section 4.2.1(iv) an average value of $\lambda = 0.073$ was calculated from the isotropic compression stages carried out in tests on speswhite kaolin. A convenient fixed point on the isotropic normal compression line is $p' = 400\text{kPa}$, $v = 2.027$. No reliable measurement of M was obtained from the tests reviewed in section 4.2. Atkinson et al (1987) reported a large number of tests on K_o consolidated speswhite kaolin and calculated that M was 0.85 in both compression and extension. This is the value that has been used.

(ii) Elastic Parameters κ and ν

The model predicts that the stress-strain response of the soil is elastic after a 180° stress path rotation, i.e. as the stress path travels back through the elastic region enclosed by the yield surface, Figure 5.3.6. The experimental results presented in section 4.2 suggest that this region is extremely small and could not be measured in the tests. To derive a value for κ it has been assumed that if $\theta = 180^\circ$ the initial value of bulk modulus, K', for a constant q' loading path represents the elastic bulk modulus of the soil. A value for κ can then be obtained using the relationship $\kappa = p'/K'$. The stress-strain data for isotropic swelling stages, which were normalised and plotted as K'/p' versus p'/p'_m in Figure 4.2.22, provided a range of values for initial K'/p' of between 110 and 190. Hence, κ varies from 0.009 to 0.005.

If these values for κ and the initial shear moduli obtained from constant p' loading paths with $\theta = 180^\circ$, are combined with equation 5.3.3 it should be possible to derive an associated range of values for Poissons ratio, ν. Values for ν calculated from these data, were either negative or extremely small. It appears that the values for elastic shear modulus and bulk modulus derived from the experimental data are not related by the expression given in equation 5.3.3, and it is therefore not possible to determine Poissons ratio in this way. For the present, Poissons ratio has been set at 0.3 which was the value calculated by Al Tabbaa (1987). Assuming Poissons ratio is 0.3, data for the initial shear stiffness immediately following a stress path reversal, $\theta = 180°$, can be combined with equation 5.3.3 to calculate a second range of possible values for κ, in this case, 0.001 to 0.003. This range is significantly different from the values 0.005 to 0.009 derived from the isotropic compression and swelling tests. To accommodate this variation in κ and also the difficulty of defining R, noted below, a number of different combinations of parameters have been tried, see Table 5.3.1.

(iii) R and ψ

R can be defined in two ways: it is the ratio between the size of the elastic region and the bounding surface and, as demonstrated in Figure 5.3.7, the ratio between the range of influence of recent stress history, $\Delta\sigma'_R$ and the size of the bounding surface. Figures 5.3.7(a) and (b) show the configuration of the two surfaces at the start of a typical isotropic compression stage in one of the stress probe test described in chapter 3. The start of the stage is identified by the point O. Figure 5.3.7(a) shows the position of the surfaces after no rotation and (b) after a 180° rotation. Figures (c) and (d) show the configuration of the surfaces after loading by a change in stress equal to the principal diameter of the kinematic yield surface, to point C. Although, the stress-strain response predicted by the model before C is different, at C the response will be the same for both (c) and (d), i.e. C is the end of the influence of recent stress history. Hence $\Delta\sigma'_R = 2Rp'_o$ for an isotropic loading stage.

Unfortunately from the data presented in section 4.2 these two ways of defining R are not consistent and it is difficult to choose an appropriate value for R. This means that the two-surface model is inadequate. Three different values have been investigated. If R represents the size of the elastic region an arbitrary value of 0.01 will ensure that the region is always very small. If R represents the size of $\Delta\sigma'_R$ then assuming $p'_o = p'_m/2$ and using the data presented in Figures 4.2.23 and 4.2.24, R varies between 0.16 and 0.23. For the purpose of this analysis these values have been approximated to 0.1 and 0.2.

The exponent of the hardening function ψ has no clear physical meaning and can only be determined by trying different values and seeing how well they fit the experimental data. The stress-strain response of the soil outside the influence of recent stress history is best suited for the comparison. Al Tabbaa (1987) used $\psi = 1.5$ to predict the results of cyclic tests on speswhite kaolin.

Table 5.3.1 gives the various permutations of material parameters which were used in the evaluation of the model.

5.3.3 Evaluation of Model Predictions

This comparison between model predictions and experimental data has two purposes. Firstly, to look at the effect on the predicted stress-strain behaviour of varying the three main parameters, R, κ and ψ and, secondly, to evaluate the main problems with the two-surface model. These problems have already been identified in the previous section as,

(i) The single kinematic yield surface is trying to model two features of the observed behaviour, the small elastic zone and the range of influence of the recent stress history effect, which needs a surface an order of magnitude larger.

(ii) Any reasonable values for the elastic stiffness parameters used in the model lead to predictions which do not correspond to the overall pattern of behaviour observed in laboratory tests.

The stress-strain behaviour predicted by the model was calculated using a single element computer program called SECUNDUS. A flow chart for the program is given in Appendix 1 and the program is described in detail in Stallebrass (1990b). The program models the behaviour of a single element of soil with properties described by the two-surface model developed by Al Tabbaa (1987). To predict the stress-strain response equivalent to test results given in Chapter 4, exactly the same series of stress probes were applied to the element of soil as those carried out during the stress path tests.

Figure 5.3.8 shows model predictions for an isotropic swelling stage from a normally consolidated state at $p' = 400$kPa. Figure 5.3.8(a) shows that the sudden decrease in K', that occurs as the soil yields is dependent on the size of the yield surface. The best approximation to the highly non-linear behaviour observed in the laboratory is for $R = 0.2$. Post yield the gradient of the K' versus p' graph increases as ψ varies from 1 to 3, see Figure 5.3.8(b).

Figures 5.3.9 and 5.3.10 show comparisons between model predictions and experimental data for isotropic compression from 100kPa after $\theta = 0°$ and $\theta = 180°$. Figure 5.3.9(a) demonstrates that if R is very small the model predicts that recent stress history has a negligible effect and the stress-strain response predicted by the model is dominated by a gradual increase in stiffness as p' increases. This effect is less marked when $R = 0.2$ and plastic deformations are greater, as shown by, for example, the curve for $\theta = 0°$ in Figure 5.3.9(b), and it is also less marked when κ decreases (Figure 5.3.10). Conversely the predictions for $\theta = 180°$ in Figures 5.3.9(b) and 5.3.10 illustrate the problems that occur if R is higher. This implies that there is a large region of elastic deformation contrary to the experimental stress-strain data which are highly non-linear and definitely inelastic. These two figures demonstrate another drawback to the model which is that although the value of κ was approximately correct at $p' = 400$kPa, it is too high by approximately a factor of two at $p' = 100$kPa.

The difficulty of using only one kinematic yield surface to predict both the effect of recent stress history and the highly non-linear stress-strain behaviour produced by a stress path rotation is confirmed in Figure 5.3.11. Figures 5.3.11(b) and (c) show model predictions for the stress probe test with a constant p' path at $p'_i = 300$kPa and $p'_m = 720$kPa. The experimental results from this test are given in Figure 5.3.11(a). As illustrated in 5.3.11(c), where an appropriate value of κ for this test was used, the only way of predicting the dramatic variation between the initial shear stiffness after $\theta = 0°$ and $\theta = 180°$ is to use a large kinematic yield surface, R

$= 0.2$. However, when the elastic region enclosed by the yield surface is traversed, as it is following a complete stress path reversal, the resulting step function is a very poor approximation to the experimental data. The experimental data for $\theta = 90^\circ$, -90° and 0° are more accurately modelled.

Figure 5.3.12 shows predictions for comparison with experimental data from a constant p' path at $p'_i = 100$kPa, $p'_m = 150$kPa. The stress-strain data from constant p' paths, analysed in section 4.2.4(ii), showed that G' is not simply proportional to p', but in the model the elastic shear modulus is solely a function of p'. Hence, although with $\kappa = 0.002$ the model predicted shear moduli, for a path at $p'_i = 300$kPa, which were approximately the correct magnitude (see Figure 5.3.11(c)) the stiffnesses predicted for a path at $p'_i = 100$kPa are too low, as shown in Figure 5.3.12. The range of influence of the effect, $\Delta\sigma'_R$, is predicted correctly by assuming $R = 0.2$ for both sets of data.

Figure 5.3.13 illustrates that the model is capable of predicting qualitatively the correct pattern of strain paths because of the associated plastic flow at the kinematic yield surface. Once again the size of the surface is critical.

The main conclusion of this comparison between experimental data and predictions using the two-surface model is that the model cannot predict both the effects of recent stress history and non-linearity with only one inner yield surface. As a result the model gives particularly poor predictions of the stress-strain response along constant q' and constant p' paths after a stress path reversal. A further conclusion is that the elastic bulk and shear moduli should not be defined by assuming that the elastic shear modulus is proportional to p' with Poissons ratio a constant.

The two surface model attempts to use a single kinematic yield surface to represent two features of the experimental observations. The data clearly show that these two features are not compatible and require two separate surfaces. In the following section a new three-surface model is proposed which incorporates a "history" surface to model the extent of the influence of recent stress history. The extra surface has a clear physical meaning and only requires the definition of one extra parameter.

5.4 Three-surface Yield Model

The new model has been derived by modifying the translation rules and hardening rules of the two-surface model (Al-Tabbaa, 1987) to accommodate an extra kinematic yield surface. Largely the same form of hardening and translation rules have been retained. The extra parameter required in the model is the size of the new surface. This three surface model is not the same as the model proposed by Hashiguchi (1985), where the extra surface is not truly kinematic.

5.4.1 Basic description of the model

The model is defined in triaxial stress space as shown in Figure 5.4.1, which identifies the three yield surfaces that constitute the model. These consist of two kinematic yield surfaces lying within the Modified Cam-clay state boundary surface. For normally consolidated clays yielding continuously the model reduces to the Modified Cam-clay soil model, as defined in section 1.2.2.

The intersection of the Modified Cam-clay state boundary surface with an elastic wall forms a yield locus in q′ : p′ space with equation;

$$(p' - p'_o)^2 + q'^2/M^2 = p'^2_o \qquad (5.4.1)$$

Following Al Tabbaa (1987) this surface is called the <u>bounding surface</u>. The two kinematic yield surfaces are similar in shape to the bounding surface but smaller in size by constant ratios. The first kinematic yield surface has centre co-ordinates (p'_a, q'_a) and the equation of the surface is;

$$(p' - p'_a)^2 + \frac{(q' - q'_a)^2}{M^2} = T^2 p'^2_o \qquad (5.4.2)$$

This is the additional yield surface and is called the <u>history surface</u>. The parameter T is the ratio between the dimensions of this surface and the bounding surface. The second kinematic yield surface is the <u>yield surface</u> which defines the region in stress space within which purely elastic deformations occur. The centre of this yield surface has coordinates (p'_b, q'_b) and the ratio between the dimensions of this surface and the history surface is denoted by S. Thus the surface is defined by the equation.

$$(p' - p'_b)^2 + \frac{(q' - q'_b)^2}{M^2} = T^2 S^2 {p'_o}^2 \tag{5.4.3}$$

When the stress state of the soil lies within the elastic region, for example when the soil has been unloaded slightly, the deformations of the soil are governed by an isotropic elastic constitutive equation of the form;

$$\begin{bmatrix} \delta\epsilon^e_v \\ \delta\epsilon^e_s \end{bmatrix} = \begin{bmatrix} \kappa/p' & 0 \\ 0 & 3G'_e \end{bmatrix} \begin{bmatrix} \delta p' \\ \delta q' \end{bmatrix} \tag{5.4.4}$$

where G'_e is the elastic shear modulus.

In chapter 4 it was established that within the influence of recent stress history G' is not solely dependent on p'. In the previous section it was clear that the predicted maximum stiffness of the soil within the influence of recent stress history is determined by the current elastic shear stiffness in the model. Hence to obtain predictions that match the experimental data, G'_e should not be solely dependent on p'. The appropriate definitions of G'_e and also κ are discussed in greater detail in section 5.4.4 when values for the model parameters are selected.

5.4.2 Translation Rules

The translation rules control the movement of the two kinematic yield surfaces as they are dragged by the current stress state during loading. The translation rule should ensure that when the surfaces meet they do not intersect but meet tangentially with a common outward normal. In addition when the surfaces are in contact, during subsequent loading, they should move so that they maintain contact for all paths which constitute continued loading, ie. paths for which the scalar product of the stress increment vector and the outward normal to the surfaces is zero or greater than zero. Al Tabbaa (1987) used a single translation rule which fulfilled the non-intersection criterion and also allowed for the expansion and contraction of the surfaces due to plastic volumetric straining, but the latter part of the rule would not maintain contact between the surfaces when the stress increment was not in the same direction as the outward normal to the surfaces.

This problem is more critical with two kinematic surfaces in contact and so for this model each surface requires two different forms of the translation rule. The first, is a rule to control the translation of a surface moving inside another surface and is similar to the translation rule described by Al Tabbaa (1987), and the second, is a rule to control the translation of surfaces which are in contact with one or more other surfaces. However, this form of translation rule could not be used to derive the hardening modulus in the same way as that used by Al Tabbaa (1987), as described in section 5.4.3.

As mentioned above any plastic volumetric strains cause the bounding surface to expand or contract according to the hardening rule:

$$\delta p_o' = \frac{p_o'}{(\lambda - \kappa)} \quad \delta \epsilon_v^p \qquad (5.4.5)$$

where λ and κ are Modified Cam-clay compression and swelling parameters derived from a lnv, lnp' graph as defined in section 1.2. When the bounding surface contracts or expands the inner yield and history surfaces also contract or expand proportionally. This feature is included in both forms of the translation rule.

(a) Translation Rules for the History Surface

The following two translation rules govern the movement of p_a' and q_a'.

(i) The translation rule for the history surface moving inside the bounding surface as shown in Figure 5.4.2(a). There are two components of the rule as in section 5.3.1(ii). The movement caused by expansion or contraction of surfaces is given by the equation:

$$\begin{bmatrix} \delta p'_a \\ \delta q'_a \end{bmatrix} = \frac{\delta p'_o}{p'_o} \begin{bmatrix} p'_a \\ q'_a \end{bmatrix} \qquad (5.4.6)$$

The second component of the rule covers the translation of the history surface as it is dragged by the current stress state. Translation must occur along the vector β, which joins the stress state, A, and its conjugate point, A_c, on the bounding surface, see Figure 5.4.2(a). This ensures that the surfaces will meet correctly. The vector β is,

$$\begin{bmatrix} \dfrac{p' - p'_a}{T} - (p' - p'_o) \\ \dfrac{q' - q'_a}{T} - q' \end{bmatrix} \qquad (5.4.7)$$

The full expression for the translation rule is:

$$\begin{bmatrix} \delta p'_a \\ \\ \delta q'_a \end{bmatrix} = \frac{\delta p'_o}{p'_o} \begin{bmatrix} p'_a \\ \\ q'_a \end{bmatrix} + W \begin{bmatrix} \dfrac{p' - p'_a}{T} - (p' - p'_o) \\ \dfrac{q' - q'_a}{T} - q' \end{bmatrix}. \qquad (5.4.8)$$

Where W can be determined using the consistency equation for the history surface, which takes the form:

$$(p' - p'_a)(\delta p' - \delta p'_a) + \frac{(q' - q'_a)}{M^2}(\delta q' - \delta q'_a) = T^2 p'_o \delta p'_o \qquad (5.4.9)$$

Hence,

$$W = \frac{(p' - p'_a)\left[\delta p' - \dfrac{\delta p'_o}{p'_o} p'\right] + \dfrac{(q' - q'_a)}{M^2}\left[\delta q' - \dfrac{\delta p'_o}{p'_o} q'\right]}{(p' - p'_a)\left[\dfrac{p' - p'_a}{T} - (p' - p'_o)\right] + \dfrac{(q' - q'_a)}{M^2}\left[\dfrac{q' - q'_a}{T} - q'\right]}$$

(5.4.10)

(ii) The translation rule for the history surface when it is in contact with the bounding surface and the loading path is such that the bounding surface is expanding.

From the geometry of the surfaces when they are in contact, as shown in Figure 5.4.2(b):

$$T(p' - p'_o) = p' - p'_a \qquad \text{and} \qquad Tq' = q' - q'_a \tag{5.4.11}$$

Differentiating these expressions gives the translation rule:

$$\begin{bmatrix} \delta p'_a \\ \delta q'_a \end{bmatrix} = (1 - T) \begin{bmatrix} \delta p' \\ \delta q' \end{bmatrix} + T \begin{bmatrix} \delta p'_o \\ 0 \end{bmatrix} \tag{5.4.12}$$

In the above cases the stress state lies on the history surface. When the stress state is inside the history surface, the surface will still move to allow for expansion or contraction of the surfaces as follows,

$$\begin{bmatrix} \delta p'_a \\ \delta q'_a \end{bmatrix} = \frac{\delta p'_o}{p'_o} \begin{bmatrix} p'_a \\ q'_a \end{bmatrix} \tag{5.4.13}$$

(b) Translation rules for the yield surface.

These translation rules govern the movement of p'_b and q'_b.

(i) The translation rule for the yield surface when it is moving inside the history surface as shown in Figure 5.4.3(a). Using a similar form to the history surface the translation rule is given by:

$$\begin{bmatrix} \delta p'_b \\ \\ \delta q'_b \end{bmatrix} = \frac{\delta p'_o}{p'_o} \begin{bmatrix} p'_b \\ \\ q'_b \end{bmatrix} + Z \begin{bmatrix} \dfrac{p' - p'_b}{S} - (p' - p'_a) \\ \dfrac{q' - q'_b}{S} - (q' - q'_a) \end{bmatrix} \tag{5.4.14}$$

where

$$\begin{bmatrix} \dfrac{p' - p'_b}{S} - (p' - p'_a) \\ \dfrac{q' - q'_a}{S} - (q' - q'_a) \end{bmatrix} = \gamma \tag{5.4.15}$$

The vector, γ, joins the current stress state, D, to its conjugate point, D_c. The expression for Z was derived using the consistency equation for the yield surface such that:

$$Z = \frac{(p' - p_b')\left[\delta p' - \dfrac{\delta p_o'}{p_o'} p'\right] + \dfrac{(q' - q_b')}{M^2}\left[\delta q' - \dfrac{\delta p_o'}{p_o'} q'\right]}{(p' - p_b')\left[\dfrac{p' - p_b'}{S} - (p' - p_a')\right] + \dfrac{(q' - q_b')}{M^2}\left[\dfrac{q' - q_b'}{S} - (q' - q_a')\right]} \qquad (5.4.16)$$

(ii) The translation rule for the yield surface when it is in contact with the history surface, as shown in Figure 5.4.3(b), is derived from the geometry of the surfaces as before:

$$\begin{bmatrix} \delta p_b' \\ \delta q_b' \end{bmatrix} = (1 - S) \begin{bmatrix} \delta p' \\ \delta q' \end{bmatrix} + S \begin{bmatrix} \delta p_a' \\ \delta q_a' \end{bmatrix} \qquad (5.4.17)$$

5.4.3 Hardening Rule

The hardening rules follow those developed for the two-surface model. As noted in section 5.3.1(iii) the functions chosen to define the second part of the hardening modulus in the two-surface model are not unique and could easily be altered if it was necessary to improve the model predictions. It was found that using the same expression to describe deformations on both the yield and history surfaces produced unacceptably inaccurate predictions and a simple modification to one section of the hardening modulus was required. Further work on the definition of the hardening modulus is required to derive more appropriate functions to differentiate between the hardening moduli for the two surfaces.

The hardening modulus is developed for the special case when all the surfaces are in contact and then generalised. Plastic deformations follow the associated flow rule so that the vector of plastic strain increments is always normal to all current yield surfaces. The Modified Cam clay hardening rule given in equation 5.4.5 also applies to all surfaces.

Equation 5.4.5 clearly links the expansion or contraction of all three surfaces to changes in volumetric plastic strain. A representation of this process is shown in Figures 5.4.4 and 5.4.5. The bounding surface is represented in q':p' space by the locus of the intersection of the state boundary surface and an elastic wall, as shown in Figure 5.4.4. Figure 5.4.5(a) shows the bounding surface and the two kinematic surfaces in q' : p' space and Figure 5.4.5(b) the projection of the isotropic compression line and the swelling lines, which represent the elastic walls, in v : p' space. When elastic strains occur the stress state moves along the current elastic wall, path AB, and the bounding surface does not expand. When the stress state reaches the kinematic surfaces and yielding occurs, loading path BCD, the stress state is moving to new elastic walls or swelling lines as shown in Figure 5.4.5(b). Hence the locus of the bounding surface expands or contracts, as do the loci of the two kinematic surfaces. Plastic shear strains are linked to plastic volumetric strains by the normality rule so the surfaces will expand or contract when yielding occurs for the majority of stress states and stress histories.

Combining the normality rule and the hardening rule, increments of plastic volumetric and shear strain on the yield surface are given by the equation:

$$\begin{bmatrix} \delta\epsilon_v^p \\ \\ \delta\epsilon_s^p \end{bmatrix} = \frac{1}{h_o} \begin{bmatrix} (p' - p_b')^2 & (p' - p_b')\dfrac{(q' - q_b')}{M^2} \\ (p' - p_b')\dfrac{(q' - q_b')}{M^2} & \left(\dfrac{(q' - q_b')}{M^2}\right)^2 \end{bmatrix} \begin{bmatrix} \delta p' \\ \\ \delta q' \end{bmatrix} \qquad (5.4.18)$$

Using the same expression that was employed in the two-surface model

$$h_o = \frac{(p' - p_b')}{(\lambda - \kappa)}\left(p'(p' - p_b') + q'\frac{(q' - q_b')}{M^2} \right)$$

which, as required, reduces to the Modified Cam-clay constitutive relationship when all three surfaces are in contact and $TS(p' - p_o') = (p' - p_b')$ and $TSq' = (q' - q_b')$. Al Tabbaa (1987) obtained this expression by substituting into the consistency equation and using the translation rule for the case when the surfaces are in contact. The new translation rule for the three-surface model is not consistent with the above expression for h_o, and cannot be used to obtain a similar expression which will also reduce to Modified Cam-clay. Further work is necessary to derive a more consistent version of either the translation or hardening rules.

As for the two-surface model h_o cannot be used on its own because the function predicts infinite strains at a number of points on the kinematic surfaces. Consequently the model follows Al Tabbaa (1987) in defining the hardening modulus h as a function of $h_o + H_1 + H_2$. As before, where instability has not been observed, when $\eta < M$, $h_o + H_1 + H_2$ must be greater than zero. The values of h_o, H_1 and H_2 are further restricted as follows:

(i) When all three surfaces are in contact $H_1 + H_2 = 0$ so that they are all predicting the same strains.

(ii) When the stress point lies within the bounding surface on the history and yield surfaces $H_2 = 0$ so that both these surfaces are predicting the same strains.

(iii) Plastic strains should be lowest when the stress state lies on the yield surface only, $H_2 \geq 0$, and greatest when the stress state lies on the bounding surface $H_1 \geq 0$.

These criteria are fulfilled by linking H_1 and H_2 to the position of the history and yield surfaces respectively. Similarly to Al Tabbaa (1987) and Hashiguchi (1985), H_1 is expressed as a function of b_1, the degree of approach of the history surface to the bounding surface, and H_2 as a function of b_2, the degree of approach of the yield surface to the history surface. b_1 and b_2 are defined geometrically for the case when the stress state lies on the yield surface only, see Figure 5.4.6.

$$b_1 = \frac{1}{Tp'_o}\left[\frac{(p' - p'_b)}{S}\left[\frac{(p' - p'_b)}{TS} - \left(\frac{(p' - p'_b)}{S} + p'_a - p'_o\right)\right]\right.$$

$$\left. + \frac{(q' - q'_b)}{SM^2}\left[\frac{q' - q'_b}{ST} - \left(\frac{(q' - q'_b)}{S} + q'_a\right)\right]\right]$$

(5.4.19)

which is the scalar product of the vector $\underline{\beta}$ and the normal to the history surface, $\underline{n}_h$, at the <u>conjugate</u> stress point $(p'_s,\ q'_s)$, see Figure 5.4.6, divided by a measure for the size of the history surface. The stresses p'_s and q'_s were eliminated from the expression using the equations

$$p'_s = \frac{(p' - p'_b)}{S} + p'_a \qquad \text{and} \qquad q'_s = \frac{(q' - q'_b)}{S} + q'_a \qquad (5.4.20)$$

A slightly simpler expression defines b_2,

$$b_2 = \frac{1}{STp'_o}\left[(p' - p'_b)\left[\frac{(p' - p'_b)}{S} - (p' - p'_a)\right]\right.$$

$$\left. + \frac{(q' - q'_b)}{M^2}\left[\frac{q' - q'_b}{S} - (q' - q'_a)\right]\right]$$

(5.4.21)

Which is the scalar product of the vector γ and the normal to the yield surface, $\underline{n}_y$, at the <u>current</u> stress point, see Figure 5.4.6, divided by a measure for the size of the yield surface.

When the two kinematic surfaces are in contact $b_2 = 0$ and the conjugate stress point used to define b_1 becomes the current stress point. Both b_1 and b_2 are normalised relative to their maximum possible values:

$$b_{1max} = 2p'_o(1 - T) \qquad b_{2max} = 2Tp'_o(1 - S)$$

The functions b_1 and b_2 are at a maximum when the surfaces are in the configuration shown in Figure 5.4.7.

The components of the hardening rule H_1 and H_2 are defined using minor modifications to the functions chosen by Al Tabbaa (1987).

$$H_1 = S^2 \left[\frac{b_1}{b_{1max}}\right]^{\psi} \frac{1}{\lambda - \kappa}\, p_o'^3 \qquad (5.4.22)$$

$$H_2 = \left[\frac{T.b_2}{b_{2max}}\right]^{\psi} \frac{1}{\lambda - \kappa}\, p_o'^3 \qquad (5.4.23)$$

The S^2 term that appears in equation 5.4.22 ensures that the strains predicted by the history and yield surfaces are the same when these surfaces are in contact. The parameter T is introduced into equation 5.4.23 to reduce the value of H_2 which ensures that model predictions of elasto-plastic deformations inside the history surface are realistic, as noted at the beginning of this section. The term $p_o'^3$ is consistent with the dimensions of h_o, as the functions $(b_1/b_{1max})^{\psi}$ and $(b_2/b_{2max})^{\psi}$ are dimensionless. The parameter ψ is an experimentally derived constant.

The constitutive relationship for plastic strain increments is thus

$$\begin{bmatrix} \delta\epsilon_v^p \\ \delta\epsilon_s^p \end{bmatrix} = \frac{1}{h} \begin{bmatrix} (p' - p_b')^2 & (p' - p_b')\dfrac{(q' - q_b')}{M^2} \\ (p' - p_b')\dfrac{(q' - q_b')}{M^2} & \left[\dfrac{(q' - q_b')}{M^2}\right]^2 \end{bmatrix} \begin{bmatrix} \delta p' \\ \delta q' \end{bmatrix}$$

where

$$h = \frac{1}{(\lambda - \kappa)} \left[(p' - p_b')\left\{p'(p' - p_b') + q'\frac{(q' - q_b')}{M^2}\right\} + \left[\frac{b_1}{b_{1max}}\right]^{\psi} p_o'^3 S^2 + \left[\frac{T.b_2}{b_{2max}}\right]^{\psi} p_o'^3 \right] \qquad (5.4.24)$$

5.4.4 Calculation of Model Parameters

The three-surface model is defined by eight parameters:

M - critical state friction coefficient.

λ - gradient of the isotropic normal compression line defined in lnv : lnp′ space.

κ - gradient of the swelling line immediately after a stress path reversal when the strains are defined as elastic, defined in lnv : lnp′ space.

G'_e - elastic shear modulus.

T - ratio between the size of the history surface, that defines the end of the influence of recent stress history, and the bounding surface.

S - ratio between the size of the elastic region, enclosed by the yield surface and the history surface.

ψ - exponent in the hardening function.

A point on the isotropic normal compression line to fix the model in lnv : lnp′ space.

As in section 5.3.2, data from the tests presented in section 4.2, will be used to calculate the values of these parameters for speswhite kaolin. The model will only be used to model the behaviour of the tests on speswhite kaolin, because the appropriate test data are not available for London Clay. The parameters λ and M, and the point on the isotropic normal compression line have the same definition as in the two-surface model and Modified Cam-clay. Hence: $\lambda = 0.073$, $M = 0.85$ and the isotropic compression line is fixed at the point, $p' = 400$kPa and $v = 2.027$. The parameters κ, T, S and ψ can all be obtained from simple swelling and recompression tests, similar to those described in section 3.6.2. The series of probes that makes up these tests provides a comparison between the stress-strain behaviour along a constant q′ compression path after a stress path reversal, $\theta = 180°$, and after no change in direction of stress path, $\theta = 0°$. The initial stiffness of the soil for $\theta = 180°$ is used to calculate κ, and S is obtained by observing the stress change for which strains are elastic. Following the same explanation that was given in section 5.3.2(iii), the change in stress at which the two curves converge gives a value for T. The parameter ψ is estimated using the stiffness curve for $\theta = 0^\circ$. Figure 5.4.8 shows diagrammatically how the parameters would be calculated from typical stiffness curves. The parameter, G'_e, can only be obtained from constant p' tests. Initial estimates of the values of the five parameters κ, G'_e, T, S, and ψ, for speswhite kaolin were calculated as described below.

(i) κ and G'_e

In the review of experimental data given in section 4.2 the factors which affect the bulk and shear stiffness of the soil were assessed for two cases: firstly, when the stress-strain response of the soil was influenced by recent stress history, $\theta = \pm 90^\circ$ and 180°, and secondly, when the stress-strain response was unaffected by recent stress history, $\theta = 0^\circ$. As indicated in section 5.3.3, the elastic moduli define the maximum stiffness that the model will predict. At any point on a loading path within the influence of recent stress history, the predicted stiffness of the soil is in part a function of the elastic stiffness. Hence the elastic moduli used in the model should be dependent on the same factors as the experimental stiffness data for soil within the influence of recent stress history and at constant $\Delta\sigma'/\Delta\sigma'_R$ and θ.

There were insufficient experimental data at very small strains for any firm conclusions to be drawn about the factors affecting K', but data demonstrated that G' was not simply proportional to p'. In the light of these rather incomplete observations and in order to keep the model as simple as possible, the elastic strains were defined as in equation 5.4.4. The strains are isotropic and controlled by a bulk modulus, K', which is equal to p'/κ, and a shear modulus, G'_e, which is a constant. The latter is the greatest approximation, as indicated in Figure 4.2.31(b). With reference to data for constant p' loading paths presented in Figures 4.2.28 to 4.2.30, G'_e varies from about 60-25MPa allowing for scatter in the data. The parameter κ is determined as before from the initial stiffness of soil subjected to isotropic swelling stages. From the data presented as plots of K'/p' versus p'/p'_m in Figure 4.2.22, κ varies in the range 0.009 to 0.005.

(ii) T, S and ψ

The first of these parameters will be calculated from the results of the stress path swelling and recompression tests given in Figures 4.2.23 and 4.2.24. Two different stiffness curves are obtained from a common isotropic compression path, for two different recent stress histories, $\theta = 0^\circ$ and $\theta = 180^\circ$. Using the same reasoning that was illustrated in Figure 5.3.7, for the two-surface model, the stress change at which these two curves meet can be used to define T. As shown in Figure 5.4.8 this stress change $\Delta\sigma_R'$ is equal to $2Tp_o'$ so if $p_o' = p_m'/2$, $T = \Delta\sigma_R'/p_m'$. From the tests represented in Figures 4.2.23 to 4.2.24, T varies between 0.16 and 0.23, as calculated in section 5.3.2(iii) when the single surface was assumed to represent the range of influence of recent stress history.

Unfortunately, S cannot be obtained from any of the experimental data presented in Chapter 4. Dynamic tests such as those undertaken by Rampello (1989) indicate that elastic strains occur at strain levels below 0.001%, which for G_e' in the range 60-25MPa is equivalent to a stress change of approximately 1kPa. These data were obtained for Todi clay, not speswhite kaolin, and it is not clear whether the size of this elastic region varies with p_m'. Estimates of the value of S should be varied to match the estimates of G_e' and κ, and to predict the correct stiffnesses at measurable stress and strain levels. The value of ψ can only be determined by trial and error.

The ranges of values for the model parameters which have been estimated were used in a small parametric study of the model. This was carried out using the computer program TERTIUS, which is described briefly in the following section. The section also describes how the predictions calculated by the program were validated.

5.4.5 Validation of the Computer Program TERTIUS

The stress-strain response predicted by the model was calculated using a single element computer program called TERTIUS. A flowchart for the program, which is similar to the program SECUNDUS, is given in Appendix II. Stallebrass (1990b) includes a more detailed description of the program and the form of data input it requires. The program models the behaviour of the sample in a triaxial test using a single element subjected to incremental applied stress or strain. For each applied increment of stress or strain the program calculates the new state of the soil using the appropriate constitutive equations for elastic or plastic deformation, equations 5.4.4 and 5.4.24, depending on the position of the current stress state relative to the three surfaces. At the end of the increment the model calculates how far the surfaces should translate during the increment.

The program has been validated by considering these two steps separately, first the translation of the surfaces and second the calculation of the correct stress or strain increment. When the program is running the position of the three surfaces is plotted in q':p' space on the screen. It is thus possible to confirm that the surfaces are translating in a reasonable manner during a loading path. The program is not iterative and so slight inaccuracies in the calculation of the stress state at which a surface is reached may occur, but these are reduced by the small increments used.

The calculation of the new strain or stress state using the constitutive equations for plastic and elastic strains was partially checked by following specific loading paths which should give known results. These paths are as follows,

(a) Isotropic compression from a normally consolidated state with all three surfaces meeting at the current stress state. The model should predict a normal compression line with a gradient of λ in lnv : lnp' space.

(b) Constant q' compression or swelling after a stress path reversal. The model should predict that the initial bulk stiffness is p'/K'.

(c) Constant p' compression or extension after a stress path reversal. The model should predict that the initial shear stiffness is equal to $G'_{\bullet}$.

The model predicts the correct response for all these loading paths. The loading path described in (a) tests the subroutines used to calculate the elasto-plastic stiffness matrix and also those routines used to solve the matrix to obtain the appropriate stress or strain increments. The only parts of the program not included in these calculations are versions of the hardening modulus used to calculate plastic strains within the bounding surface. These equations have been carefully checked, and the predictions made by the program are considered to be reasonable, as they can all be explained with reference to the equations given in section 5.4.1.

When predictions are compared to experimental data, exactly the same loading paths are applied to the single element as were applied to the triaxial sample. All those predictions which are compared to the results of stress controlled probing tests were calculated from incremental stress paths. The increments of stress are always 0.05kPa or less and a decrease in the size of the increments by a factor of ten makes no visible difference to the stiffness curves predicted by the model. Undrained compression tests are modelled using strain increments which ensure that $\delta\epsilon_v = 0$. The increments of strain were 0.002% or less. The paths modelled in section 5.4.7 used stress and strain increments. When yielding at constant p' and near to failure the minimum increment of strain was increased to 0.01%.

5.4.6 Parametric Study

The primary object of this study is to examine the sensitivity of the model to the five parameters, ψ, κ, G_e', T and S. The secondary aim is to make better estimates of the values of these parameters for speswhite kaolin. The study is divided into three sections beginning with an investigation into the effect of ψ, the exponent in the hardening modulus. In the second part the influence of κ and G_e', the elastic stiffness parameters, is assessed. The study ends by looking at the effect of T and S.

For this parametric study the computer program TERTIUS was used to model predictions of the variation of stiffness with stress change for three sets of experimental data: an isotropic swelling stage from p' = 400 kPa, when the soil was normally consolidated, to p' = 100kPa; an isotropic compression stage, at $p_i' = 100$kPa, $p_m' = 300$kPa, for two different recent stress histories $\theta = 180°$ and $\theta = 0°$; and a constant

p' loading path at $p'_i = 300$kPa, $p'_m = 720$kPa, also for $\theta = 180°$ and $\theta = 0°$. The predictions are compared with the experimental data for these loading paths.

(i) ψ

For these predictions the values of the parameters were set at $M = 0.89$, $\lambda = 0.073$, $\kappa = 0.007$, $T = 0.2$, $S = 0.1$ and $G'_e = 40$MPa. The parameter ψ was varied between 1.5 and 3.0. This is the least well defined of all the model parameters and it is necessary to determine a sensible value for ψ before continuing the parametric study. Figure 5.4.9 shows that when the stress state lies within the history surface at the start of the unloading stage increasing ψ alters the shape of the stiffness curve. Once the stress state lies on the history surface increasing ψ increases the gradient of the stiffness curves. These effects are also illustrated in Figures 5.4.10(b) and 5.4.11(b) which show data for constant q' and constant p' compression paths respectively. As ψ increases the stiffness tends to decrease more rapidly immediately after the elastic region. Once the yield surface is reached values of both bulk and shear stiffness should decrease as plastic straining occurs. Unfortunately, if ψ is low the plastic strains are too small to counteract the increase in elastic stiffness caused by the increase in p', and the overall bulk stiffness predicted by the model increases, as shown in Figure 5.4.10(b) for $\psi = 1.5$. The graphs for constant q' and constant p' paths with $\theta = 0°$, Figures 5.4.10(a) and 5.4.11(a), confirm that once the stress state reaches the history surface, i.e outside the influence of recent stress history for the model, predicted values for stiffness decrease with increasing ψ.

If the corresponding stiffness curves for $\theta = 0°$ and $\theta = 180°$ predicted by the model are plotted on the same graphs, the curves meet when the stress state reaches the edge of the history surface or the end of the influence of recent stress history. Hence not much additional information is gained by considering the behaviour of the model for $\theta = 0°$. Stiffness curves plotted from experimental data, as shown in section 4.2.4, particularly curves showing the variation of bulk stiffness with stress change do not always converge in this way, see for example Figures 4.2.23 and 4.2.24.

(ii) κ and G'_e

By inspection of the curves discussed above, $\psi = 2.5$ was chosen as a suitable value to be used for the remainder of the evaluation of the model. The basic set of parameters used to investigate κ and G'_e is $\psi = 2.5$, $T = 0.2$ and $S = 0.1$. Figures 5.4.12 and 5.4.13(a) illustrate the sensitivity of the model predictions to κ as it is varied from 0.003 to 0.007. Figure 5.4.13(b) compares the stiffness curves predicted for $G'_e = 60$MPa and $G'_e = 40$MPa. Only data for $\theta = 180°$ are used. The initial increase in stiffness which results from decreasing κ, gradually reduces as plastic straining occurs. This is shown by the gradual convergence of the three sets of curves for the constant q' paths in both Figures 5.4.12 and 5.4.13(a). Figure 5.4.13(a) also shows how decreasing κ changes the shape of the initial part of the bulk stiffness curve. As κ decreases the elastic bulk modulus becomes too small to influence the change in the modulus with p', which is then dominated by the change in plastic hardening modulus. This is the opposite situation to that discussed in section (i), where the magnitude of the elastic bulk modulus was constant and the shape was influenced by the changing magnitude of the plastic modulus.

The two stiffness curves illustrated in Figure 5.4.13(b) show that the initial difference in shear stiffness caused by the different values of G'_e, decreases dramatically once plastic straining begins. Varying G'_e has a negligible effect on the stiffness of the soil once the history surface is reached.

(iii) T and S

The parameters already evaluated were assigned values as follows: $\psi = 2.5$, $\kappa = 0.005$, $G'_e = 60$MPa. The influence of T the ratio of the sizes of the history and bounding surfaces is illustrated in Figures 5.4.14(a), 5.4.15(a) and 5.4.16(a). To keep the size of the elastic region constant for these predictions S is varied so that the product T.S representing the size of elastic region is equal to 0.02 for all of these stiffness curves. Figures 5.4.14(b), 5.4.15(b) and 5.4.16(b) demonstrate the effect of changing the size of the elastic region and for these curves T is constant and equal to 0.2. Decreasing the product T.S has approximately the same effect as decreasing ψ. For lower values of T.S there is a less dramatic decrease in stiffness when plastic straining first occurs, i.e. at the end of the elastic region. This feature is best illustrated in Figure 5.4.16(b) which shows shear stiffness curves for a constant p′ path. Unlike ψ, the model is only sensitive to changes in T.S for stress states inside the history surface. Changes in T have a more long term effect on the stiffness curves, particularly for constant q′ loading, Figures 5.4.14(a) and 5.4.15(a). Within the history surface increasing T changes the shape of the stiffness curves in approximately the same way as decreasing S or ψ. The shear stiffness plots for the constant p′ loading show an approximately constant increase in stiffness with T once yielding first occurs and before the history surface is reached, Figure 5.4.16(a). As expected the stress change required to reach the history surface increases as T increases. At this point the stiffness is lowest for the highest value of T.

(iv) Summary

The parametric study investigated the effect of the model parameters ψ, κ, G'_e, T and S on predicted curves showing the variation in bulk modulus or shear stiffness along typical loading paths. There are essentially four main aspects of these stiffness curves. Firstly, the difference between the maximum stiffness predicted for $\theta = 180°$ and the maximum stiffness predicted for $\theta = 0°$, which characterises the sensitivity of the model to recent stress history effects. Secondly, the range of the recent stress history effect, $\Delta\sigma'_R$. Thirdly, the way in which stiffness decreases with stress change, i.e. the shape of the curve, within the influence of recent stress history and, finally, the shape of the curve outside the influence of recent stress history.

The results of the parametric study show which parameters have most influence on these features.

(a) If the stiffness at very low stresses is used to evaluate the sensitivity of the model to recent stress history effects, then κ and G'_e are the most significant parameters. At higher stresses, once deformations are elasto-plastic, the effect of T also becomes important.

(b) The range of the effect, $\Delta\sigma'_R$, is purely dependent on T.

(c) Although, the parameters T and ψ are the main influence on the shape of both bulk and shear stiffness curves, the variation in shear stiffness with stress change is also sensitive to the product TS. The magnitude of bulk stiffness predicted by the model is also determined by κ.

(d) The stiffness predicted for $\theta = 0°$ and the shape of the stiffness curves outside the influence of recent stress history are influenced predominantly by ψ and also by T.

Overall the main features of the variation of stiffness with stress change are most sensitive to changes in T and ψ. The elastic parameters G'_e and κ determine the magnitude of the predicted stiffness for $\theta = 180°$, but the influence of G'_e, in particular, decreases rapidly once deformations are elasto-plastic. The value of the product TS appears to be significant for the predictions of shear stiffness, but the value of TS does vary by a factor of three, a much greater amount than any of the other parameters. Unfortunately the size of the yield surface, which is represented by TS cannot be reliably measured in stress path triaxial tests.

The comparison between model predictions and experimental data presented in Figures 5.4.10 to 5.4.17 helped to optimize the set of seven model parameters chosen to represent speswhite kaolin. The parameters were: $M = 0.89$, $\lambda = 0.073$, $\kappa = 0.005$, $G'_e = 60\text{MPa}$, $\psi = 2.5$, $T = 0.25$, $S = 0.08$ ($T.S = 0.02$) and $v = 2.027$ when $p' = 400\text{kPa}$. This set of parameters will be used for <u>all</u> subsequent predictions that are compared with data from stress path tests on speswhite kaolin.

5.4.7 General Characteristics of the Three-surface Model

The three-surface model was developed specifically to predict the behaviour of overconsolidated soils at small strain or stress changes. This section examines the influence of the two kinematic surfaces on the prediction of soil behaviour at larger deformations with reference to two particular loading conditions, loading to failure at highly overconsolidated stress states and predicted stress paths during one-dimensional swelling and compression.

(i) Failure at highly overconsolidated stress states

The Modified Cam-clay model predicts that at highly overconsolidated states, dry of critical state, the soil will deform elastically until the stress state reaches the yield surface and then dilate as the deviator stress decreases and the soil moves towards a critical state. This behaviour is illustrated in Figure 5.4.17(a) which shows plots of stress ratio against shear strain for constant p′ loading to failure as predicted by Modified Cam-clay. There are three curves at different values of mean effective pressure. These represent different overconsolidation ratios as p'_m is constant and equal to 400kPa. The figure also shows corresponding curves predicted by the three surface model. The latter data exhibit almost no peak behaviour, except the curve for p′ = 50kPa. This occurs for two reasons. Firstly, as shown by the corresponding strain paths, Figure 5.6.17(b), the plastic deformations that occur inside the bounding surface are dilatant and so the surfaces contract throughout the shearing stage reducing the likelihood of the soil reaching a high peak state. Secondly, as observed by Al Tabbaa (1987) and Al Tabbaa and Wood (1989) for $\eta > M$, $h_o + H$ or in this case $h_o + H_1 + H_2$, section 5.4.3, may become equal to zero before the stress state reaches the bounding surface. Hence, softening behaviour can be observed within the bounding surface, as shown in the slight peak exhibited for p′ = 50kPa.

(ii) One-dimensional compression, swelling and recompression

In Figure 5.4.18 the stress paths predicted by Modified Cam-clay for a one-dimensional compression, swelling and recompression cycle are compared to those predicted by the three-surface model. The three surface model predicts that K_{onc} for speswhite kaolin is 0.79 which is rather high compared to experimentally derived values of 0.69 (Al Tabbaa, 1987) and 0.66 (Atkinson et al, 1987). Nevertheless, the plastic deformations that occur within the bounding surface mean that much more realistic predictions of unloading and reloading paths are obtained. Within the Modified Cam-clay state boundary surface the gradient of a one-dimensional stress path is determined purely as a function of Poissons ratio. This causes steps to occur in the stress path when the stress state reaches the yield locus. The stress state has to move around the yield locus to the correct point for the start of one-dimensional compression when the soil is yielding. The cycle starts from a state that is slightly overconsolidated, so this step is illustrated in Figure 5.4.18(a) at the start of the one-dimensional compression line. This problem does not occur for the three surface model. Figure 5.4.19 shows a standard plot of K_0 against OCR, defined as the maximum vertical effective stress divided by the current vertical effective stress.

This section shows that the two kinematic surfaces used in the new model significantly influence the predicted behaviour of the model at large deformations within the bounding surface.

5.5 Evaluation of Model

5.5.1 Introduction

The aim of this section is to establish whether the three-surface model is capable of predicting the main characteristics of the stress-strain behaviour of overconsolidated soil. These characteristics were identified from the results of stress path triaxial tests and were reported in section 4.5. The model is used as a numerical experiment with a fixed set of soil parameters representing the behaviour of speswhite kaolin. These were listed at the end of section 5.4.4. Where model predictions are compared with experimental data the model follows the same stress paths that were used in the tests. When appropriate the model predictions are explained with reference to sketches and plots of the position of the three surfaces during loading.

5.5.2 Non-linearity and Inelasticity

The experimental data showed that the stress-strain response of the soil was both highly non-linear and inelastic.

(i) Non-linearity

The non-linear stress-strain response of the soil was observed in all the test data, but it is best illustrated by curves of stiffness against stress change for constant p' and constant q' loading following a complete stress path reversal, $\theta = 180°$. Comparisons between model predictions and experimental data for a constant q' compression path from $p_i' = 100$kPa, $p_m' = 400$kPa and also a constant p' compression path at $p_i' = 300$kPa, $p_m' = 720$kPa are given in Figures 5.5.1 and 5.5.2. These figures also show sketches of the position of the three surfaces at the start of the paths.

The model predicts non-linear stress-strain behaviour for both loading paths. The predicted stiffness curves also show qualitatively the correct difference between the variation in bulk stiffness and shear stiffness with stress change. The way in which the various model parameters influence the predicted change in stiffness with loading was discussed in section 5.4.6. An important factor was the size of the history surface represented by T. When all the parameters are constant, the size of the history surface is dependent on the overall stress history. Hence the overall stress history, for example, the preconsolidation pressure, p_m', will affect the shape of the predicted stiffness versus stress change curve.

(ii) Inelasticity

In Figure 5.5.2 there is a small stress change during which predicted G' is constant, when the loading path passes through the elastic region. This is intended to represent the elastic deformations observed in dynamic tests. The experimental data reported in section 4.5 show that for stress changes and at strain levels greater than those made in dynamic measurements, all deformations are inelastic. In the model, once the yield surface surrounding the elastic region has been reached all predicted deformations are also inelastic.

In section 4.5 two main features of the soil stress-strain response were used as evidence that the deformations were inelastic. These were the strain paths obtained during the tests and the effect of recent stress history. A comparison of strain path data with model predictions is given in section 5.5.3(iii). In section 4.5 it was observed that due to the effect of recent stress history strains could only be conserved for a loading cycle with $\theta = 180°$ at the beginning of the cycle. Data for constant p' cycles confirmed this assumption. Figure 5.5.3(a) shows a comparison between the experimental data and model predictions for these cycles. This comparison illustrates two differences in predicted and experimental behaviour. Firstly, at the end of loading the predicted stiffness is considerably lower than the experimental stiffness resulting in higher shear strains, and secondly, the predicted strains are not conserved during the final cycle, in fact, the model predicts a significant net increase in strain. The predicted stiffness is lower once the stress state reaches the history surface. This is due to the choice of hardening modulus and indicates that further modifications are necessary. These could include using a different form of hardening modulus or two separate values for the exponent ψ. The model will always predict a net increase in shear strain for this type of constant p' cycle, where $\theta = 180°$ for both paths, because the hardening modulus is partially dependent on the distance of the stress state from the bounding surface. Thus, if the recent stress history is constant the soil has a lower stiffness at (2) or (4) than at (3), see Figure 5.5.3(a). Figure 5.5.3(b) shows plots of the positions of the surfaces during the cycles. As mentioned previously, the model does not include time effects such as creep. The creep or secondary consolidation that occurred during the rest period before the final loading stage in the stress path test cancelled out the increase in shear strain during this stage.

5.5.3 Influence of Recent Stress History

The third major characteristic of the stress-strain response, already mentioned above, is that recent stress history affects both the stiffness of the soil and the shape of the strain paths or effective stress paths resulting from drained or undrained loading.

(i) Stiffness

Figure 5.5.4(a) shows predicted stiffness curves for a constant p' compression path at p'_i = 300kPa, p'_m = 720kPa. Plots in q':p' space showing the size and location of the three surfaces at the start and finish of the common loading stage, for each of four different stress path rotations, are given in Figure 5.5.5. This typical set of predictions qualitatively follows the same pattern as the corresponding experimental data shown in Figure 5.5.4(b). The experimental data can only be compared to the predictions for stress changes greater than about 20kPa, particularly for $\theta = 180°$, -90° and 90°, since, at lower stresses the experimental data are unreliable.

One of the main features of the effect of recent stress history which is reproduced by the model is the influence of the stress path rotation, θ, on the stress-strain response of the soil. The initial stiffness is at a maximum when $\theta = 180°$ and at a minimum for $\theta = 0°$. At very low stress changes the maximum stiffness also applies to θ = 90° and $\theta = -90°$. In Figure 5.5.6 values of G' at $\Delta\sigma'/\Delta\sigma'_R = 0.3$ are plotted against θ. The figure includes stiffnesses calculated using the model, for additional values of θ not investigated during this particular test. The graph shows that at this fixed stress level G' decreases as θ decreases and G' is lower for negative rotations.

The second important feature of the effect which is reproduced by the model is that the stiffness decreases relatively smoothly with stress change. At a change in stress, $\Delta\sigma'_R$, shown in Figure 5.5.4, the different stiffness curves converge and the stress-strain behaviour of the model is independent of θ. The way in which the stiffness decreases with change in stress is largely dependent on the detail of the position and size of the three surfaces at the start of loading path. This is in turn dependent on the stress paths before the approach path. The influence of stress paths before the approach path on experimental data has already been recognised and discussed under the heading of approach path length. The importance of this factor to the predicted stiffnesses is best illustrated by contrasting the shapes of the curves for 90° and -90°. The approach path length for θ = 90° was particularly long and the history and yield surfaces are completely re-orientated along this path by the start of the common path, see Figure 5.5.5 (a). As a result the stiffness varies smoothly during loading. The approach path length for $\theta = -90°$ was not long enough for the history and yield surfaces to translate into the correct position by the start of the main loading stage, see Figure 5.5.5 (c). When loaded along the common path the stress state passes through parts of the elastic region and inside the history surface. The resulting stiffness curve has a completely different shape to the curve for 90°. The additional factor determining the variation in stiffness is the size of the surfaces, as noted in section 5.3.2. The model predicts plastic volumetric strains that cause the surfaces to change in size significantly during the test. For example, the surfaces are larger for $\theta = 90°$ than $\theta = 180°$.

In the model the current size of the history surface determines $\Delta\sigma'_R$, the range of influence of recent stress history. Hence $\Delta\sigma'_R$ is largely determined by overall stress history, but also changed when plastic volumetric strains cause the surfaces to change size. It should be noted that the definition $\Delta\sigma'_R = 2Tp'_o$ given in section 5.4.4 is only true for the special case of isotropic compression or swelling. Three of the constant q′ compression tests described in section 4.2.4 (i) started at the same initial value of p′ but the samples had been compressed to different preconsolidation pressures. The estimated values of $\Delta\sigma'_R$ obtained from these tests increase with increasing p'_m, see Figure 4.2.26. This is consistent with the model, but the magnitude of $\Delta\sigma'_R$ predicted by the model is greater than the stress change identified from the experimental data, see for example Figure 5.5.1. The end of the influence of recent stress history is predicted correctly for the shear stiffness data, Figure 5.5.4.

In the model, within the influence of recent stress history, the initial bulk and shear stiffness of a loading path passing though the elastic region is well defined by elastic stiffness parameters. Additionally, the stiffness predicted by the model is generally dependent on θ and $\Delta\sigma'/\Delta\sigma'_R$. Unfortunately it is impossible to determine whether the model predictions are also dependent on state and overconsolidation ratio, ie p′ and R_o. This is because the predictions are very sensitive to the particular location and size of the surface at the start of any loading path and there is no straightforward relationship between the initial elastic stiffness and the subsequent stiffness. As the influence of p' and R_o on stiffnesses within the influence of recent stress history is not well defined experimentally either, no comparisons have been made.

The experimental data indicate that outside the influence of recent stress history, ie for $\theta = 0°$, the bulk modulus is not only dependent on p' but also R_o. Figure 5.5.7 compares experimental data and model predictions showing the variation in normalised stiffness with R_o, represented by p'/p'_m, for four constant q' compression paths starting at states identified by A, B, C and D in Figure 4.2.20. The same pattern of behaviour is predicted by the model.

(ii) Strain paths

Experimental data show that within the influence of recent stress history, the shape of the strain path resulting from a common loading stage is determined by θ. Figure 5.5.8(a) shows a comparison between strain paths predicted by the model and experimental data for a constant p' path at $p'_i = 100$kPa, $p'_m = 150$kPa. The pattern of strain paths predicted by the model is similar to the experimental data, although the predicted strains are greater. This is either because the hardening modulus is incorrect as noted in section 5.5.2 (ii), or because the history surface is too small which causes the shear modulus to decrease rapidly. The strain paths are only curved initially and corresponding curves of strain increment ratio against stress change converge, see Figure 5.5.8(b), after a stress change approximately equal to $\Delta\sigma'_R$.

Figure 5.5.9 shows model predictions for a constant p' path at $p'_i = 100$kPa, $p'_m = 400$kPa compared to experimental data. Once more the predicted strains are too high, but the pattern of strain paths is similar. The significant difference is that the model predicts that for $\theta = 0°$ the heavily overconsolidated soil will dilate. The experimental data clearly shows that the soil initially compresses.

The translation of the history and yield surfaces during a loading stage following a stress path rotation of 90° is illustrated diagrammatically in Figure 5.5.10(a). These plastic potentials can be compared to strain increment vectors plotted from experimental data, Figure 5.5.10(b). This clearly illustrates how the model predicts the same pattern of strain paths that were observed experimentally.

5.5.4 Undrained Compression Tests

Experimental data from undrained compression tests provide a rigorous check on the model which was derived wholly from the results of drained stress path tests. Figure 5.5.11 shows a comparison between predictions and experimental data for the pattern of effective stress paths followed during undrained compression. The effective stress paths are for undrained compression at $p_i' = 200\text{kPa}$, $R_o = 3$. The model predictions are similar to the experimental data except for the stress path for $\theta = 0°$. Again the model predicts that because the soil is dry of critical it will tend to dilate not compress as indicated by the experimental stress path. The model predicts qualitatively the correct variation in undrained shear stiffness with change in stress, particularly at higher stress levels, as shown in Figure 5.5.12.

5.5.5 Different Soils and Time Effects

(i) Different Soils

Richardson (1988) testing a variety of soils observed that the stress-strain response became less sensitive to the effect of recent stress history as the plasticity of the soil decreased. This would be characterised in the model by reducing the relative size of the history surface and would therefore be accompanied by a reduction in the range of influence of the effect. Unfortunately, there were insufficient reliable data to calculate all the model parameters for soils other than speswhite kaolin.

(ii) Time Effects

As stated previously, time effects are not included in the model at present. A possible development of the model to include time effects would be to allow plastic volumetric strains to occur at a constant stress state at a rate controlled by a creep equation. The surfaces would all expand but the stress state would remain stationary. When loading recommenced the soil state would lie inside the elastic region and high stiffnesses would be predicted initially. Creep involving negative plastic volumetric strains would not be possible. Figure 5.5.13 illustrates the process diagrammatically.

5.5.6 Summary

The model predictions reviewed in this section were all obtained using a single set of material parameters. All of these parameters may be derived from appropriate tests as illustrated in section 5.4.4 and with the exception of ψ, they all have a physical meaning.

Qualitatively, the model is capable of correctly predicting the three main characteristics of the behaviour of overconsolidated soils. These are, firstly, that the stress-strain response is highly non-linear, secondly, that except at very low stress levels the deformations are inelastic and thirdly that the stress-strain response is dependent on recent stress history.

The effect of recent stress history on the deformation of the soil, as predicted by the model, has most of the features observed in the experimental data. The predicted stress-strain response is dependent both on θ and $\Delta\sigma'/\Delta\sigma'_R$. The initial stiffness is a maximum for $\theta = 180°$ and a minimum for $\theta = 0°$ and at a certain stress change $\Delta\sigma'_R$ the effect of recent stress history runs out. Generally, at a given stress change, the predicted stiffness decreases with θ, and is lower for negative rotations. The factors which effect $\Delta\sigma'_R$ in the model appear to be consistent with experimental data. Additionally, the model predicts approximately the correct pattern of strain paths and effective stress paths.

Quantitatively, the model predictions are mostly within a factor of two of the experimental data, with some exceptions which are discussed later. An important characteristic of the model, which particularly effects the quantitative predictions of stiffness within the range of the recent stress history effect is the influence of stress paths before the approach path. Outside the influence of recent stress history, i.e. for $\theta = 0°$, predicted curves of bulk stiffness versus stress change for different values of R_0 and p′ followed approximately the same pattern as the experimental data.

As noted above, there are some aspects of the behaviour observed experimentally that the model does not predict well quantitatively. These aspects are listed below.

(a) At stress changes beyond $\Delta\sigma'_R$, i.e. for states on the history surface, the model predicts a fairly rapid decreases in stiffness as the surface approaches the boundary surface, which is not observed in the experimental data. The agreement could be improved by adjusting the expression used for the hardening modulus.

(b) For $\theta = 0°$, i.e. for states outside the influence of recent stress history, the model predicts that strain paths or effective stress paths, from drained or undrained loading respectively, are determined by whether the stress state is dry or wet of critical. The experimental data did not fit this pattern for states dry of critical.

(c) The predicted value of $\Delta\sigma'_R$ for the bulk stiffness data are significantly different from the points identified in section 4.2.4. This may be because the stress change corresponding to $\Delta\sigma'_R$ is not always clearly defined by the experimental stiffness curves.

As discussed in section 5.4.4 the definition of the elastic parameters G'_e and κ used in the model is only an approximation to the experimental data. Unfortunately this is one of the main aspects of the model predictions which cannot be reliably checked against the present experimental data.

The model has not been evaluated for soils other than speswhite kaolin, and does not include time dependent effects such as creep or secondary consolidation. A method has been proposed, however, to expand the model to include these effects. Time effects were just kept constant for sets of tests, they were not eliminated, and are significant when examining the data as a whole.

CHAPTER 6 SUMMARY AND CONCLUSIONS

6.1 Effect of Recent Stress History on the Behaviour of Overconsolidated Soils.

A series of laboratory tests was carried out on both reconstituted and undisturbed soil samples. The tests provided data on the stress-strain response of overconsolidated soil which added to the results obtained by Richardson (1988). The tests used Bishop and Wesley hydraulic stress path cells mostly with standard instrumentation which, with the optimum combination of transducers and load cells, could measure strains accurate to about ±0.004%. Some of the tests on undisturbed soil samples also employed internal strain gauges to improve the reliability of the measurements. The high initial stiffness of the soil in many of the tests meant that the strains being measured were close to or smaller than the limit of the accuracy of the equipment. The results of the tests enable most of the important features of the behaviour to be identified although some details are still unclear.

6.1.1 Typical Characteristics

The stress-strain response of overconsolidated soils loaded along a new stress path is highly non-linear, not elastic (except possibly for very small changes in stress) and dependent on recent stress history, defined by θ, the angle of rotation of the stress path. As the soil is loaded the effect of recent stress history gradually runs out and different stiffnesses or strain increment ratios converge after the same change in stress, $\Delta\sigma'_R$.

The recent stress history determines the stiffness of the soil such that the stiffness is greatest when $\theta = 180°$ and least when $\theta = 0°$. The angle of rotation, θ, also effects the shape of the strain paths, characterised by the strain increment ratio, $d\epsilon_v/d\epsilon_s$. The maximum variation in strain increment ratio is between $\theta = 90°$ and $\theta = -90°$.

These characteristics were originally identified by Richardson (1988) and were confirmed by the results of the stress path triaxial tests carried out as part of this project. The behaviour must be inelastic, firstly because of the different continuously varying strain paths observed during the tests and secondly, because the dependence of the stress-strain response on θ means that strains are not recoverable.

6.1.2 Effect of Recent Stress History on Undisturbed Soil Samples

Stiffnesses and strain paths measured during stress paths applied to samples of undisturbed London clay are sensitive to recent stress history in qualitatively the same way as those measured in tests on reconstituted samples. To determine the details of the behaviour, it is necessary to measure very small strains more accurately than was possible even using internal strain gauges.

6.1.3 Detailed Features of Recent Stress History Effects

A number of stress path triaxial tests have been carried out to investigate different aspects of the recent stress history effect in more detail. These tests were undertaken both as part of this project and by Richardson (1988) and Lewin (1990). The main aspects investigated during this project were the influence of overconsolidation ratio, R_o, and the current mean effective pressure. The data obtained from these tests, which used both constant q′ and constant p′ paths to investigate bulk and shear stiffness, was not always conclusive because of the limited number of tests that were completed and because in many tests the strains were close to the limits of accuracy of the equipment, but they yielded the following observations.

(a) For states within the influence of recent stress history, when θ and $\Delta\sigma'/\Delta\sigma'_R$ are constant, G′ is not simply proportional to p′ or straightforwardly related to R_o.

(b) Outside the influence of recent stress history K′ and probably G′ are proportional to p′ and decrease slightly as R_o decreases.

(c) The range of influence of the recent stress history effect, $\Delta\sigma'_R$, is not solely dependent on p′ but also on R_o.

It was not possible to draw any firm conclusions about the variation of K′ with p′ and R_0, within the range of influence of the effect.

Tests were also carried out with undrained compression as the common loading path. These tests showed that θ has the same type of effect on the effective stress paths obtained from undrained loading as was observed for the strain paths from drained loading. As expected, for approximately equivalent loading paths, plots of strain increment ratio against stress change are mirrored by curves showing variation in gradient of the effective stress path, dp′/dq′, with stress change.

Sets of strain paths obtained from a variety of constant p′ loading paths indicate that R_0 may effect the pattern of strain increment ratio curves within the influence of recent stress history. The effect of R_0 is more significant outside the influence of recent stress history when the paths approach the state boundary surface.

Tests by Richardson (1988) on London Clay confirmed the observations of the influence of p′ and R_0 on G′ given above. Further tests on London Clay established that there is no evidence that the initial compression history of the samples (i.e. isotropic or anisotropic) has any noticeable effect on the different elements of the recent stress history effect. By testing a variety of soils Richardson (1988) found that the effect of recent stress history was accentuated in high plasticity clays.

The true triaxial test carried out by Lewin (1990) showed that the current definition of θ may be inadequate if the behaviour is to be investigated in three-dimensional stress space.

6.2 Modelling the Recent Stress History Effect

A new constitutive soil model has been developed which is an extension of the Modified Cam-clay soil model and was derived from the kinematic yielding models of Al Tabbaa (1987) and Hashiguchi (1985). The model accounts for the small strain behaviour of overconsolidated soils observed in laboratory tests using three nesting yield surfaces.

These three surfaces consist of an outer surface defined by the Modified Cam-clay state boundary surface and two inner kinematic surfaces.

6.2.1 Why Use a Three-surface Model

The three-surface model has two kinematic surfaces inside the state boundary surface. These kinematic surfaces are required to model two major features of the experimental stress-strain data, non-linearity and the effect of recent stress history. One surface is a yield surface, defining the onset of plastic deformations, and the second surface defines the end of the influence of recent stress history. Both surfaces provide a level of memory of previous stress paths. The behaviour predicted by the two-surface model, presented in section 5.3.7, clearly shows that these features are not compatible and cannot be modelled by a single kinematic surface. Additional surfaces would have no physical meaning and are therefore unnecessary.

6.2.2 Model Parameters

The model uses eight soil parameters, M, λ, κ, G'_e, T, S, ψ and a point on the isotropic normal compression line. These are material parameters and they may be evaluated from the results of relatively simple laboratory tests.

The basic critical state parameters M, λ and the point on the isotropic normal compression line may be calculated from the results of standard isotropic and triaxial compression tests. The value of κ, which defines the elastic bulk stiffness in the model, may be calculated from the maximum stiffness at the start of an isotropic swelling or recompression path when $\theta = 180°$. Similarly, the elastic shear modulus, G'_e is the maximum stiffness at the start of a constant p′ path when $\theta = 180°$. It is best to average data from more than one test because inaccuracies in the experimental measurements may be made at these low strain levels. The choice of values for G'_e and κ is also linked to the value of S, which effectively defines the size of the yield surface. Theoretically, the stress change for which the bulk stiffness is constant at the start of an isotropic swelling or recompression loading path, determines the value of the product TS.

In practice this part of the curve is at very small changes of stress and is not measurable in stress path triaxial tests. The value of the product TS has a considerable influence on the predicted shape of shear stiffness versus stress change curves. Therefore, if S is estimated, predicted data should be checked against appropriate shear stiffness curves. The parameter defining the size of the history surface, T, can be derived by comparing the two stiffness against stress change curves obtained from isotropic compression paths when $\theta = 0°$ and $\theta = 180°$. The curves converge at $\Delta\sigma'_R = 2Tp'_0$. Unfortunately the precise stress change equivalent to $\Delta\sigma'_R$ is not always clear and again it may be advisable to check the value for T in the same way. The final parameter ψ which is the exponent in the hardening modulus can only be obtained by trial and error. The correct value of ψ should fit stiffness data for isotropic compression or swelling paths when $\theta = 0°$.

The parametric study showed that the parameters T and ψ and the product TS have the greatest influence on behaviour predicted by the model.

The values of most of the model parameters used in section 5.5 to represent speswhite kaolin were actually selected by using the results of the parametric study to produce a optimum combination. Only M, λ and the point on the isotropic normal compression line were calculated solely using the method outlined above. As discussed above, the parametric study showed the significant influence on the predicted behaviour of the parameters T and ψ and the product TS and confirmed the importance of testing values against both bulk and shear stiffness data. For this set of predictions the value of T fitted the shear stiffness data but not the bulk stiffness data.

6.2.3 Evaluation of Model Predictions Against Experimental Data

The predictions were all obtained using the same set of model parameters. All the non-linearity and effects of recent stress history are in the definition of the three-surface model. Qualitatively the model can predict most aspects of the observed stress-strain response. These are:

(a) Highly non-linear stress-strain behaviour.

(b) Predominantly inelastic deformations.

(c) A stress-strain response that is dependent on θ and $\Delta\sigma'/\Delta\sigma'_R$. For a given stress path when $\theta = 180°$ the initial stiffness is at a maximum and if $\theta = 0°$ the initial stiffness is a minimum. After a stress change $\Delta\sigma'_R$ the effect has run out.

(d) Strain paths and effective stress paths obtained during drained and undrained loading respectively are determined by θ.

(e) A general decrease in stiffness with θ at a given stress change and a lower stiffness if θ is negative.

(f) The variation in $\Delta\sigma'_R$ with overall history for bulk stiffness data.

(g) The effect of p' and R_o on bulk stiffness when $\theta = 0°$.

Quantitatively, the model predictions of the aspects of the behaviour of overconsolidated soils listed above are within a factor of two of the experimental data except when the stress state reaches the history surface, as noted later. An important feature of the predictions that it has not been possible to evaluate against the experimental data is the influence of stress paths previous to the approach path, if the latter is not particularly long. Additionally, it has not been possible to establish whether the model predictions show the same influence of R_o and p' within the influence of recent stress history that was observed in the experimental data. This is because the influence of R_o and p' are not well defined by the experimental data and also because the predictions are very sensitive to other factors such as stress paths previous to the approach path as noted above, which obscure the effect of R_o and p'.

Some aspects of the behaviour are not predicted satisfactorily by the model.

(a) The decrease in stiffness for states on the history surface is too rapid.

(b) Experimentally measured strain paths or effective stress paths for drained or undrained loading at states outside the influence of recent stress history are not purely determined by whether the state is wet or dry of critical. In the model they are.

(c) The predicted values of $\Delta\sigma'_R$ for the bulk stiffness data are too high when a value of T is chosen which fits the shear stiffness data.

Of these problems, only the first can be improved by adjusting the existing model, in this case by modifying the hardening modulus. The other two are inherent characteristics of the model. In comparing the experimental data and predictions it should be noted that the model does not include time effects. Time effects were not eliminated in the stress path tests, just held constant for certain sets of tests.

6.3 Further Work

The research described in this thesis has used laboratory tests to define and clarify the small strain behaviour of overconsolidated soils and derived a new constitutive soil model which predicts all the important features of this behaviour. Nevertheless, there are still some aspects of the soil behaviour which are not understood or well defined and some elements of the model which are unsatisfactory and require further development.

6.3.1 Further Experimental Work

Further experimental data are required, firstly because further developments of the model would require additional data if they were to be evaluated properly and secondly, because some aspects of the behaviour are not well defined, as follows:

(i) The stiffness at the start of a loading path after $\theta = 180°$ when the behaviour may be elastic.

(ii) The effect of recent stress history on soil samples which have been compressed to very high preconsolidation pressures, such as samples of undisturbed London clay.

(iii) The influence of p' and R_0 on the stress-strain response of overconsolidated soils.

The initial stiffness of a soil after $\theta = 180°$ may be determined using dynamic testing techniques or alternatively by making significant improvements to the measurements of strain in a stress path cell. Improvements to the measurement of radial strains can be achieved by using internal gauges similar to the local axial strain gauges. However it is unlikely that significant improvements in the measurement of axial strains are possible.

Stress path tests investigating the effect of rest period and further tests using the true triaxial equipment would be required to evaluate developments in the model.

6.3.2 Further Developments of the Model

Two basic modifications to the model should be carried out, firstly an adjustment of the translation rule which would make it fully consistent with the hardening modulus and secondly some development of the hardening modulus so that it would satisfactorily differentiate between deformation within and outside the influence of recent stress history. The model must also be expanded into general stress space if it is to be installed in a finite element program. A further addition to the model would be to include the effect of rest period on the stiffness of overconsolidated soils.

The ultimate aim of this work is to obtain better predictions of ground movements around structures constructed in overconsolidated soils. To quantify the improvement in the prediction of ground movements offered by the type of non-linear model proposed in this thesis, the model must be installed in a finite element program and evaluated for boundary value problems. It would then be possible to establish the significance of inaccuracies in the model and hence the relative importance of carrying out the various items of further work discussed above.

6.4 Conclusions

The stress-strain behaviour of overconsolidated soil is basically inelastic, although there may be a very small elastic region, and highly non-linear. For new loading paths, at small strains or relatively small stress changes, the stress-strain response is significantly influenced by recent stress history.

A new constitutive soil model has been developed, which can account for all the basic features of the experimentally observed behaviour. The inelastic behaviour is modelled by elasto-plastic yielding and hardening inside the state boundary surface which is controlled by two kinematic yield surfaces. One of these surfaces defines the limit of elastic behaviour and the second the extent of the influence of recent stress history. Both surfaces model the effect of recent stress history. The model requires only eight basic soil parameters which are all soil properties.

The basic characteristics of the stress-strain behaviour of overconsolidated soil, given above, were confirmed and more detailed aspects of the behaviour investigated using a program of stress path triaxial tests on reconstituted and undisturbed soil samples. The resulting experimental data provided, an increased understanding of the effect of recent stress history on strain paths and undrained effective stress paths, data confirming that undisturbed samples are affected by recent stress history in qualitatively the same way as reconstituted samples and some data on the influence of p' and R_0. The tests also enabled the model parameters to be evaluated for speswhite kaolin.

The main limitations of the work are as follows:

(i) The understanding of the soil behaviour obtained from laboratory tests is incomplete, particularly the behaviour at very small strains and the effect of p' and R_o.

(ii) The model requires further development primarily the modification of the translation rule and hardening modulus and the extension of the model into general stress space.

APPENDIX I - Flowchart for the computer program SECUNDUS.

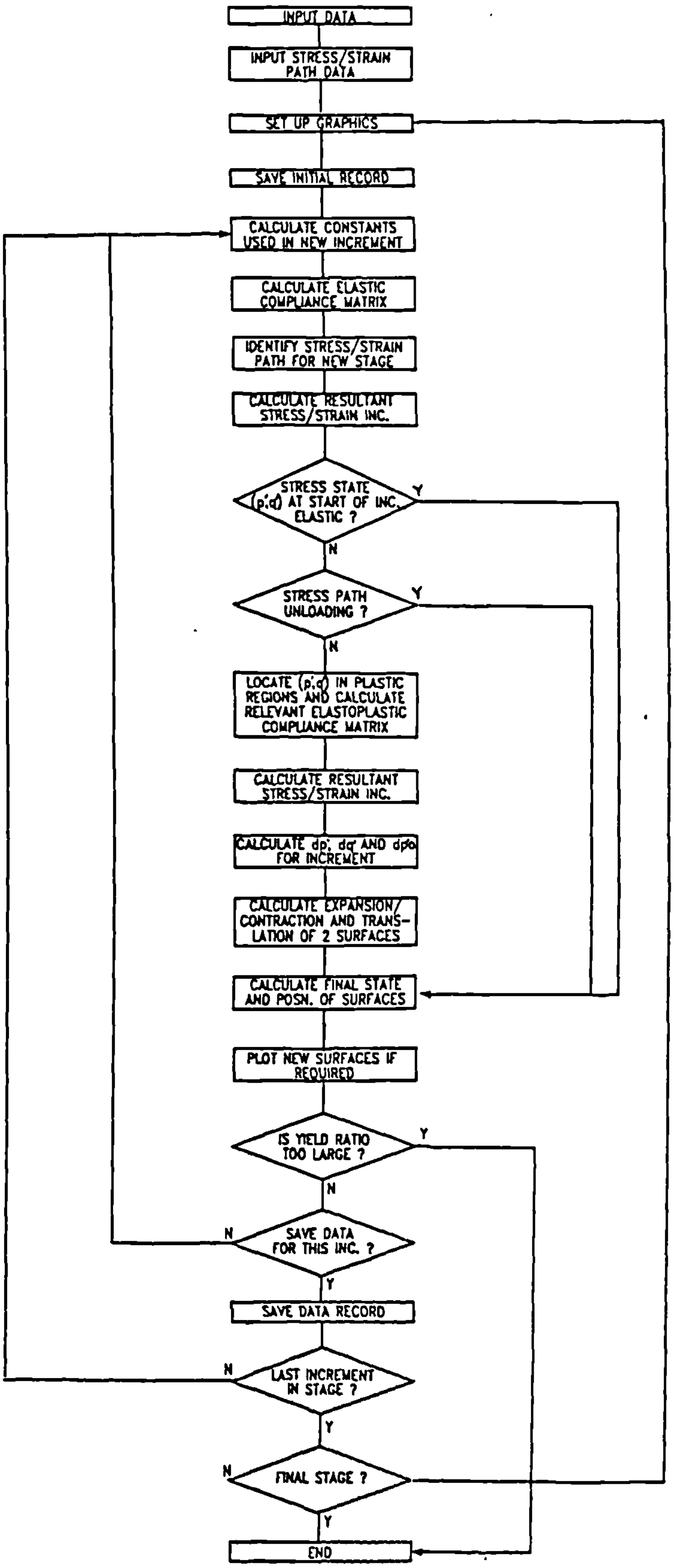

APPENDIX II - Flowchart for the computer program TERTIUS.

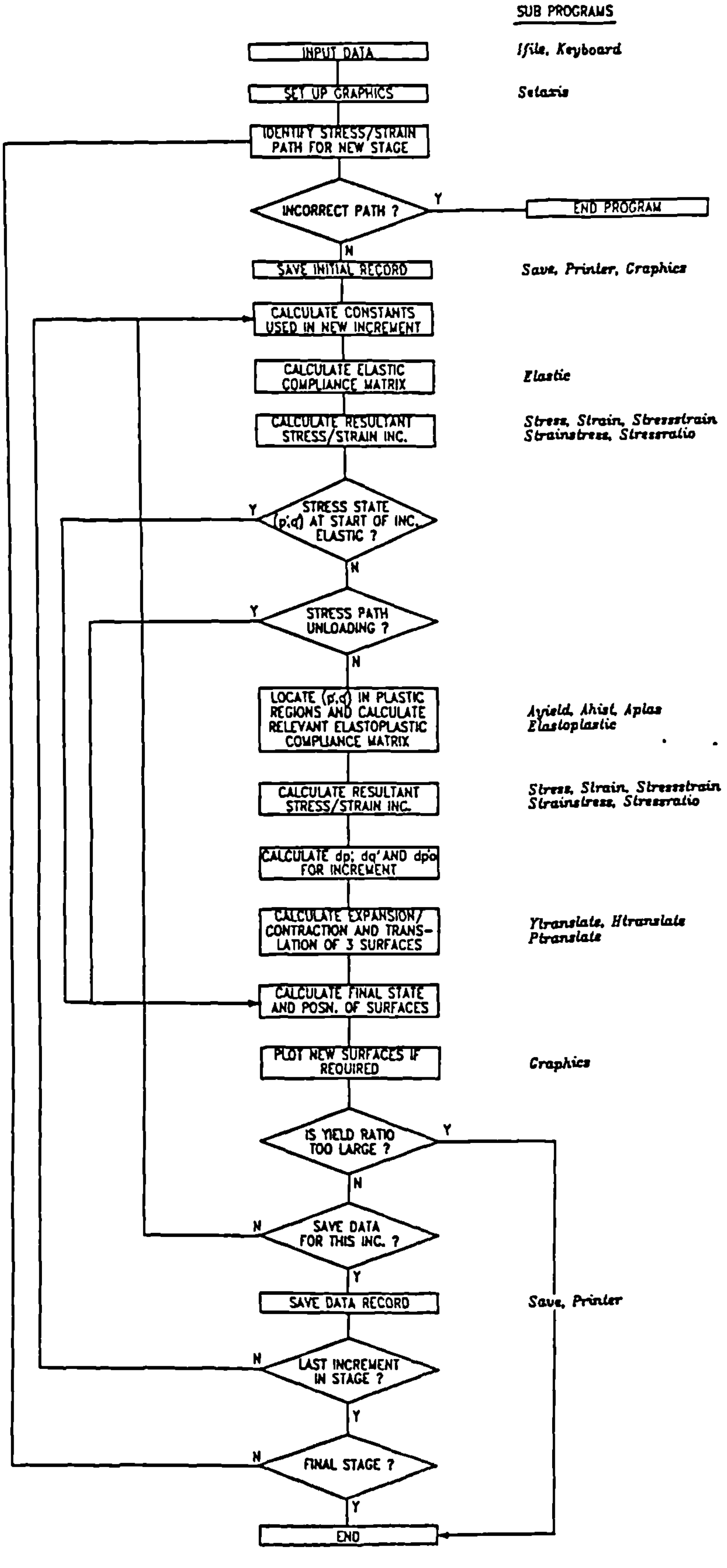

REFERENCES

Ackerly, S.K., Hellings, J.E. and Jardine, R.J. (1987). Discussion on: Clayton, C.R.I. and Khatrush, S.A. (1986). A new device for measuring local axial strains on triaxial specimens. Geotechnique, Vol. 37, No. 3, pp. 414-415.

Al Tabbaa, A. (1987). Permeability and stress-strain response of speswhite kaolin. Ph.D. Thesis, University of Cambridge.

Al Tabbaa, A. and Wood, D.M. (1989). An experimentally based "bubble" model for clay. Proc. Third Int. Conf. on Numerical Models in Geomechanics. Niagara Falls.

Atkinson, J.H. (1973). The deformation of undisturbed London Clay. Ph.D. Thesis, University of London.

Atkinson, J.H. (1983). Effects of stress path and stress history on the stiffness of soils near trenches. Geotechnical Engineering Research Centre Research Report GE/83/7. The City University.

Atkinson, J.H. (1984). Rate of loading in drained and undrained stress path and triaxial tests. Geotechnical Engineering Research Centre Research Report GE/84/1. The City University.

Atkinson, J.H. (1985). Simple and inexpensive pressure control equipment for conventional and stress path triaxial testing of soils. Geotechnique. Vol. 35, No. 1, pp. 61-63.

Atkinson, J.H. and Bransby, P.L. (1978). The Mechanics of Soils. McGraw-Hill, London.

Atkinson, J.H. and Evans, J.S. (1985). Discussion on: Jardine, R.J., Symes, M.J.R.P. and Burland, J.B. (1984). The measurement of soil stiffness in the triaxial apparatus. Geotechnique, Vol. 35, No. 3, pp. 378-382.

Atkinson, J.H., Evans, J.S. and Ho, E.W.L. (1985). Non-uniformity of triaxial samples due to consolidation with radial drainage. Geotechnique, Vol. 35, No. 3, pp. 353-355.

Atkinson, J.H., Evans, J.S. and Scott, C.R. (1983). Development of a new microcomputer based controller for stress path testing. Geotechnical Engineering Research Centre Research Report GE/83/2. The City University.

Atkinson, J.H., Evans, J.S. and Scott, C.R. (1984). Developments in stress path testing equipment for measurement of soil parameters. Geotechnical Engineering Research Centre Research Report GE/84/2. The City University.

Atkinson, J.H. and Richardson, D. (1985). Elasticity and normality in soil - experimental examinations. Geotechnique, Vol. 35, No. 4, pp. 443-450.

Atkinson, J.H., Richardson, D. and Robinson, P.J. (1987). Compression and extension of K_0 normally consolidated kaolin clay. ASCE. Journal of Geotechnical Engineering, Vol. 113, No. 12, pp. 1468-1482.

Atkinson, J.H., Richardson, D. and Stallebrass, S.E. (1990). Effect of recent stress history on the stiffness of overconsolidated soil. Geotechnique. To be published.

Balasubramaniam, A.S. (1976). Local strains and displacement patterns in triaxial specimens of a saturated clay. Soils and Foundations, Vol. 16, No. 1, pp. 101-114.

Bishop, A.W. and Henkel, D.J. (1962). The Measurement of Soil Properties in the Triaxial Test. Edward Arnold, London.

Bishop, A.W. and Wesley, L.D. (1975). A hydraulic triaxial apparatus for controlled stress path testing. Geotechnique, Vol. 25, No. 4, pp. 657-670.

Brown, S.F. and Snaith, M.S. (1974). The measurement of recoverable and irrecoverable deformation in the repeated load triaxial test. Geotechnique, Vol. 24, No. 2, pp. 255-259.

Bullen and Partners (1989). Personal communication.

Burland, J.B., Simpson, B. and St John, H.D. (1979). Measurements around excavations in London Clay. Proc. Seventh Eur. Conf. Soil Mechanics, Brighton. Vol. 1, pp. 13-29.

Burland, J.B. and Symes, M.J.R.P. (1982). A simple displacement gauge for use in the triaxial apparatus. Geotechnique, Vol. 32, No. 1, pp.62-64.

Butterfield, R. (1979). A natural compression law for soils. Geotechnique, Vol. 29, No. 4, pp. 469-480.

Cherrill, H.E. (1990). Personal communication.

Clayton, C.R.I. and Khatrush, S.A. (1986). A new device for measuring local axial strains on triaxial specimens. Geotechnique, Vol. 36, No. 4, pp. 593-597.

Clayton, C.R.I., Khatrush, S.A., Bica, A.V.D. and Siddique, A. (1988). The use of Hall effect semiconductors in geotechnical instrumentation. ASTM, Geotechnical Testing Journal, Vol. 12, No. 1, pp. 69-76.

Clinton, D.B. (1987). The determination of soil parameters for design from stress path tests. Ph.D. Thesis, The City University.

Costa Filho, L. de M. (1979). Discussion: Design parameters for soft clays. Proc. Seventh Eur. Conf. Soil Mechanics, Brighton. Vol. 4, pp. 125-128.

Costa Filho, L. de M. (1985). Measurement of axial strains in triaxial tests on London clay. ASTM, Geotechnical Testing Journal, Vol. 8, No. 1, pp. 3-13.

Costa Filho, L. de M. and Vaughan, P.R. (1980). Discussion on: Simpson, B., O'Riordan, N.J. and Croft, D.D. (1979). A computer model for the analysis of ground movements in London clay. Geotechnique, Vol. 30, No. 3, pp. 336-339.

Dafalias, Y.R. and Herrmann, L.R. (1982). Bounding surface formulation of soil plasticity in Pande, G.N. and Zienkiewicz, O.C. (Ed). Soil Mechanics - Transient and Cyclic Loads. John Wiley and Sons. Chichester.

Davis, E.H. and Poulos, H.G. (1968). The use of elastic theory for settlement and predictions under three-dimensional conditions. Geotechnique, Vol. 18, No. 1, pp. 67-91.

Duncan, J.M. and Chang, C-Y. (1970). Non-linear analysis of stress and strain in soils. ASCE. Journal of the Soil Mech. and Fdn. Eng. Div., Vol. 96, SM5, pp. 1629-1653.

Gibson, R.E. (1974). The analytical method in soil mechanics. The Fourteenth Rankine Lecture. Geotechnique, Vol. 24, No. 1, pp. 115-140.

Graham, J. and Houlsby, G.T. (1983). Anisotropic elasticity of a natural clay. Geotechnique, Vol. 33, No. 2, pp. 165-180.

Graham, J.H., Crooks, A. and Lau, S.L.K. (1988). Yield envelopes: Identification and geometric properties. Geotechnique, Vol. 38, No. 1, pp. 125-134.

Hashiguchi, K. (1985) Two- and three-surface models of plasticity. Proc. Fifth Int. Conf. on Numerical Methods in Geomechanics, Nagoya, pp. 285-292.

Hight, D. W., Gens, A. and Jardine, R.J. (1985). Evaluation of geotechnical parameters from triaxial tests on offshore clay. Soc. Underwater Technology Conf. on Offshore Site Investigations, London.

Hird, C.C. and Yung, P. (1987). Discussion on: A new device for measuring local axial strains on triaxial specimens. Clayton, C.R.I. and Khatrush, S.A. (1986). *Geotechnique*, Vol. 37, No. 3, pp. 413-414.

Ho, E.W.L. (1988). Geotechnical properties of deep-ocean sediments: a critical state approach. Ph.D. Thesis, The City University.

Houlsby, G.T., Wroth, C.P. and Wood, D.M. (1982). Predictions of the results of laboratory tests on a clay using a critical state model. Proc. Int. Workshop on Constitutive Behaviour of Soils, Grenoble, pp. 99-121. Balkema, Rotterdam.

Isenhower, W.M. (1979). Tortional simple shear/resonant column properties of San Francisco Bay mud. Ms. Thesis, University of Texas, Austin.

Jardine, R.J. (1985). Investigations of pile-soil behaviour with special reference to the foundations of offshore structures. Ph.D. Thesis, University of London.

Jardine, R.J. and Potts, D.M. (1988). Hutton tension leg platform foundations: prediction of driven pile behaviour. Geotechnique, Vol. 38, No. 2, pp. 231-252.

Jardine, R.J., Potts, D.M., Fourie, A.B. and Burland, J.B. (1986). Studies of the influence of non-linear stress-strain characteristics in soil-structures interaction, Geotechnique, Vol. 36, No. 3, pp. 377-396.

Jardine, R.J., Potts, D.M., Hight, D.W. and Burland, J.B. (1985). Assessing the safety of offshore piles by displacement monitoring. Proc. Conf. Behaviour of Offshore Structures, pp. 611-622. Elsevier Science Publishers B.V., Amsterdam.

Jardine, R.J., Symes, M.J.R.P. and Burland, J.B. (1984). The measurement of soil stiffness in the triaxial apparatus. Geotechnique, Vol. 34, No. 3, pp. 323-340.

Lau, W.H.W. (1988). The behaviour of clay in simple shear and triaxial tests. Ph.D. Thesis. The City University.

Lewin, P.I. (1990). Private communication.

Lewin, P.I. and Burland, J.B. (1970). Stress probe experiments on satuarated normally consolidated clay. Geotechnique, Vol. 20, No. 1, pp. 38-56.

Love, A.E.H. (1942). A Treatise on the Mathematical Theory of Elasticity. 2 Vols. Cambridge University Press.

Menzies, B. K., Sutton, H. and Davies, R.E. (1977). A new system for automatically simulating K_0 consolidation and K_0 swelling in the conventional triaxial cell. Geotechnique, Vol. 27, No. 4, pp. 593-596.

Mröz, Z. and Norris, V.A. (1982). Elastoplastic and viscoplastic constitutive models for soils with application to cyclic loading in Pande, G.N. and Zienkiewicz, O.C. (Ed). Soil Mechanics - Transient and Cyclic Loads. John Wiley and Sons.

Mröz, Z., Norris, V.A. and Zienkiewicz, O.C. (1979). Application of an anisotropic hardening model in the analysis of elasto-plastic deformation of soils. Geotechnique, Vol. 29, No. 1, pp. 1-34.

Mröz, Z., Norris, V.A. and Zienkiewicz, O.C. (1981). An anisotropic, critical state model for soils subject to cyclic loading. Geotechnique, Vol. 31, No. 4, pp. 451-469.

Nova, R. (1982). A constitutive model for soil under monotonic and cyclic loading in Pande, G.N. and Zienkiewicz, O.C. (Ed). Soil Mechanics - Transient and Cyclic Loads. John Wiley and Sons. Chichester.

O'Connor, K.J.P. (1990). Personal communication.

Parry, R.H.G. and Nadarajah, V. (1973). A volumetric yield locus for lightly overconsolidated clays. Geotechnique, Vol. 23, No. 3, pp. 450-453.

Pender, M.J. (1978). A model for the behaviour of overconsolidated soil. Geotechnique, Vol. 28, No. 1, pp. 1-25.

Pender, M.J. (1982). A model for the cyclic loading of overconsolidated soil in Pande, G.N. and Zienkiewicz, O.C. (Ed). Soil Mechanics - Transient and Cyclic Loads. John Wiley and Sons. Chichester.

Pickering, D.J. (1970). Anisotropic elastic parameters for soil. Geotechnique, Vol. 20, No. 3, pp. 271-276.

Pickles, A.R. (1989). The application of critical state soil mechanics to predict ground deformations below an embankment constructed on soft alluvium. Ph.D. Thesis. The City University.

Rampello, S. (1989). Effeti del rigonfiamento sul comportamento meccanico di argille fortemente sovraconsolidate. Ph.D. Thesis. University of Rome.

Richardson, D. (1988). Investigations of threshold effects in soil deformations. Ph.D. Thesis. The City University.

Richart, F.E., Hall, J.R. and Woods, R.D. (1970). Vibration of Soils and Foundations. Prentice-Hall Inc., New Jersey.

Roscoe, K.H. and Burland, J.B. (1968). On the generalised stress-strain behaviour of "wet" clay. Engineering Plasticity. Cambridge University Press.

Schofield, A.N. and Wroth, C.P. (1968). Critical State Soil Mechanics. McGraw-Hill, London.

Schulteiss, P.J. (1981). Simultaneous measurements of P and S wave velocities during conventional laboratory testing procedures. Marine Geotechnology, Vol. 4, No. 4, pp. 343-367.

Skempton, A.W. and Henkel, D.J. (1957). Tests on London Clay from deep borings at Paddington, Victoria and the South Bank. Proc. Fourth Int. Conf. Soil Mechanics, London, Vol. 1, pp. 100-106.

Simpson, B., O'Riordan, N.J. and Croft, D.D. (1979). A computer model for the analysis of ground movements in London Clay. Geotechnique, Vol. 29, No.2, pp. 149-175.

Som, N.N. (1968). The effect of stress path on the deformation and consolidation of London Clay. Ph.D. Thesis, University of London.

Stallebrass, S.E. (1990a). Stress path tests on undisturbed London clay using local axial strain gauges. Geotechnical Engineering Research Centre Research Report GE/90/22. The City University.

Stallebrass, S.E. (1990b). Operator manual for the computer programs SECUNDUS and TERTIUS. Geotechnical Engineering Research Centre Research Report GE/90/23. The City University.

Sun, J.I., Golesorkhi, R. and Bolton Seed, H. (1988). Dynamic moduli and damping ratios for cohesive soils. Earthquake Engineering Research Centre Research Report UCB/EERC-88/15. University of California.

Viggiani, G. (1990). Personal communication.

Webb, D.L. (1967). The mechanical properties of undisturbed samples of London Clay and Pierre shale. Ph.D. Thesis, University of London.

Wroth, C.P. (1971). Some aspects of the elastic behaviour of overconsolidated clay. Proc. Roscoe Memorial Symp., Foulis, pp. 347-361.

Zytinski, M., Randolph, M.F., Nova, R. and Wroth, C.P. (1978). On modelling the unloading - reloading behaviour of soils. Int. Journal for Numerical and Analytical Methods in Geomechanics, Vol. 2, pp. 87-94.

Control system/ cell type	Transducer	Resolution (kPa)	Sources of Error				Overall[2] Accuracy
			Noise (kPa)	Hysteresis % reading	Drift[1] % reading	Non-linearity % reading	
Spectra (38mm)	Imperial College Load cell	0.027	±1.4	±0.2	±0.2	±0.3	±1.4 kPa ±0.8%
IBM (200mm)	Imperial College Load cell	0.08	±0.2	±0.2	±0.1	±0.3	±0.2 kPa ±0.6%
BBC (38mm)	Surrey University Load cell	0.5	±1.5	±0.4	±0.2	±0.1	±1.5 kPa ±0.7%
Spectra/ BBC/IBM	Pore or cell pressure transducer	0.03/0.4 /0.03	±0.2	±0.2	-	±0.4	± 0.2 kPa ±0.6%

(a)

Control system/ cell type	Transducer	Resolution (%)	Sources of Error				Overall[2] Accuracy
			Noise (%)	Hysteresis % reading	Drift[1] % reading	Non-linearity % reading	
Spectra	Axial strain -Resistance[3]	0.002	±0.01	-	±0.02	±0.2	±0.01% ±0.22%
	Volume strain -Resistance[3]	0.004	±0.01	-	±0.05	±0.5	±0.01% ±0.55%
BBC	Axial strain — LVDT[4]	0.0005	±0.002	-	±0.03	±0.4	±0.002% ±0.43%
	Volume strain - LVDT[4]	0.001	±0.005	-	±0.1 (±0.5)	±0.2	±0.005% ±0.3% (±0.7)
	Local axial strains- Hall effect	0.001	±0.004	-	±0.7	±0.4	±0.004% ±1.1%
IBM	Axial strain - LVDT[4]	0.0001	±0.001	-	±0.03	±0.2	±0.001% ±0.23%
	Volume strain - LVDT[4]	0.002	±0.002	-	±0.02 (±0.1)	±0.2	±0.005% ±0.22% (±0.3)
	Local axial strains Hall effect	0.001	±0.004	-	±0.7	±0.4	±0.004% ±1.1%

(b)

Notes
1. The percentage error due to drift is calculated as discussed in section 3.2.3
2. Overall accuracy consists of the absolute error due to noise plus the percentage error due to hysteresis, drift and non-linearity.
3. The resistance transducers were MPE LSC TypeHS.
4. The LVDTs were from RDP Electronics, type LDC500A

Table 3.2.1 Tables showing the accuracy of (a) stress and (b) strain transducers

Soil	Test numbers	t_{100} (hours)
London Clay – undisturbed	TT1-4	6
	LAS5	2.6
	DLC4	6
London Clay – reconstituted	ULC1, ULC2	1.6
Speswhite kaolin	UK5-7, DKP1, DKSR1, DKSR3	0.08

(a)

Soil	Critical state parameters ^{2}				References
	M_e	M_c	λ^1	N^1	
London Clay	0.692	0.89	0.157	2.710	Richardson (1988)
Speswhite kaolin	0.85	0.85	0.19		Atkinson et al. (1987)
			0.19	3.29	Richardson (1988)

Notes:
1. λ and N derived from conventional v:lnp' plots.
2. The definition of κ changes between references and so values for κ are not given here

(b)

Table 3.3.1 (a) t_{100} of soil used in stress path tests. (b) Typical critical state parameters for London Clay and speswhite kaolin.

Test No	Site	Depth (m)	Sampling Technique	Estimated In Situ Stress State			Initial Water Content
				σ'_v (kPa)	σ'_h (kPa)	p'_m (kPa)	
TT1	N.E London (Site 1)	15-15.45	Thin-walled tube	200	280	c. 650	0.310
TT2	N.E. London (Site 1)	15-15.45	Thin-walled tube	200	280	c. 650	0.288
TT3	N.E London (Site 1)	15-15.45	Thin-walled tube	200	280	c. 650	0.308
TT4	N.E London (Site 1)	15-15.45	Thin-walled tube	200	280	c. 650	0.317
LAS5	Central London (Site 2)	7-7.6	Thin-walled tube	100	110	c. 1900	0.291
DLC4	Central London (Site 3)	30.25-30.52	Rotary coring	425	490	c. 2200	0.245

Table 3.3.2 Location and estimated in situ state of undisturbed samples of London clay

Test No	Soil	Sample type	Initial state			Final state		
			p'_o (kPa)	q'_o (kPa)	v_o	p'_f (kPa)	q'_f (kPa)	v_f
TT1	London clay	Undisturbed	300	0	1.853	253	19	1.849
TT2			344	0	1.792	450	0	1.770
TT3			248	0	1.848	250	183	1.813
TT4			203	0	1.872	200	0	1.803
LAS5			152	0	1.800	200	−105	1.795
DLC4			212	0	1.674	300	119.7	1.666
ULC1	London clay	Reconstituted	20	0	2.460	286.5	224.7	1.979
ULC2			20	0	2.485	208.6	140	2.018
UK5	Speswhite kaolin	Reconstituted	18	0	2.493	200	0	2.046
UK6			16	0	2.451	200	−150	2.021
UK7			20	0	2.462	227	200	1.984
DKP1	Speswhite kaolin	Reconstituted	18	0	2.430	134.6	111	2.078
DKSR1			16	0	2.378	147	136	2.076
DKSR3			25	0	2.455	300	150	2.005

Table 3.6.1 Initial and final states of soil samples used in all stress path tests

Test No	common path						rotations θ°	approach path length (kPa)	rest period (hrs)
	Type	p'_i (kPa)	q'_i (kPa)	p'_m (kPa)	length (kPa)	loading rate (kPa/hr)			
TT1	constant p' comp.	253.3	−80	c.650	99	3	−90, 141.5	99/100	4/2
TT2	constant q' comp	350	0	c.650	100	4	180, 158.2	150	2
TT3	constant q' swelling	350	0	c.650	−150	3	38.7, 90, 135, 0, 180	150	2
TT4	constant p' comp.	350	0	c.650	150	7.5	128.7, 45, 90, 0, 180	150	2/3
LAS5	constant p' comp	200	0	c.1900	105	3	90, −90, 180	100/105	40/22 /20
DLC4	constant p' comp.	300	0	c.2200	120	4.8	0, −90, 90 180	120	24

Table 3.6.2 (a) Description of tests on samples of undisturbed London clay

Test No	common path						rotations θ°	approach path length (kPa)	rest period (hrs)
	Type	p'_i (kPa)	q'_i (kPa)	p'_m (kPa)	length (kPa)	loading rate (kPa/hr)			
ULC1	undrained comp.	200	0	663.5	150	3	90	100	22
ULC2	undrained comp	200	0	663.5	150	3	−90	100	23
UK5	undrained comp	200	0	663.5	150	5	−90, 90	100	27/28
UK6	undrained comp.	200	0	663.5	150	5	180	100	27
UK7	undrained comp	200	0	663.5	150/ 100	5	0, 180, 90 −90, 0	100/96	27

Table 3.6.2 (b) Description of tests with an undrained common stress path using samples of reconstituted soil,

Test No	common path						rotations θ°	approach path length (kPa)	rest period (hrs)
	Type	p'_i (kPa)	q'_i (kPa)	p'_m (kPa)	length (kPa)	loading rate (kPa/hr)			
DKP1	constant p' comp.	100	0	150	60	4.8	90, 0, -90, 180	50/60	12/14
	constant p' comp.	100	0	400	60	4.8	-90, 0, -90 180, 90	50/60	11/16
DKSR1	constant q' comp.	100	0	200	100	1	0, 180	50/100	48
	constant q' comp.	100	0	300	100	1	0, 180	50/100	24
DKSR3	constant q' comp.	100	0	400	100	1	0, 180	50/100	24
	constant q' comp.	200	0	400	100	1	0, 180	100	24
	constant p' comp.	300	0	720	150	4.2	90, 0, -90 180	150/200	11.5

Table 3.6.2 (c) Description of drained, constant p' and constant q' tests on samples of reconstituted soil.

Test No	Common path	p'i (kPa)	q'i (kPa)	p'm (kPa)
TT1	constant p'	253.3	-80	c. 650
TT2	constant q'	350	0	c. 650
TT3	constant q'	350	0	c. 650
TT4	constant p'	350	0	c. 650
LAS5	constant p'	200	0	c. 1900
DLC4	constant p'	300	0	c. 2200

Table 4.2.1 Table showing the estimated overall history and the state at the start of the common path for the six tests on undisturbed London clay

Test type	Number of deviations of path	Soil	Number of tests
Isotropic compression and swelling only		Slate dust	3
		Ware till	2
		Speswhite kaolin	2
		Cowden till	2
		London Clay	7
Stress path threshold tests.	8	Slate dust	5
Constant p', increasing q' paths.	14	Ware till	6
p' = 200kPa, overconsolidation ratio = 2.	8	Speswhite kaolin	5
Isotropically compressed.	8	Cowden till	4
	18	London Clay	15
Stress path threshold tests , isotropically compressed.		London Clay	
(constant p', q' increasing paths).			
Overconsolidation ratio's = 1.5, 4, 8.	4 each		3
Total stress path deviations.	4 each		2
Extended rest periods (two periods).	3		3
Length of approach path (5 lengths).	1		1
Tests with OCR = 2.0 and p' = 100,300kPa.	4		2
Stress path threshold tests , isotropically compressed.		London Clay	
Constant p', q' reducing path.	4		1
Constant q', p' increasing path.	4		1
Constant q', p' reducing path.	4		1
Compressed with:- $\eta'_0 = 0.25$	5	London Clay	1
$\eta'_0 = 0.75$	5		1
η'_0 = two dimensional	5		1
One dimensionally compressed.		London Clay	
Constant p', q' increasing paths with			
Overconsolidation ratios = 1.5, 2.0, 4.0, 8.0.	5 each		4

Table 4.3.1 Summary of tests conducted by Richardson (1988) to investigate the influence of recent stress history. (after Richardson, 1988)

Rest period (hrs)	Initial normalised stiffness of sample $\frac{\delta q'}{vp'\,\delta\varepsilon_s}$ $(\Delta\eta' = 0.05)$	θ°
3	98	0
241	174	
3	412	90
48	607	
246	749	
3	765	180
242	1303	

Table 4.3.2 The effect of periods of rest on the stiffness of London clay (after Richardson, 1988)

M	λ	κ	R	ψ	ν
0.85	0.073	0.007	0.01	1.5	0.3
0.85	0.073	0.007	0.1	1.5	0.3
0.85	0.073	0.007	0.2	1.5	0.3
0.85	0.073	0.002	0.1	1.5	0.3
0.85	0.073	0.002	0.2	1.5	0.3
0.85	0.073	0.007	0.1	1	0.3
0.85	0.073	0.007	0.1	3	0.3

Table 5.3.1 Combinations of model parameters used to evaluate the two-surface model.

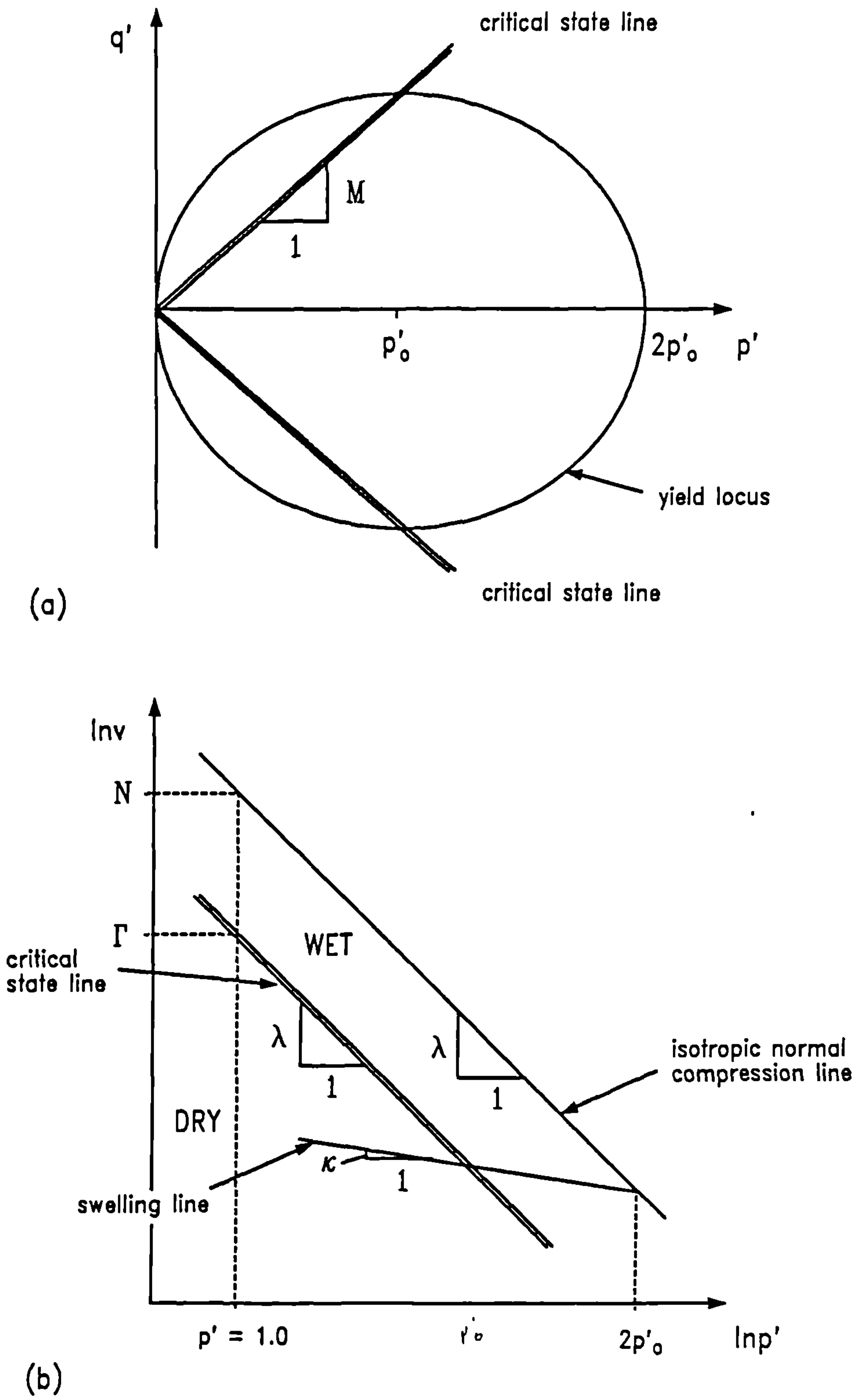

Figure 1.2.1 Diagram defining the main parameters used in the Modified Cam-clay model.

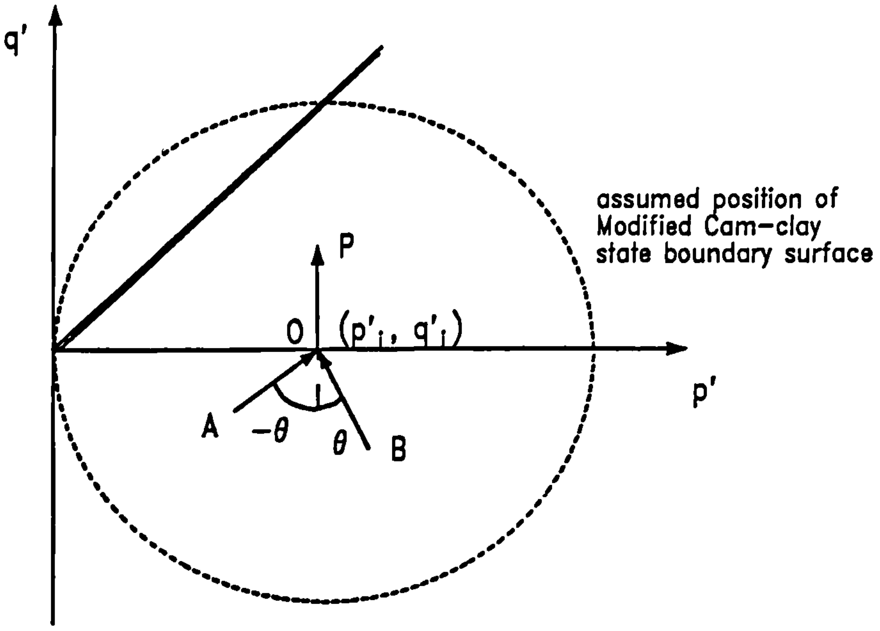

Figure 1.2.2 Diagram showing a typical set of stress probes for the basic test to investigate the recent stress history effect

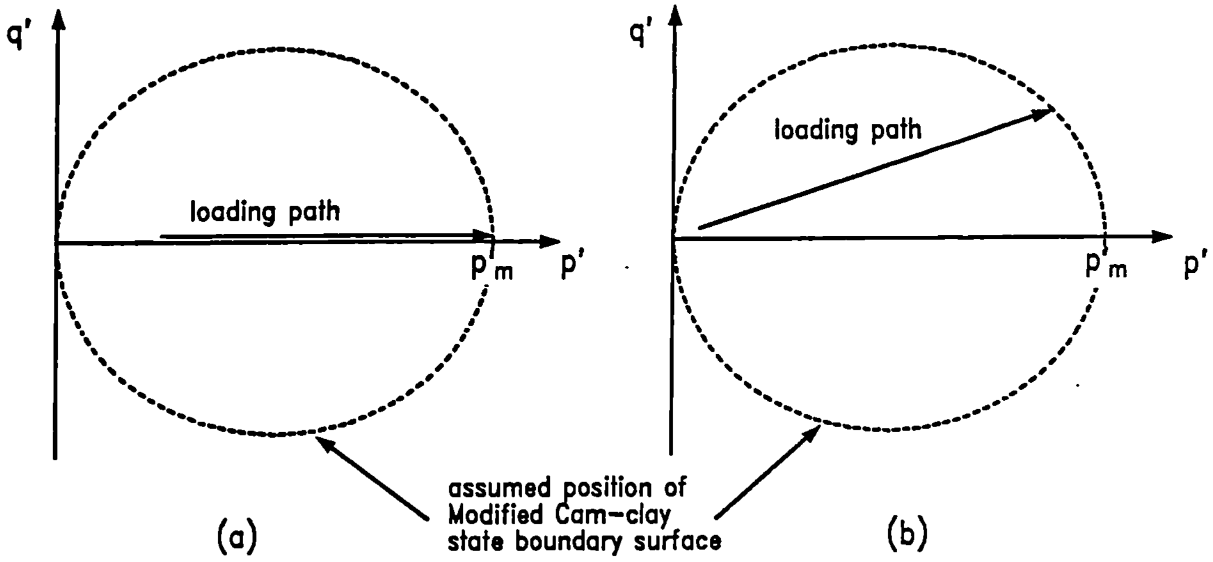

Figure 1.2.3 Diagram showing the definition of p'm for (a) isotropic and (b) anisotropic loading

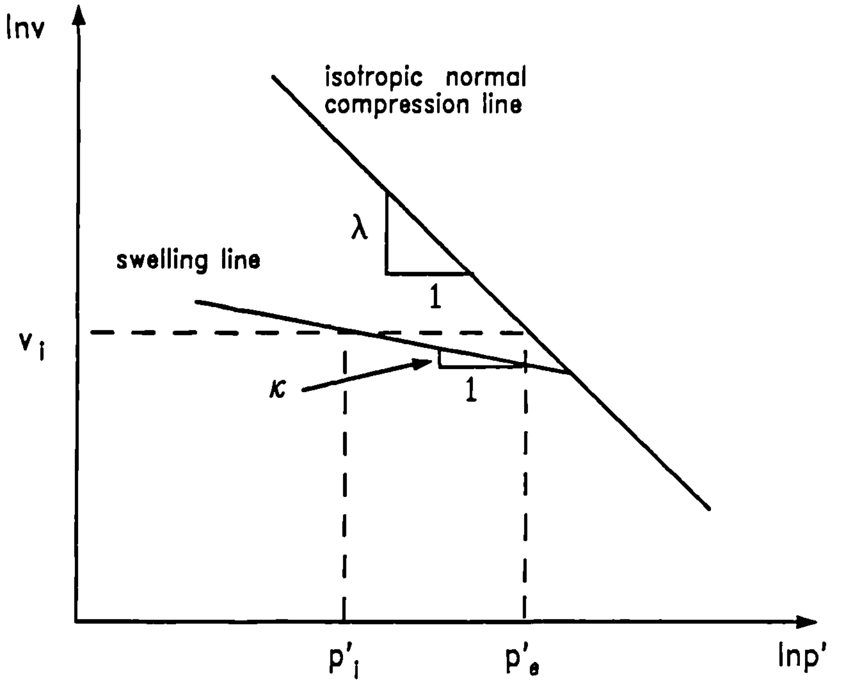

Figure 1.2.4 Diagram defining p'_e, the equivalent pressure in lnv : lnp' space

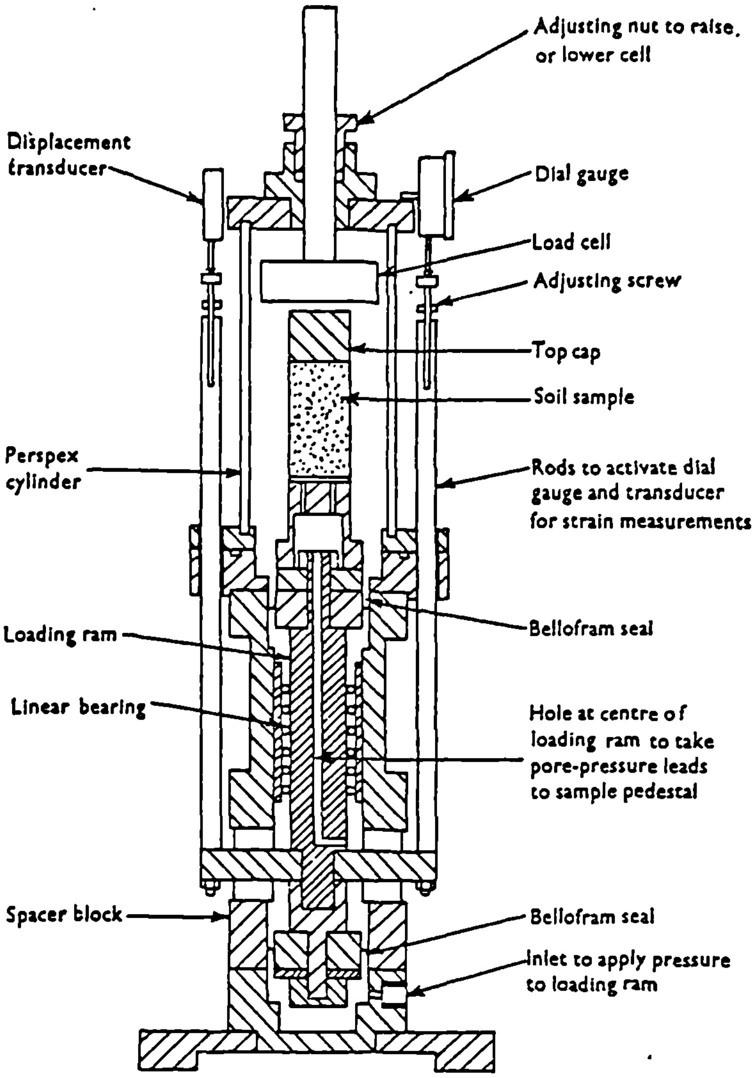

Figure 2.2.1 Cross-section of the hydraulic stress path cell (after Bishop and Wesley, 1975).

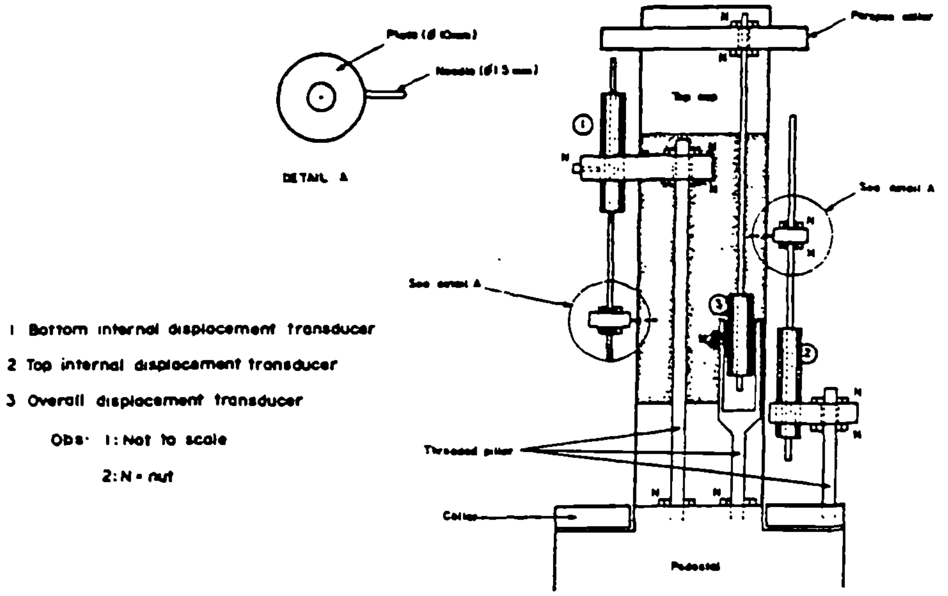

Figure 2.2.2 General arrangement for the measurement of axial strains inside the cell using miniature LVDTs (after Costa Filho, 1985)

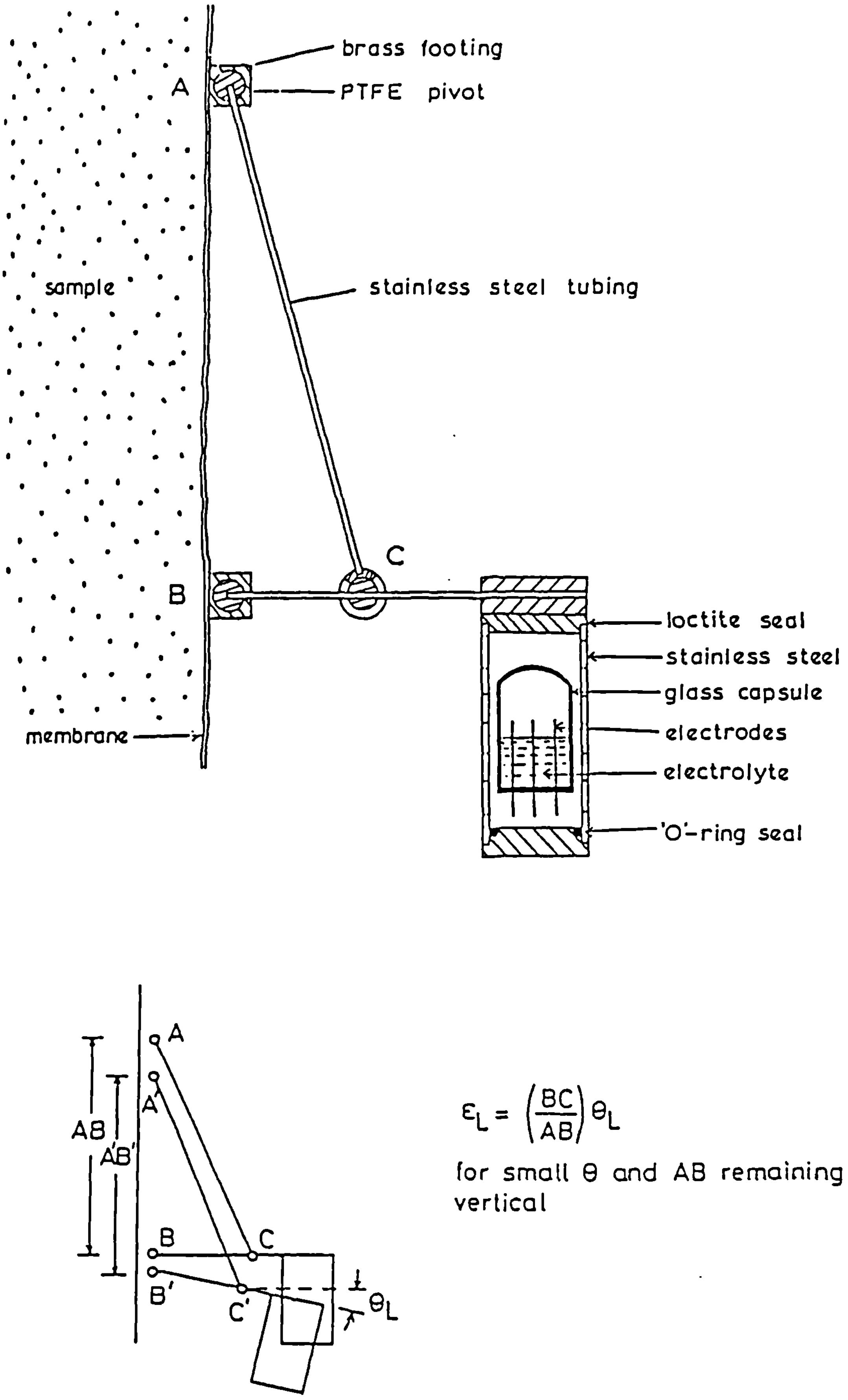

$$\varepsilon_L = \left(\frac{BC}{AB}\right)\theta_L$$

for small θ and AB remaining vertical

Figure 2.2.3 Sketch showing the construction of the electrolevel strain gauges and the way in which axial strain is converted to rotation of the capsule (after Jardine et al., 1984)

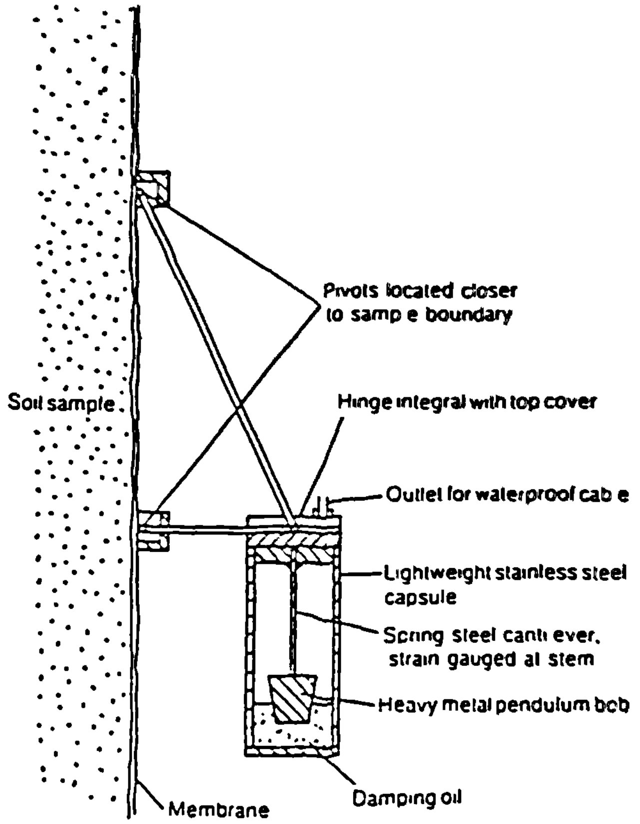

Figure 2.2.4 Sketch showing the design of pendulum inclinometer gauges (after Ackerly et al., 1987)

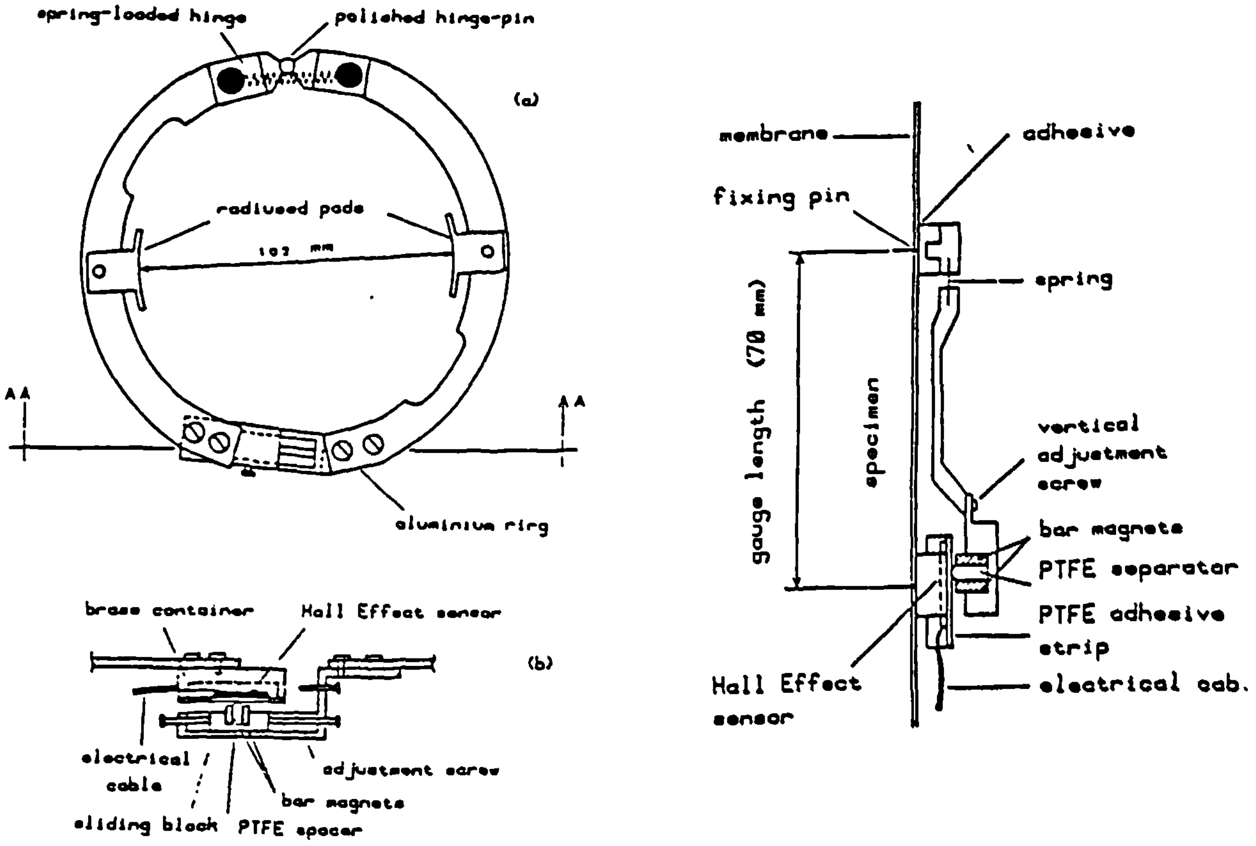

Figure 2.2.5 Configuration of Hall effect axial and radial strain gauges (after Clayton et al., 1989)

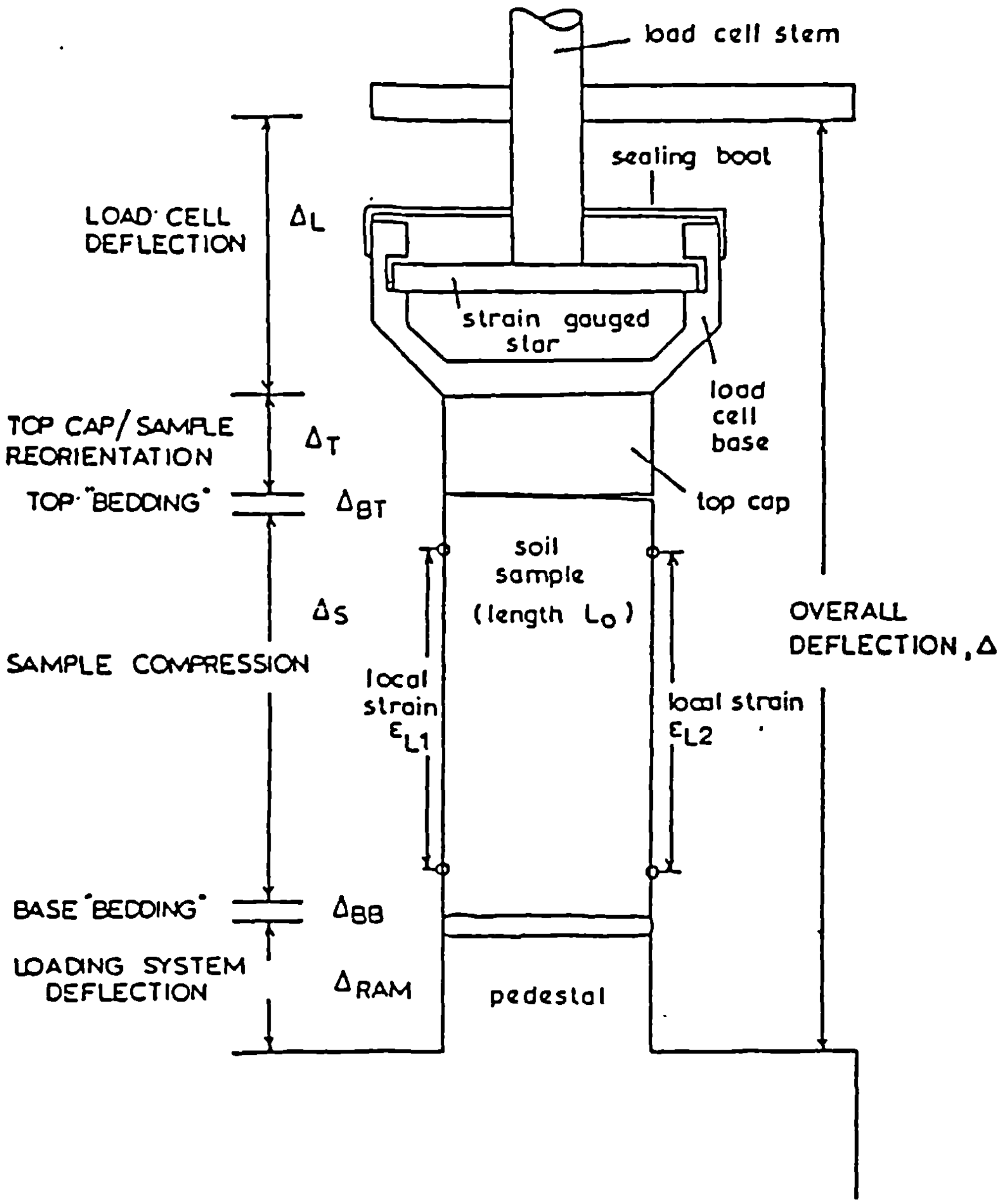

Figure 2.2.6 Sources of error in external measurements (after Jardine et al., 1984)

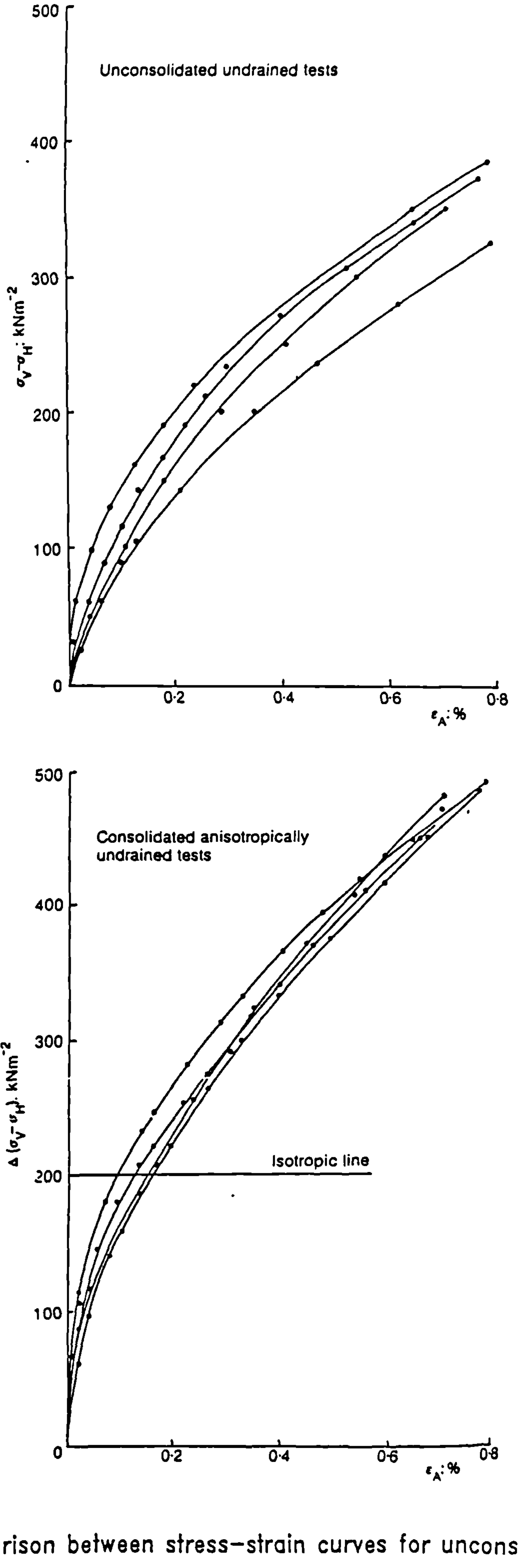

Figure 2.3.1 Comparison between stress–strain curves for unconsolidated undrained tests and anisotropically consolidated undrained tests on samples of undisturbed London clay (after Costa Filho, 1979)

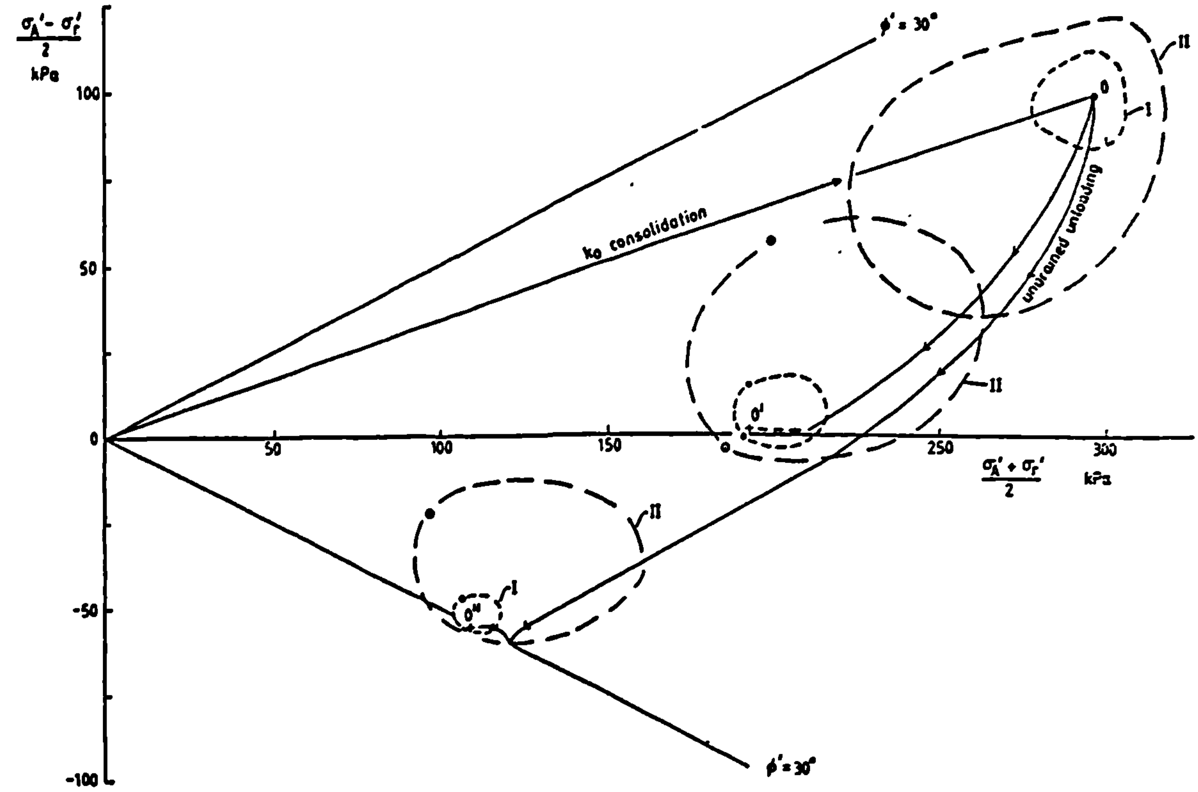

Figure 2.3.2 Sketched boundaries for zones of different classes of deformation after Ko consolidation, after perfect sampling and after extension to 5% axial strain tests on North Sea clay (after Jardine, 1985)

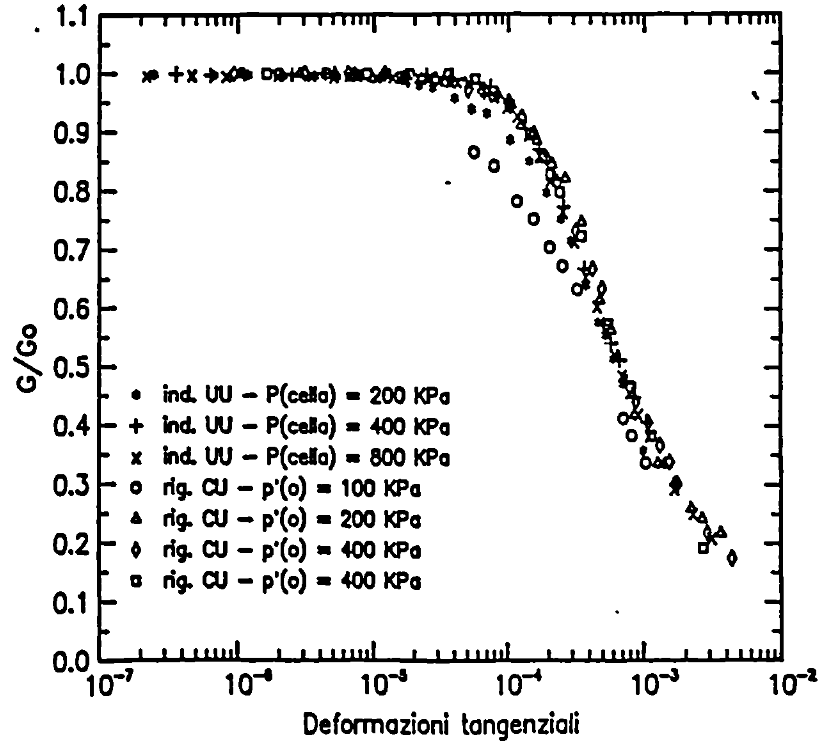

Figure 2.3.3 Graph showing the decay of shear stiffness, G, normalised by the initic shear stiffness, Go, with torsional shear strain for a selection of tests on Todi clay (after Rampello, 1989)

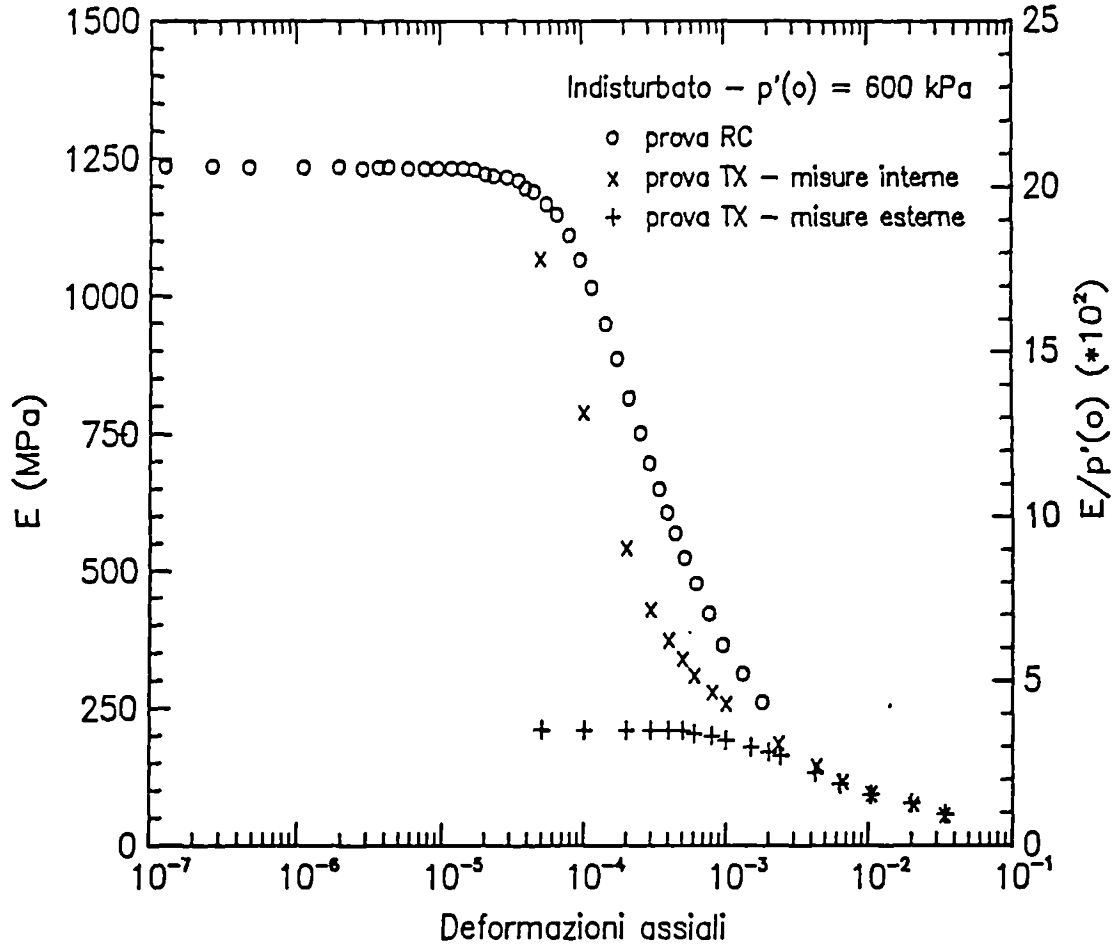

Figure 2.3.4 Comparison between the decay of shear stiffness with axial strain measured using a resonant column and internally or externally in a triaxial cell. Tests on Todi clay. (after Rampello, 1989)

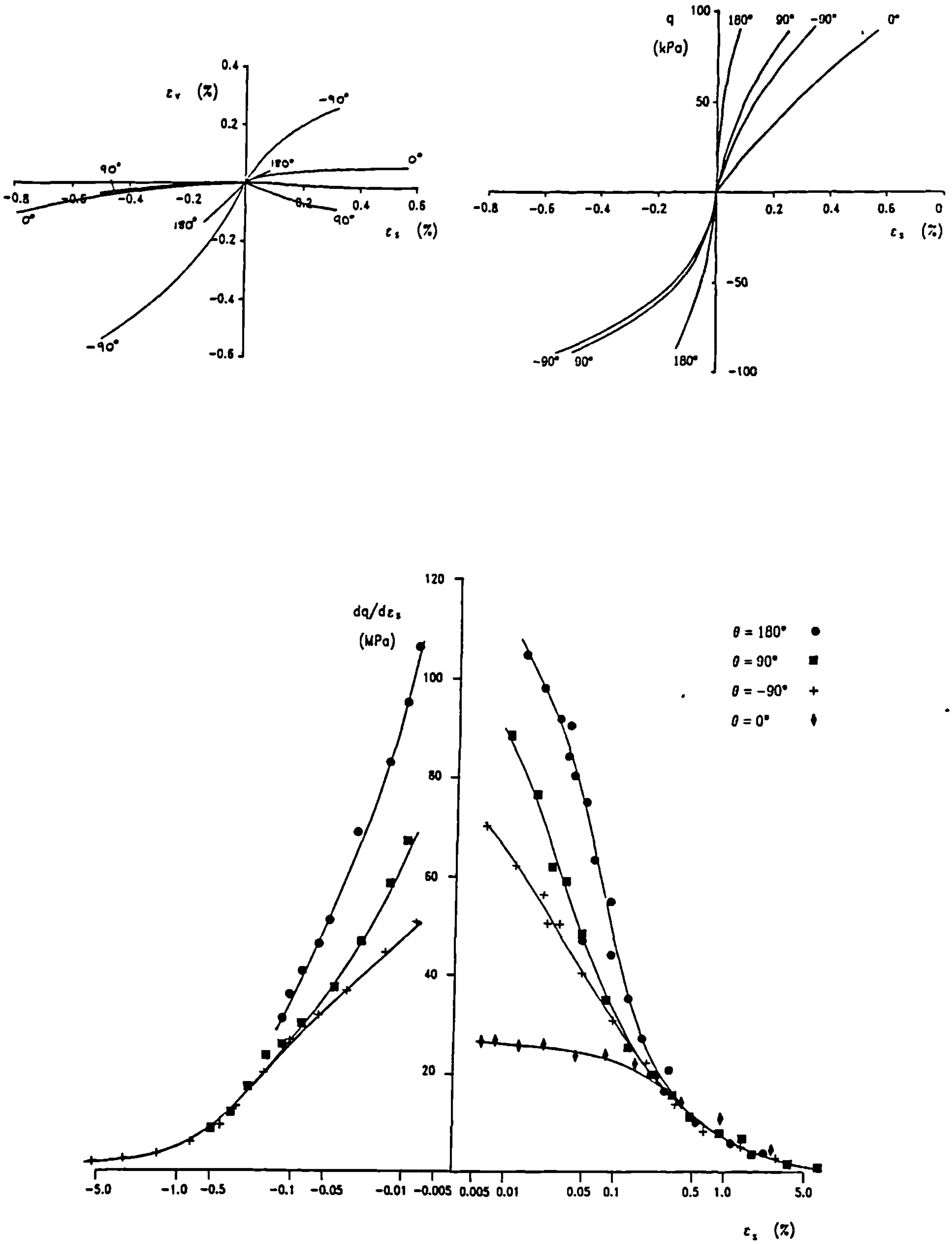

Figure 2.3.5 Graphs showing the effect of recent stress history on the stress–strain response of London clay along constant p' extension and compression paths at p' = 200kPa, p'm = 400kPa (after Atkinson et al., 1990)

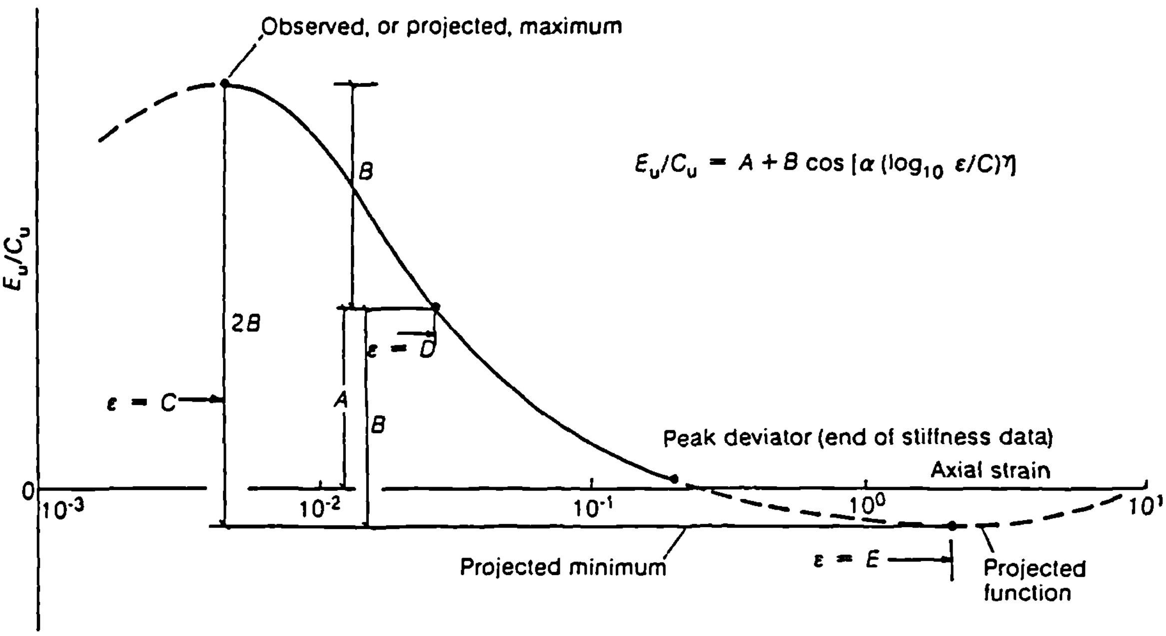

Figure 2.4.1 Diagram showing the definition of the constants in the periodic logarithmic function used to curve fit non-linear stiffness-strain data (after Jardine et al., 1986)

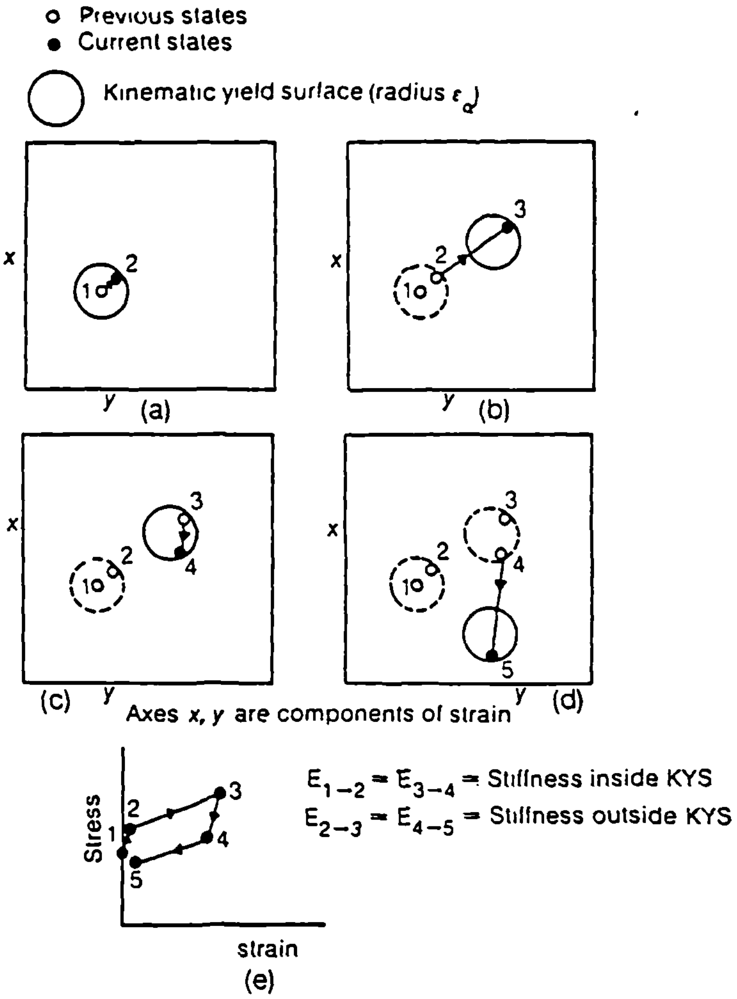

Figure 2.4.2 Diagram describing the kinematic yield surface effect (after Simpson et al., 1979)

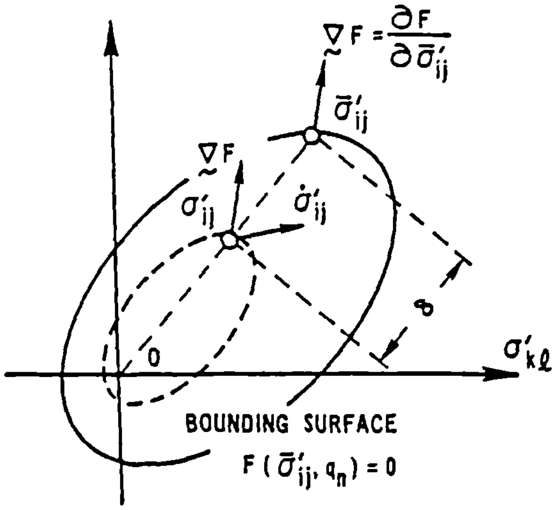

Figure 2.4.3 Schematic illustration of the bounding surface and definition of image points in general stress space (after Dafalias and Herrman, 1982)

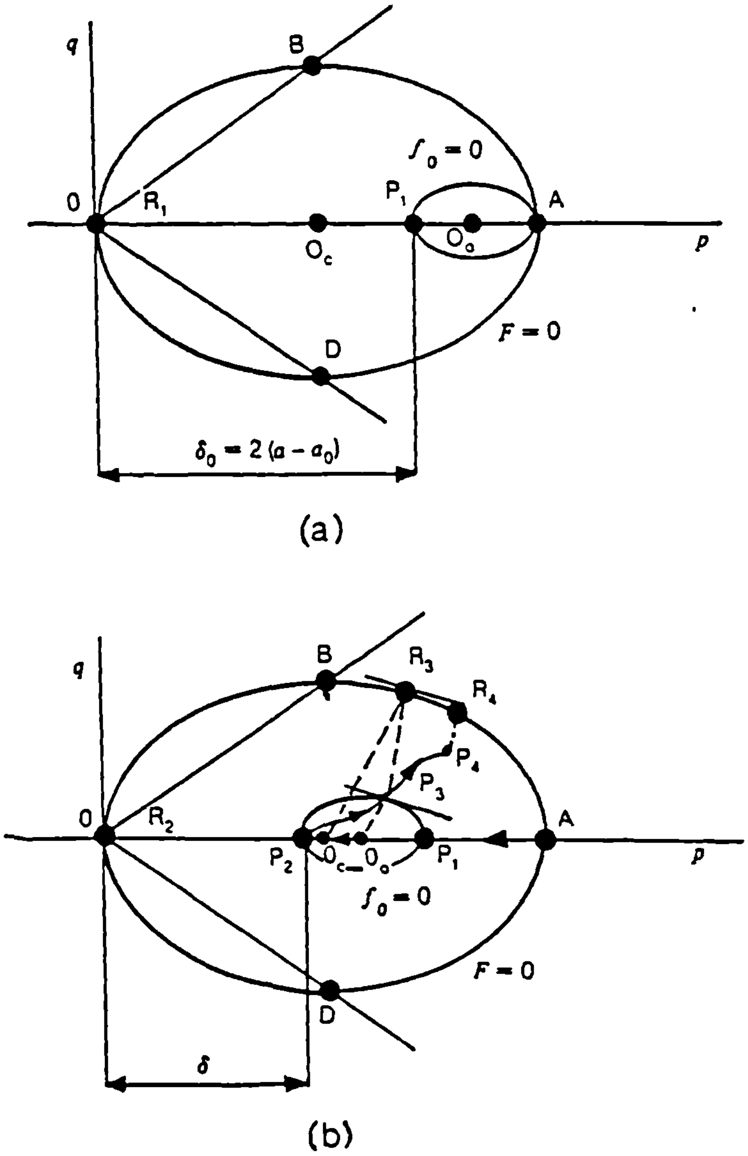

(a)

(b)

Figure 2.4.4 Relative configuration of the yield and consolidation surfaces in the two-surface model (a) after isotropic consolidation OA (b) for the stress history O-A-P1-P2-P3 (after Mroz et al., 1979)

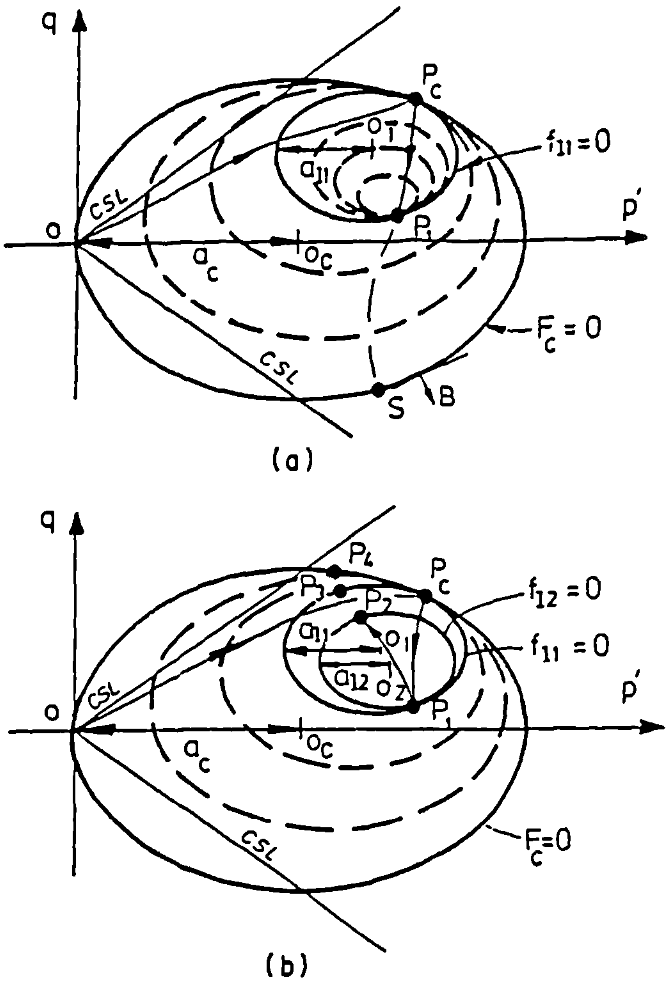

Figure 2.4.5 Model with an infinite number of surfaces: (a) first reverse loading (b) second reverse loading (after Mröz and Norris, 1982)

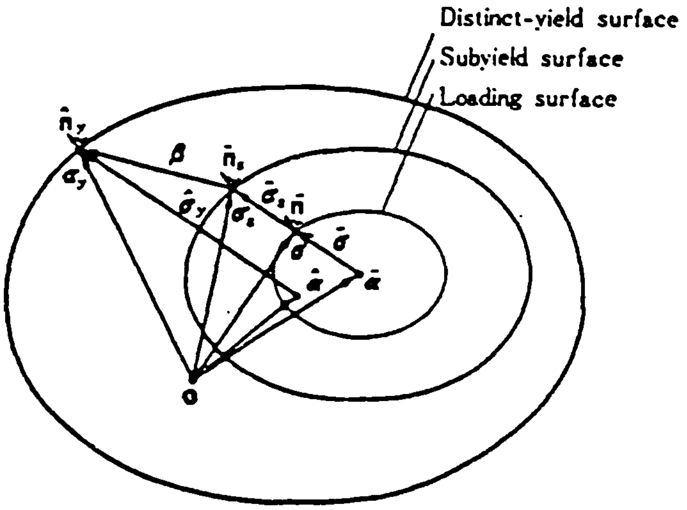

Figure 2.4.6 Typical configuration of surfaces in the three–surface model proposed by Hashiguchi (1985). (after Hashiguchi, 1985)

B	Bishop ram
R	Resistance transducer
M	Manostat
P	Load cell
C	Continuous motor
T	Pressure transducer
V	Volume gauge

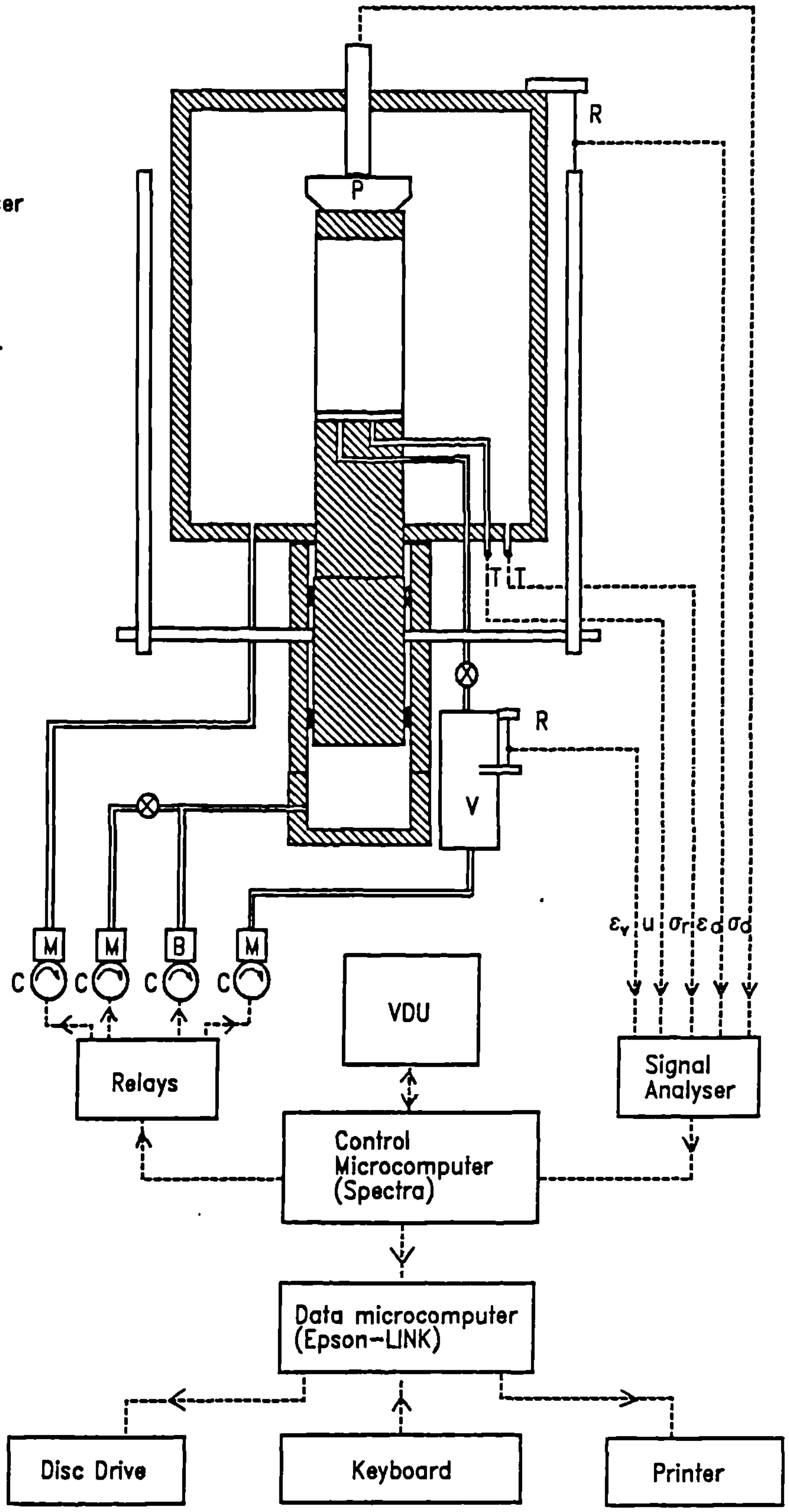

Figure 3.2.1 Schematic diagram of "Spectra" control system for stress path cells used to test 38mm diameter samples.

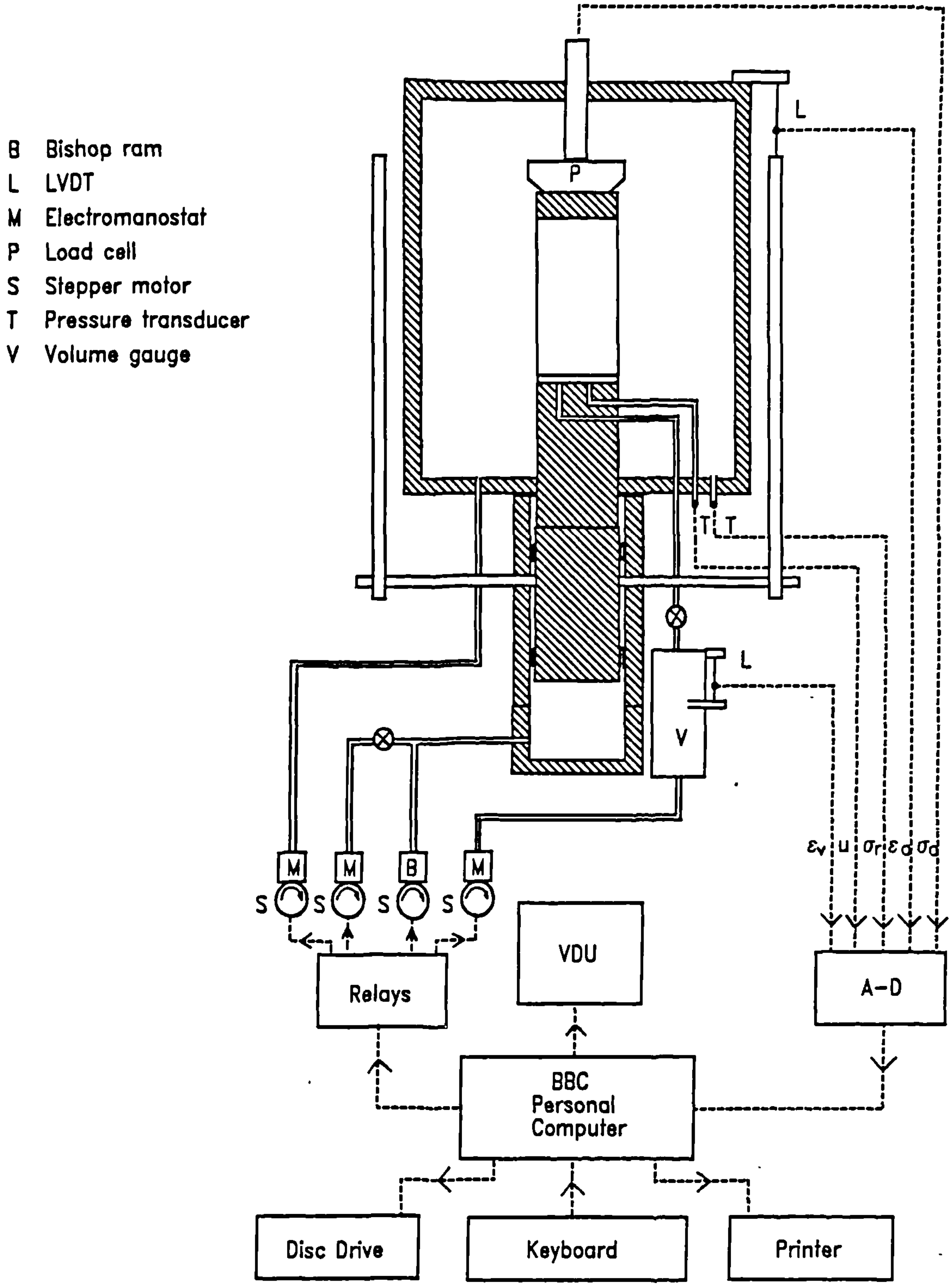

Figure 3.2.2 Schematic diagram of "BBC" control system for stress path cells used to test 38mm diameter samples.

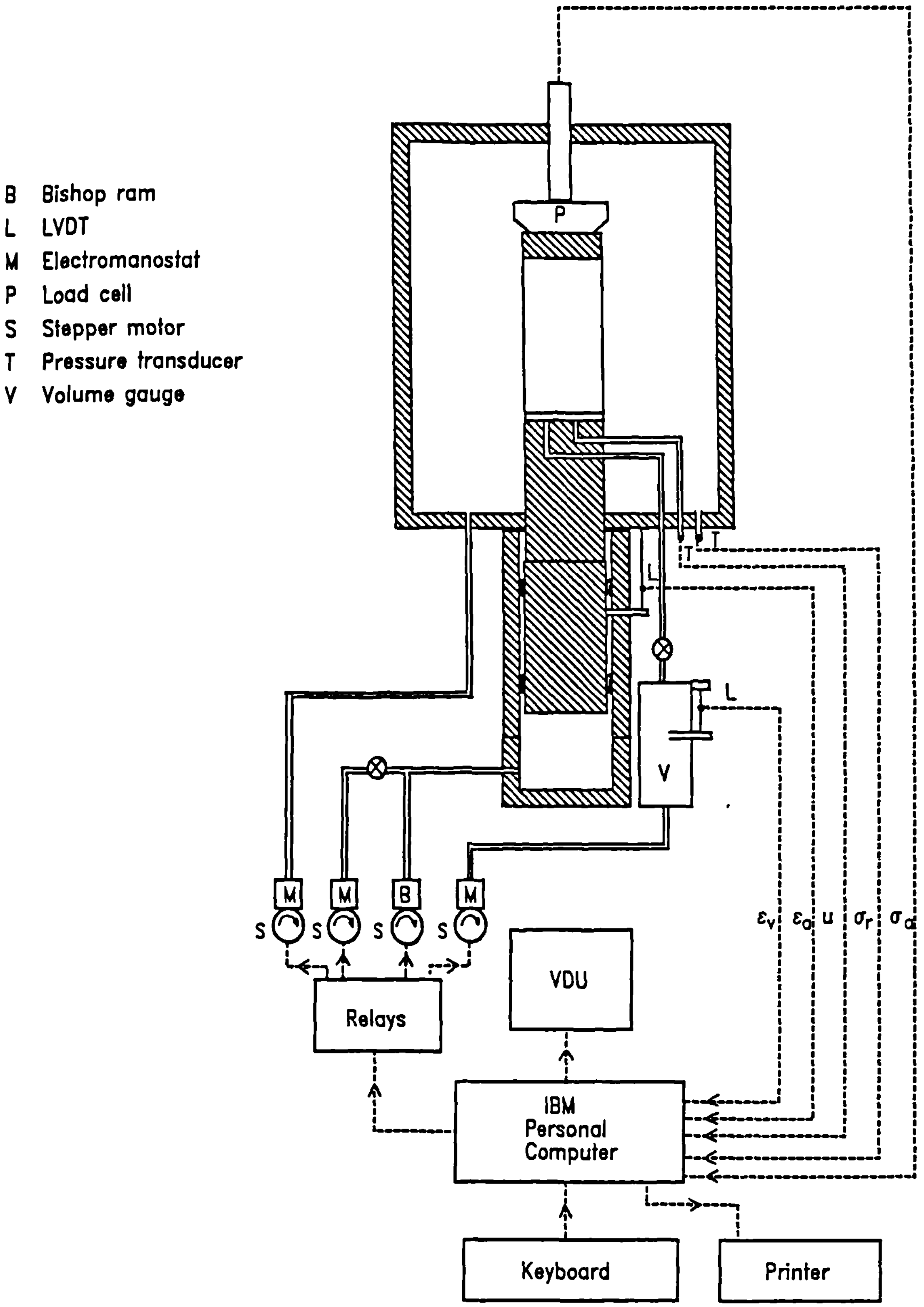

Figure 3.2.3 Schematic diagram of "IBM" control system for stress path cells used to test 100mm diameter samples.

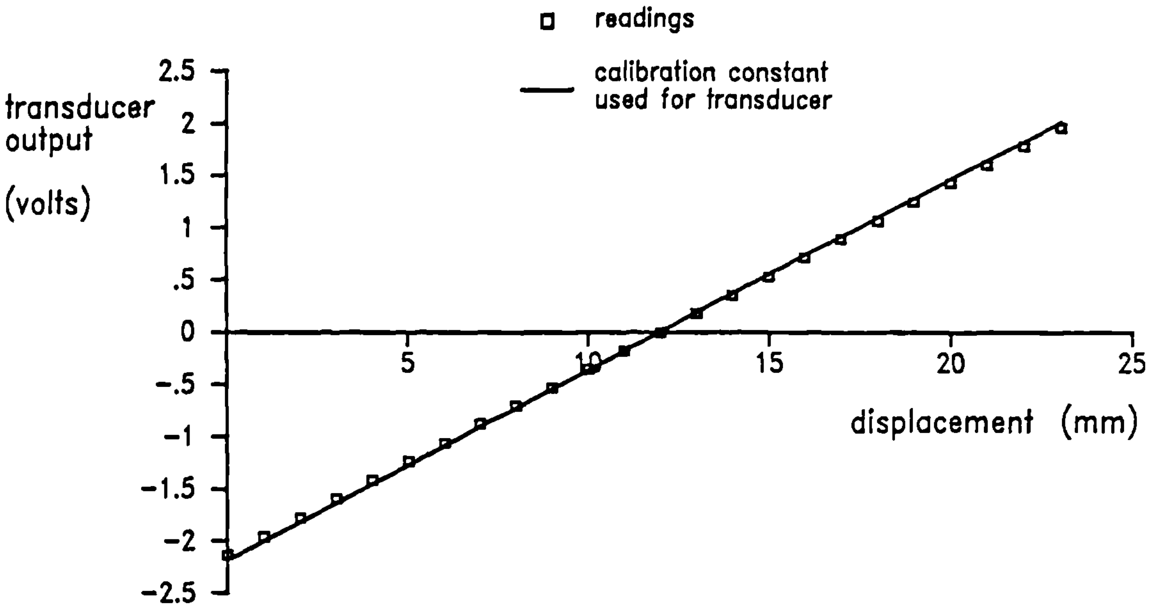

Figure 3.2.4 Typical calibration curve for a LVDT used to measure axial strains

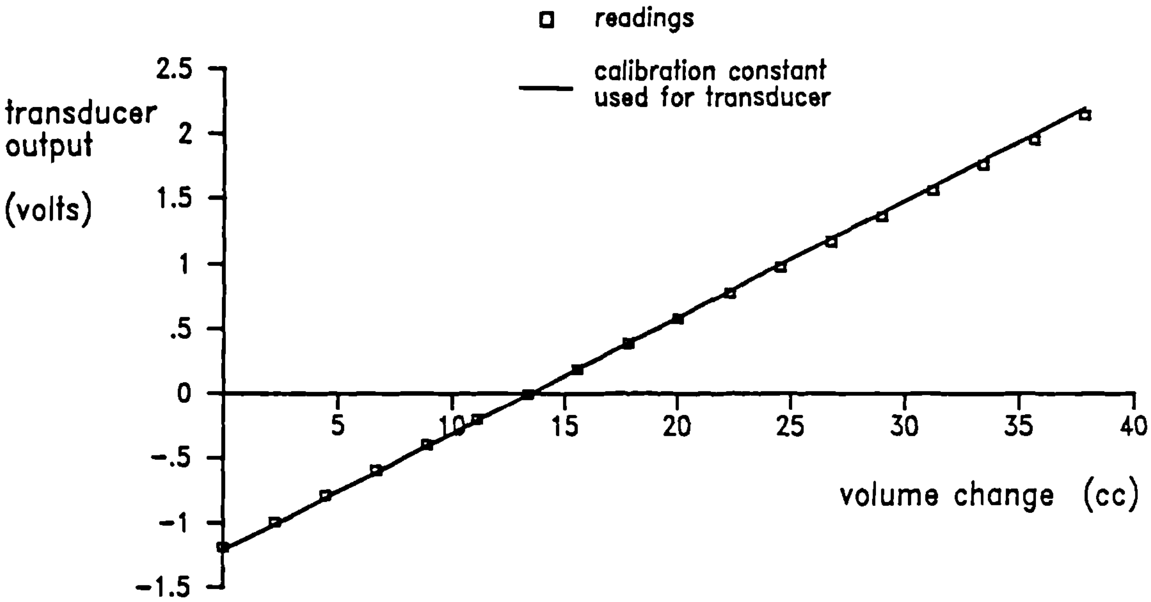

Figure 3.2.5 Typical calibration curve for a LVDT used with a volume gauge.

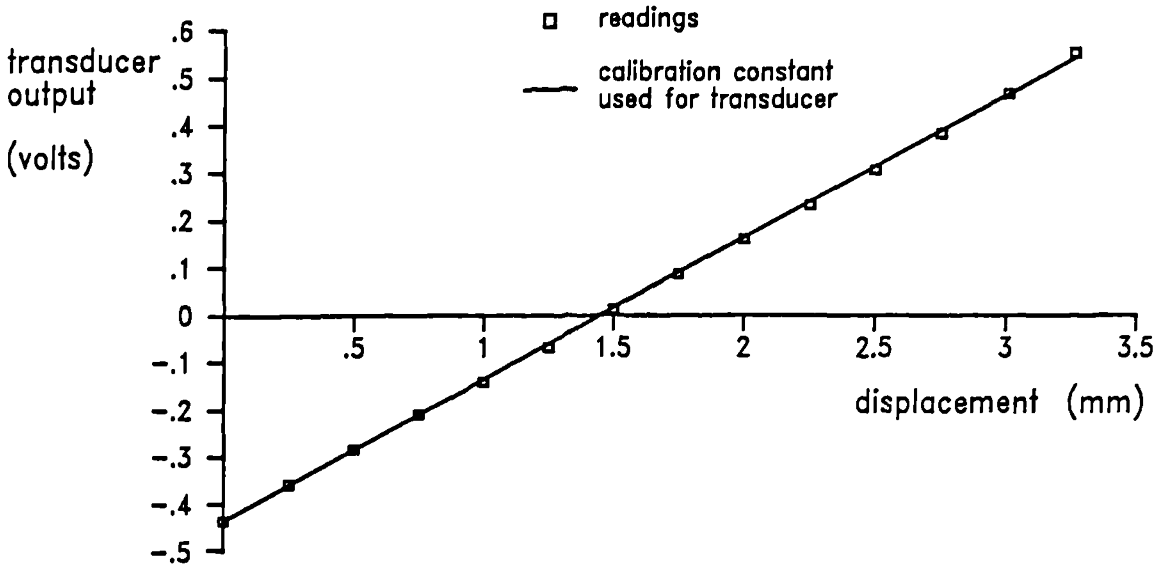

Figure 3.2.6 Typical calibration curve for a Hall effect local axial strain gauge.

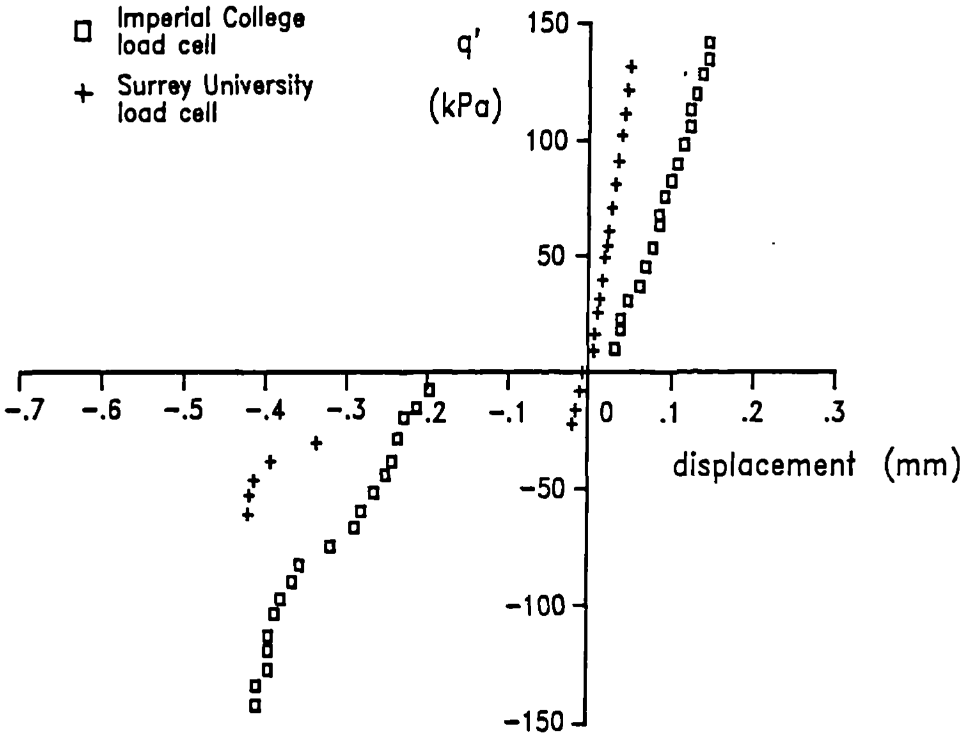

Figure 3.2.7. Compliance curves for Imperial College and Surrey University designed load cells.

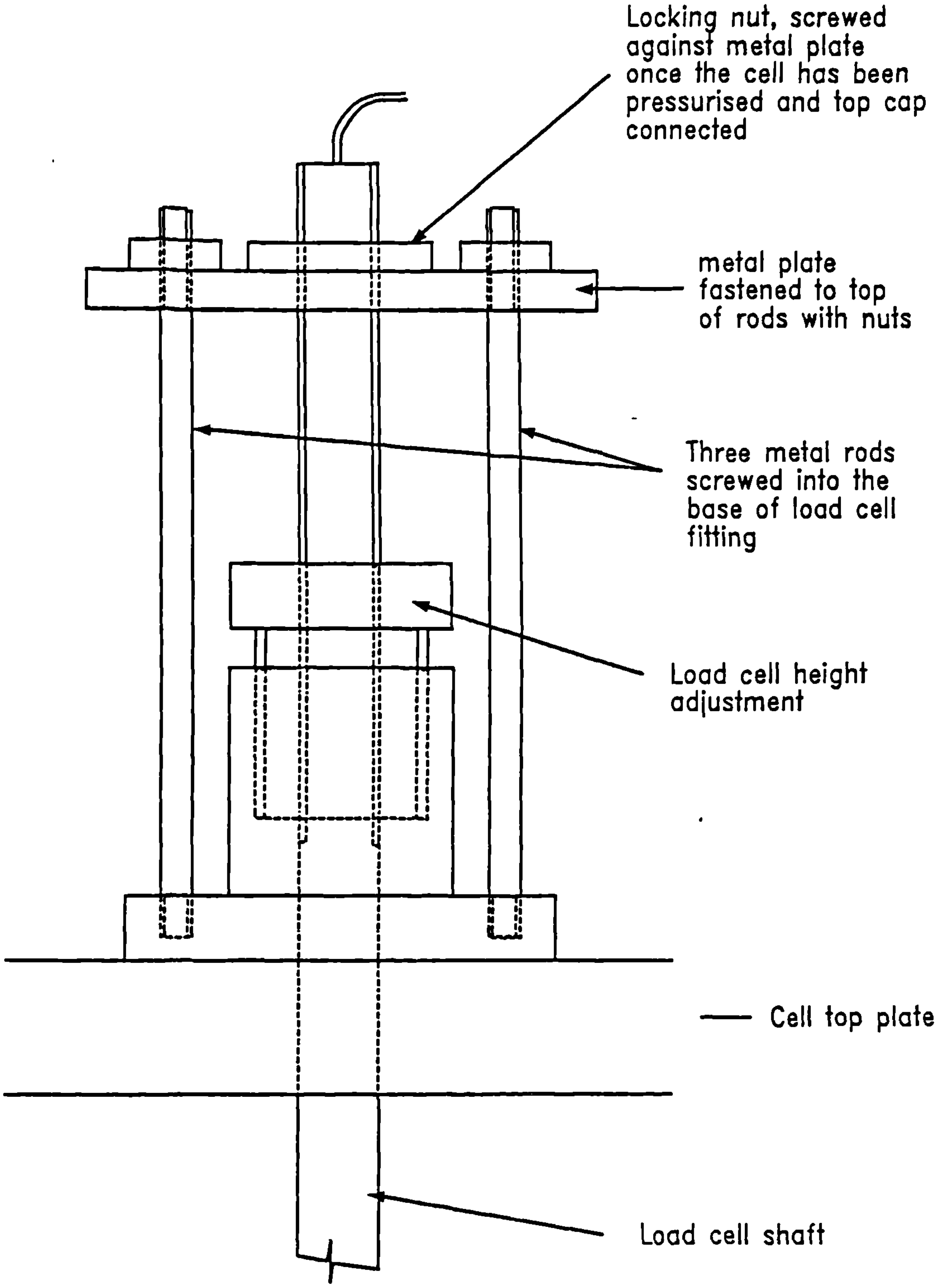

Figure 3.2.8 Diagram showing the simple restraining device used to stop movement of the load cell shaft. (after Cherrill, 1990)

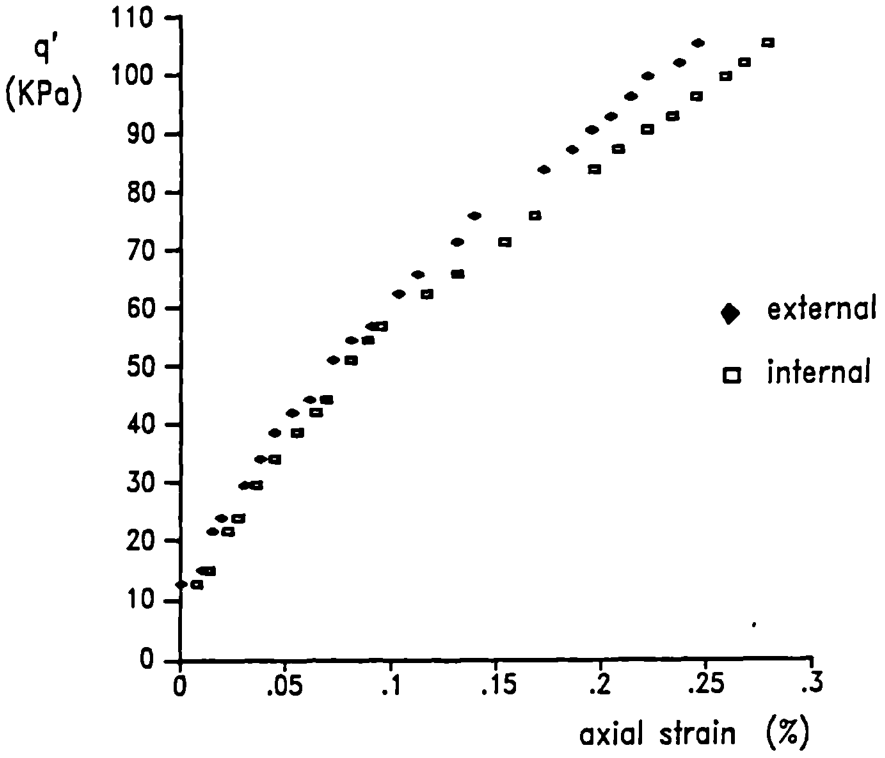

Figure 3.2.9 Typical set of stress–strain data from test LAS5 comparing axial strains measured internally and externally for a constant p' loading path.

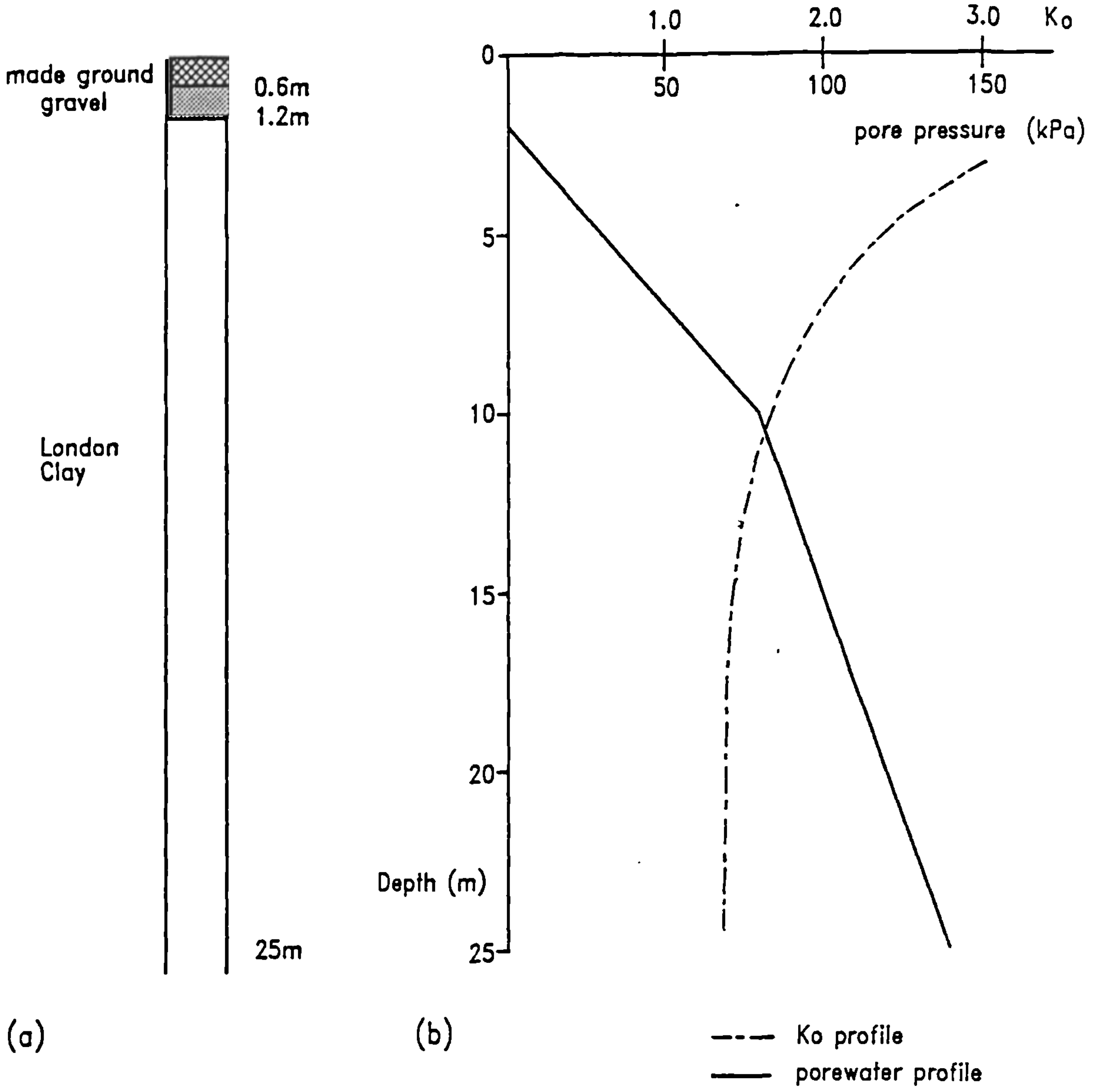

Figure 3.3.1 (a) Typical soil profile (b) Typical porewater and Ko profiles for Site 1 in north London. (after Bullen and Partners, 1989)

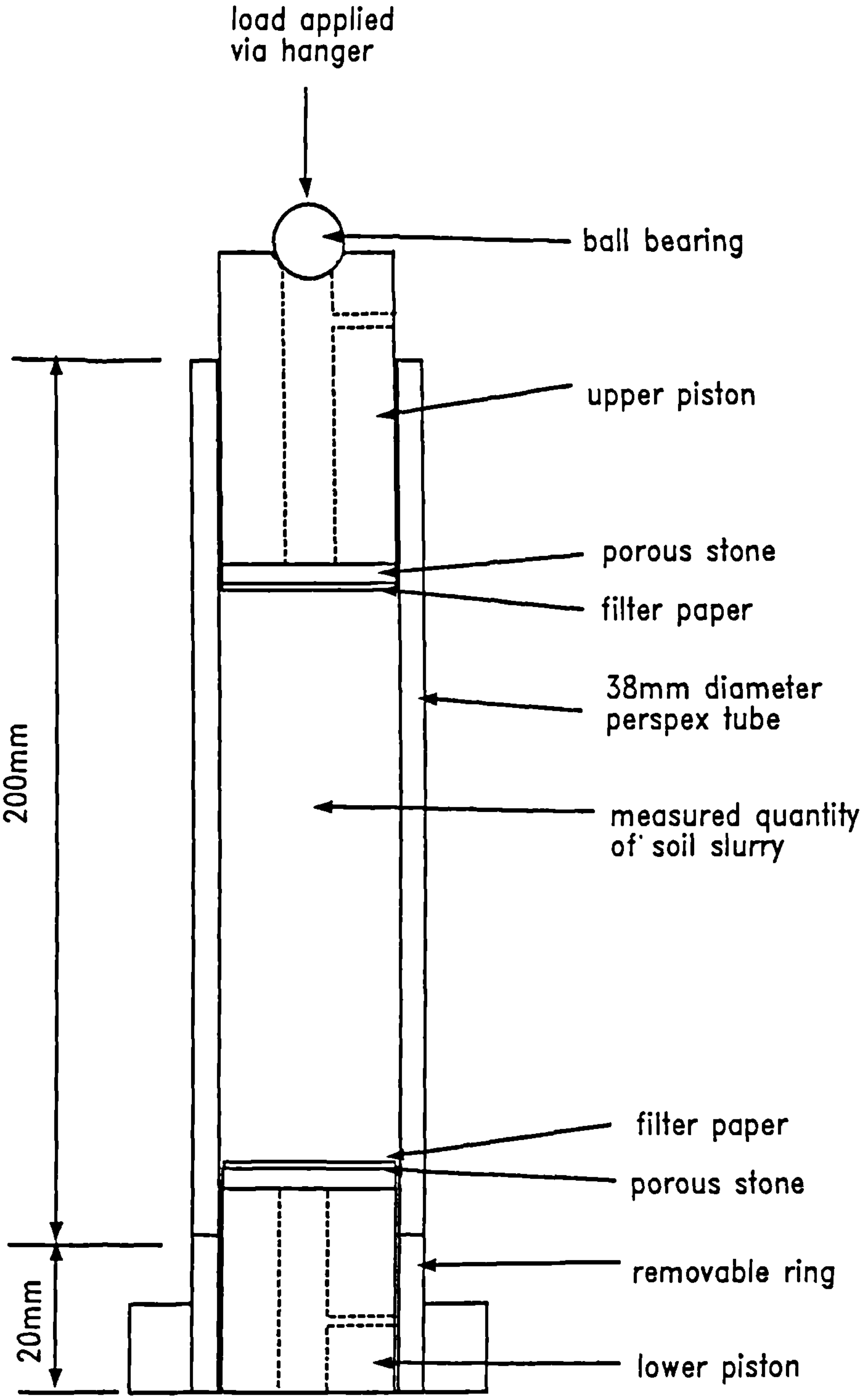

Figure 3.4.1 Diagram of perspex floating ring consolidation press.

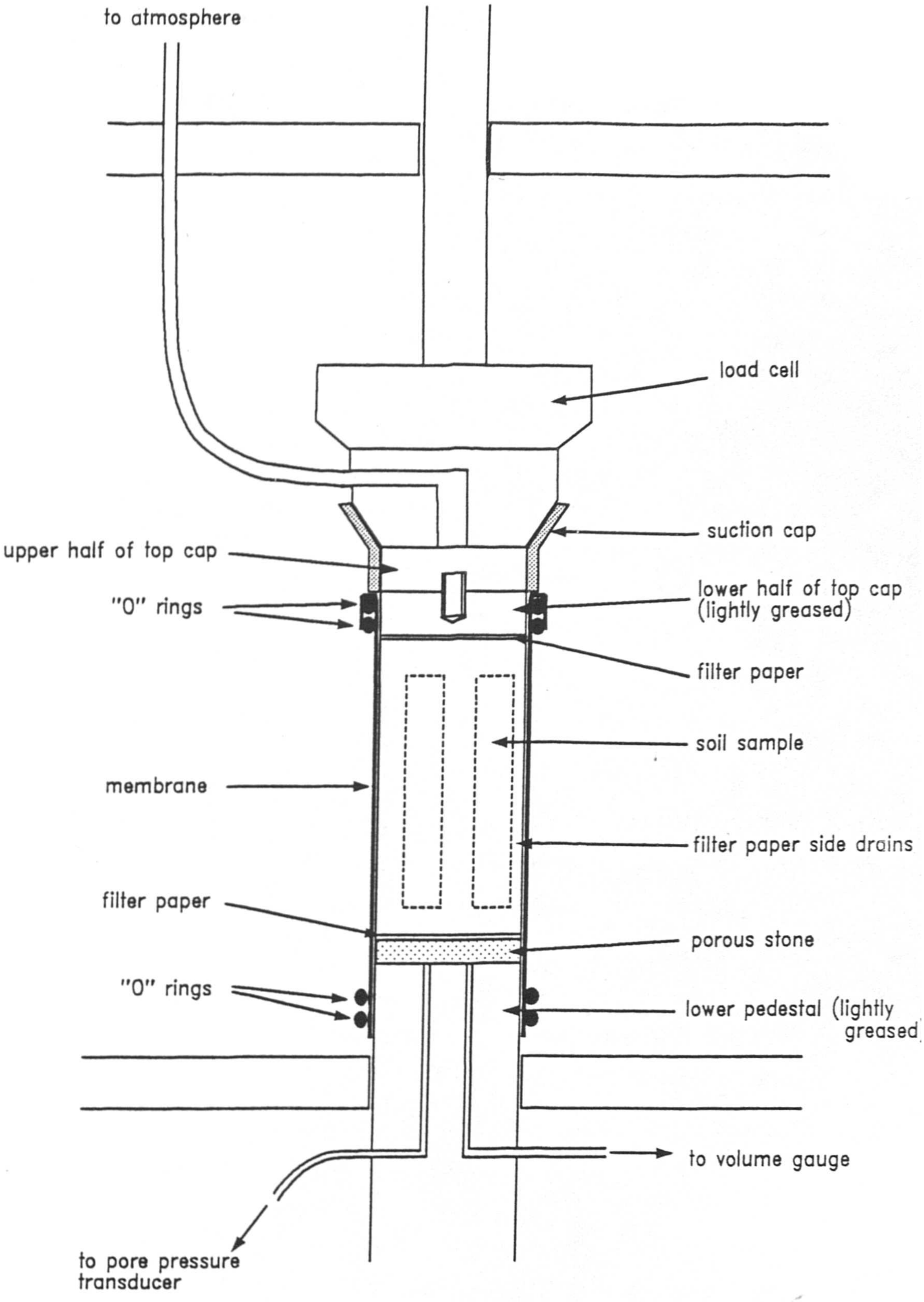

Figure 3.5.1 Diagram showing a soil sample set up in a stress path cell

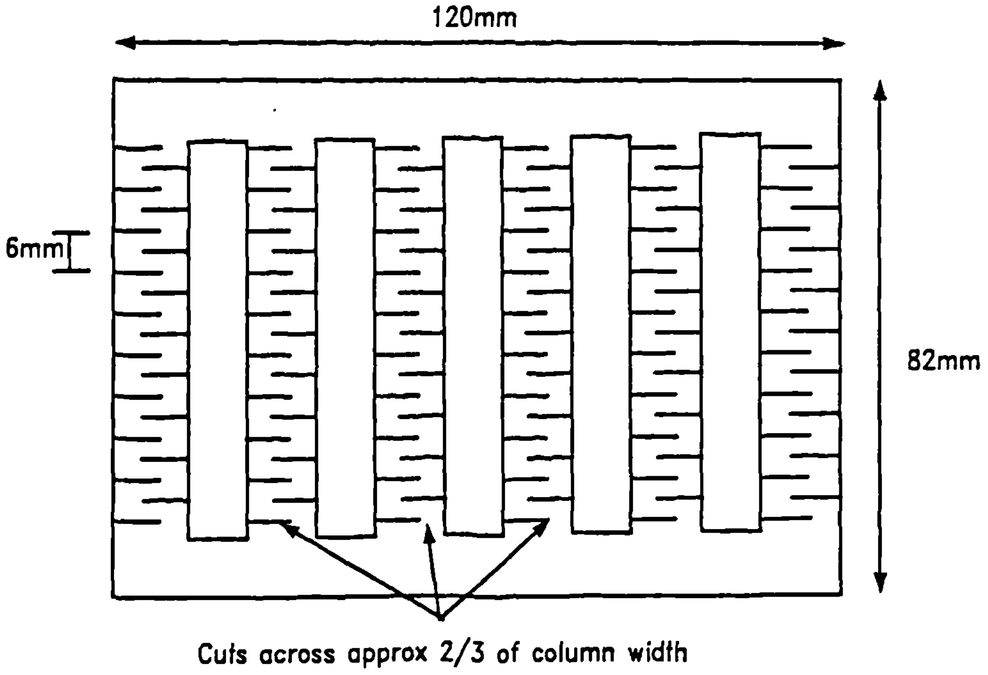

Figure 3.5.2 Diagram showing modified filter paper side drains. (after Pickles, 1989)

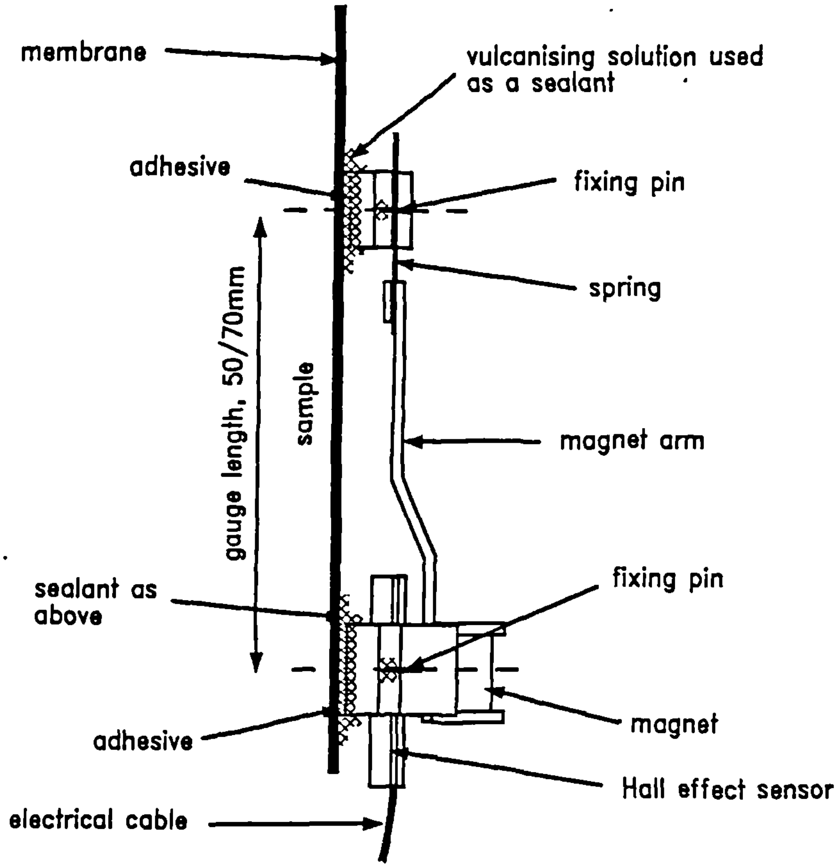

Figure 3.5.3 Diagram showing a local axial strain gauge fitted to a sample

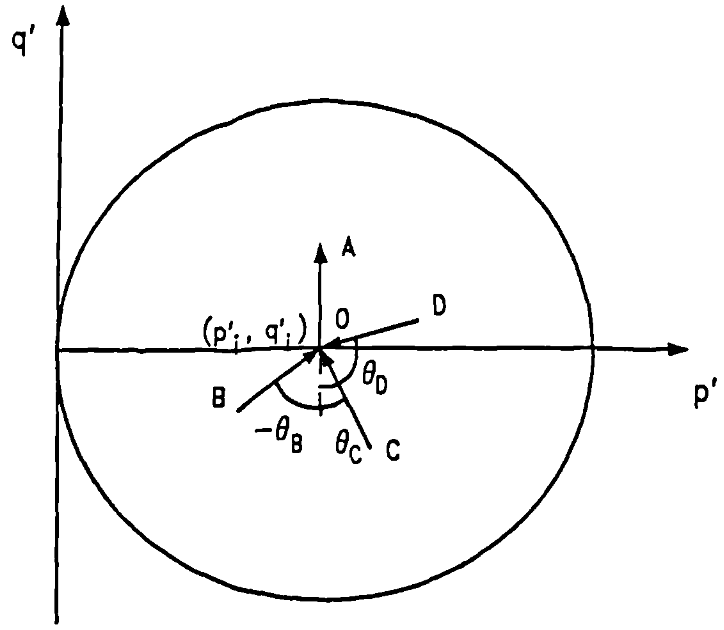

Figure 3.6.1 Diagram showing a typical set of stress probes for the basic test to investigate the recent stress history effect

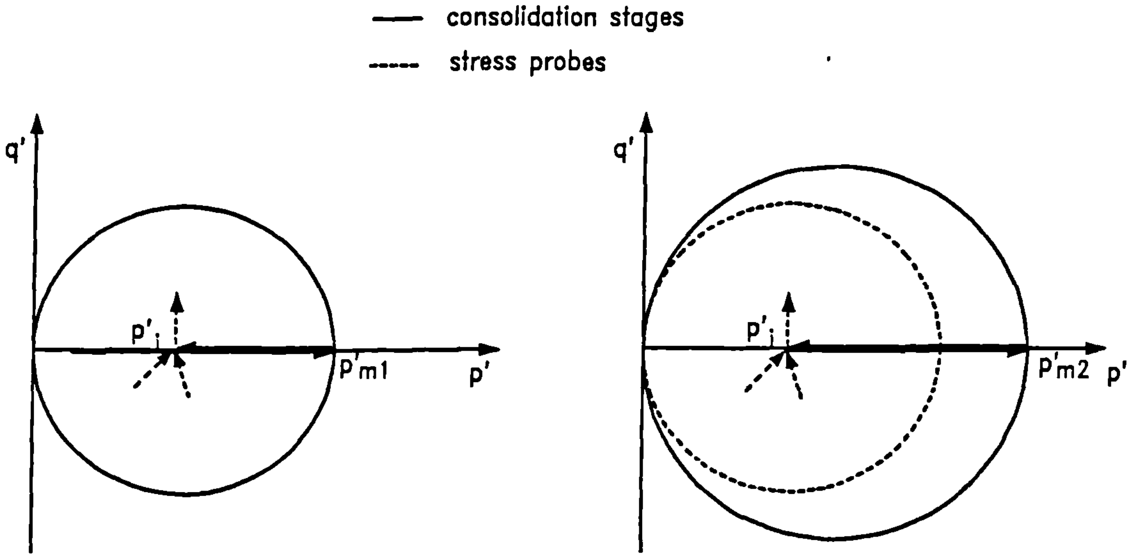

(a) First set of stress probes

(b) Set of stress probes at a new overconsolidation ratio

Figure 3.6.2 Diagram showing the sequence of loading paths followed to investigate the effect of recent stress history at different states using the same soil sample.

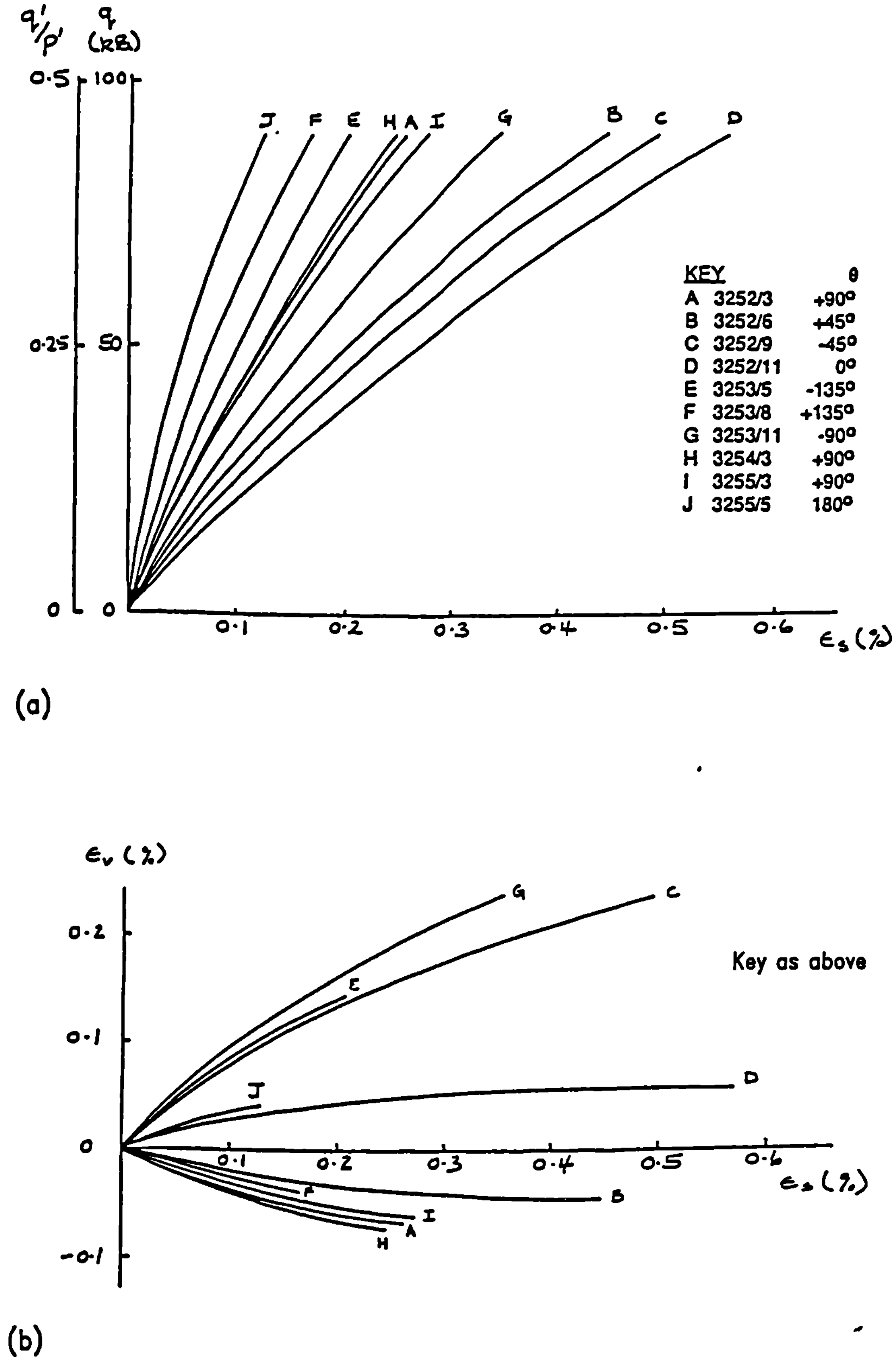

Figure 4.1.1 (a) stress–strain curves and (b) strain paths for constant p' loading. Samples of reconstituted Cowden till, isotropically compressed, p'i = 200kPa, p'm = 400kPa. (after Richardson, 1988)

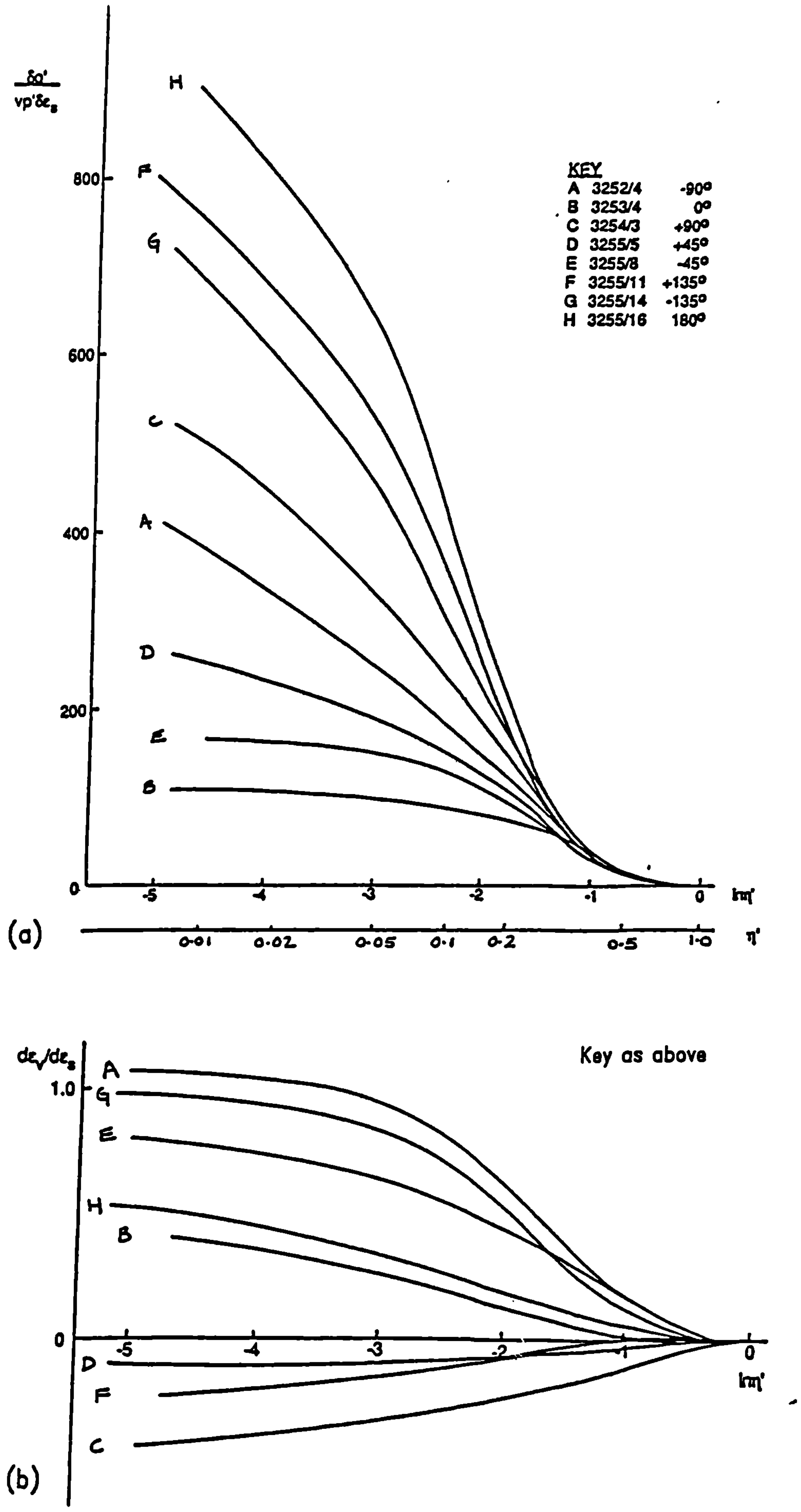

Figure 4.1.2 Plots of (a) normalised stiffness and (b) strain increment ratio against the logarithm of stress ratio for constant p' loading. Cowden till as for 4.1.1. (after Richardson, 1988)

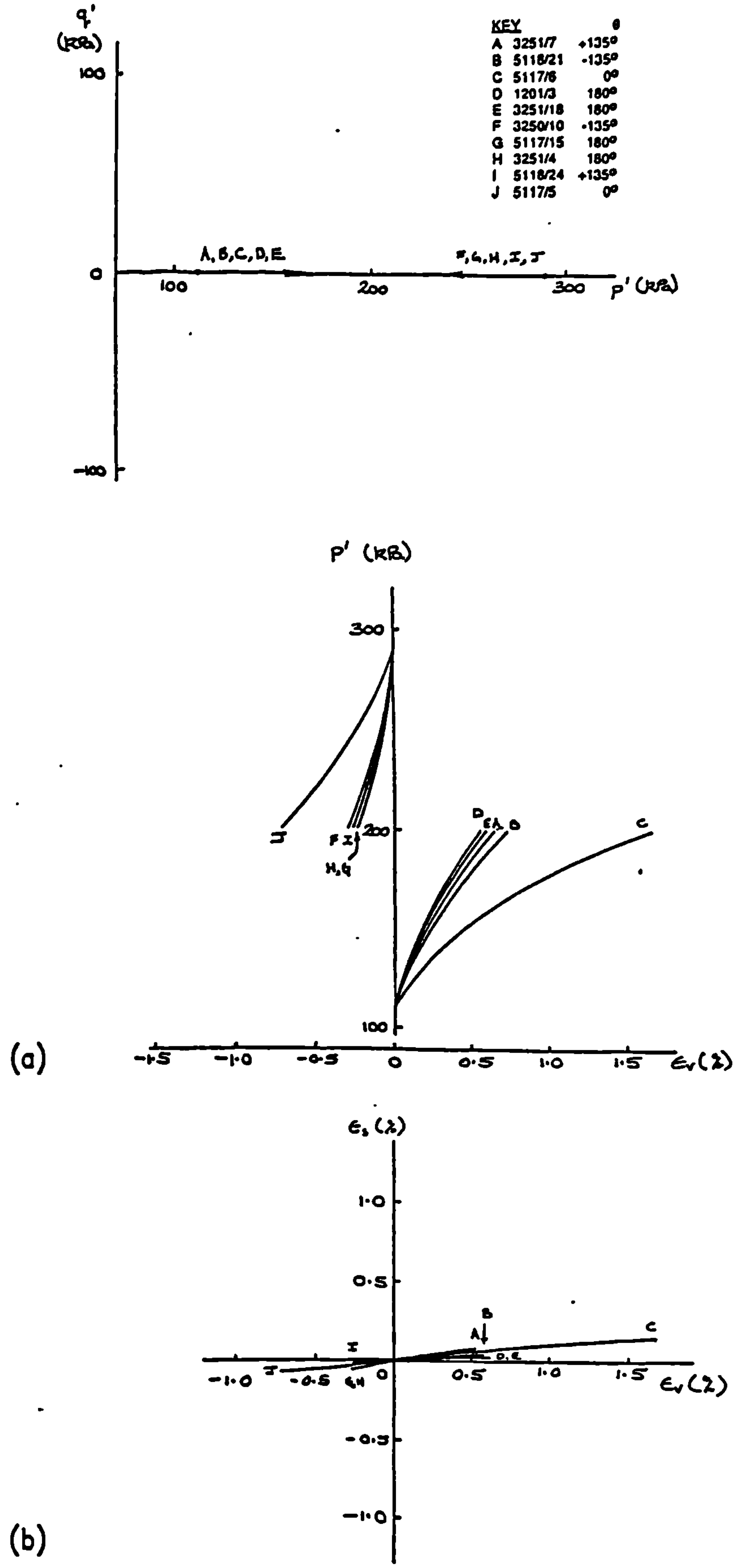

Figure 4.1.3 (a) stress-strain curves and (b) strain paths for constant q' loading. Samples of reconstituted London clay, isotropically compressed, p'i = 200kPa, p'm = 400kPa. (after Richardson, 1988)

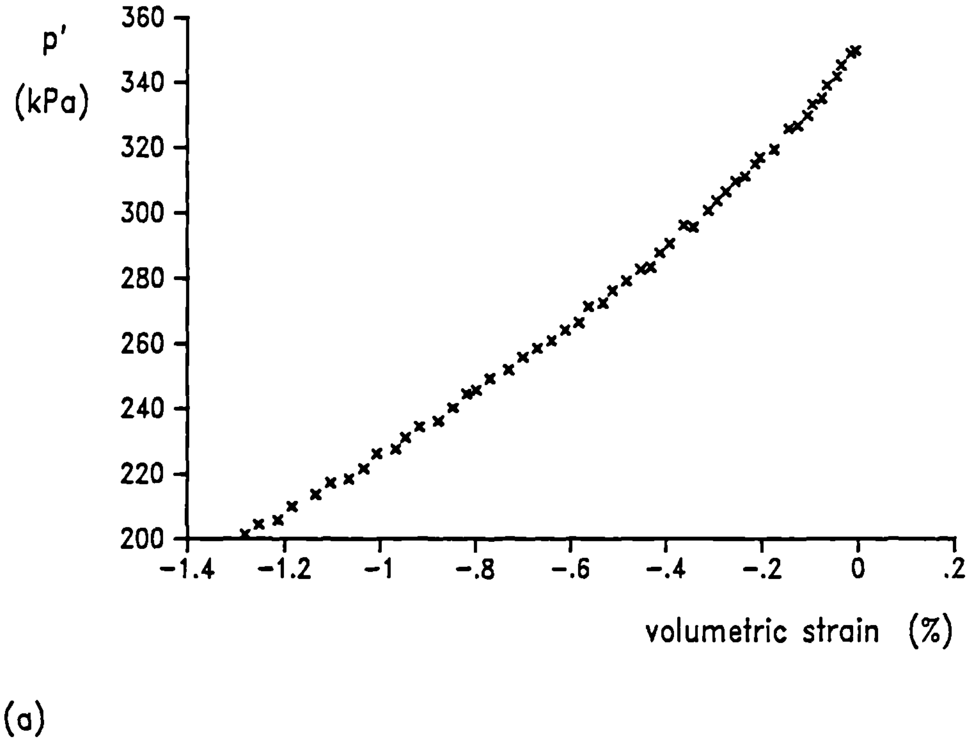

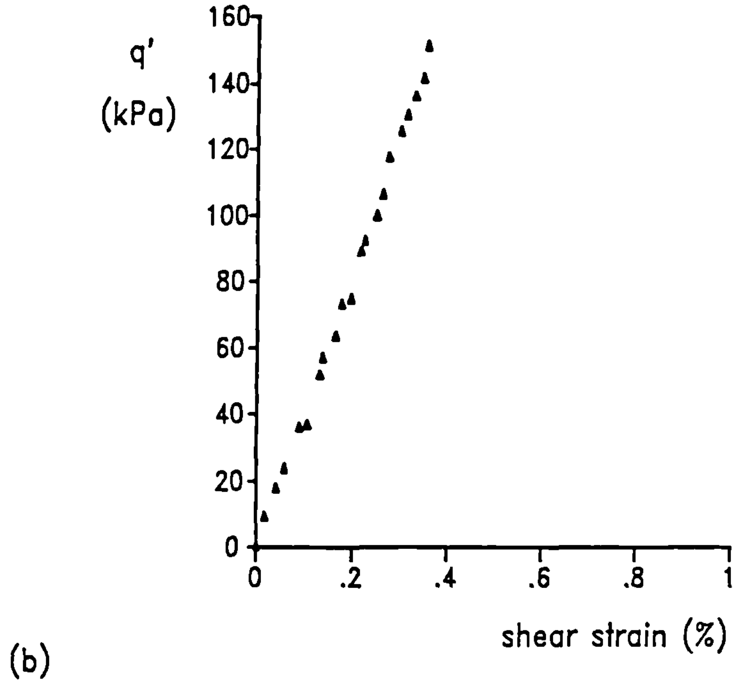

Figure 4.2.1. Typical stress–strain data for (a) Test TT3, constant q' loading, angle of rotation 39 degrees (b) Test TT4, constant p' loading, angle of rotation 90 degrees

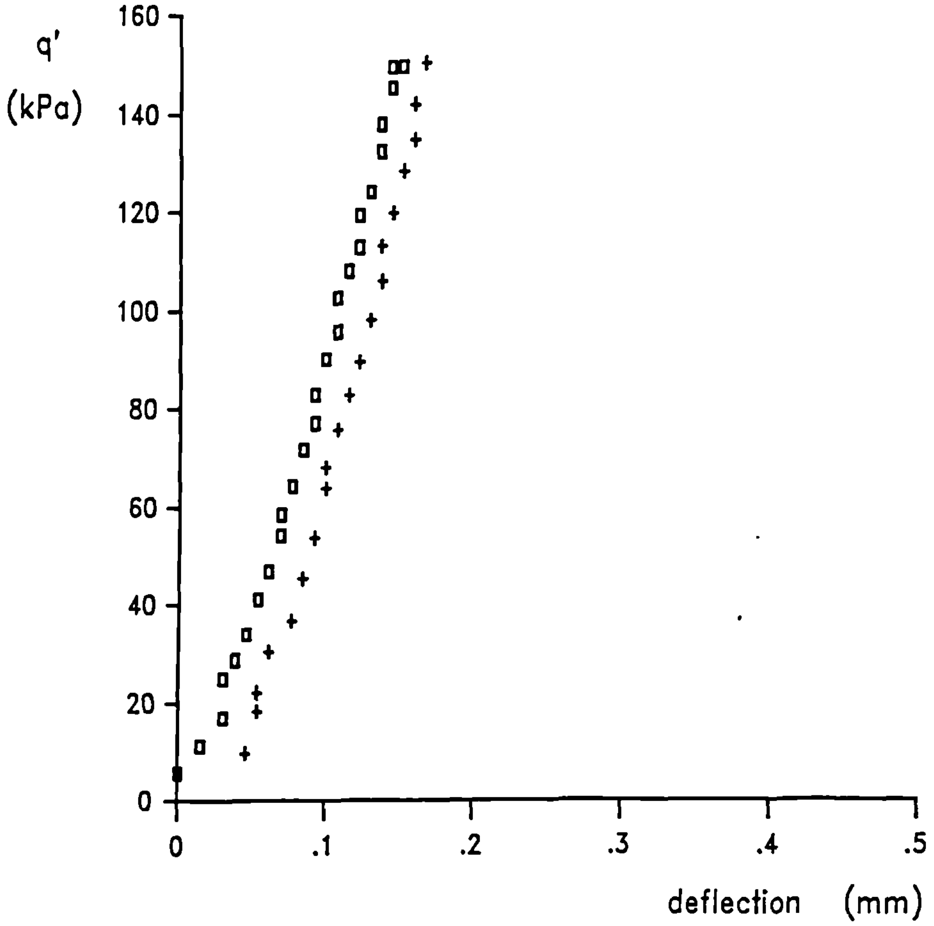

Figure 4.2.2. Two compliance curves for an Imperial College load cell obtained by loading a steel sample along the same path, constant p' with p' = 200kPa

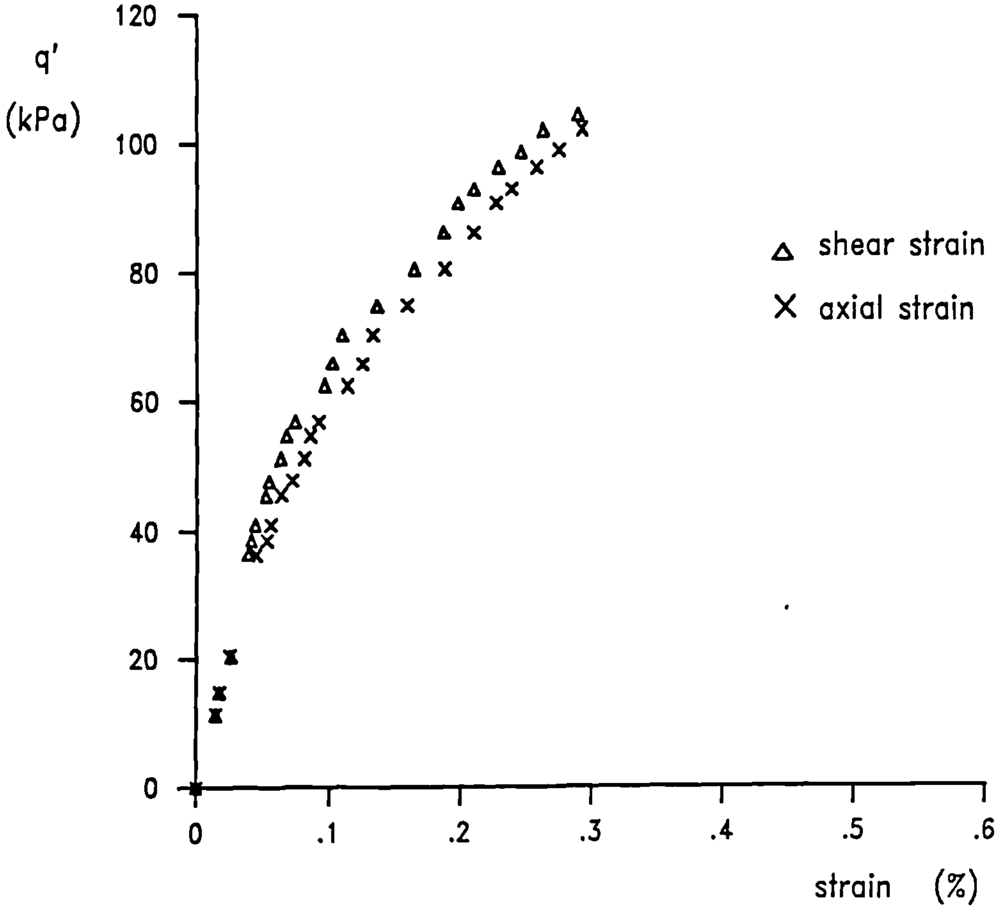

Figure 4.2.3. Comparison between typical curves of deviator stress against axial strain and shear strain, for constant p' loading after a rotation of 90 degrees, taken from test LAS5

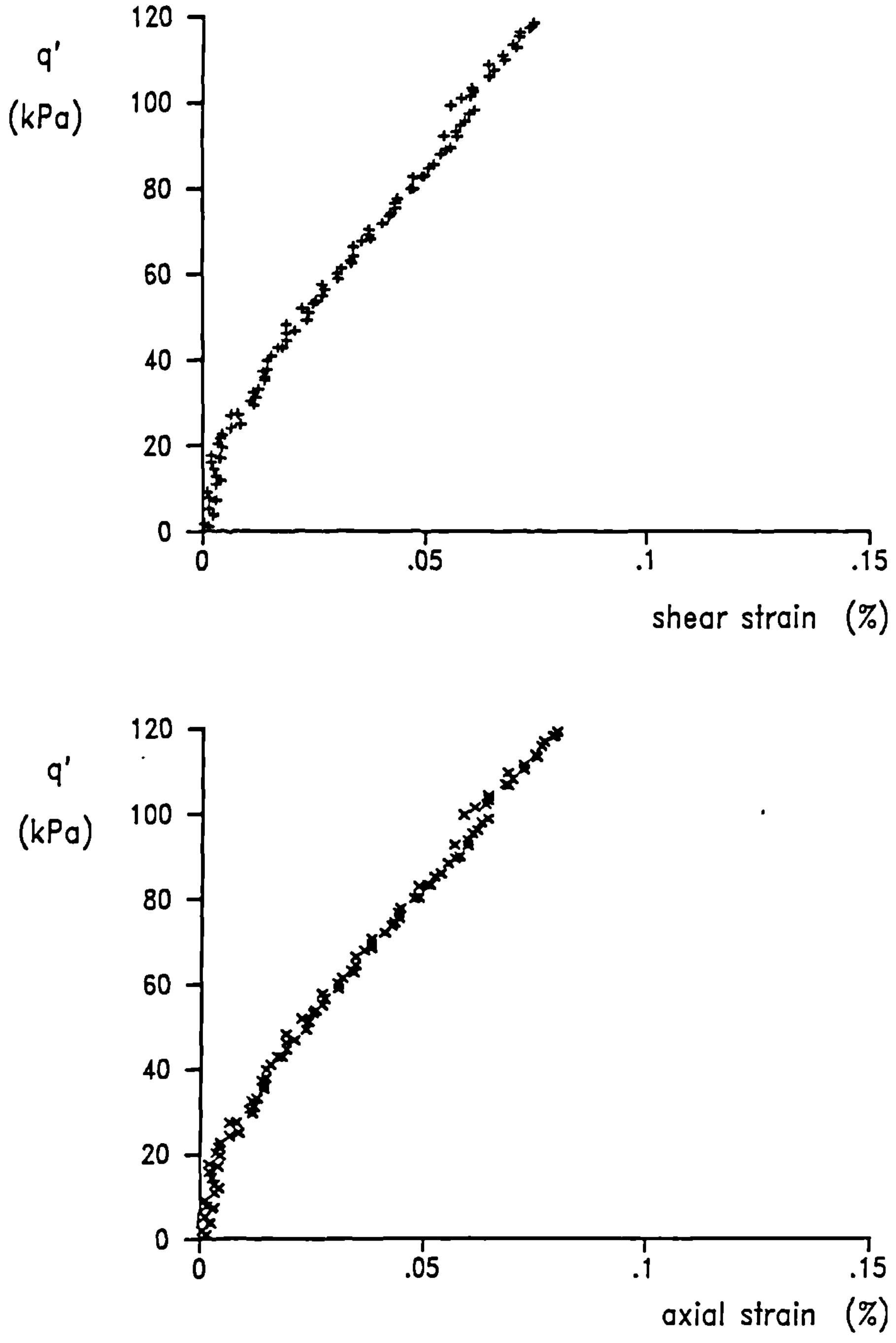

Figure 4.2.4. Comparison between typical curves of deviator stress against axial strain and shear strain, for constant p' loading after a rotation of 90 degrees, taken from test DLC4

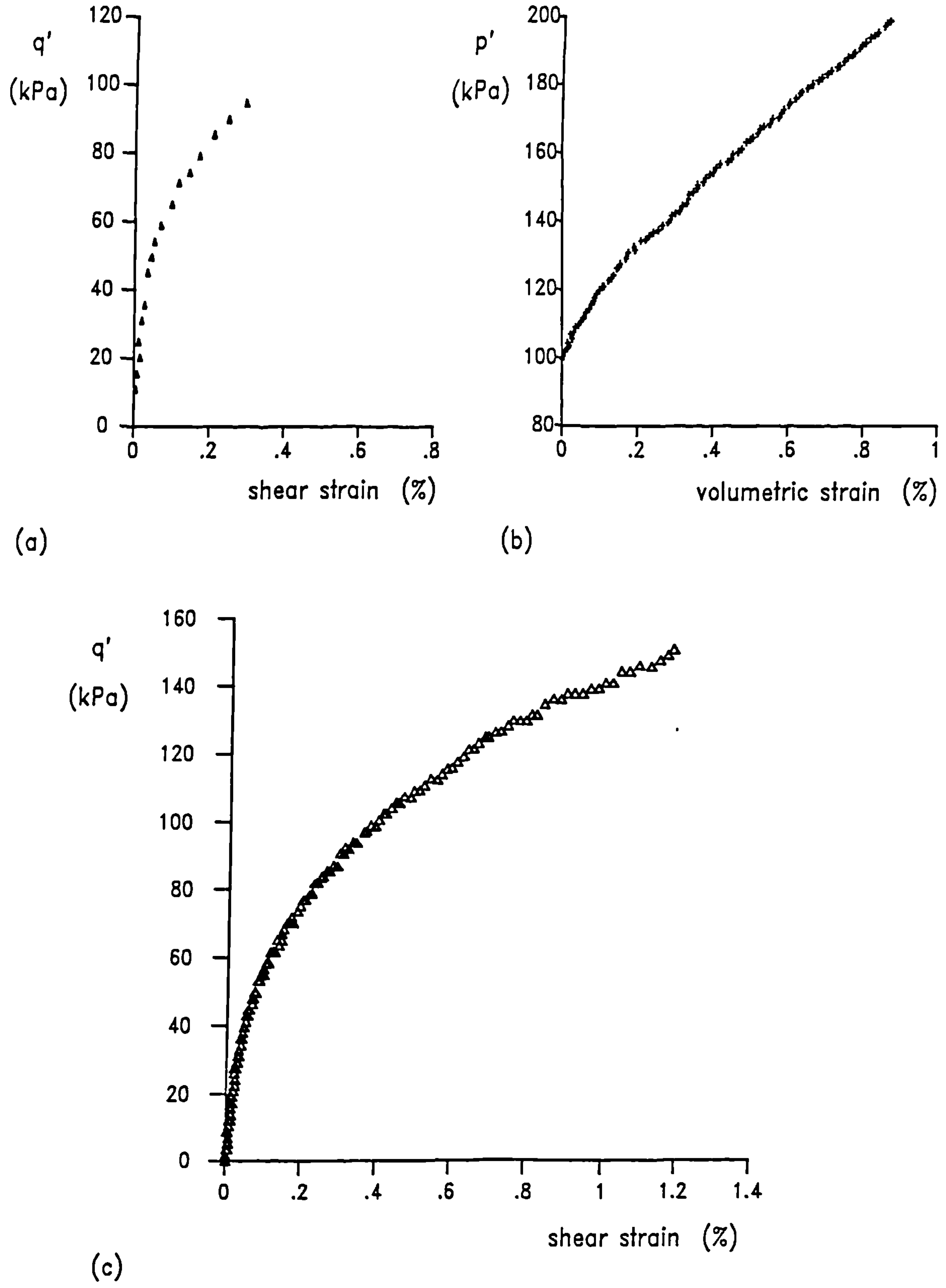

Figure 4.2.5 Typical graphs of deviator stress against shear strain for (a) Test UK7, undrained loading, 90 degrees rotation (b) Test DKSR3, constant q' loading, 180 degrees rotation (c) Test DKSR3, constant p' loading, 90 degrees rotation

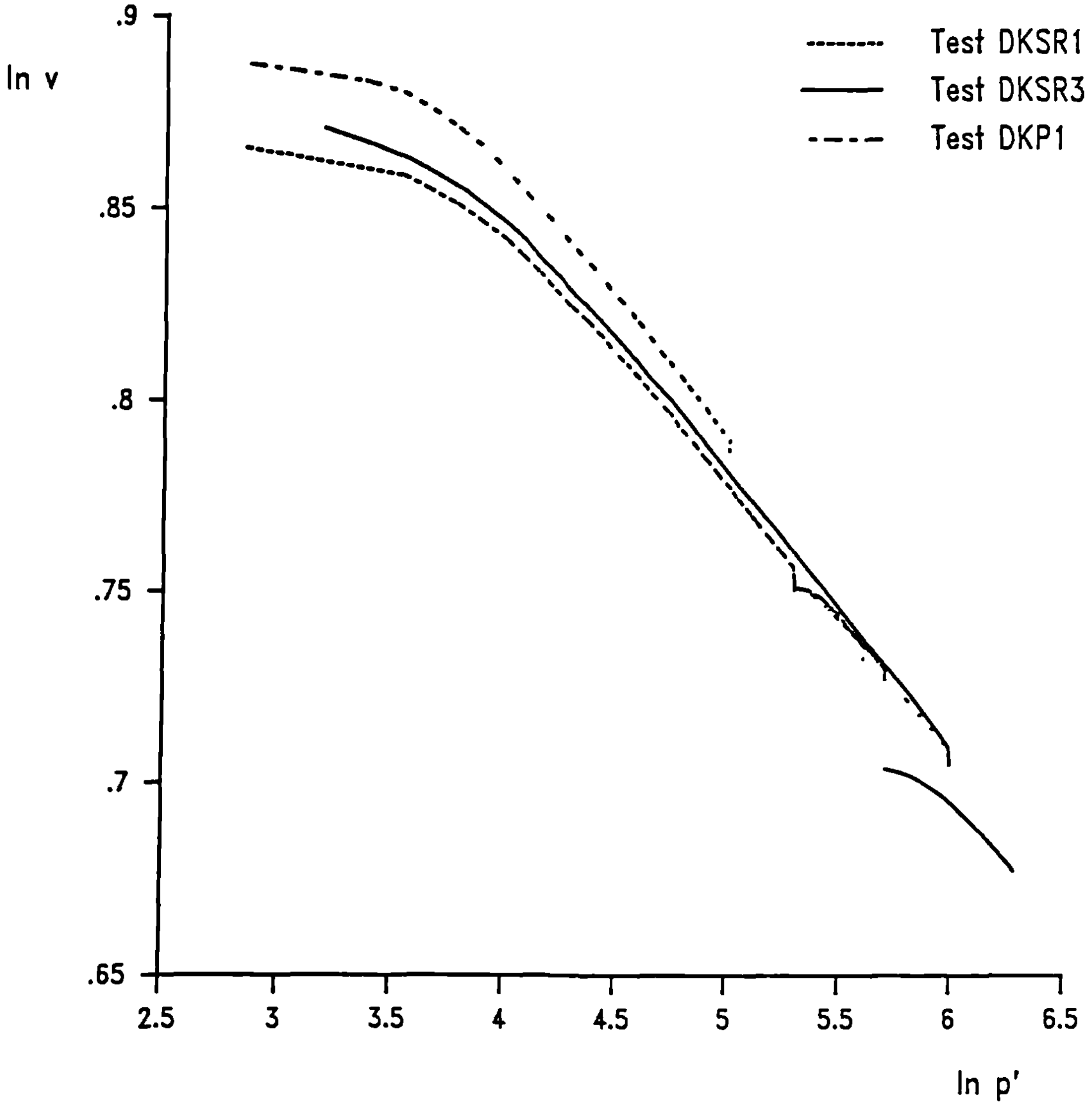

Figure 4.2.6. Isotropic normal compression data for speswhite kaolin

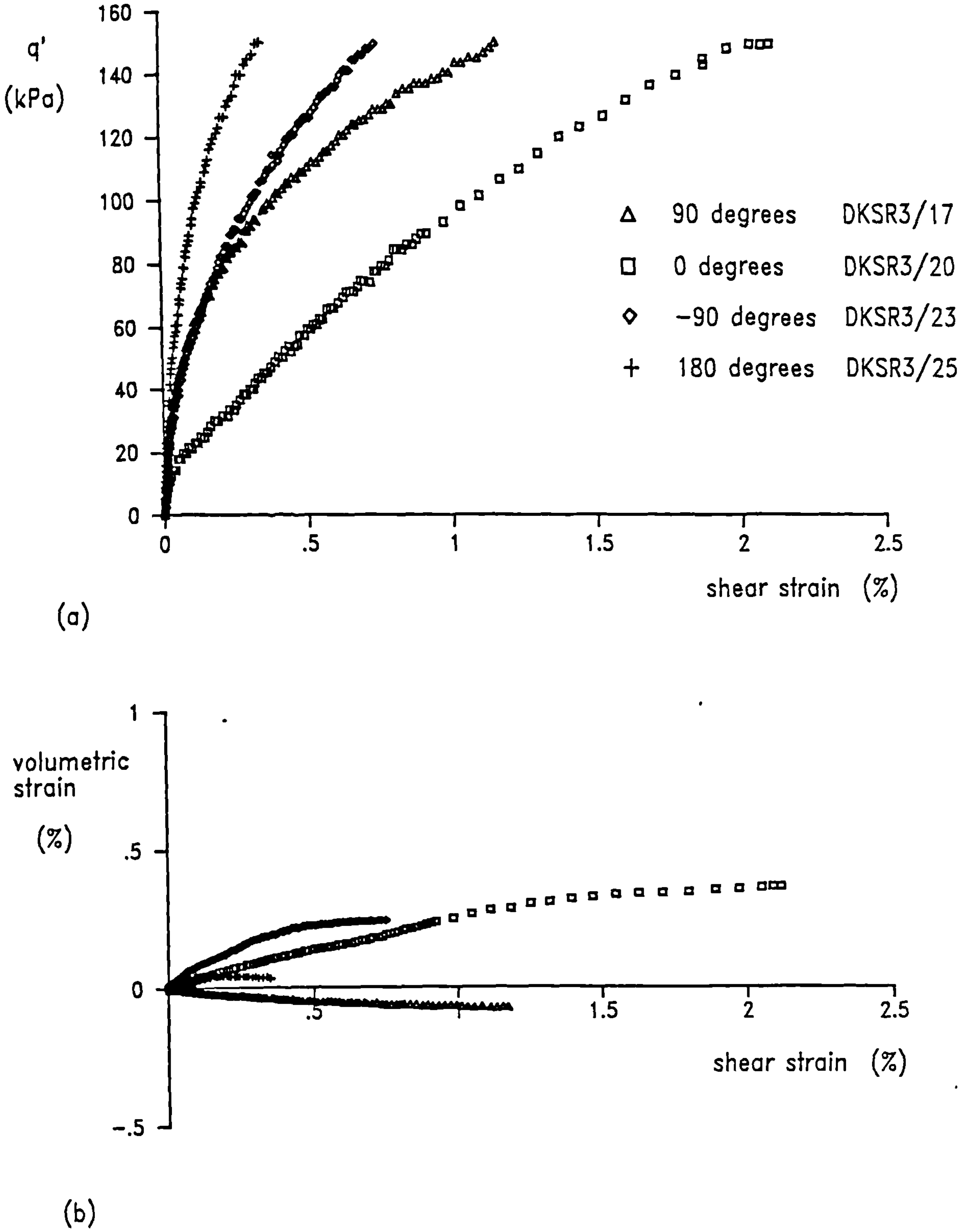

Figure 4.2.7 Stress−strain curves and strain paths for test DKSR3, constant p' loading, p'i = 300kPa, p'm = 720kPa.

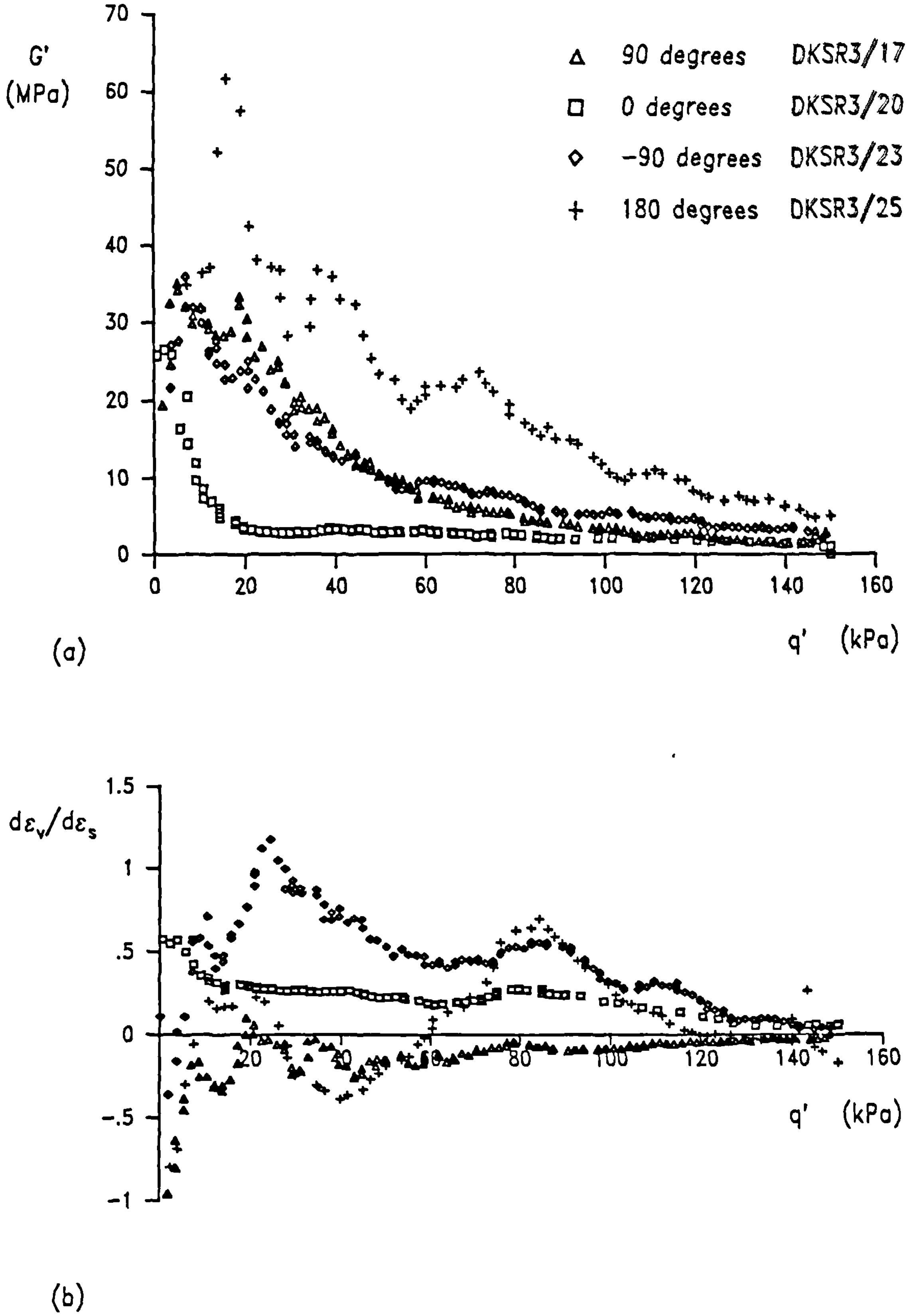

Figure 4.2.8 Curves of (a) stiffness and (b) strain increment ratio against stress change for test DKSR3, constant p' loading, p'i = 300kPa, p'm = 720kPa.

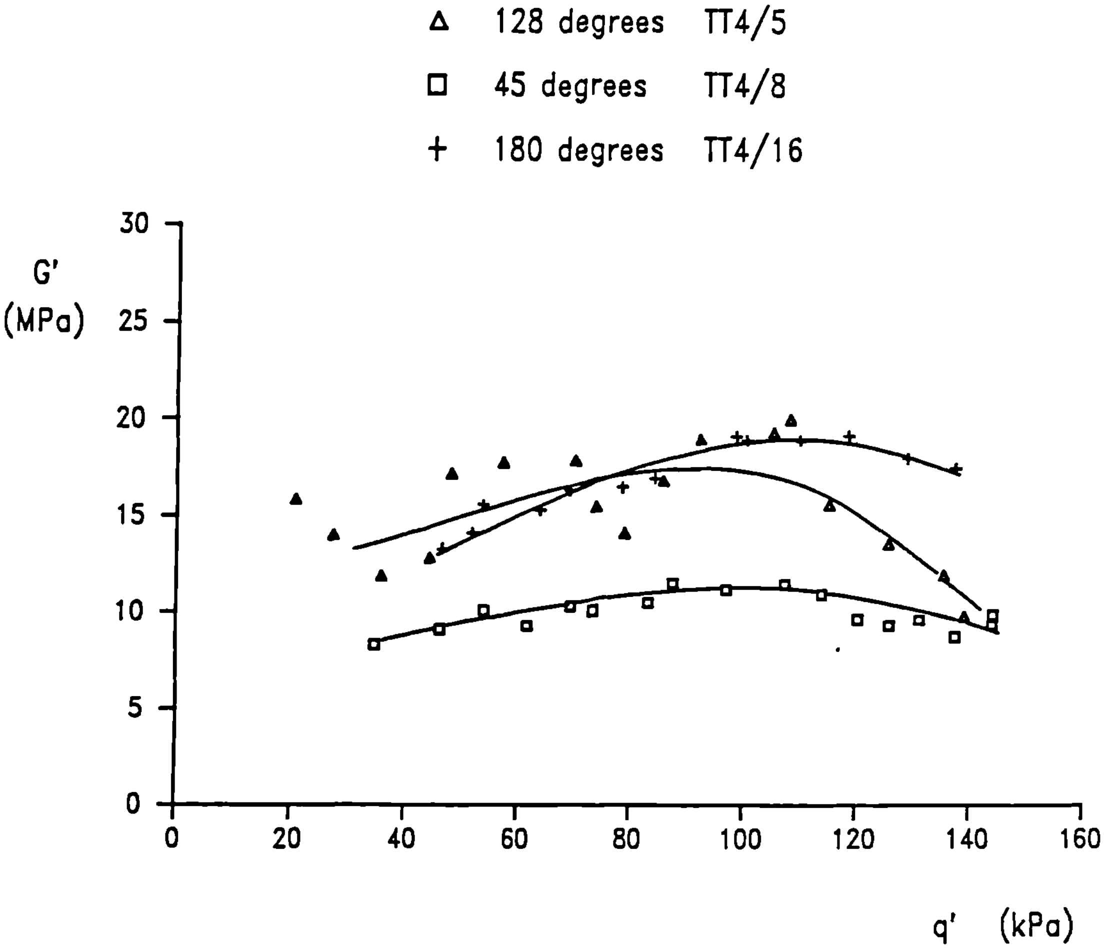

Figure 4.2.9 Curves of shear stiffness against stress change for test TT4, constant p' loading from p'$_i$ = 350kPa. Undisturbed London clay.

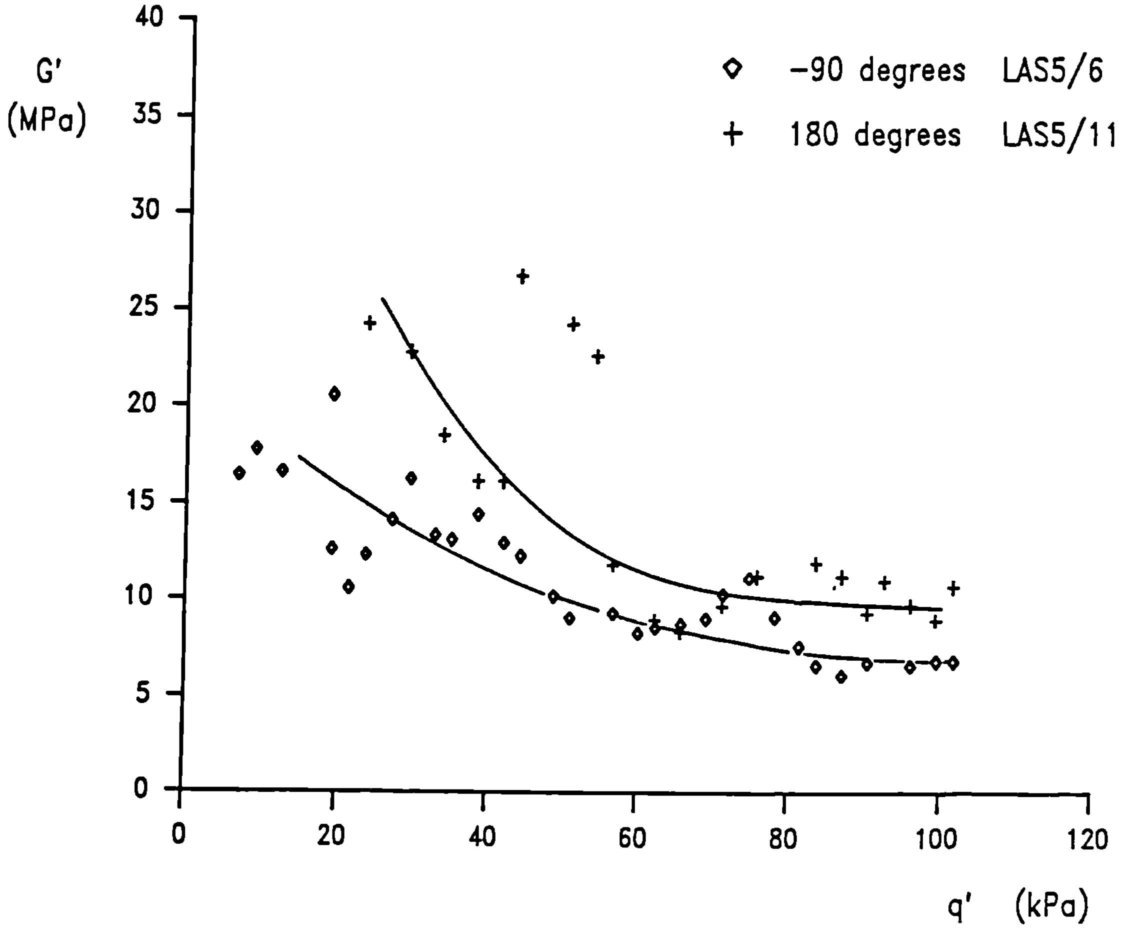

Figure 4.2.10 Curves of shear stiffness against stress change for test LAS5, constant p' loading from p'_i = 200kPa. Undisturbed London clay.

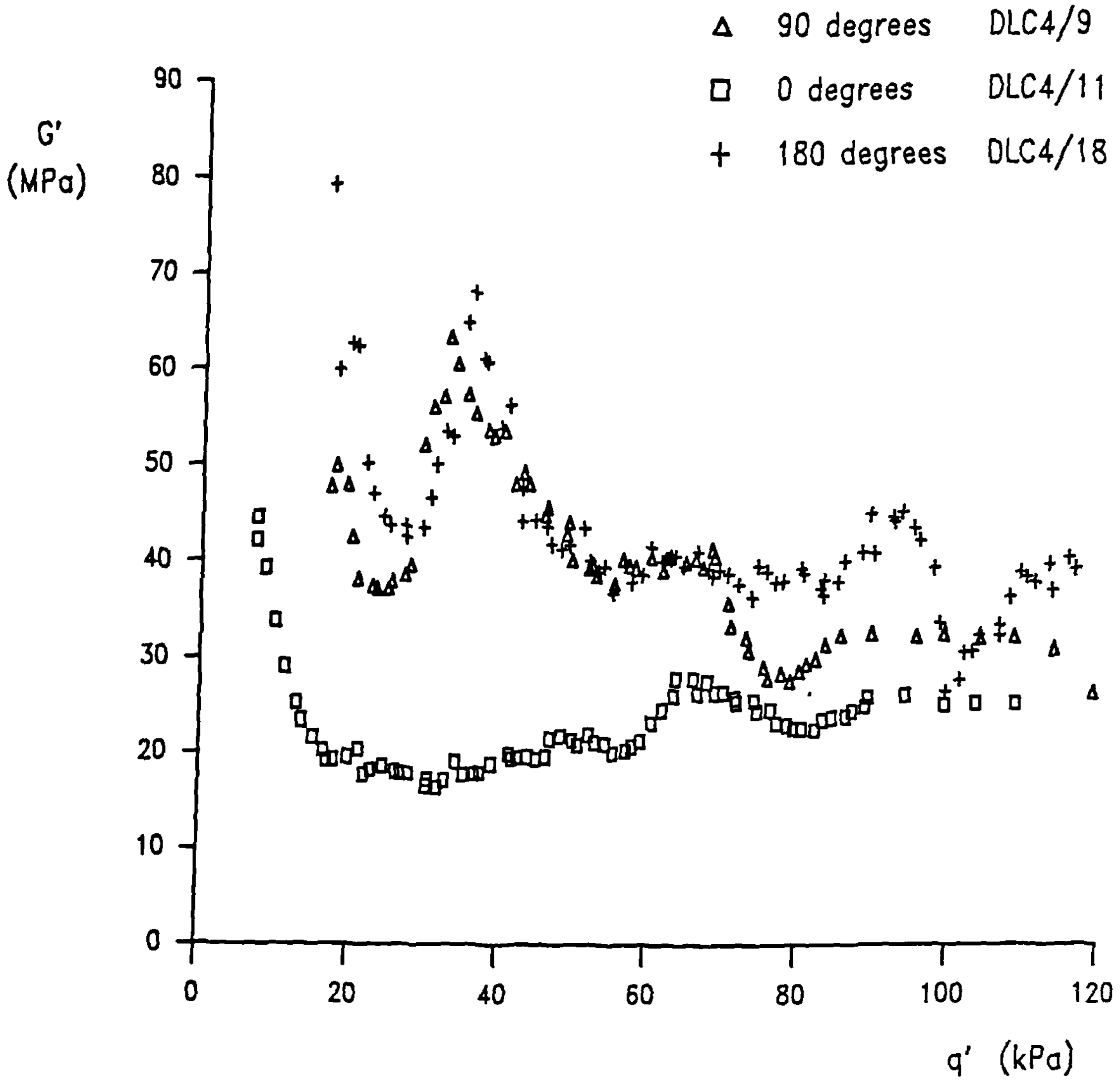

Figure 4.2.11 Curves of shear stiffness against stress change for test DLC4, constant p' loading from p'i = 300kPa. Undisturbed London clay.

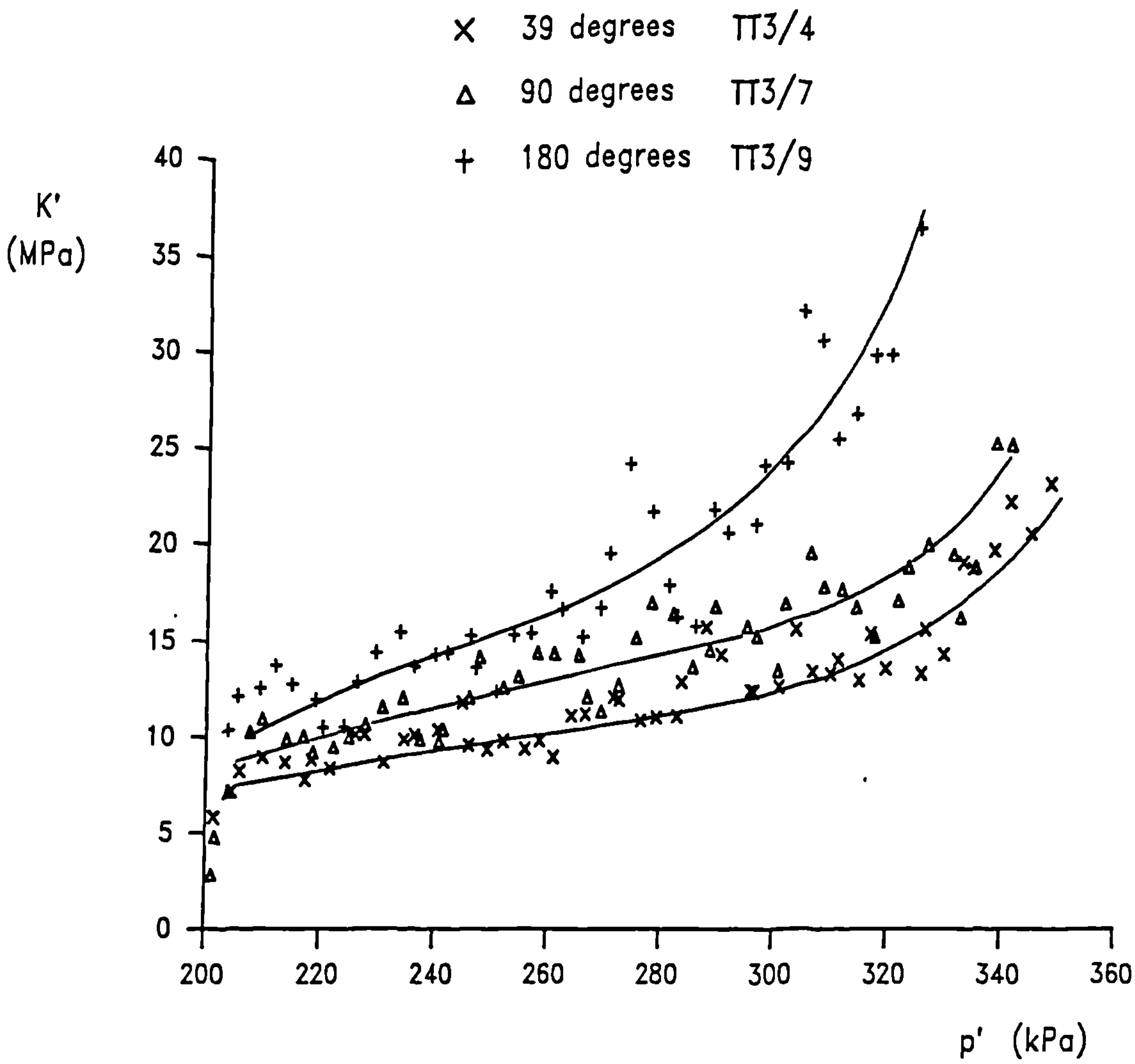

Figure 4.2.12 Curves of bulk stiffness against stress change for test TT3, constant q swelling from p'i = 350kPa, q'i = 0. Undisturbed London clay.

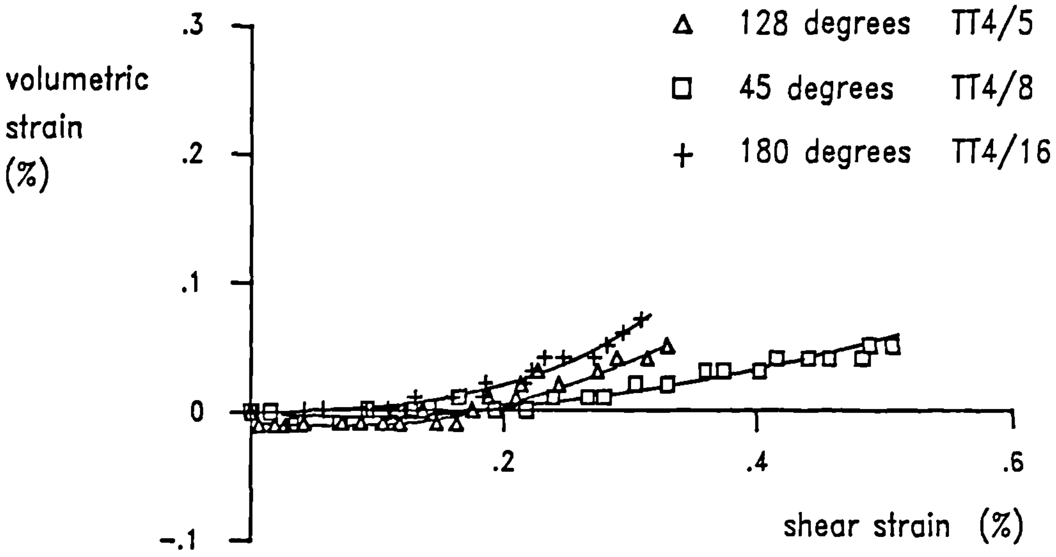

Figure 4.2.13 Strain paths for test TT4, constant p' loading from p'_i = 350kPa. Undisturbed London clay.

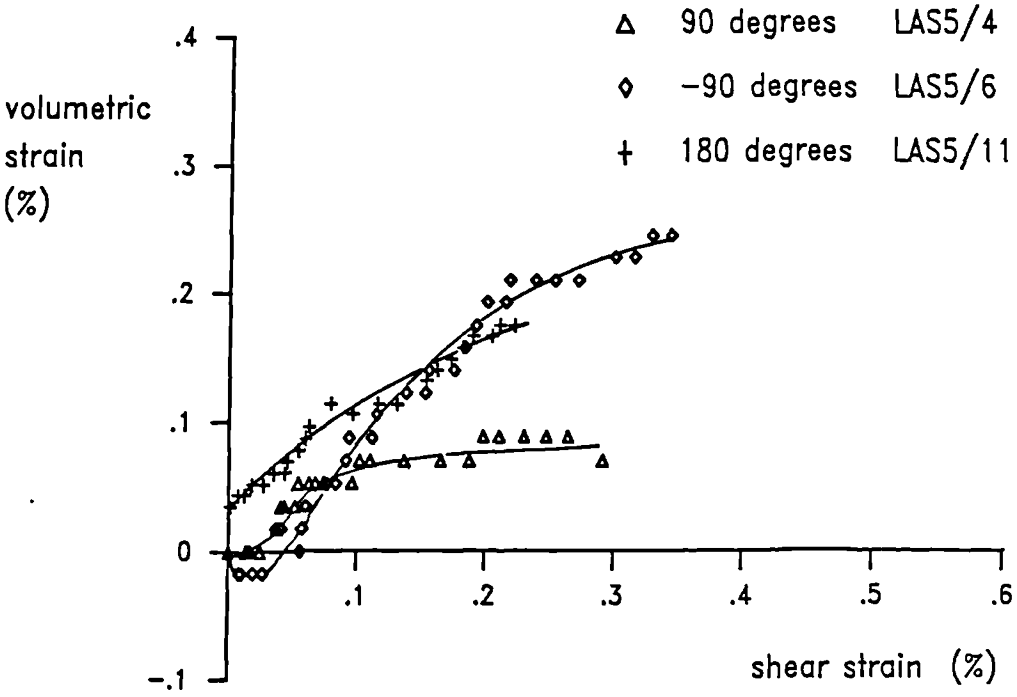

Figure 4.2.14 Strain paths for test LAS5, constant p' loading from p'_i = 200kPa. Undisturbed London clay.

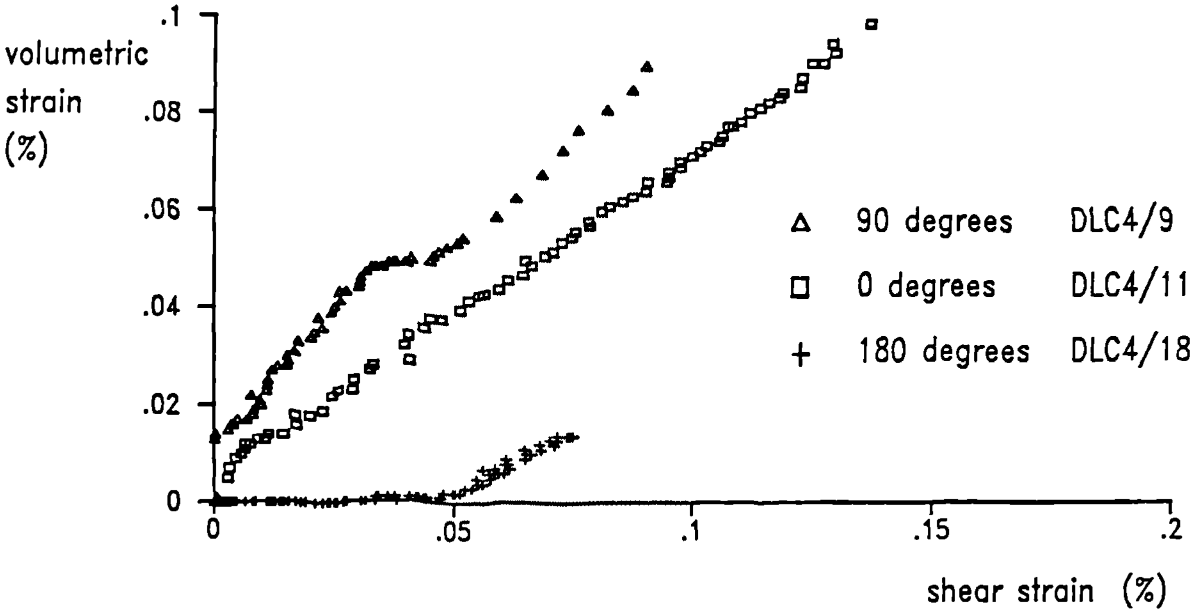

Figure 4.2.15 Strain paths for test DLC4, constant p' loading from p'i = 300kPa. Undisturbed London clay.

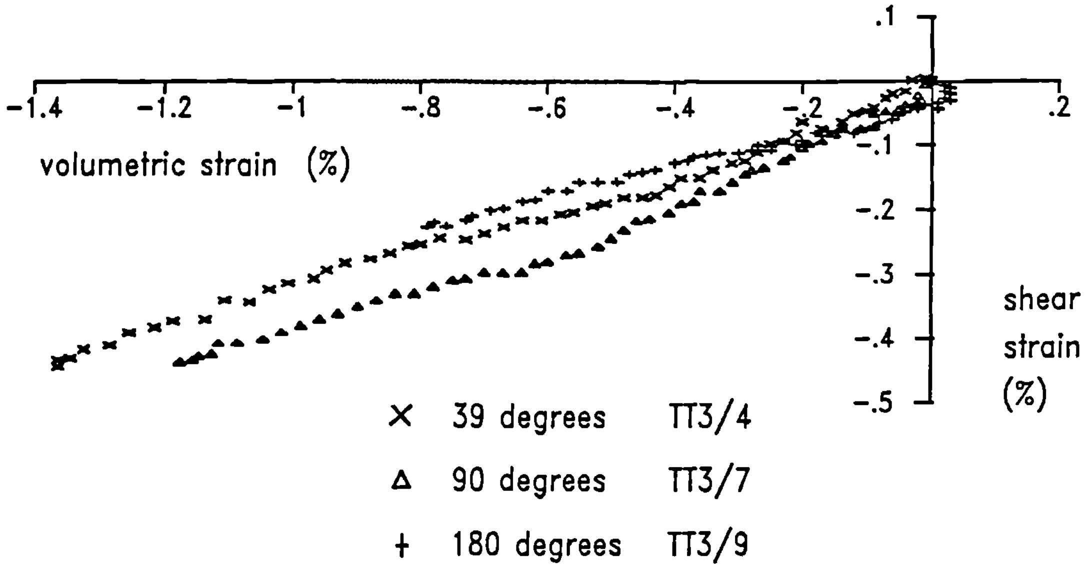

Figure 4.2.16 Strain paths for test TT3, constant q' swelling from p'i = 350kPa, q'i = 0. Undisturbed London clay.

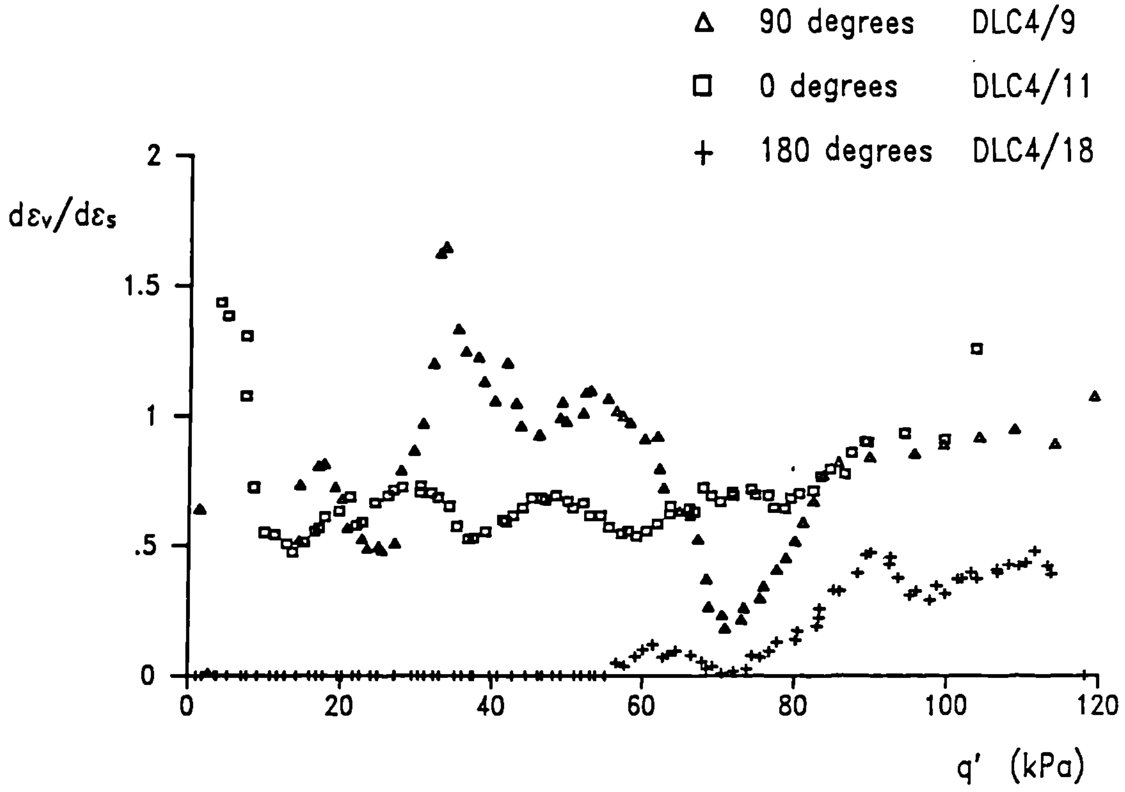

Figure 4.2.17 Plots of stress increment ratio against stress change for test DLC4, constant p' loading from p'i = 350kPa. Undisturbed London clay

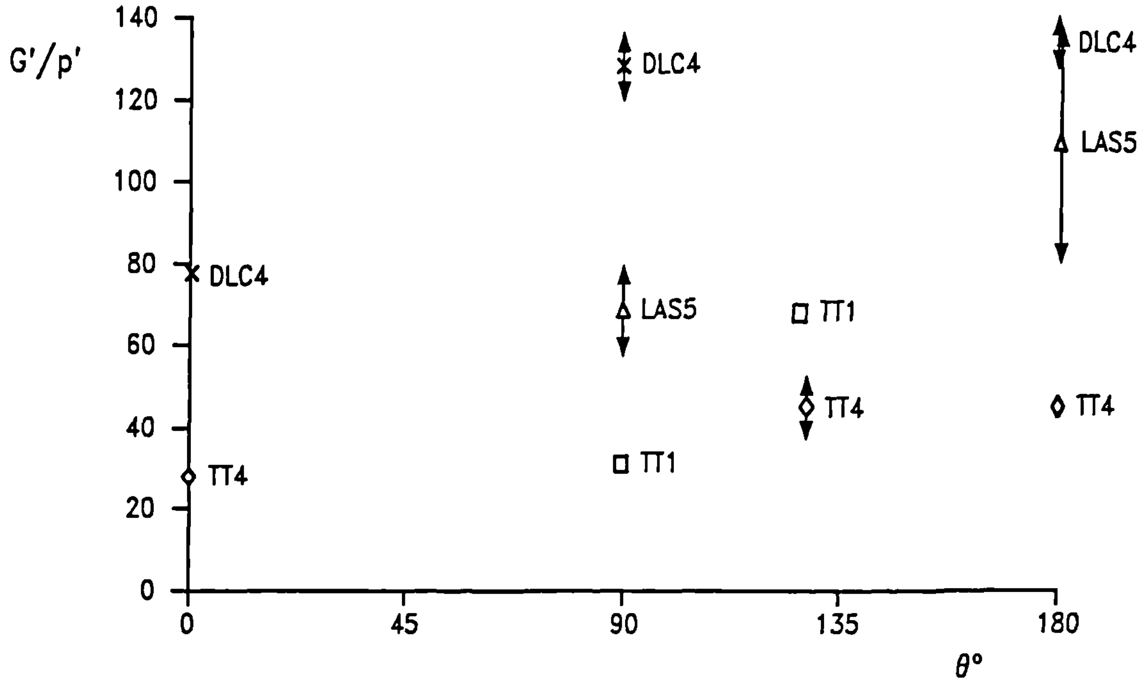

Figure 4.2.18 Plots of normalised shear stiffness, G'/p', at $\Delta q'/p' = 0.2$ against angle of stress path rotation, θ. Data taken from tests at constant p' on undisturbed London clay.

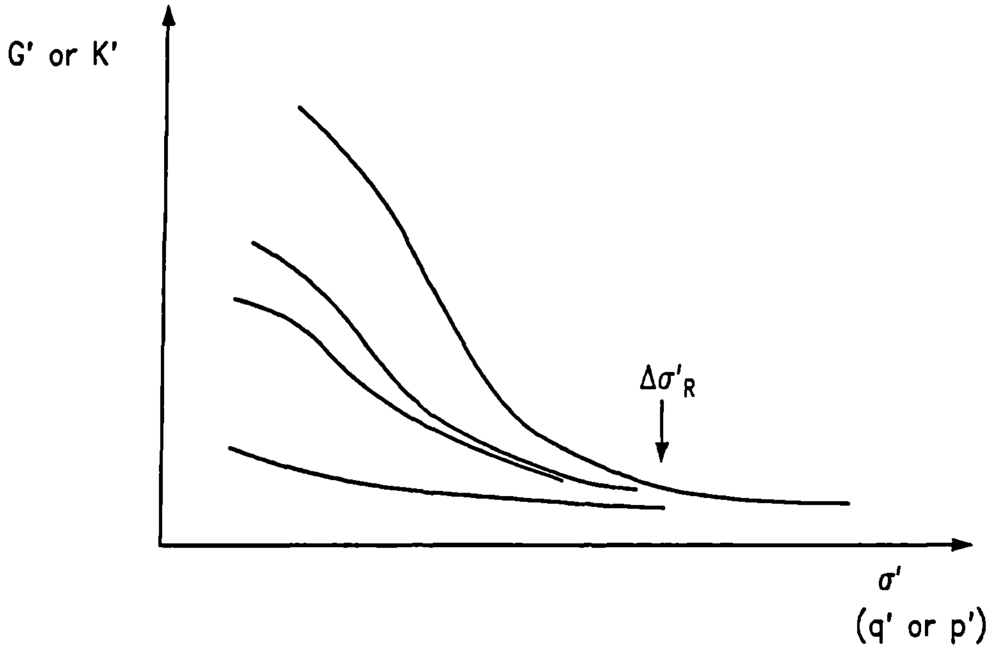

Figure 4.2.19 Definition of $\Delta\sigma'_R$ using a schematic representation of typical stiffness data.

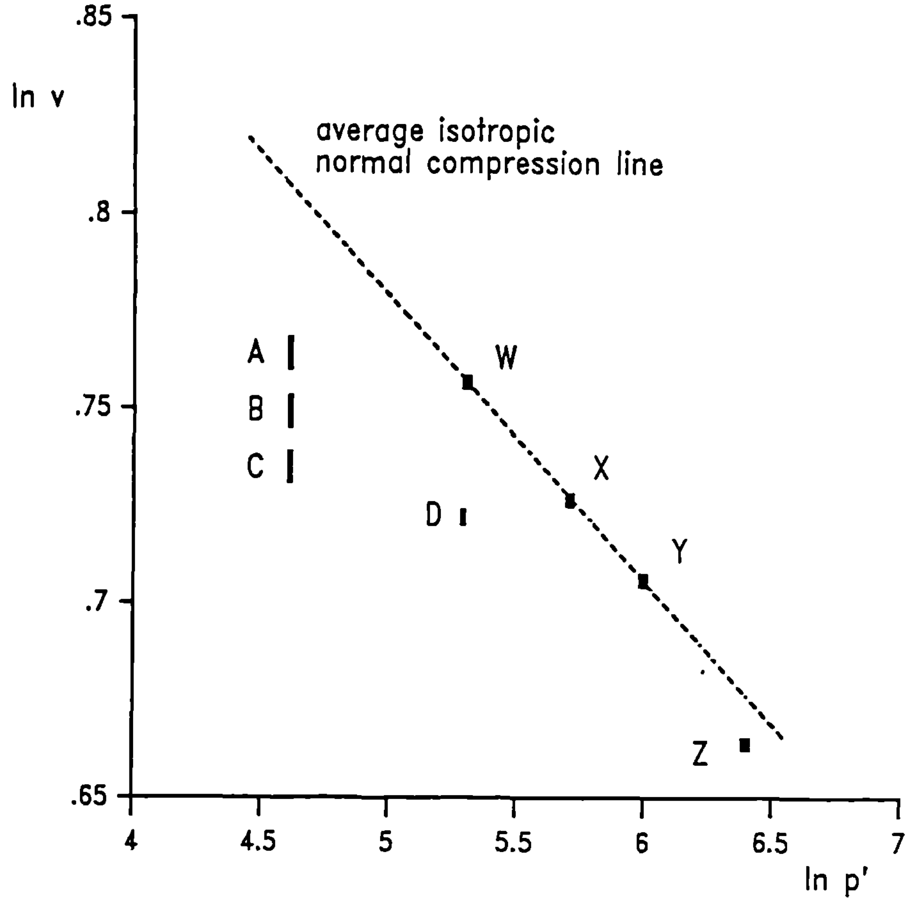

Figure 4.2.20 Graph showing the initial states of the constant q' loading paths relative to the isotropic normal compression line in lnv:lnp' space

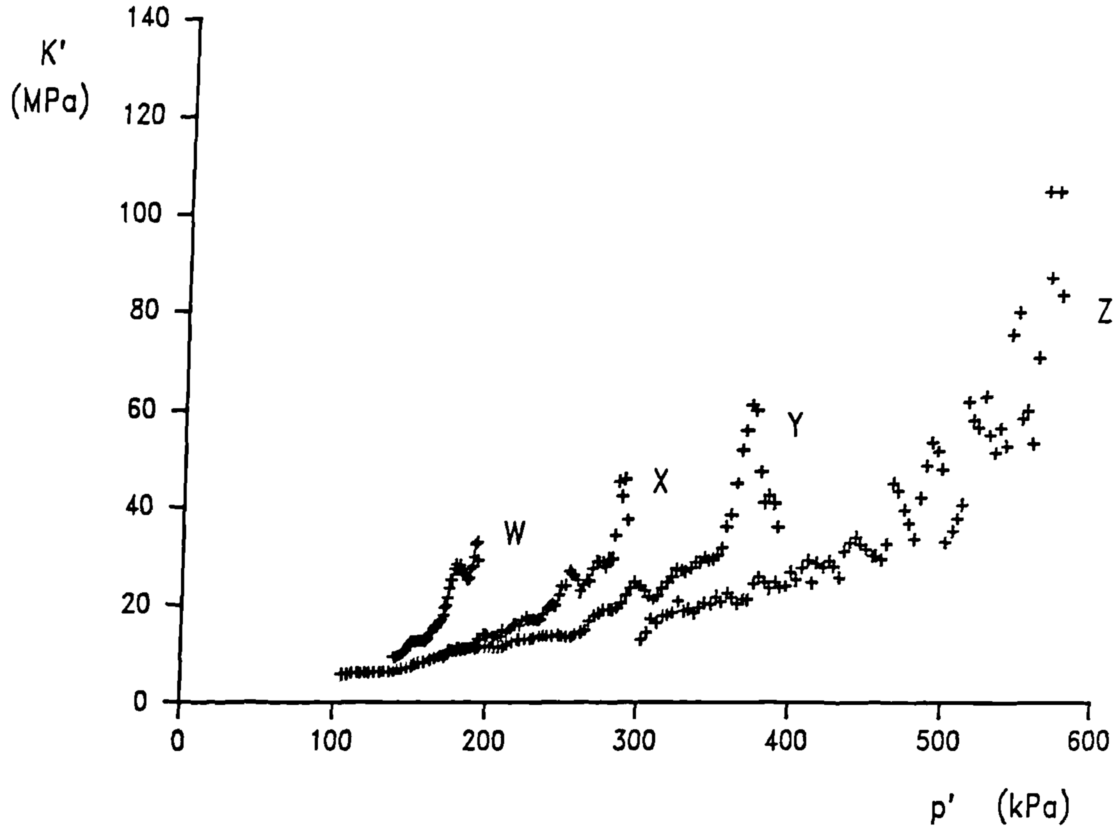

Figure 4.2.21 Curves showing the variation in bulk stiffness with p' for samples of reconstituted speswhite kaolin swelled back from four different normally consolidated states.

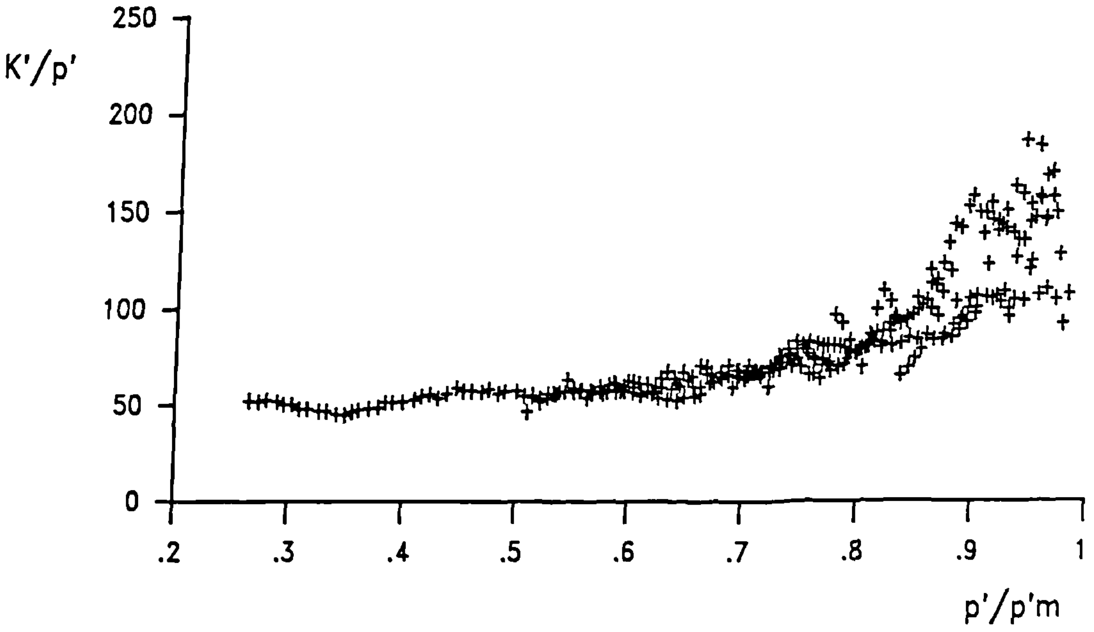

Figure 4.2.22 Stiffness data from the isotropic swelling stages shown in Figure 4.2.21 normalised with respect to p' and plotted against p'/p'm (1/Ro).

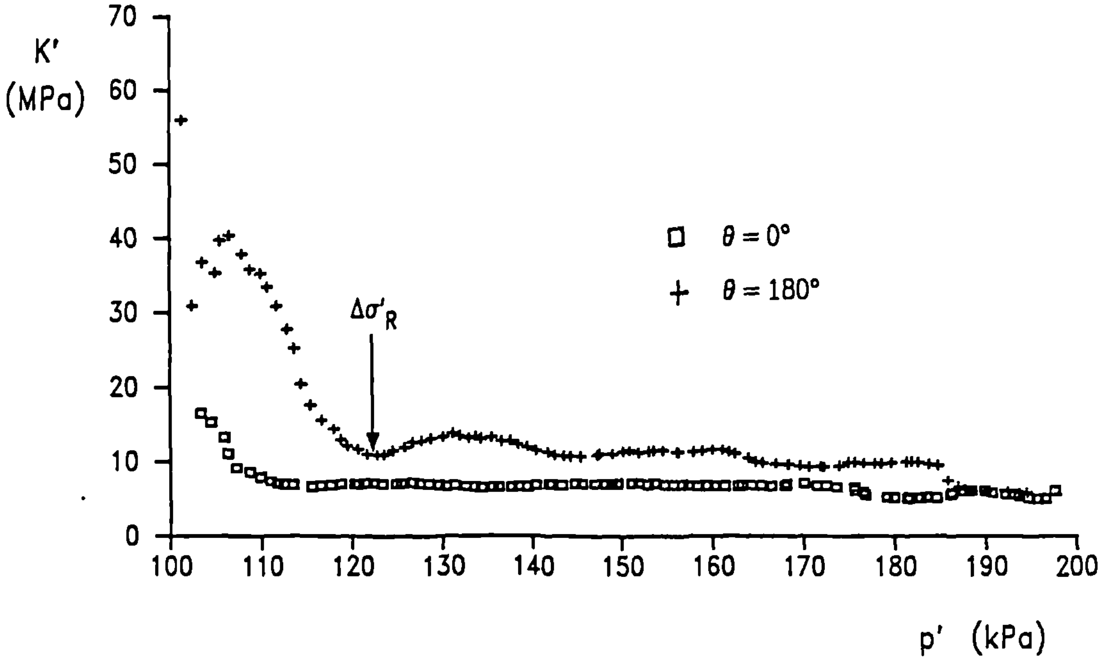

(a) path starting at A

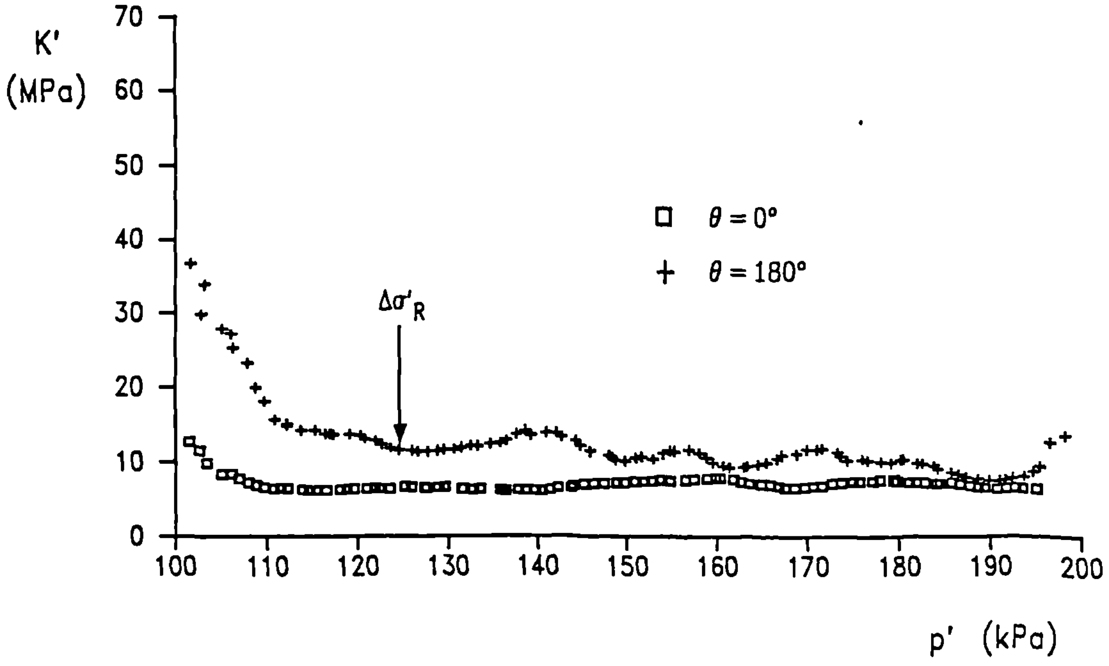

(b) path starting at B

Figure 4.2.23 Curves showing the variation in bulk stiffness with p' after rotations of 180 and 0 degrees, along a constant q' path from (a) p'i = 100kPa, p'm = 200kPa (b) p'i = 100kPa, p'm = 300kPa

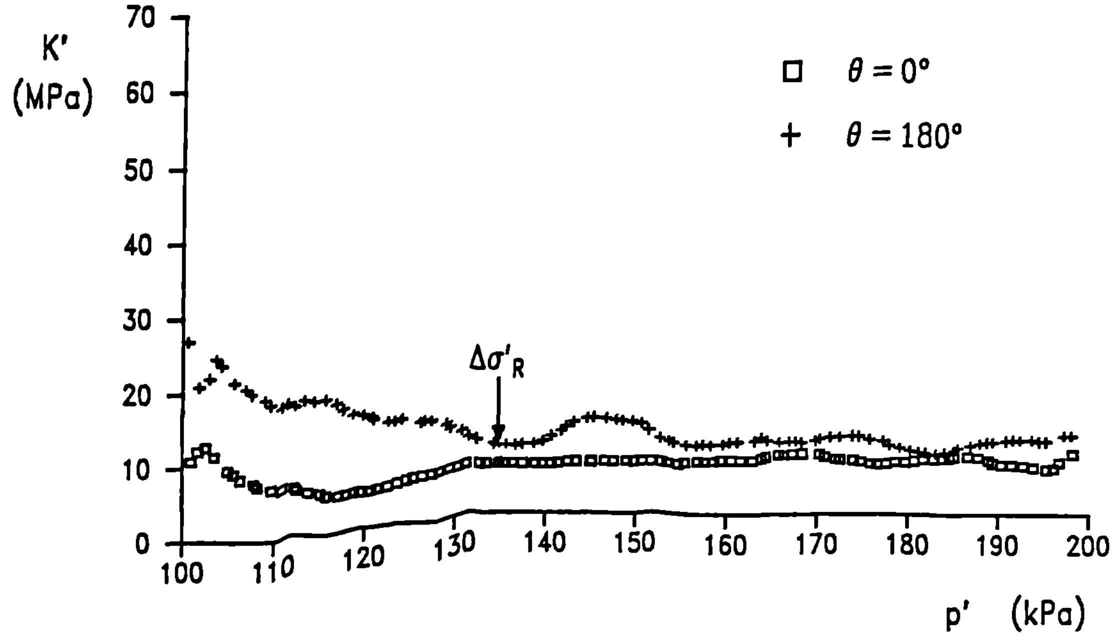

(a) path starting at C

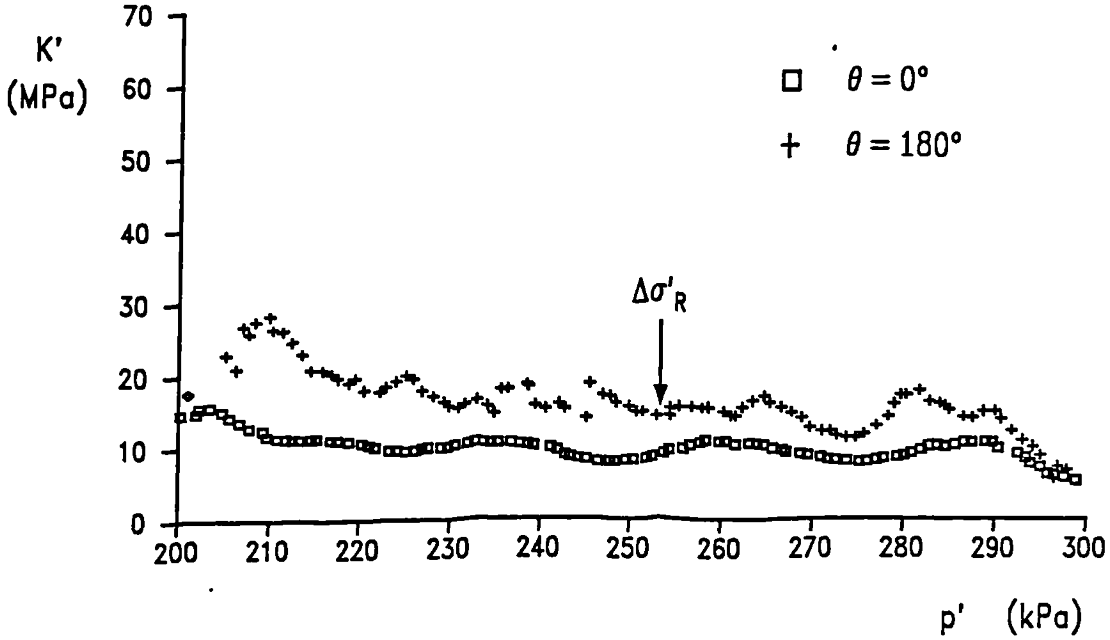

(b) path starting at D

Figure 4.2.24 Curves showing the variation in bulk stiffness with p' after rotations of 180 and 0 degrees, along a constant q' path from (a) p'i = 100kPa, p'm = 400kPa (b) p'i = 200kPa, p'm = 400kPa (data for 180° - O'Connor, 1990)

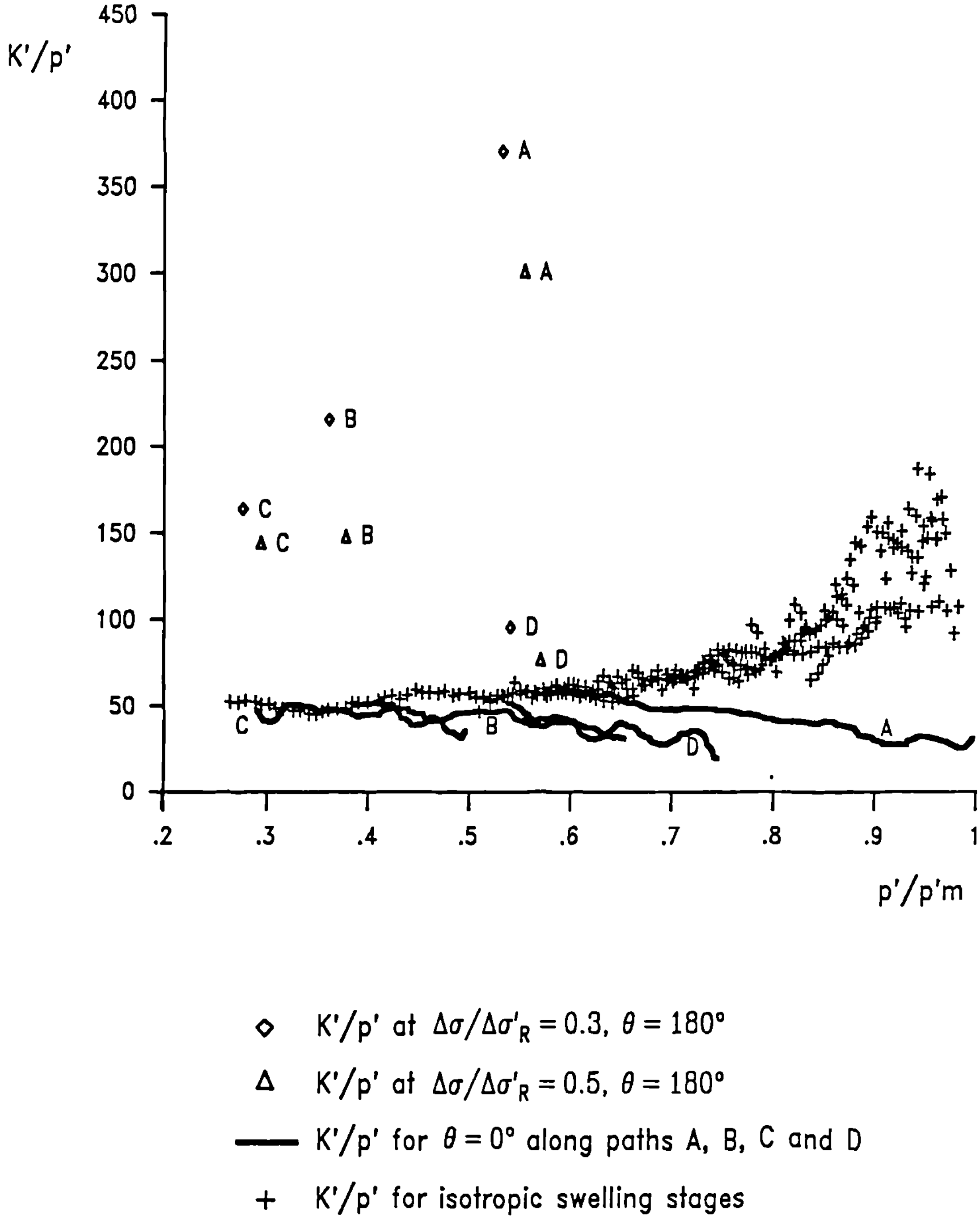

Figure 4.2.25 Plot of normalised bulk stiffness against p'/p'm for all isotropic swelling or compression stages

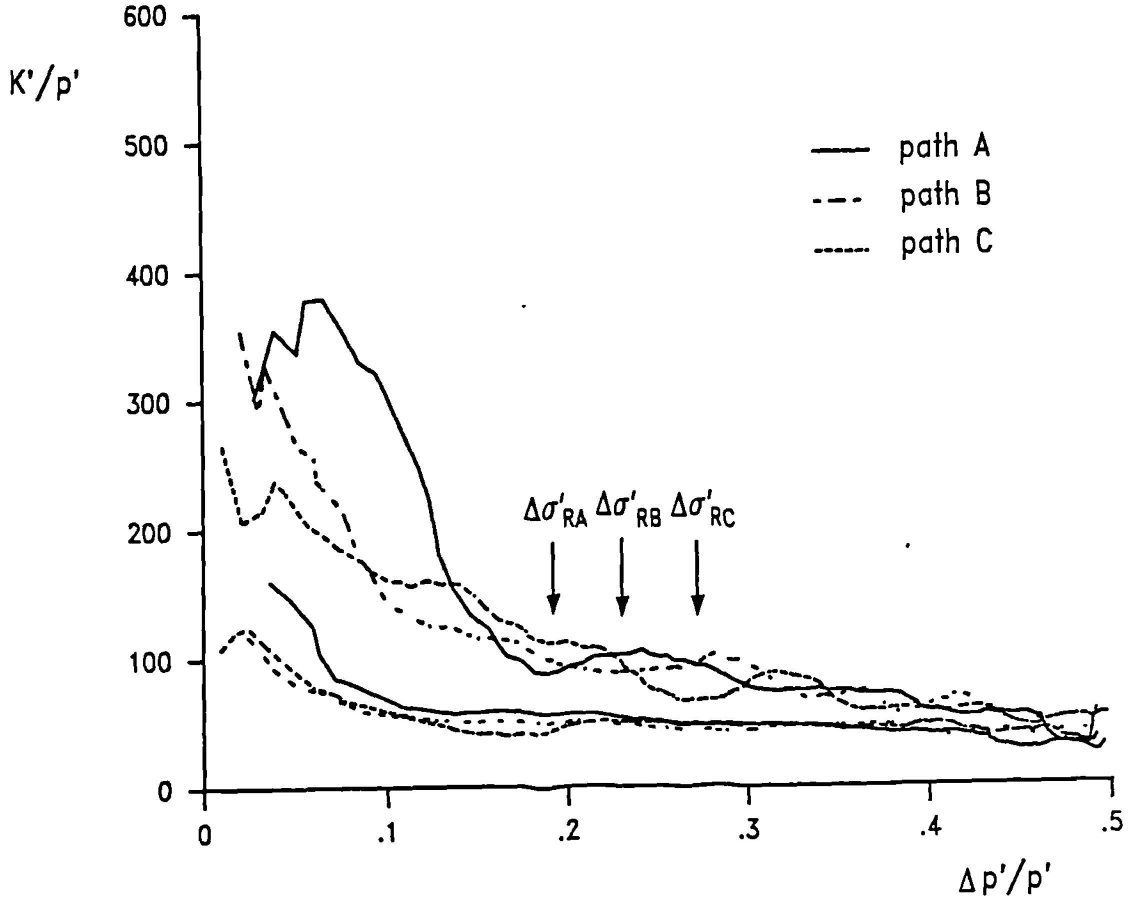

Figure 4.2.26 Graphs of normalised stiffness against normalised stress change along the constant q' paths A, B and C, after 180 and 0 degree rotation.

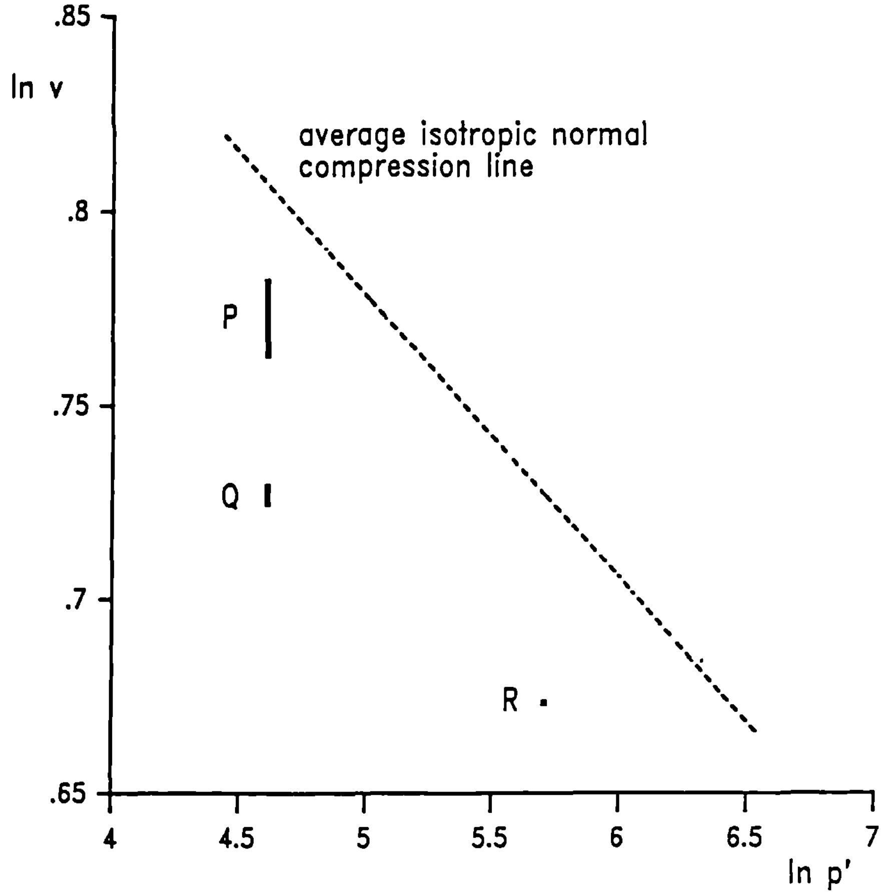

Figure 4.2.27 Graph showing the initial states of the constant p' paths, relative to the isotropic normal compression line, in lnv: lnp' space

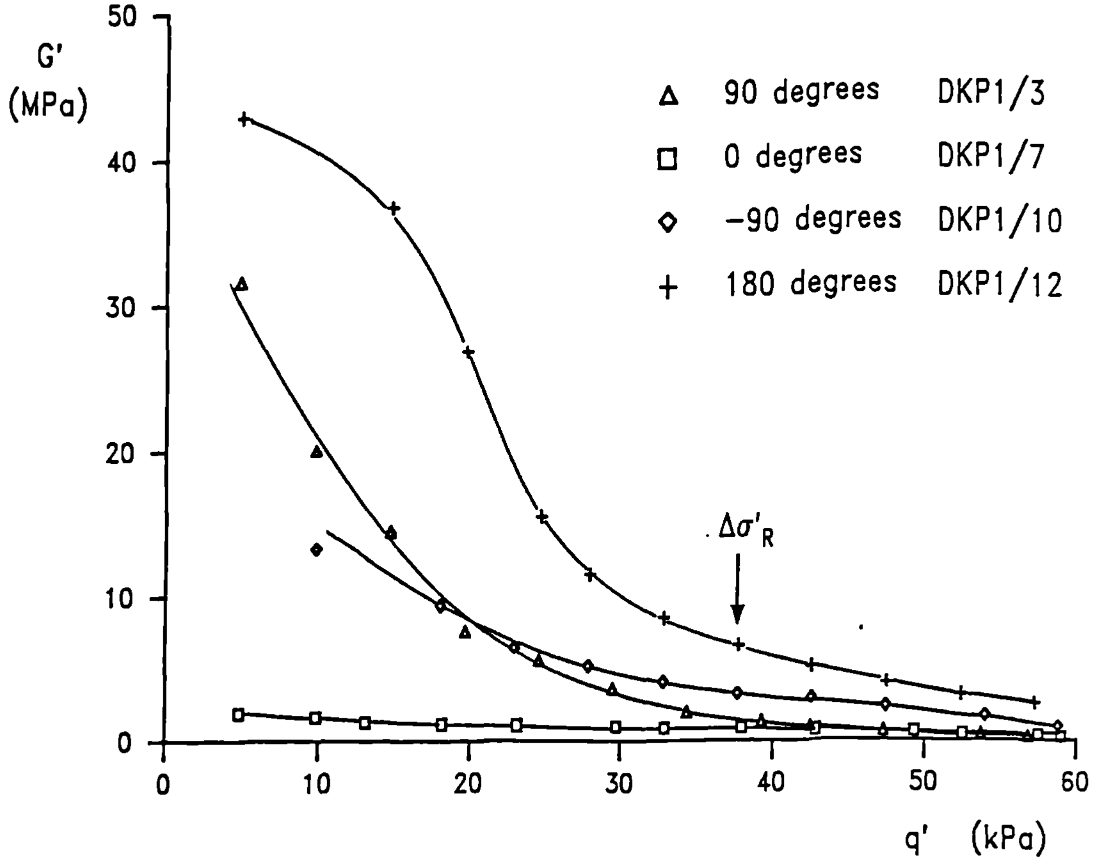

Figure 4.2.28 Curves of shear stiffness against stress change for constant p' loading, path P, p'i = 100kPa, p'm = 150kPa and four different stress path rotations

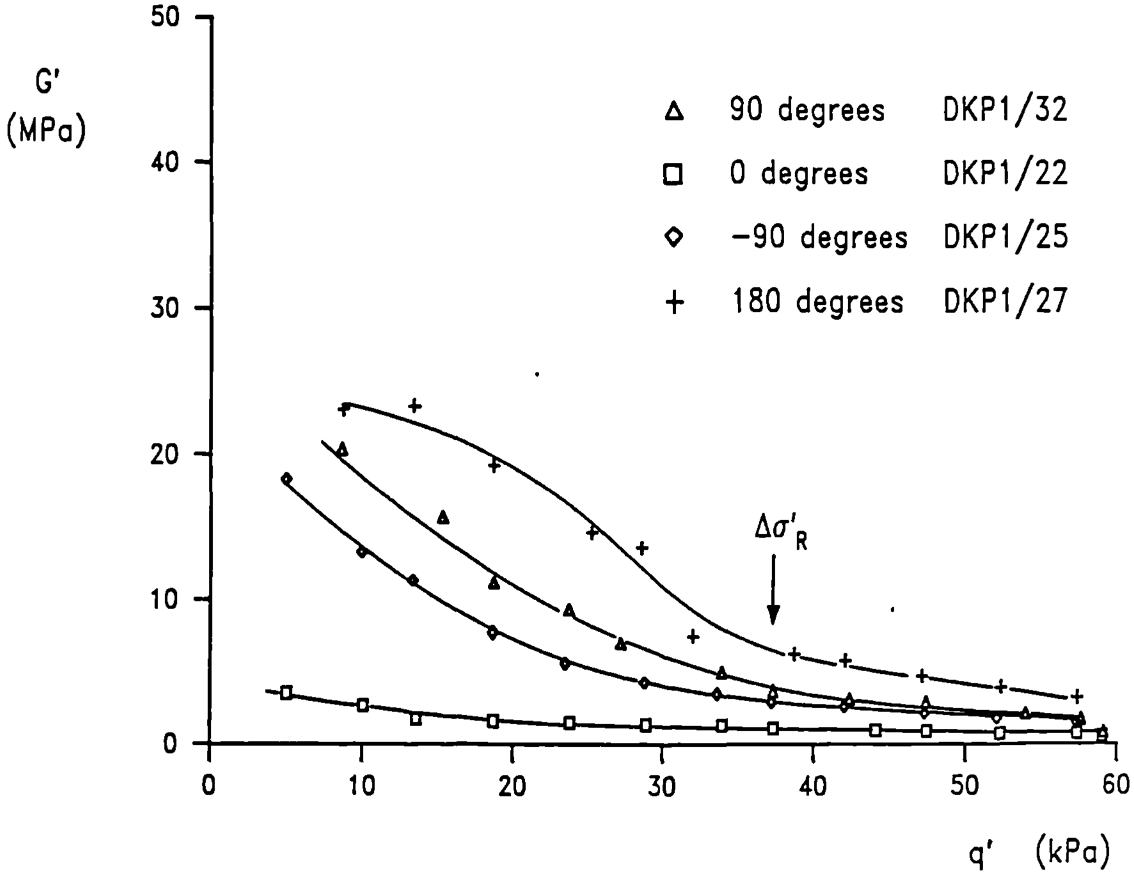

Figure 4.2.29 Curves of shear stiffness against stress change for constant p' loading, path Q, p'i = 100kPa, p'm = 400kPa and four different stress path rotations

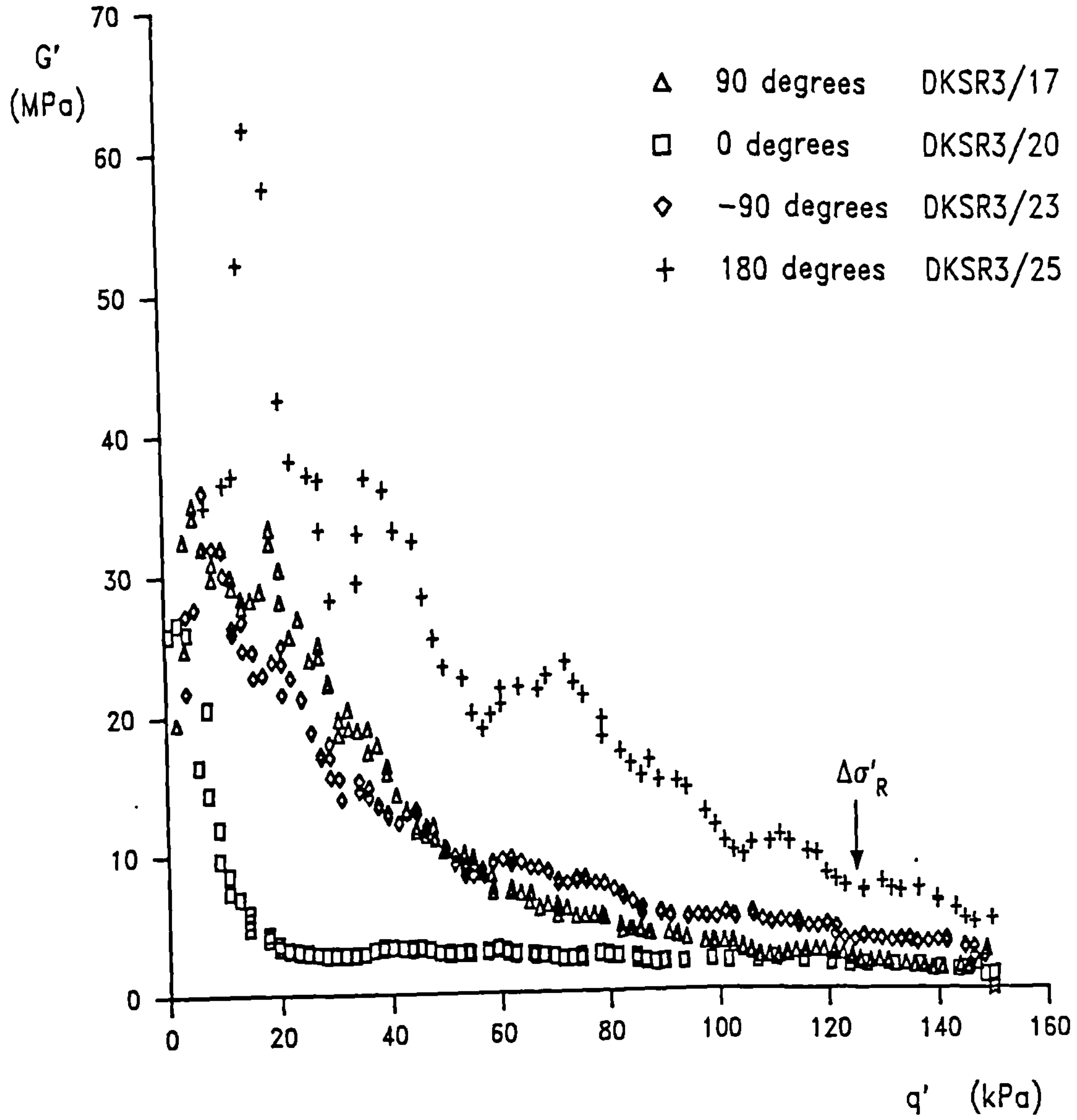

Figure 4.2.30 Curves of shear stiffness against stress change for constant p' loading, path R, p'i = 300kPa, p'm = 720kPa and four different stress path rotations

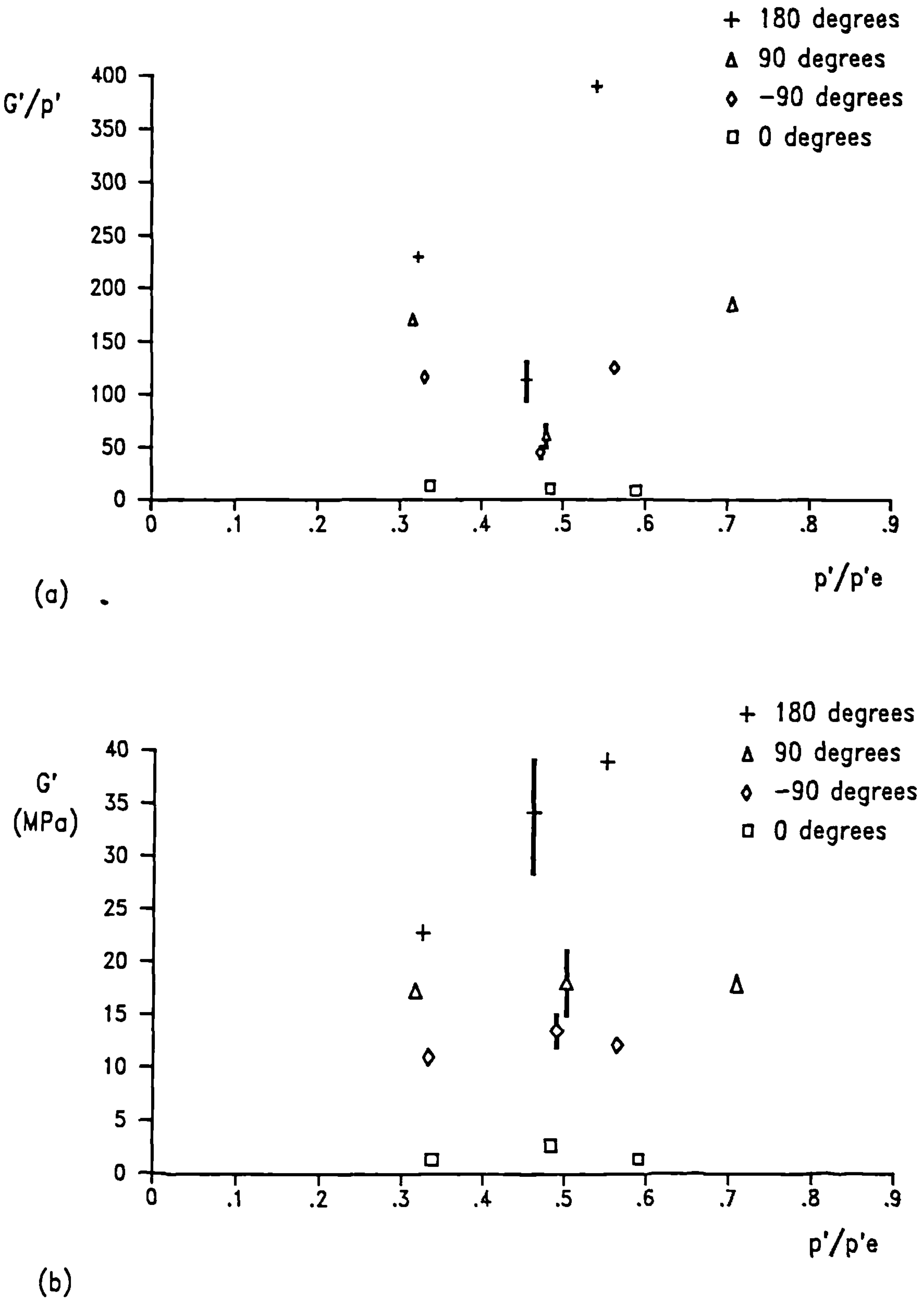

Figure 4.2.31 Plots showing the variation of (a) G'/p' and (b) G' with p'/p'e for constant p' loading. Stiffness measured at $\Delta\sigma'/\Delta\sigma'_R = 0.3$

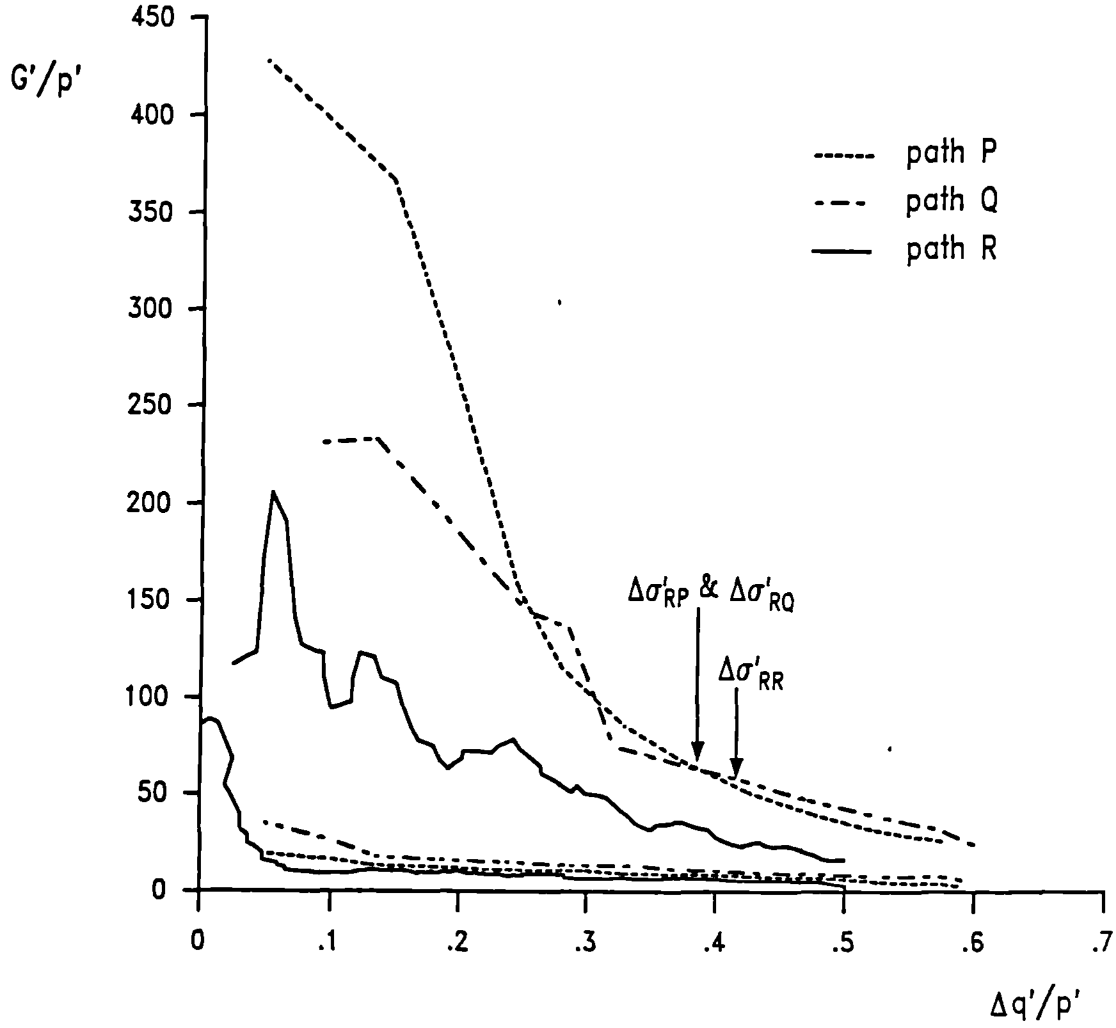

Figure 4.2.32 Stiffness data after rotations of 180 and 0 degrees, from the three paths, P, Q and R, plotted against change in stress normalised by p'.

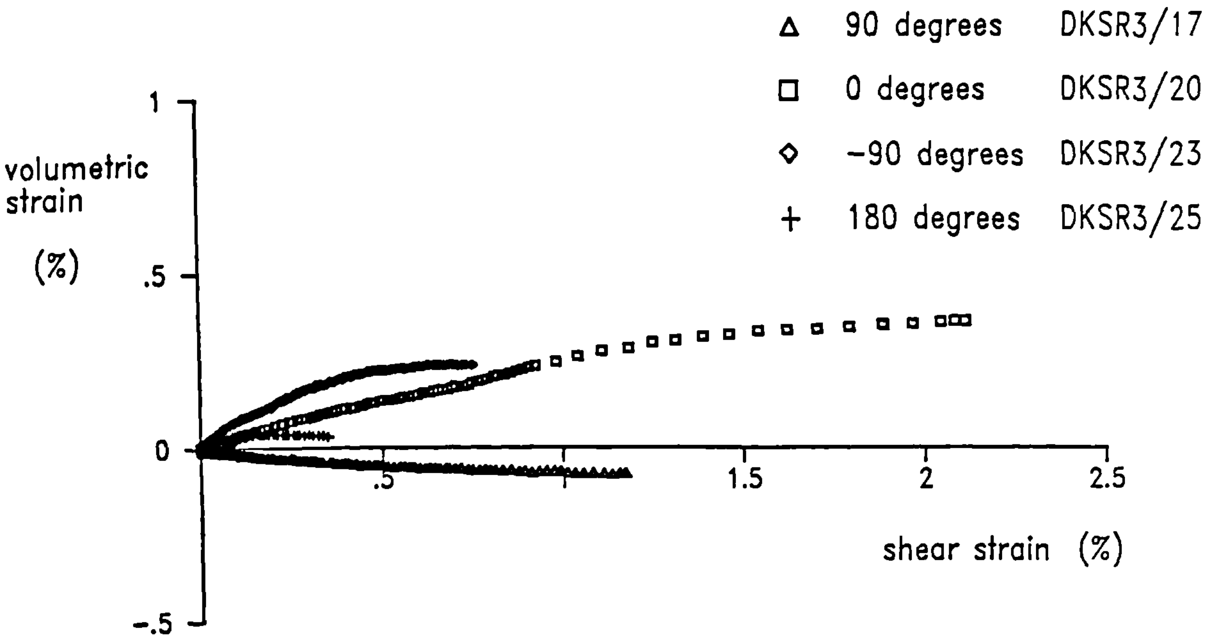

Figure 4.2.33 Strain paths for test DKSR3, constant p' loading, p'i = 300kPa, p'm = 720kPa.

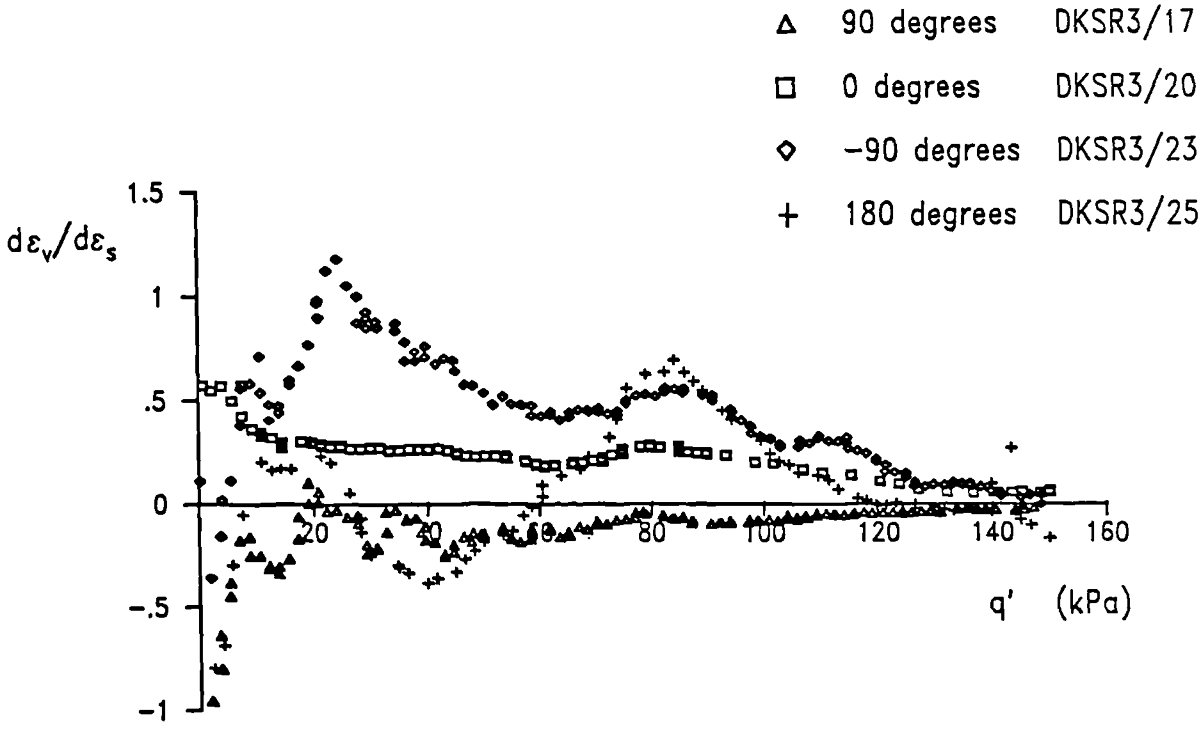

Figure 4.2.34 Curves of strain increment ratio against stress change for test DKSR3, constant p' loading, p'i = 300kPa, p'm = 720kPa.

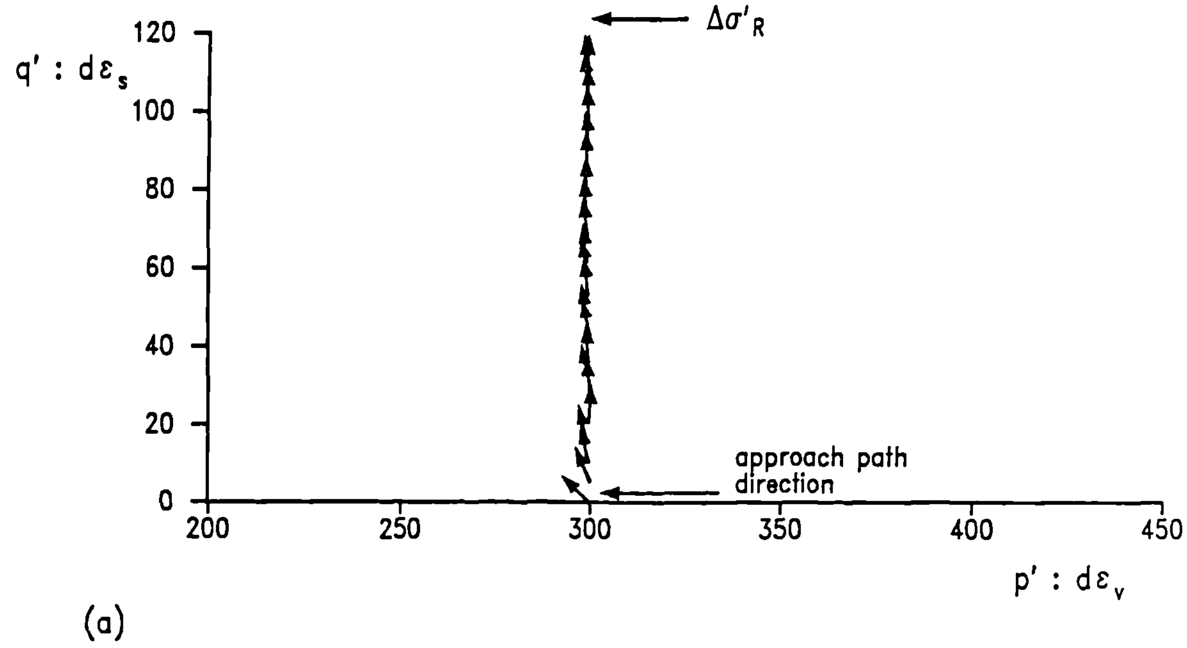

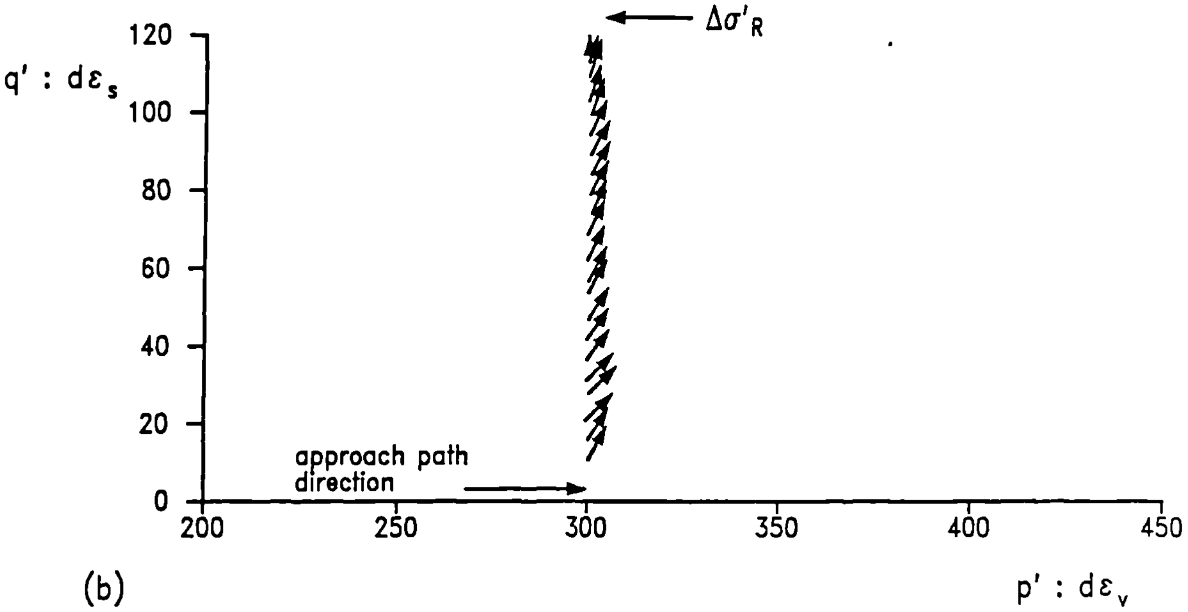

Figure 4.2.35 Strain increment vectors plotted at stages along a constant p' loading path, after (a) 90 degrees rotation (b) −90 degrees rotation

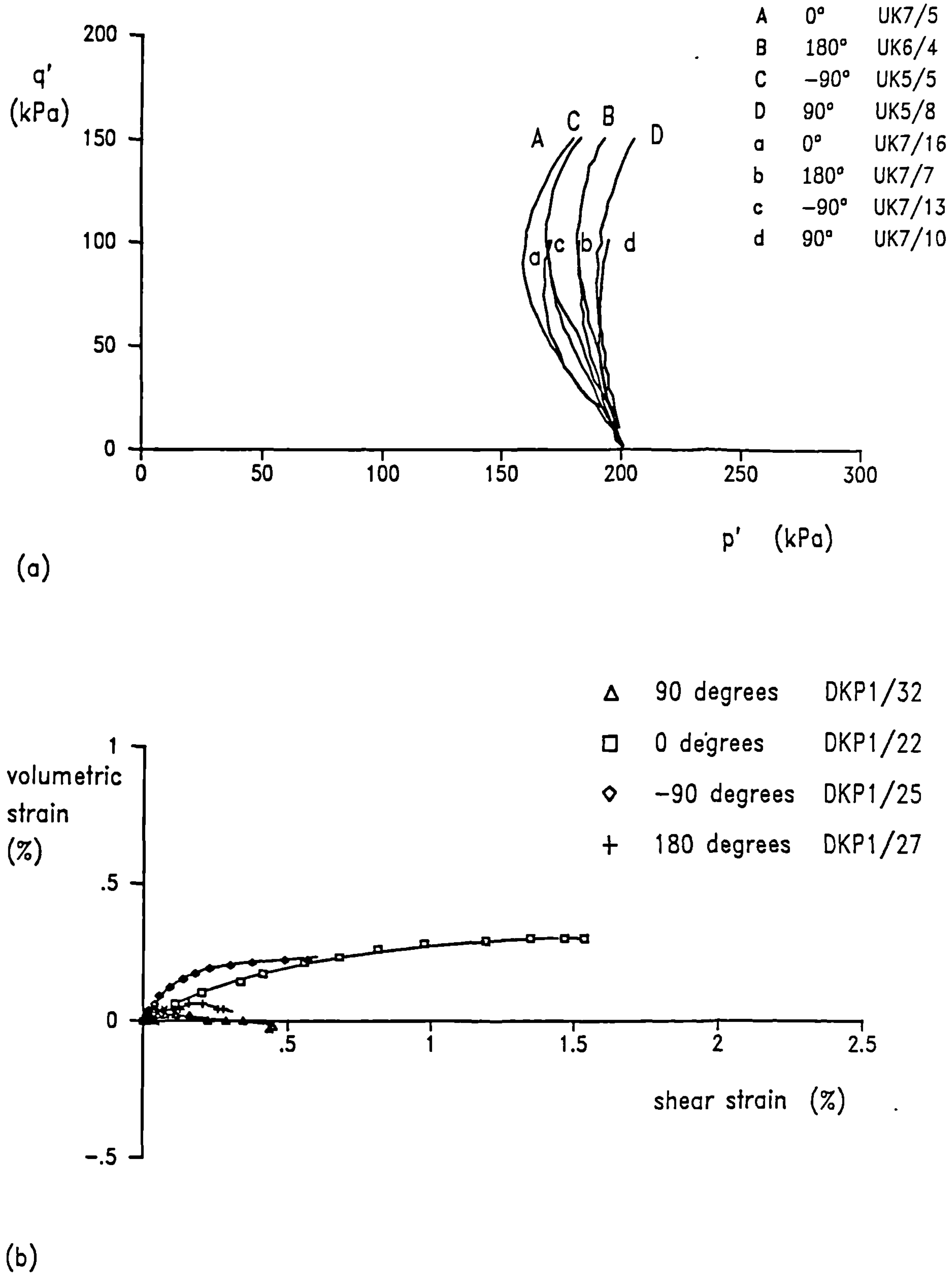

Figure 4.2.36 Comparison between (a) undrained effective stress paths, p'i = 200kPa, Ro ~ 3 and (b) drained strain paths, constant p' loading, p'i = 100kPa, Ro = 4 for four different stress path rotations.

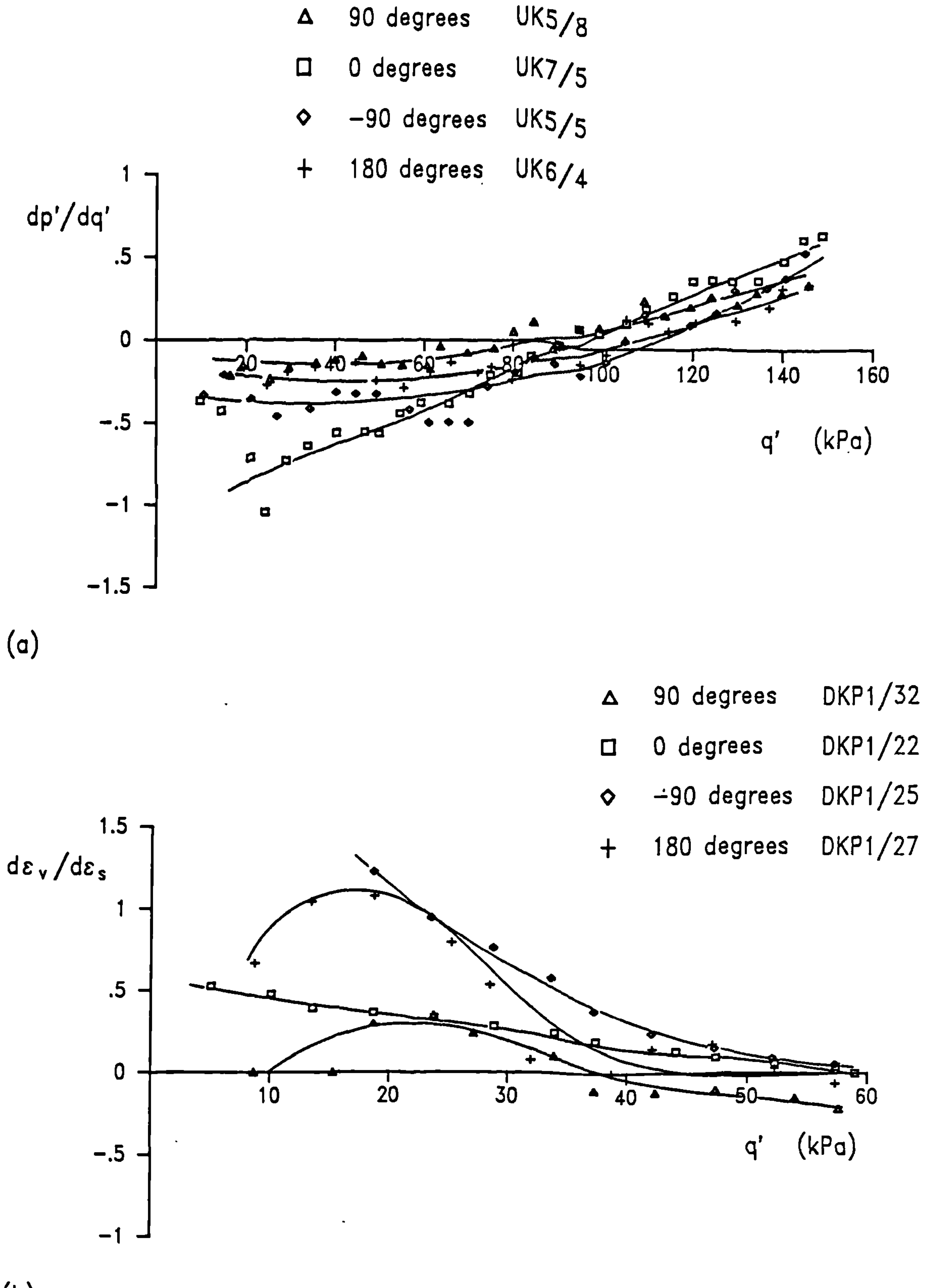

Figure 4.2.37 Comparison between (a) plots of dp'/dq' for undrained effective stress paths, p'i = 200kPa, Ro ~ 3 and (b) strain increment ratios from drained strain paths, constant p' loading, p'i = 100kPa, Ro = 4 against stress change.

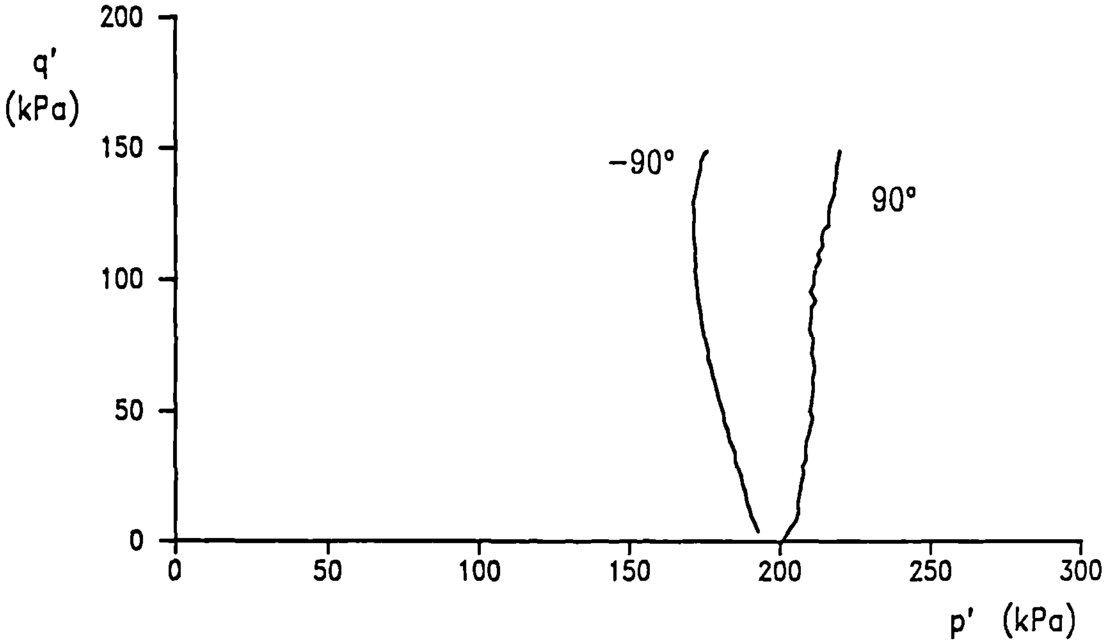

Figure 4.2.38 Undrained effective stress paths for reconstituted samples of London clay following stress path rotations of 90 and −90 degrees, p'i = 200kPa, Ro ~ 3

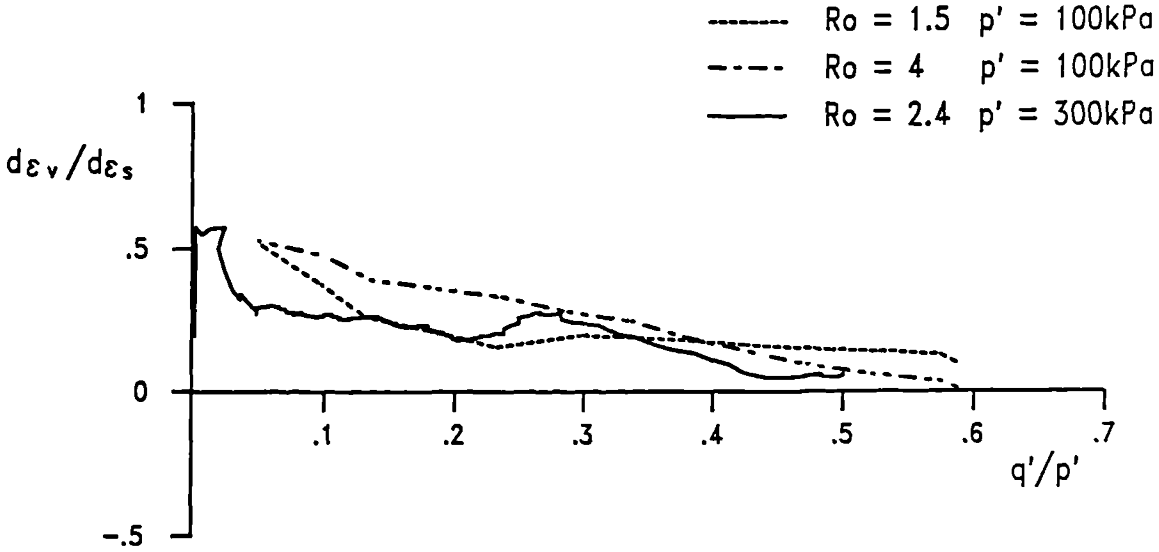

Figure 4.2.39 Plots of strain increment ratio against q'/p' for constant p' drained paths and undrained compression paths following no change in stress path direction

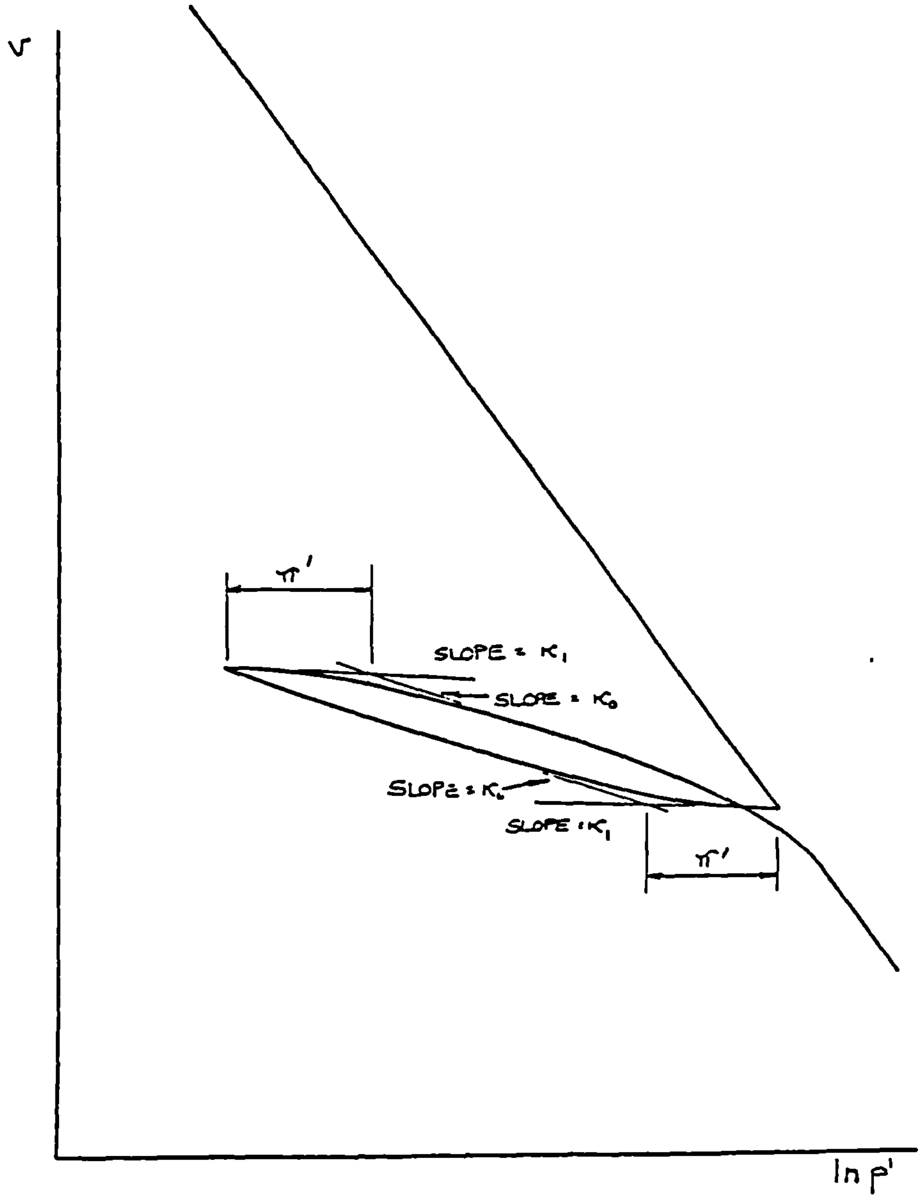

Figure 4.3.1 Diagram defining κ_1 and κ_0 for isotropic recompression and swelling stages and showing how the range of influence of recent stress history (threshold effect) was estimated from these curves. (after Richardson, 1988)

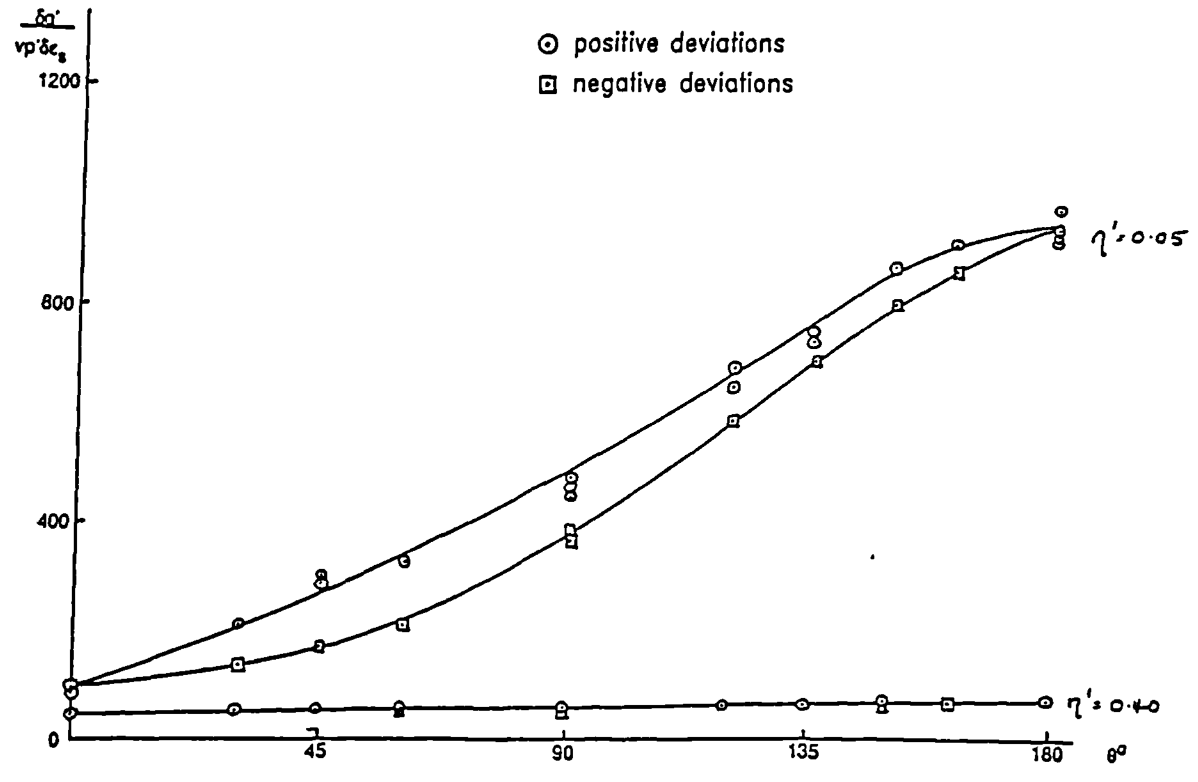

Figure 4.3.2 Variation of normalised stiffness with stress path rotation measured from constant p' loading paths, samples of reconstituted London clay. (after Richardson, 1988)

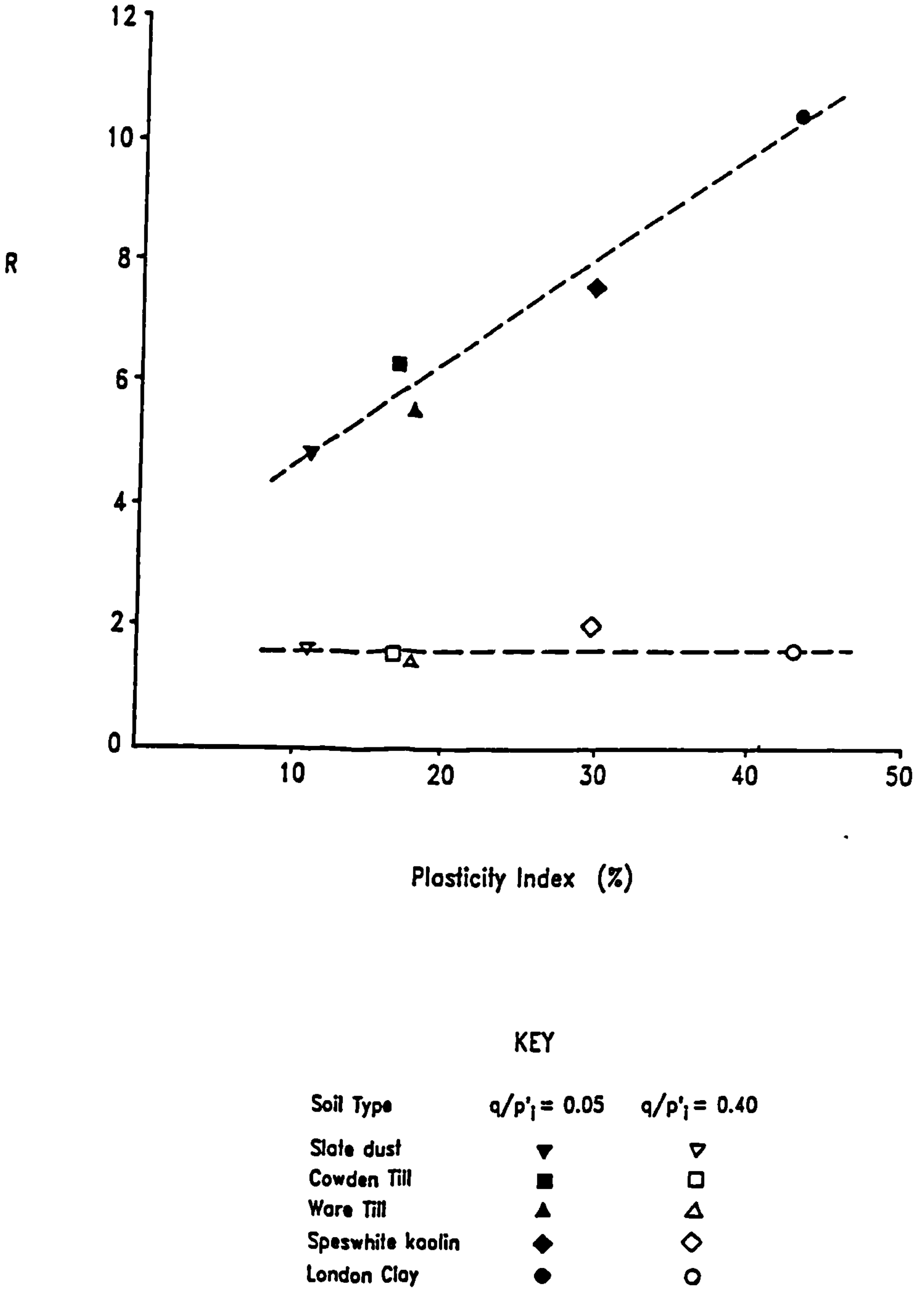

Figure 4.3.3 Variation in the range of stiffness, R, with plasticity. Data from tests on reconstituted samples. (after Richardson, 1988)

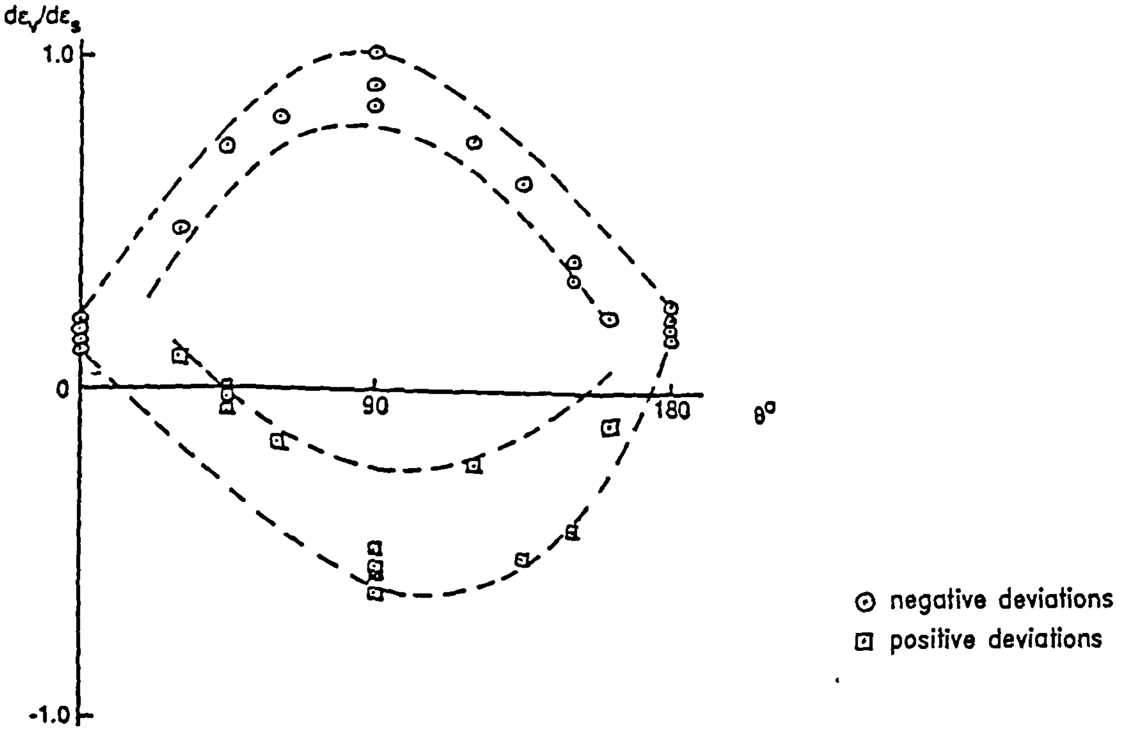

Figure 4.3.4 Variation of strain increment ratio with stress path rotation measured from constant p' loading paths, reconstituted samples of London clay. (after Richardson, 1988)

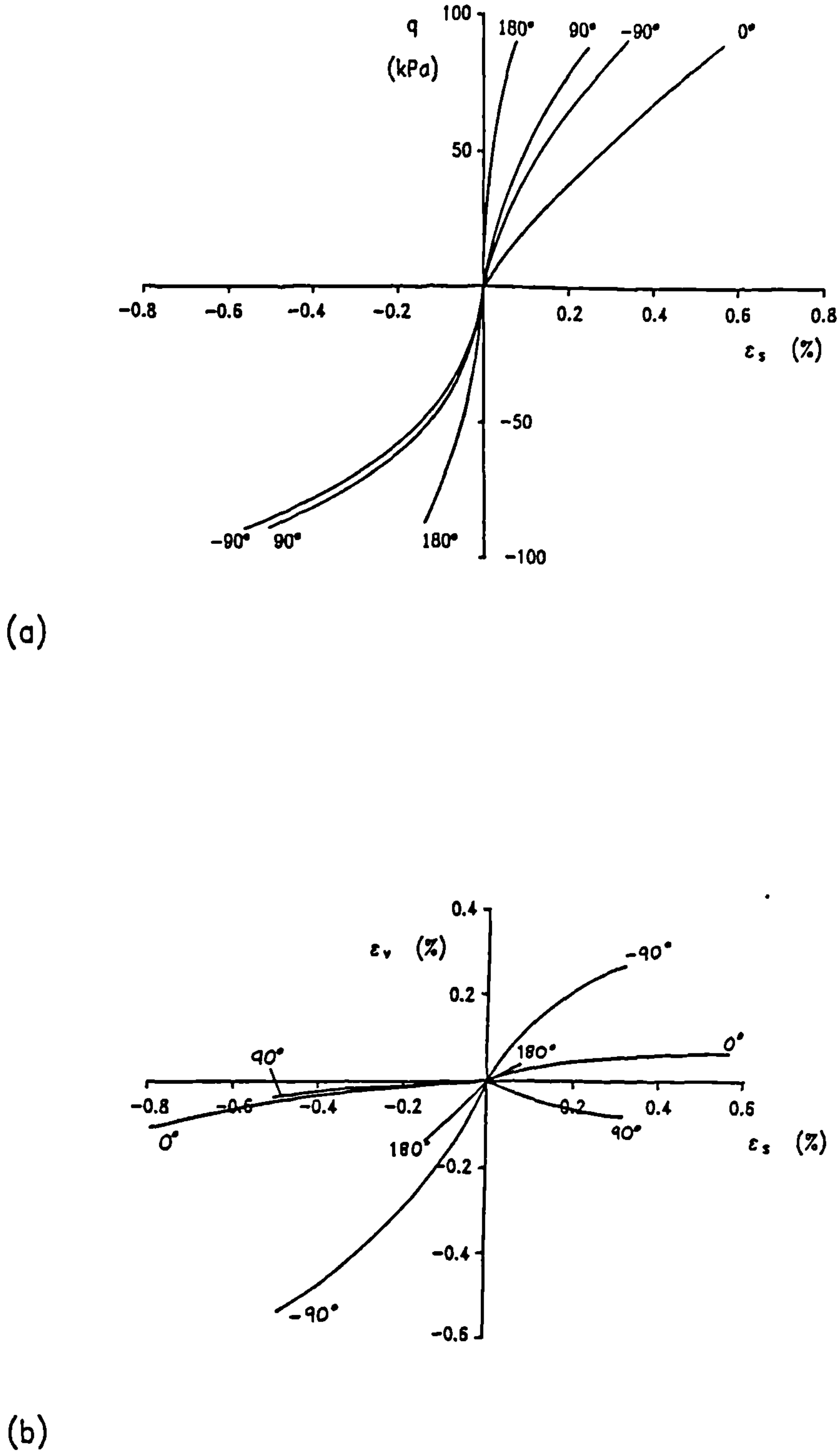

Figure 4.3.5 (a) stress-strain curves and (b) strain paths for constant p' compression and extension loading paths, samples of reconstituted London clay p'i = 200kPa, p'm = 400kPa. (after Atkinson et al. 1990)

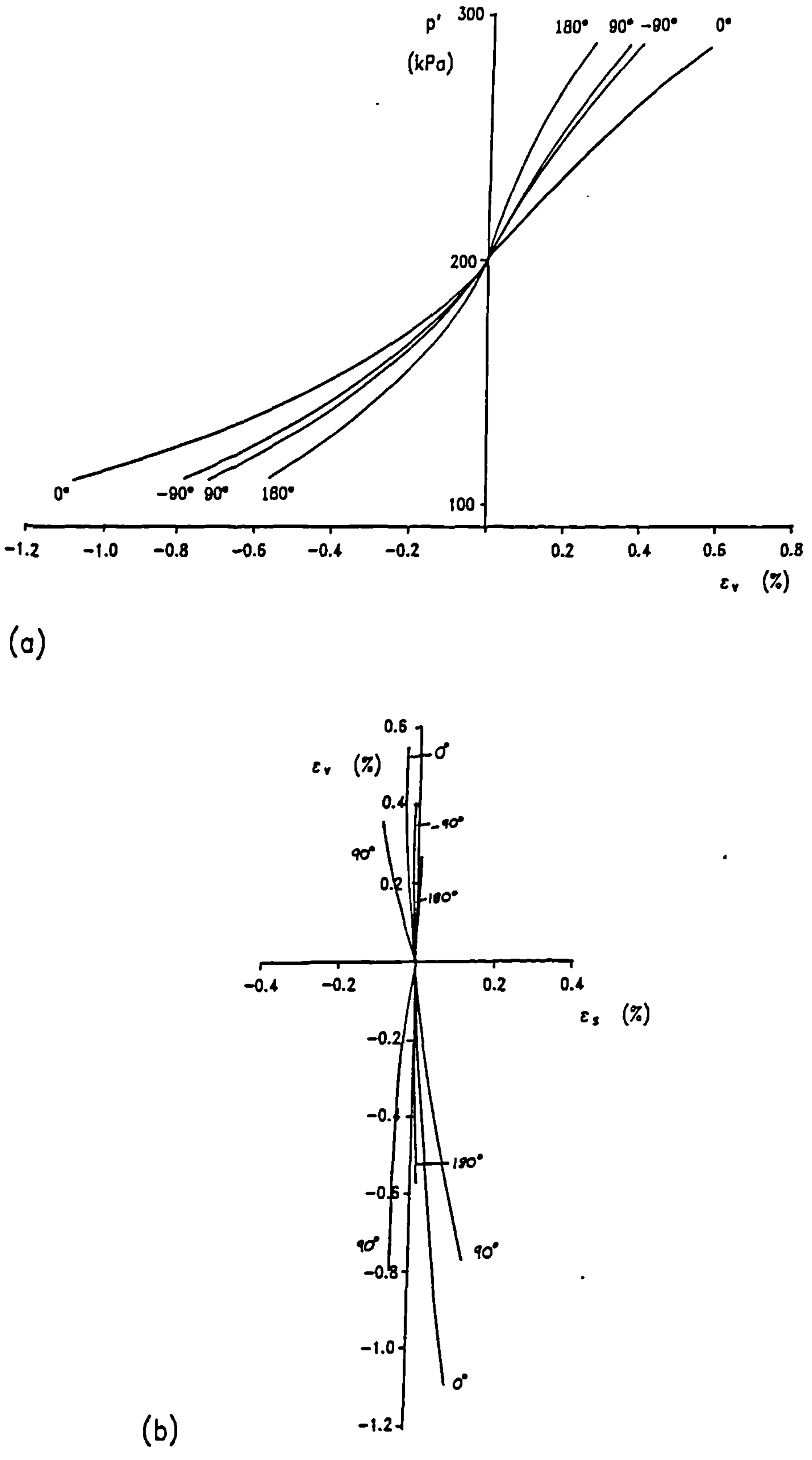

Figure 4.3.6 (a) stress–strain curves and (b) strain paths for constant q' compression and swelling paths, samples of reconstituted London clay p'i = 200kPa, p'm = 400kPa. (after Atkinson et al. 1990)

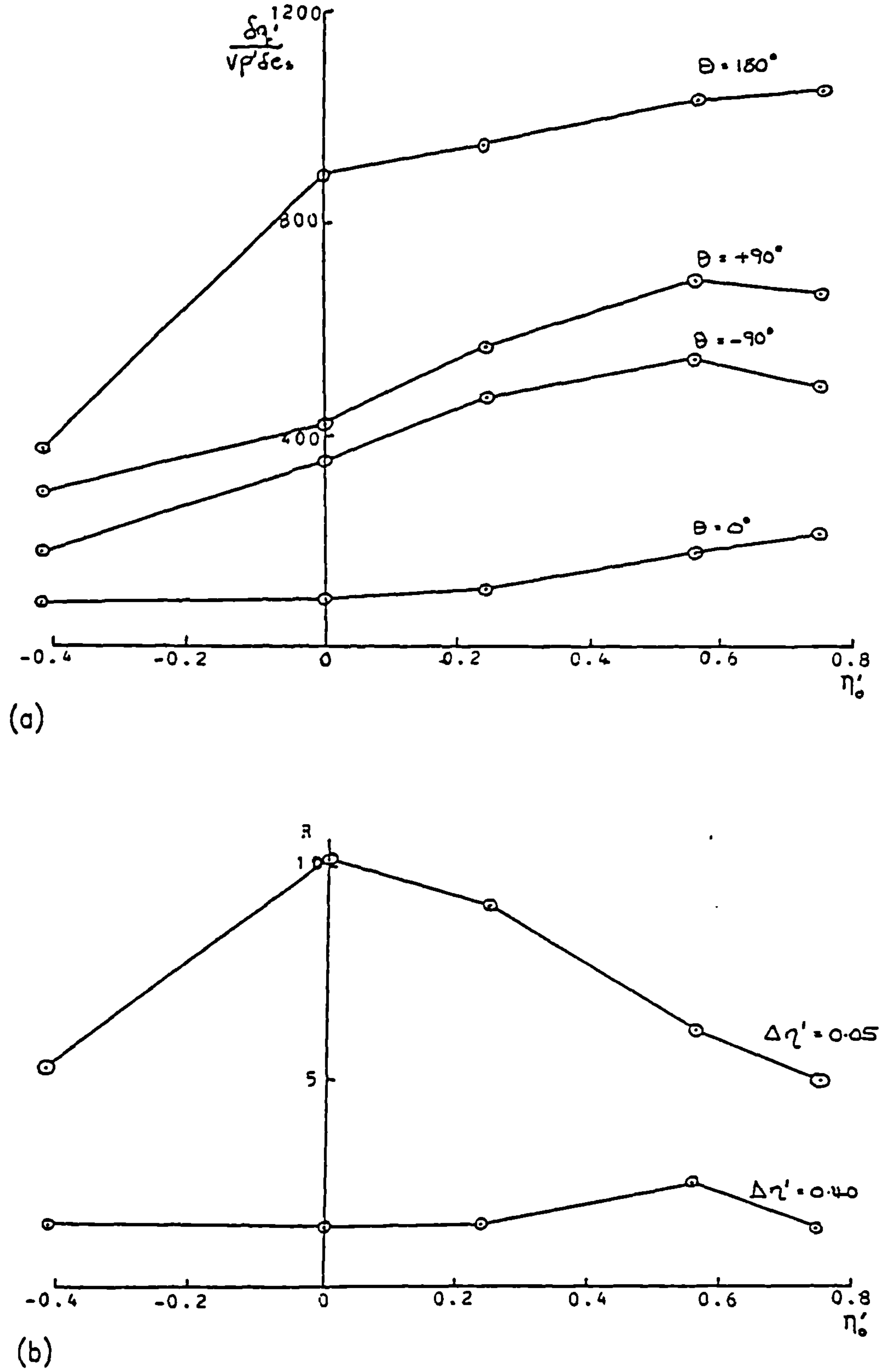

Figure 4.3.7 Variation of (a) normalised stiffness and (b) range of stiffness with η'_0, the stress ratio during initial compression. (after Richardson, 1988)

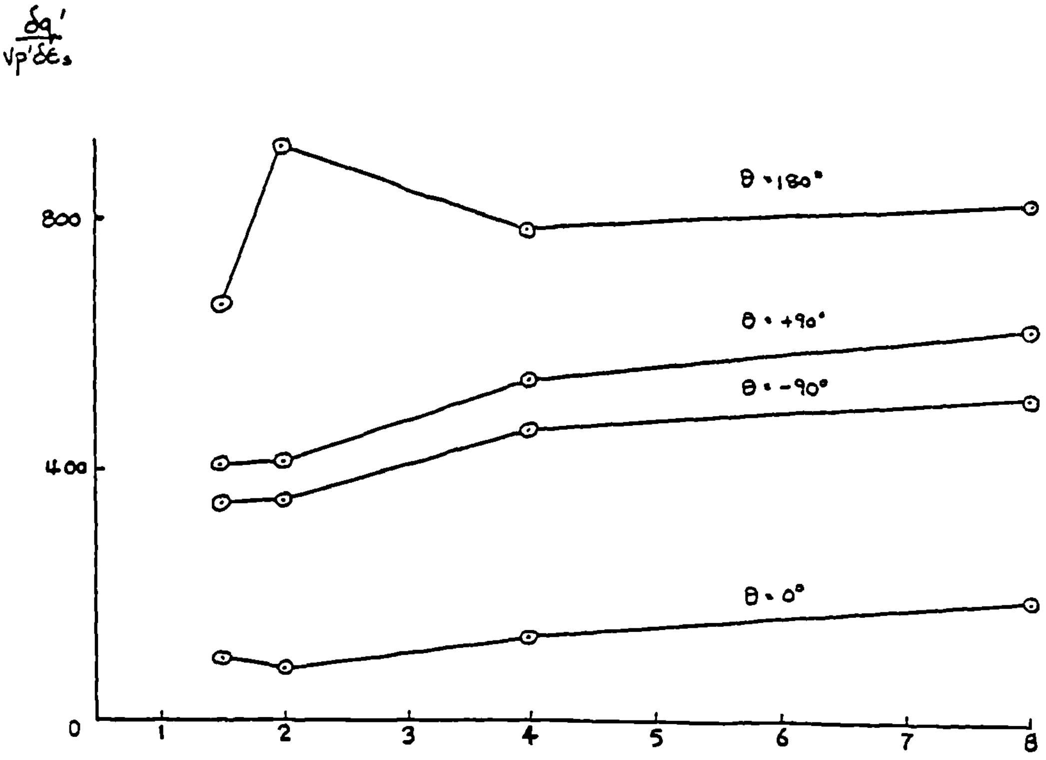

Figure 4.3.9 Variation of normalised stiffness at Δq'/p' = 0.05 with over-consolidation ratio for one-dimensionally compressed samples of London clay. (after Richardson, 1988)

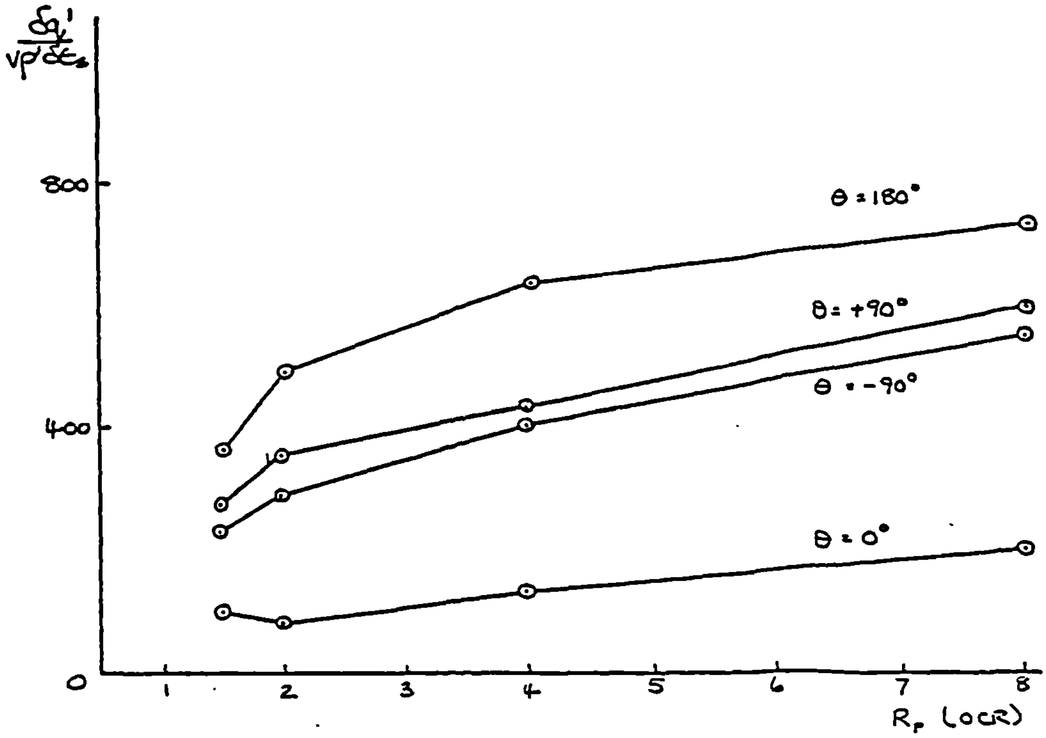

Figure 4.3.8 Variation of normalised stiffness at Δq'/p' = 0.05 with over-consolidation ratio for isotropically compressed London clay. (after Richardson, 1988)

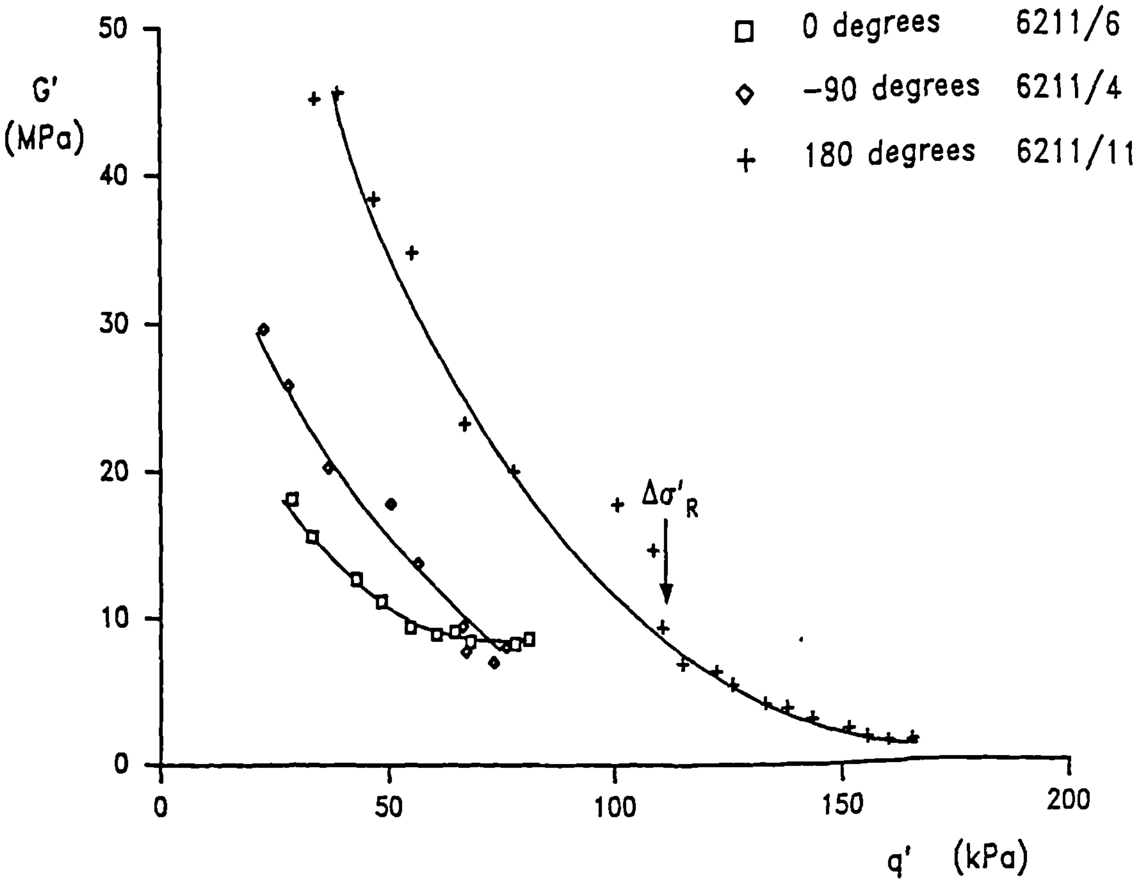

Figure 4.3.10 Curves of shear stiffness against stress change for constant p' loading, p'i = 267kPa, p'm = 400kPa. Data from tests on reconstituted samples of London clay by Richardson (1988)

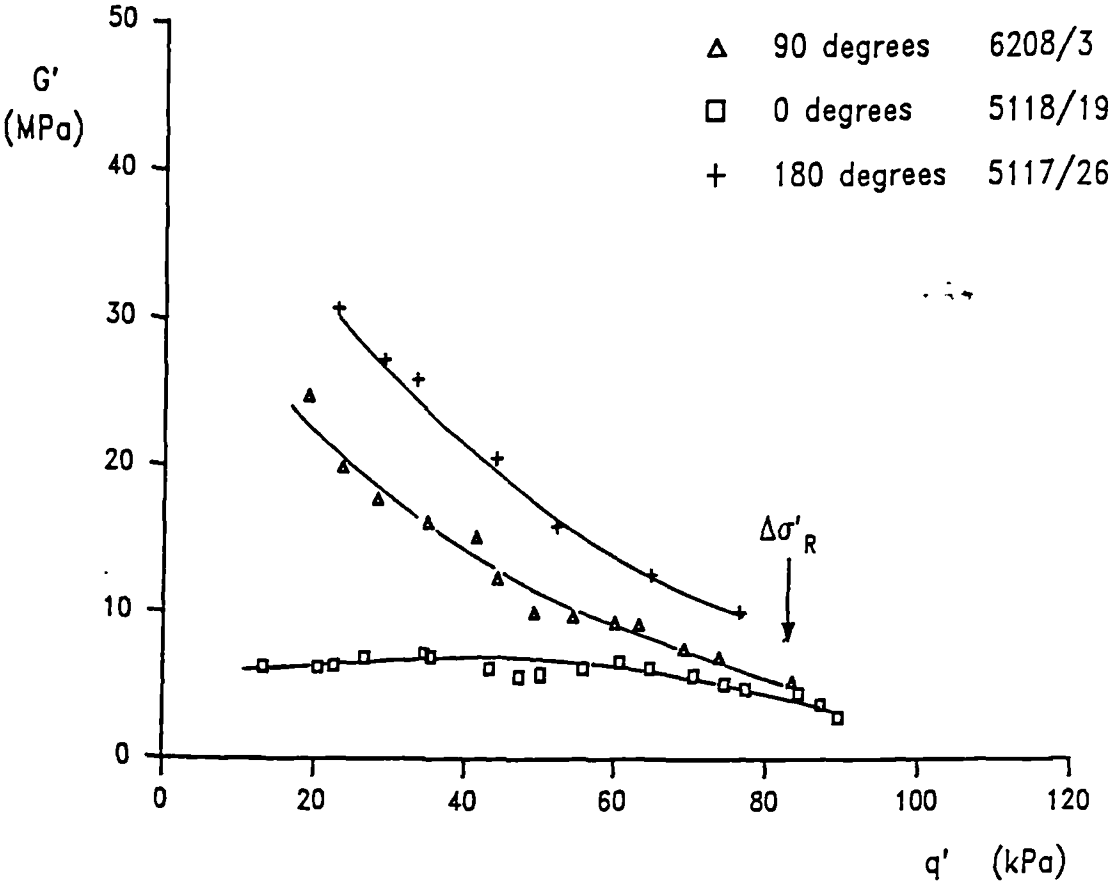

Figure 4.3.11 Curves of shear stiffness against stress change for constant p' loading, p'i = 200kPa, p'm = 400kPa. Data from tests on reconstituted samples of London clay by Richardson (1988)

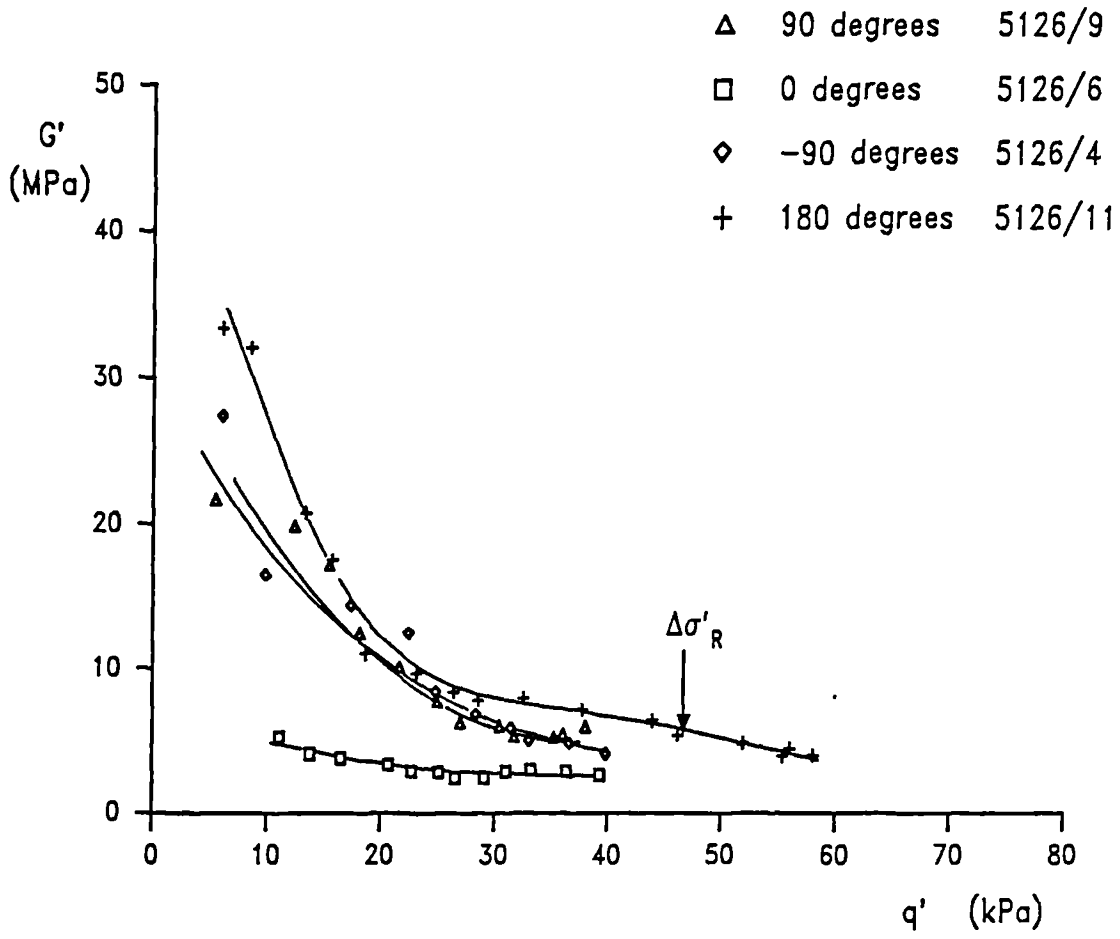

Figure 4.3.12 Curves of shear stiffness against stress change for constant p' loading, p'i = 100kPa, p'm = 400kPa. Data from tests on reconstituted samples of London clay by Richardson (1988)

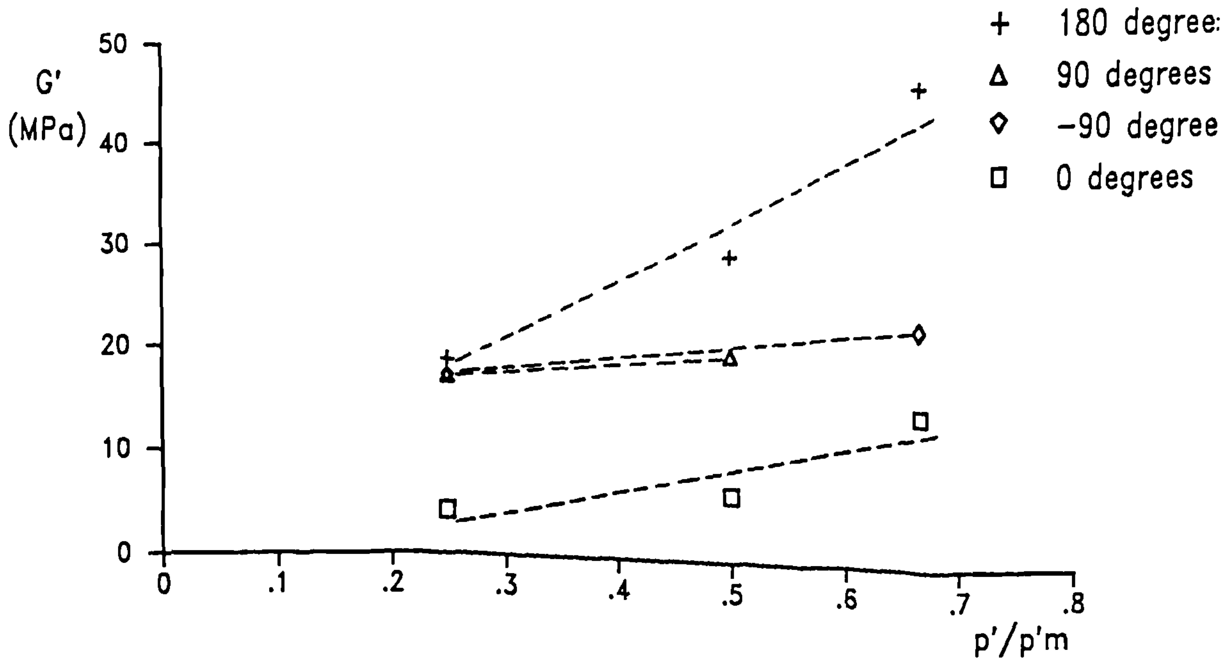

Figure 4.3.13 Plots showing the variation of G' with p'/p'm for constant p' loading. Data from three sets of tests on London clay by Richardson (1988)

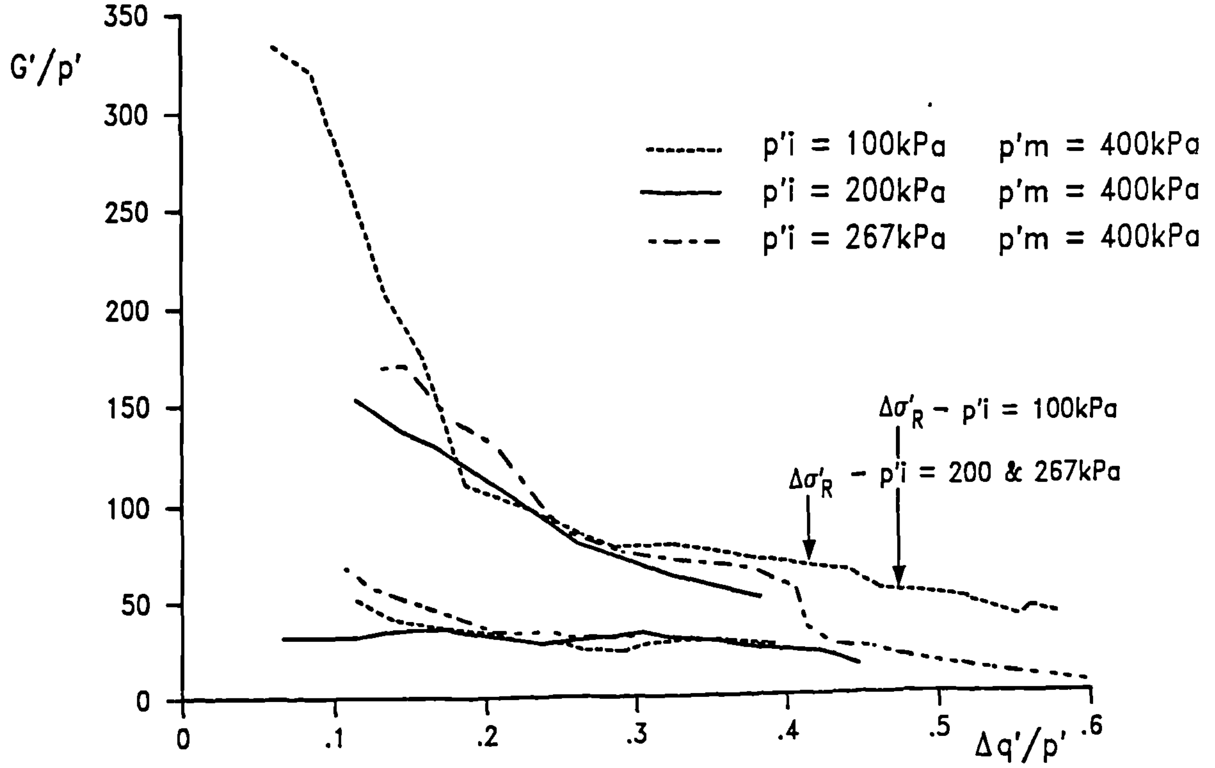

Figure 4.3.14 Curves of stiffness, after rotations of 180 and 0 degrees, plotted against change in stress normalised by p'. The data are from the three sets of tests on London clay by Richardson (1988)

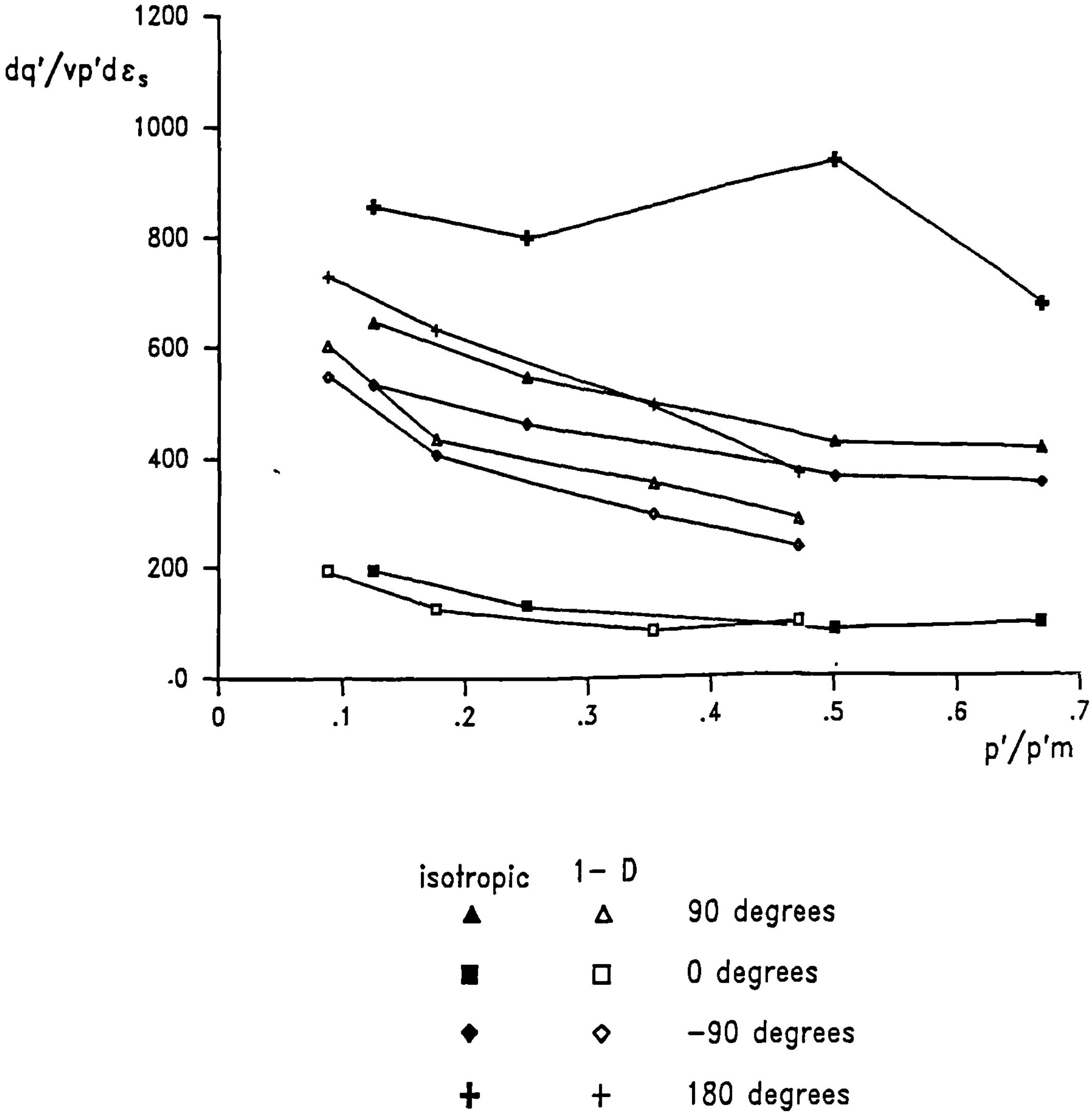

Figure 4.3.15 Stiffnesses for a given stress level plotted against p'/p'm. Data from Richardson (1988) replotted in a new format.

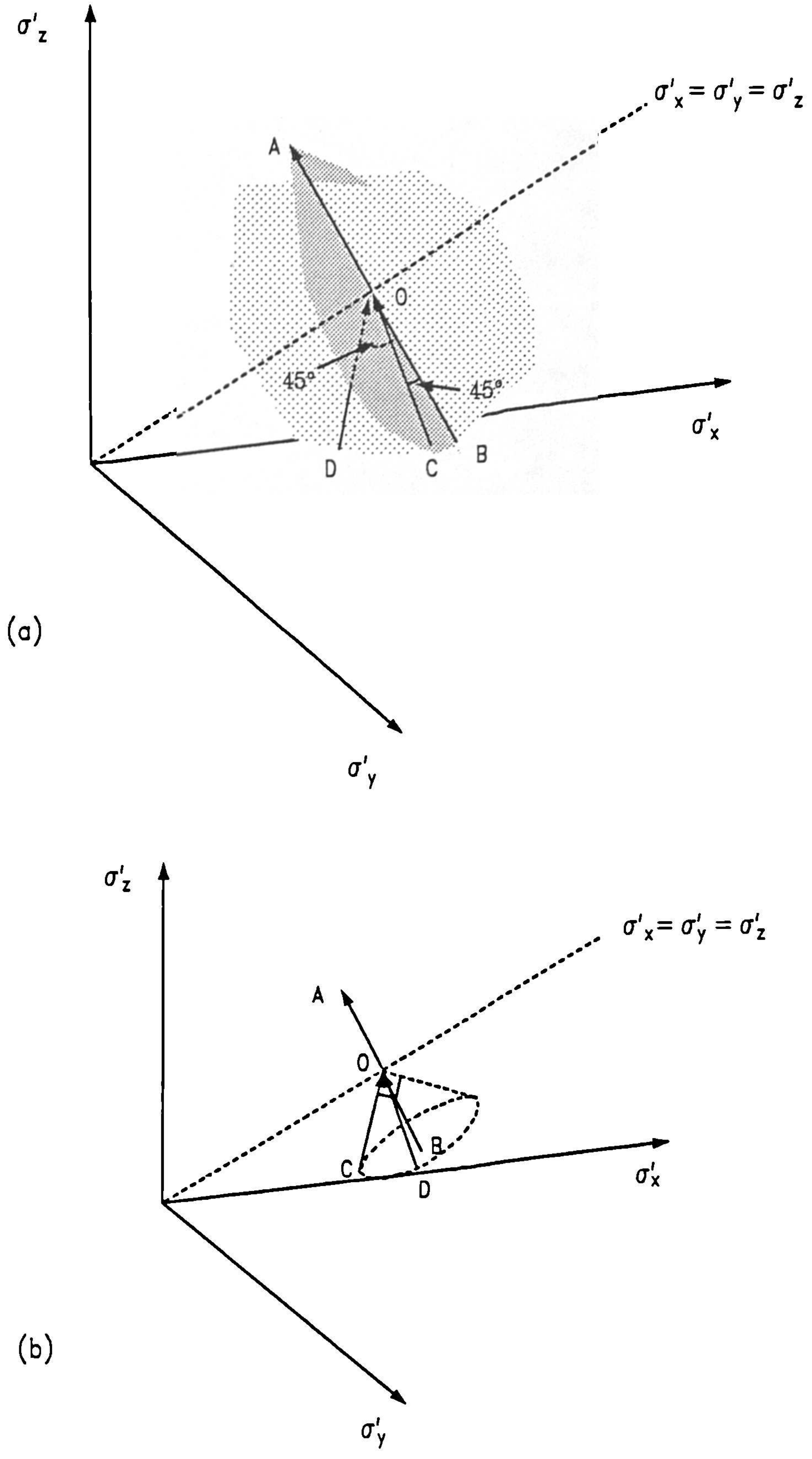

Figure 4.4.1 Diagrams showing the common path (OA) and approach paths (BO, CO and DO) used in the true triaxial tests,

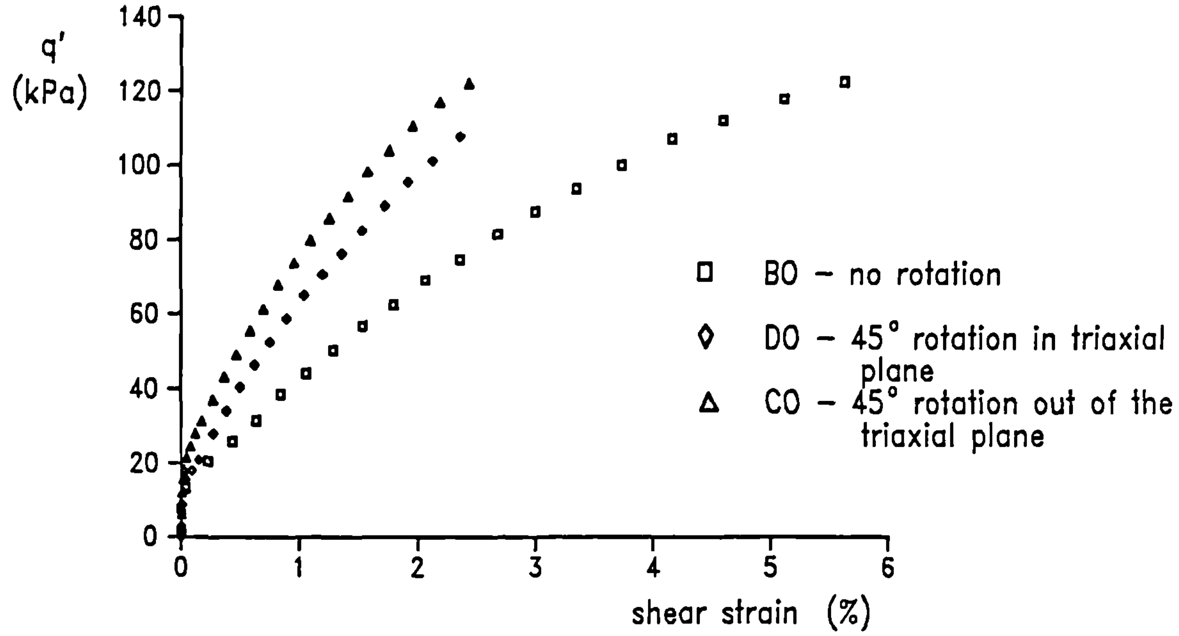

Figure 4.4.2 Plots of deviatoric stress against shear strain for constant p' loading, showing the effect of stress path rotation in 3D stress space. (after Lewin 1990)

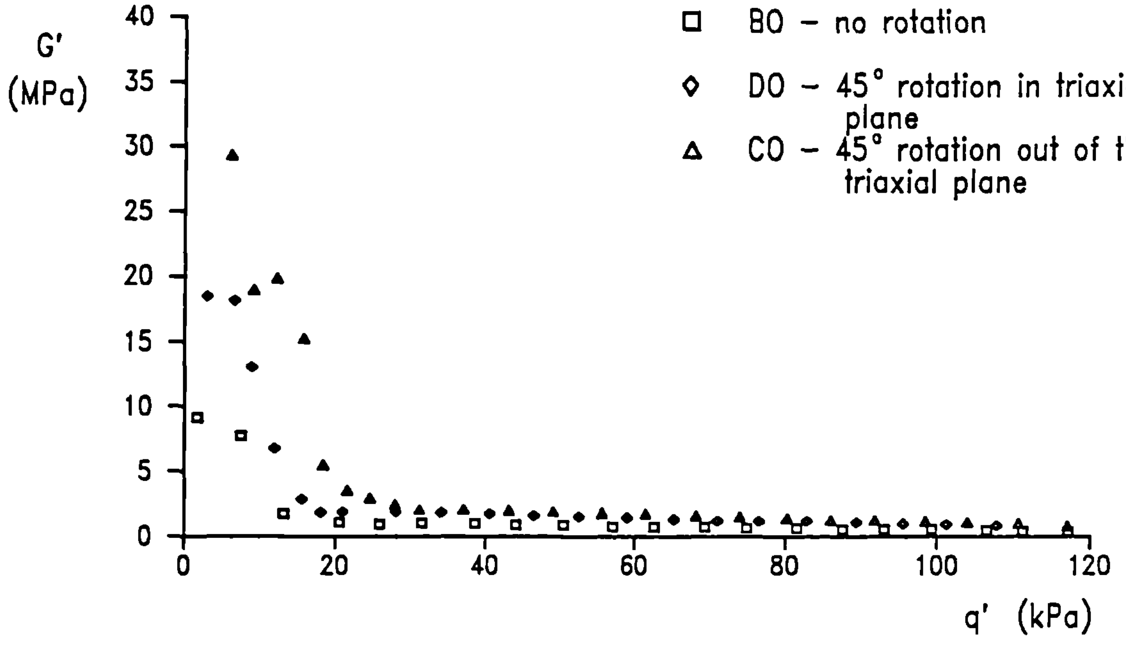

Figure 4.4.3 Plots showing the variation of shear stiffness with stress change for constant p' loading, showing the effect of stress path rotations in 3D stress space. (after Lewin, 1990)

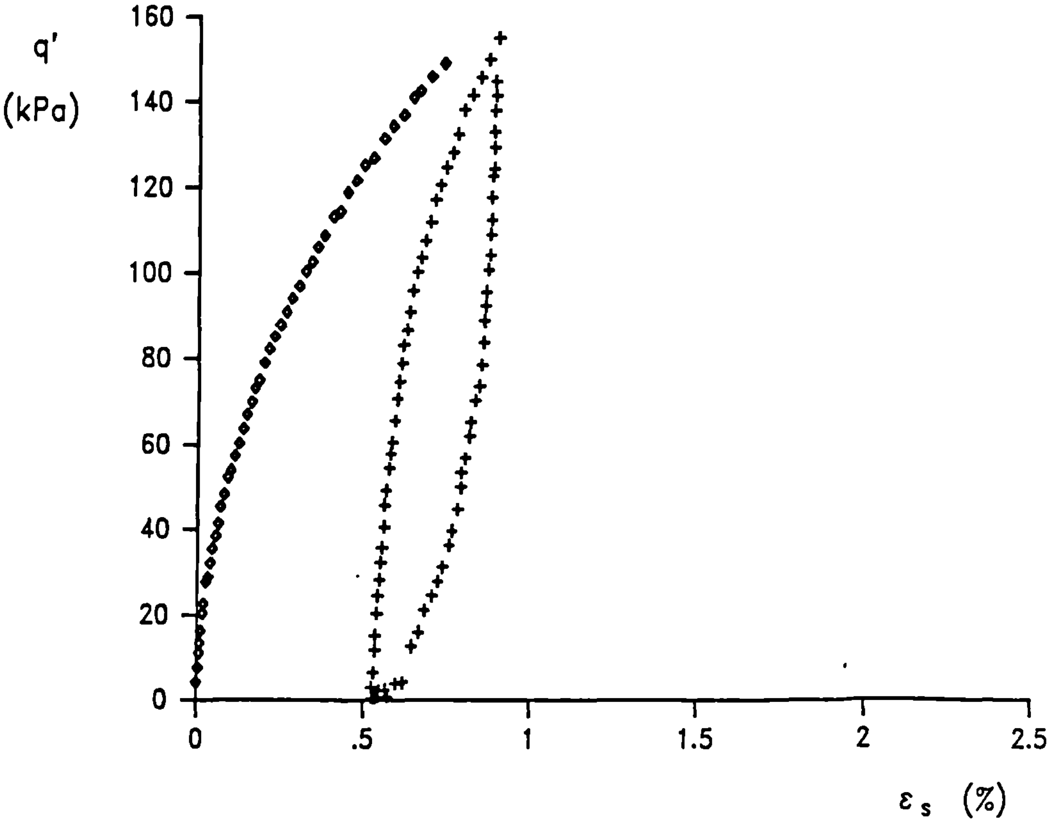

Figure 4.5.1 Cycles of constant p' loading at p'i = 300kPa, p'm = 720kPa, for reconstituted speswhite kaolin

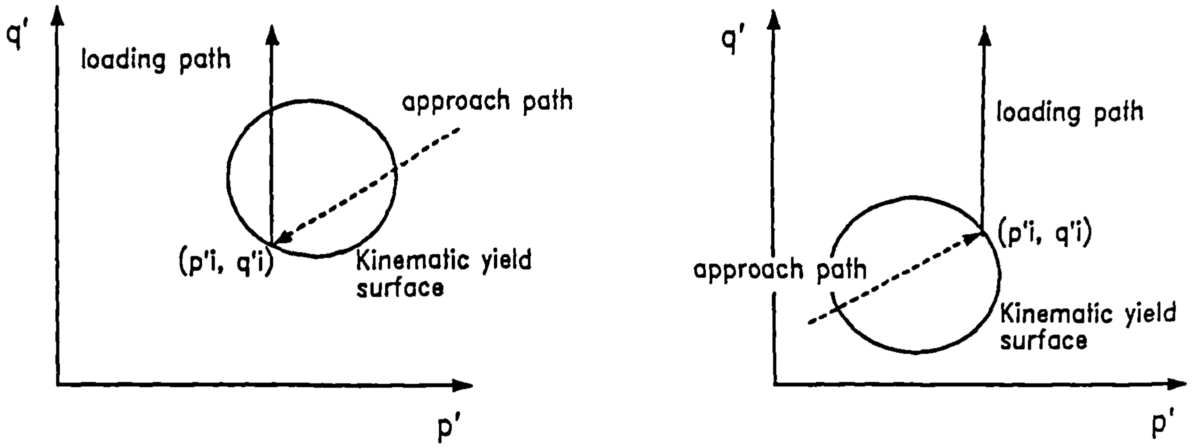

Figure 5.2.1 Diagram illustrating how the position of the kinematic yield surface relative to the current stress state is dependent on the approach stress path

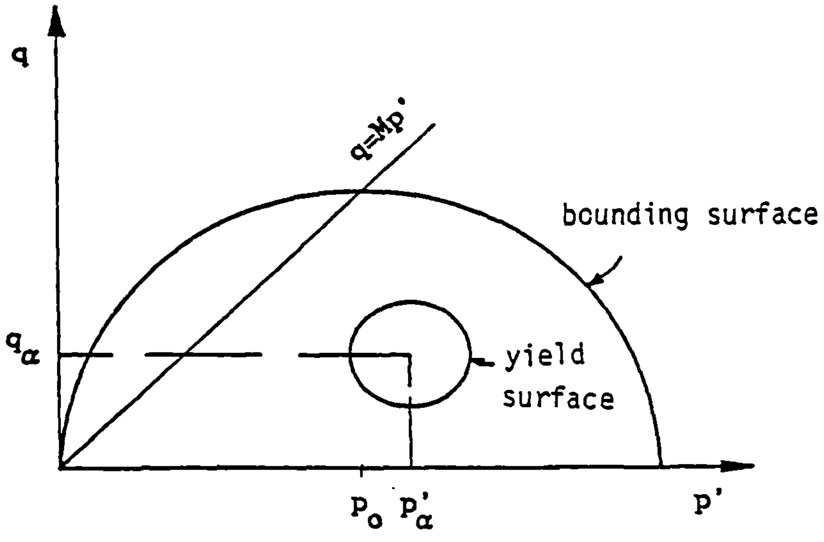

Figure 5.3.1 Diagram showing the yield and bounding surfaces and the symbols chosen for their centres (after Al Tabbaa, 1987)

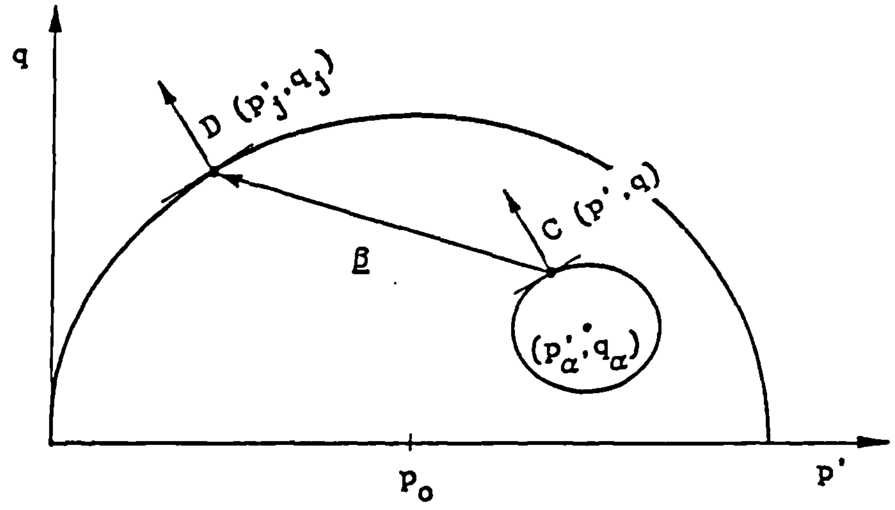

Figure 5.3.2 Assumed relative motion of yield of bounding surfaces along the vector β, joining point C to its conjugate point D (after Al Tabbaa, 1987)

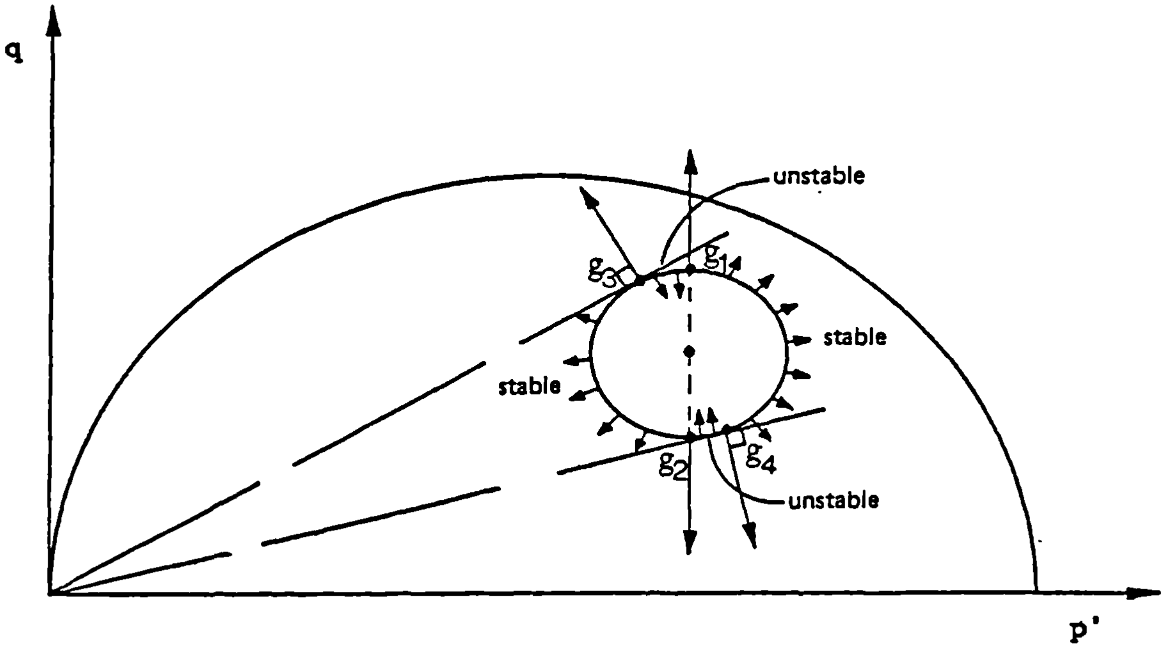

Figure 5.3.3 Diagram showing singularity points and unstable regions on the yield surface due to the function h_o (after Al Tabbaa, 1987)

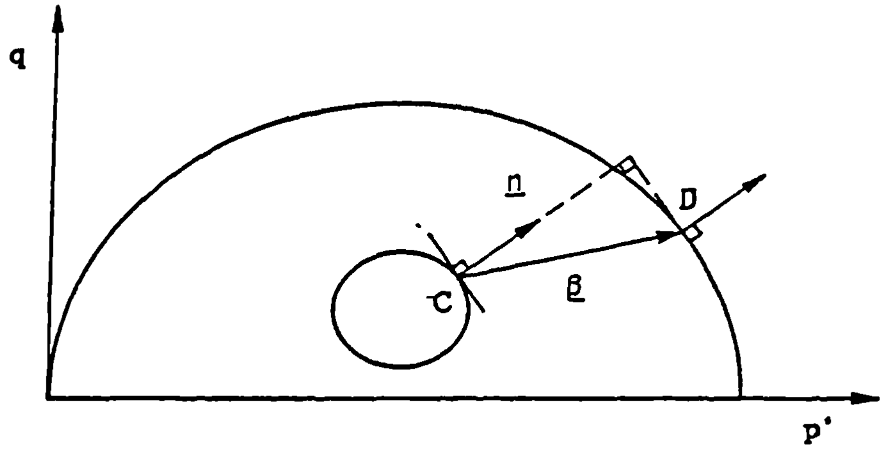

Figure 5.3.4(a) A diagram showing the vector β and the vector n (after Al Tabbaa, 1987)

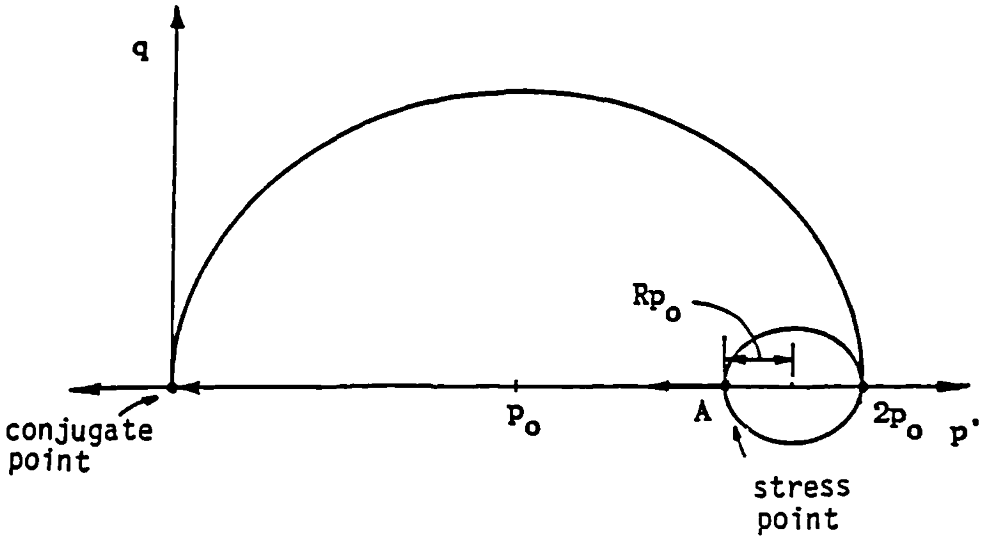

Figure 5.3.4(b) A diagram showing the position of the stress point A for the maximum value of b, b_{max} (after Al Tabbaa, 1987)

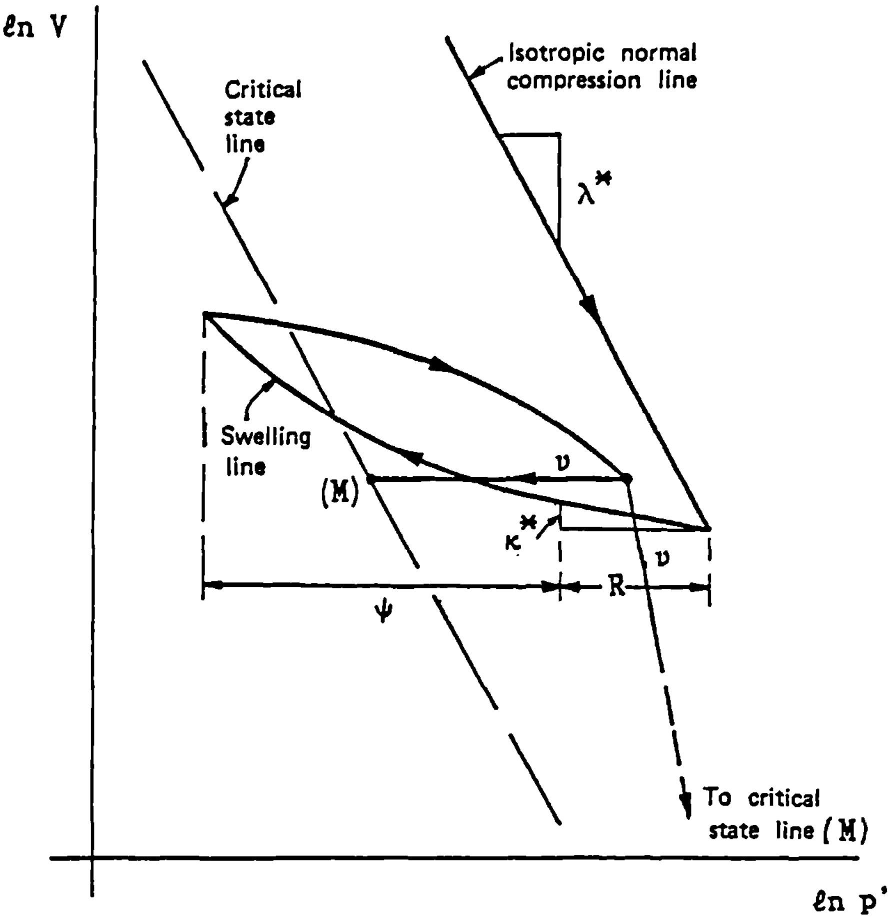

Figure 5.3.5 Example of one triaxial multi-stage test from which all the model parameters can be obtained (after Al Tabbaa, 1987)

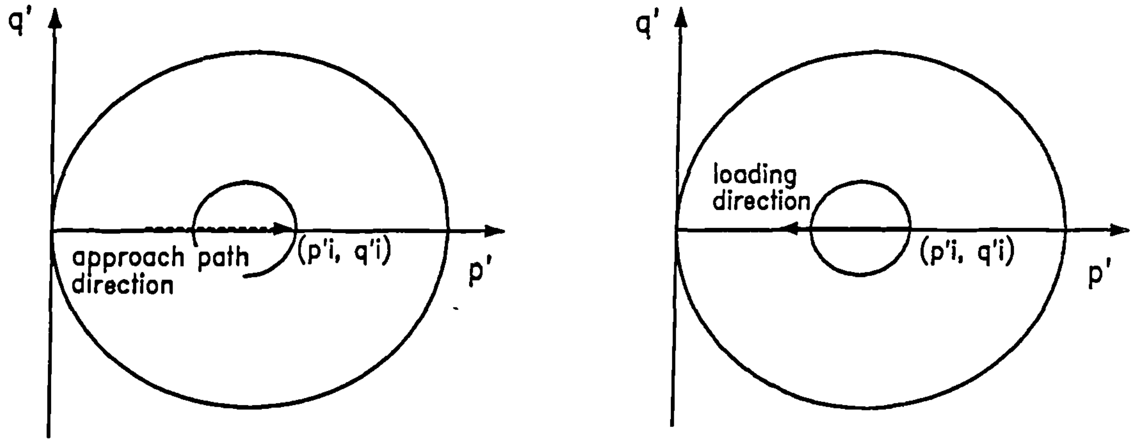

Figure 5.3.6 Diagram showing the position of the yield surface enclosing the elastic region at the start of a stress path following a stress path reversal.

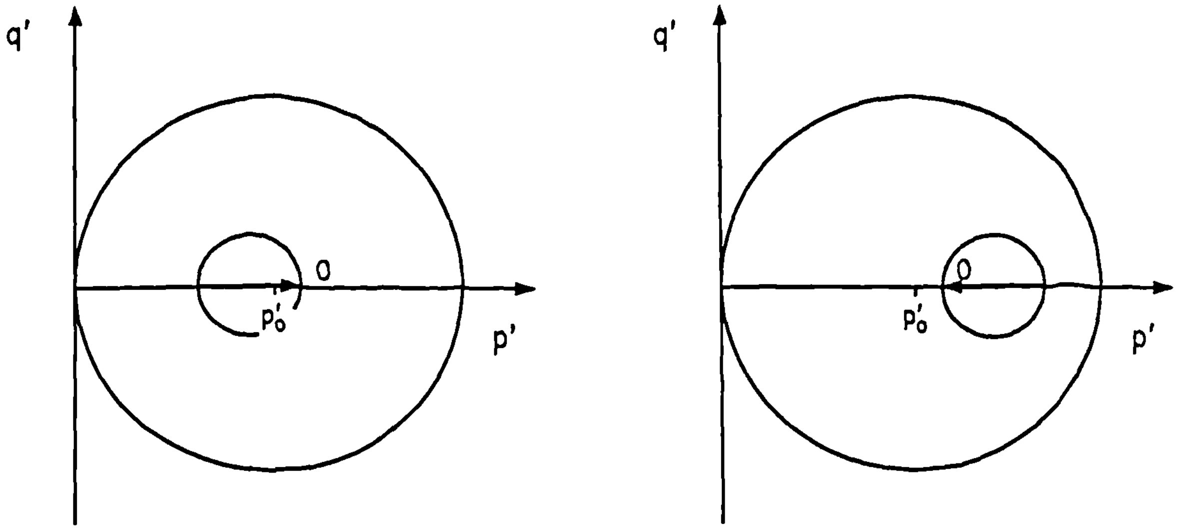

(a) approach path at 0 degrees

(b) approach path at 180 degrees

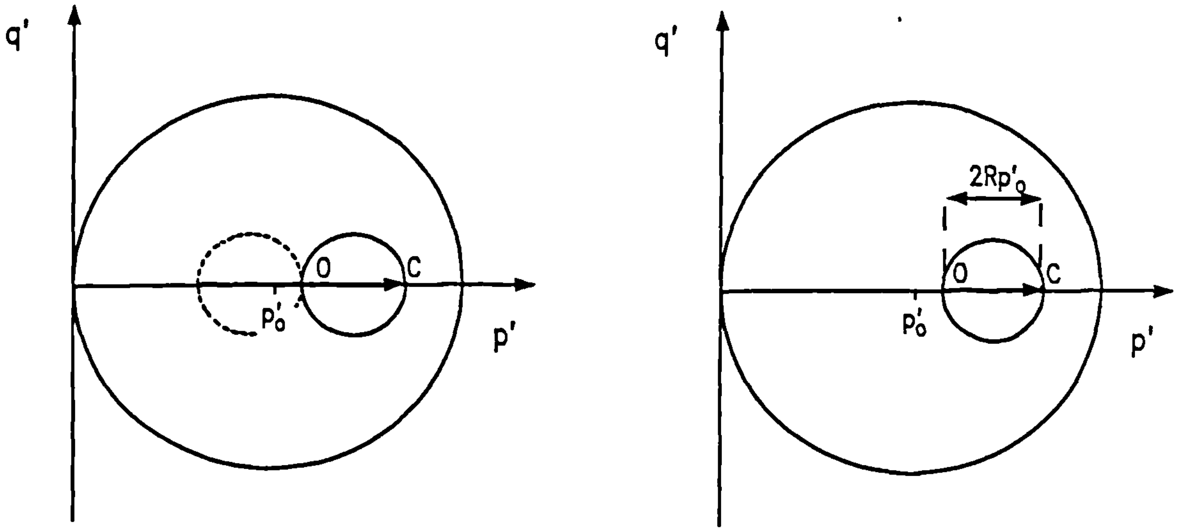

(c) loading along common path dragging yield surface

(d) loading along common path back through elastic region

Figure 5.3.7 Diagrams illustrating that for isotropic swelling or compression paths the stiffness curves for different rotations will converge at a stress change 2Rp'o

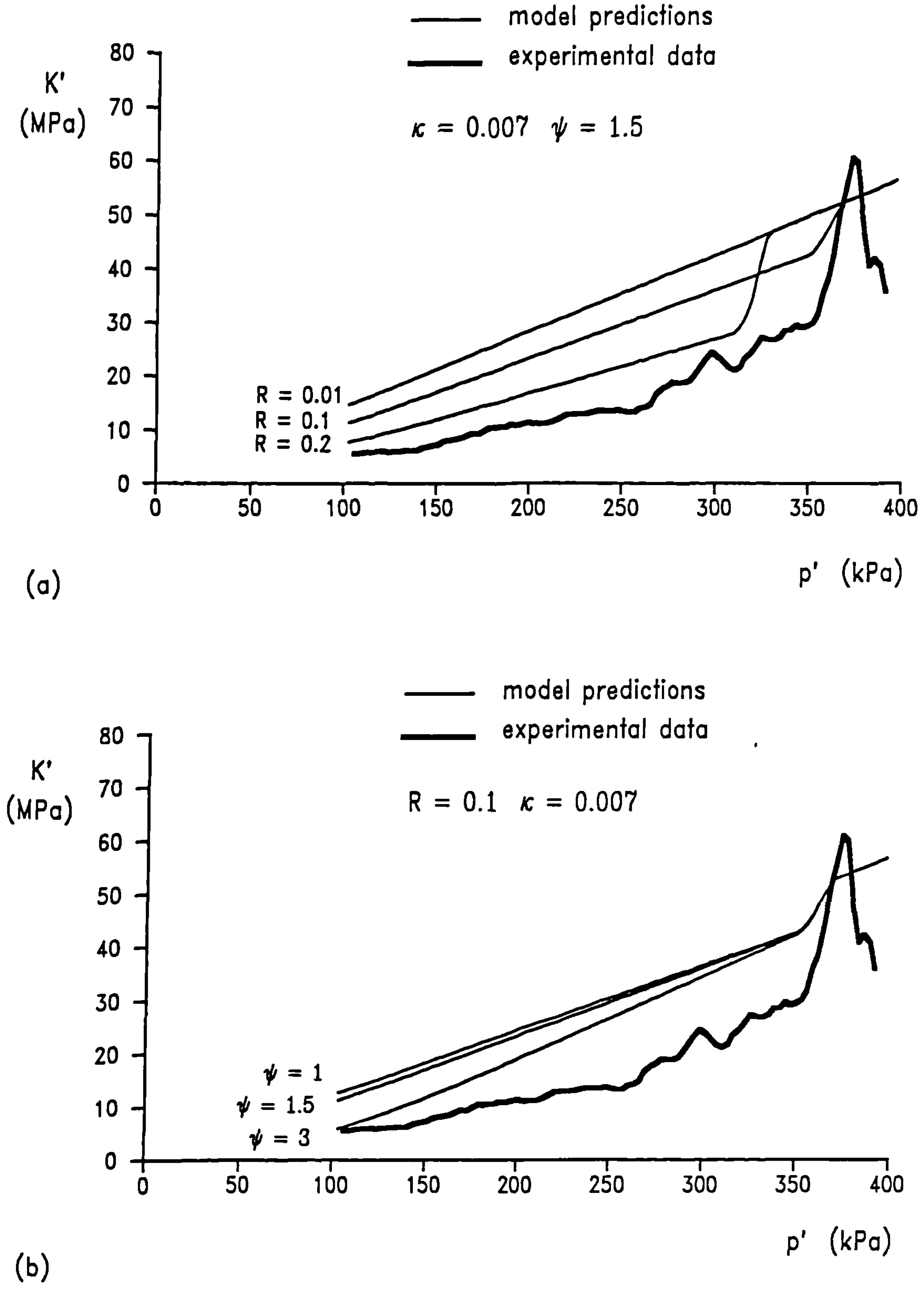

Figure 5.3.8 A comparison between the stress–strain response predicted by the two-surface model and experimental data for an isotropic swelling path from a normally consolidated state at p' = 400kPa.

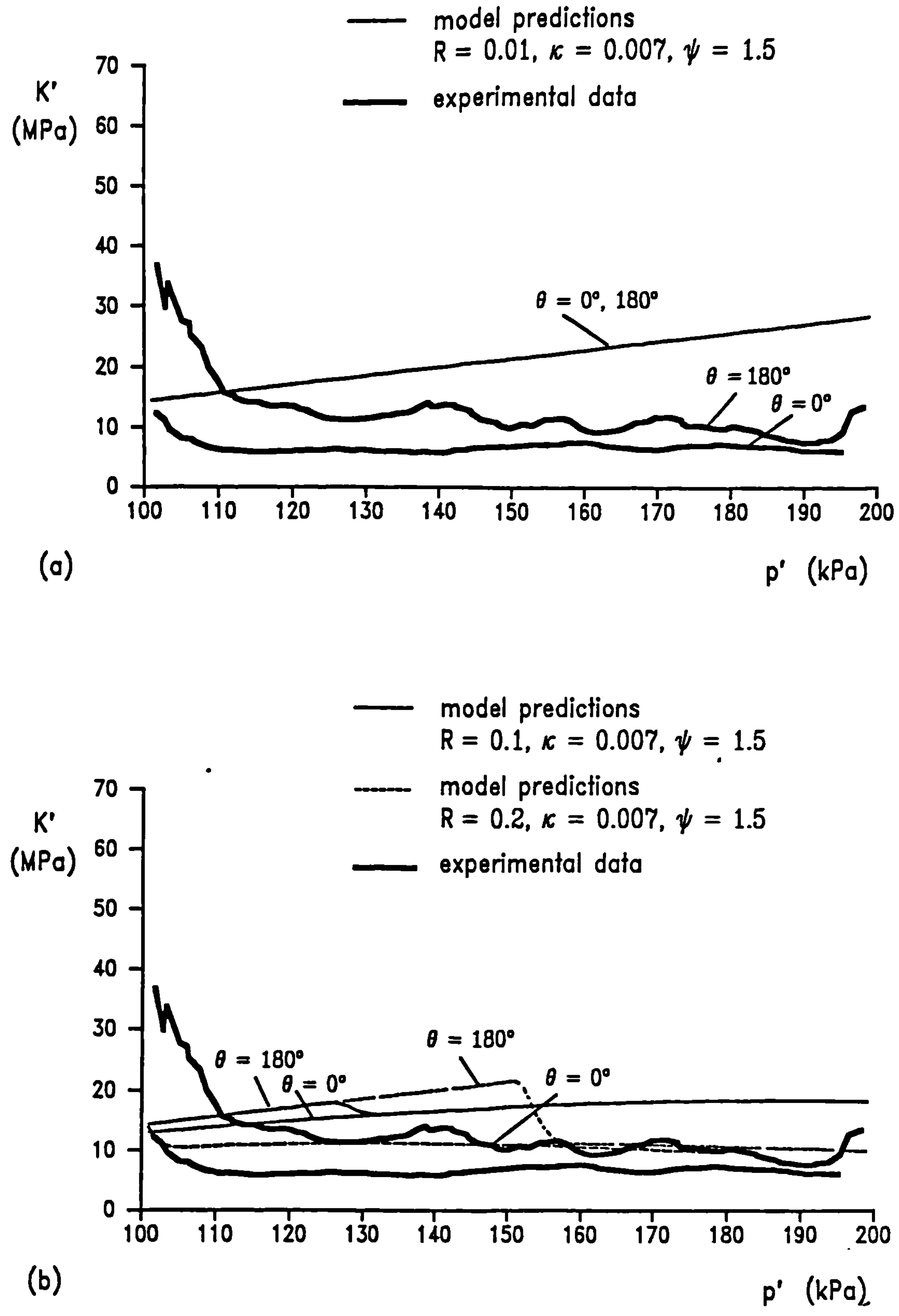

Figure 5.3.9 A comparison between the stress–strain response predicted by the two–surface model and experimental data for a constant q' compression path from p'i = 100kPa, p'm = 300kPa

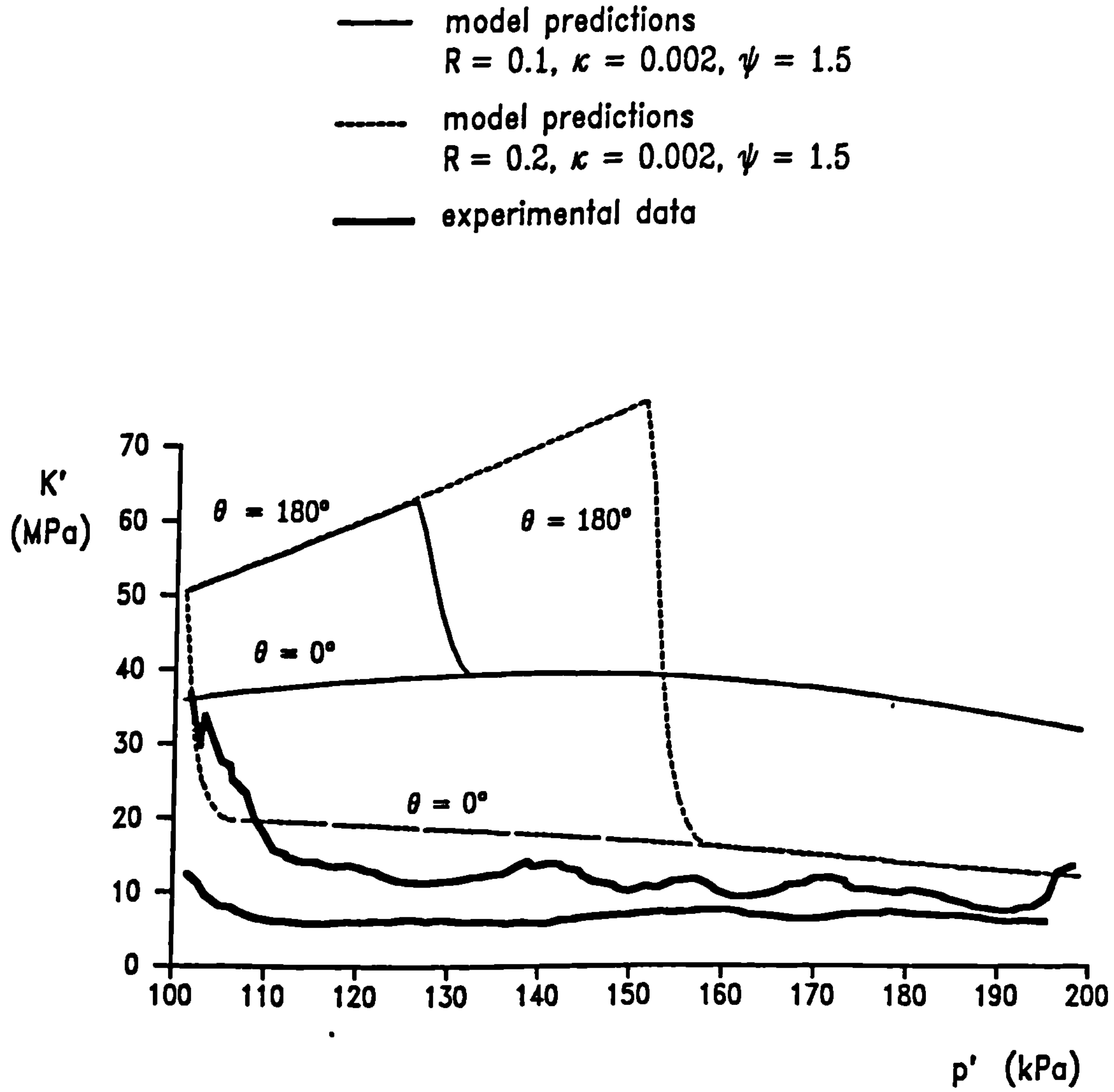

Figure 5.3.10 A comparison between the stress-strain response predicted by the two-surface model and experimental data for a constant q' compression path from p'i = 100kPa, p'm = 300kPa

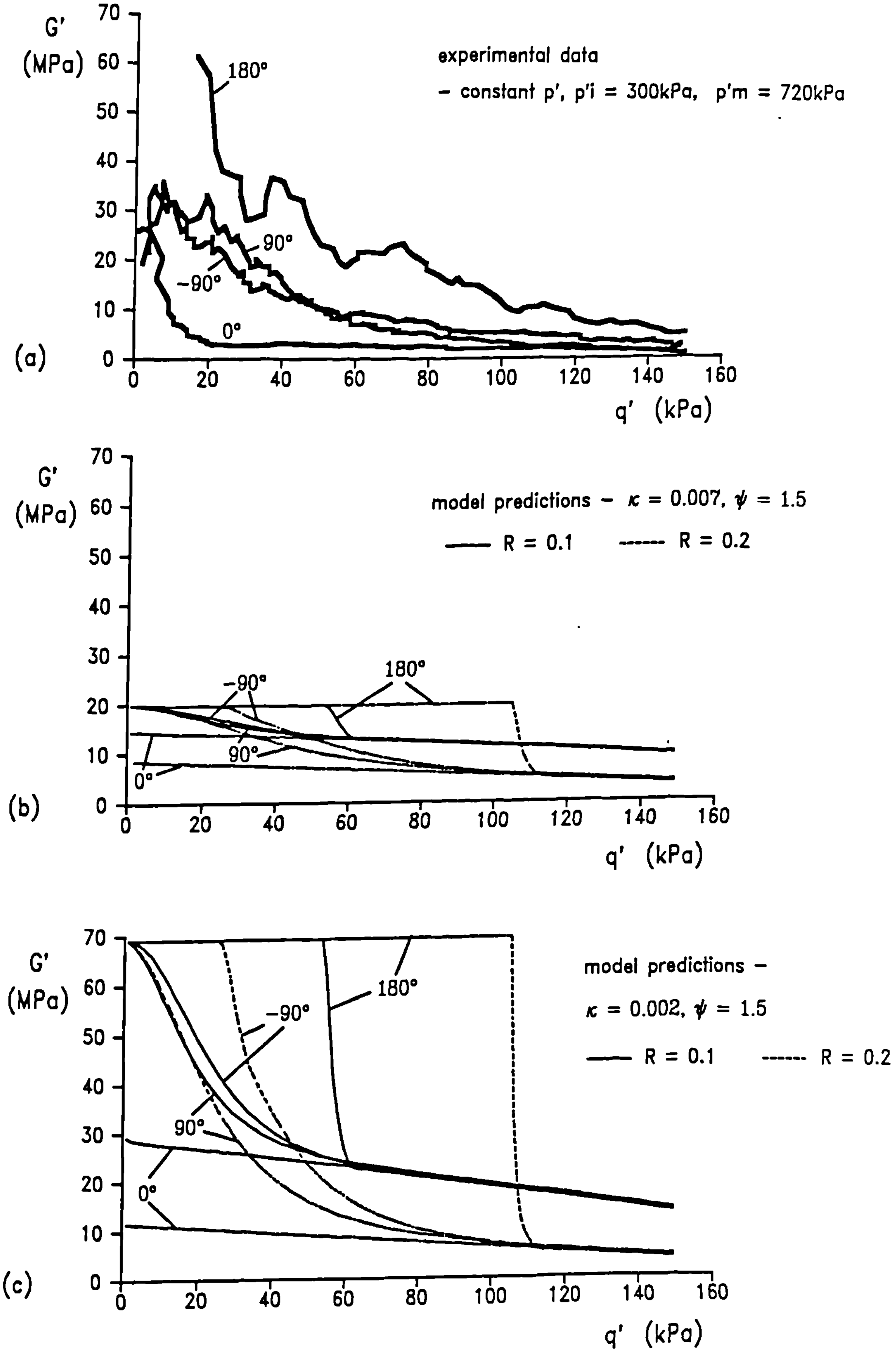

Figure 5.3.11 A comparison between predicted and experimental stiffness data for a constant p' path

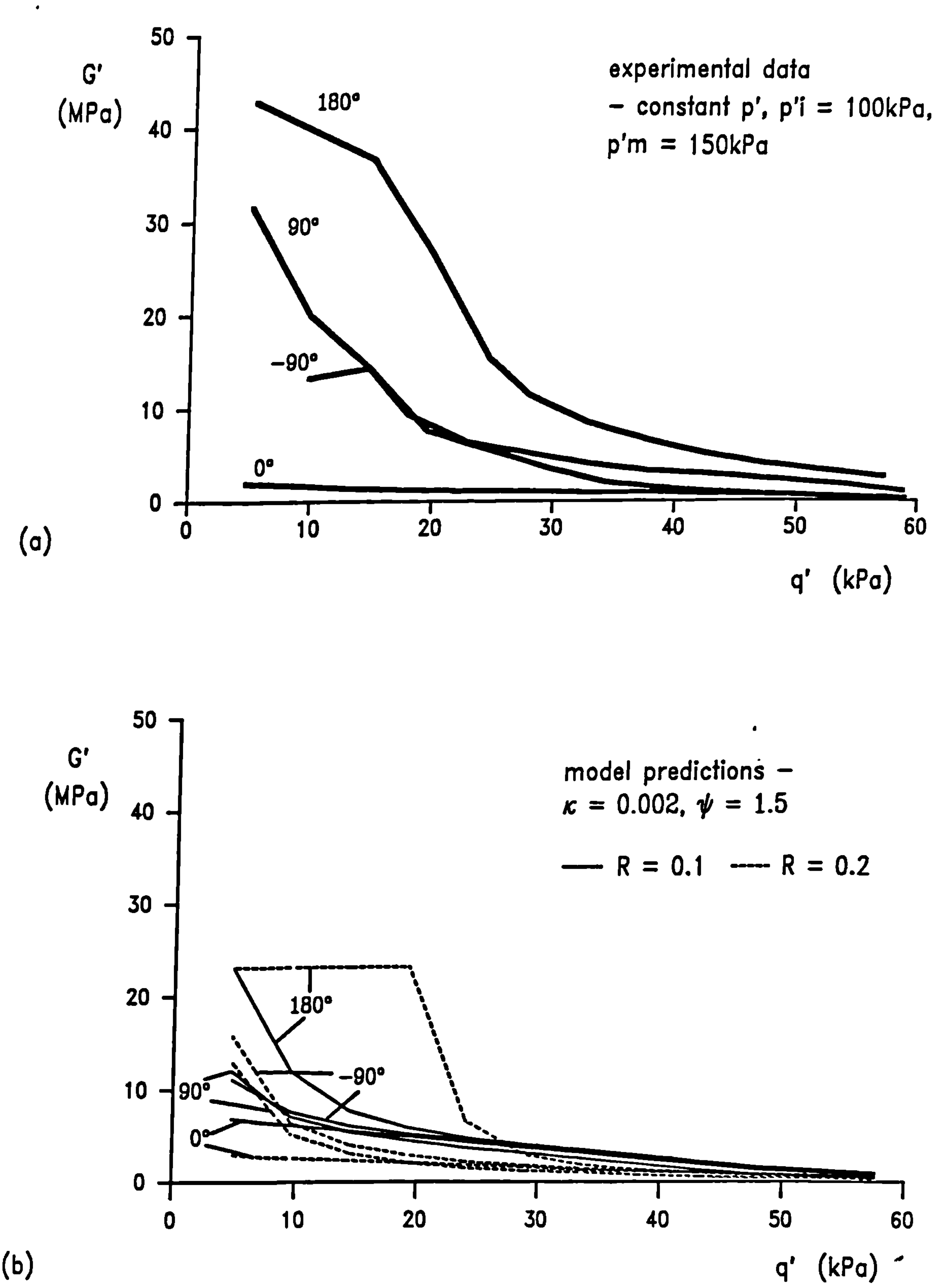

Figure 5.3.12 A comparison between predicted and experimental stiffness data for a constant p' path.

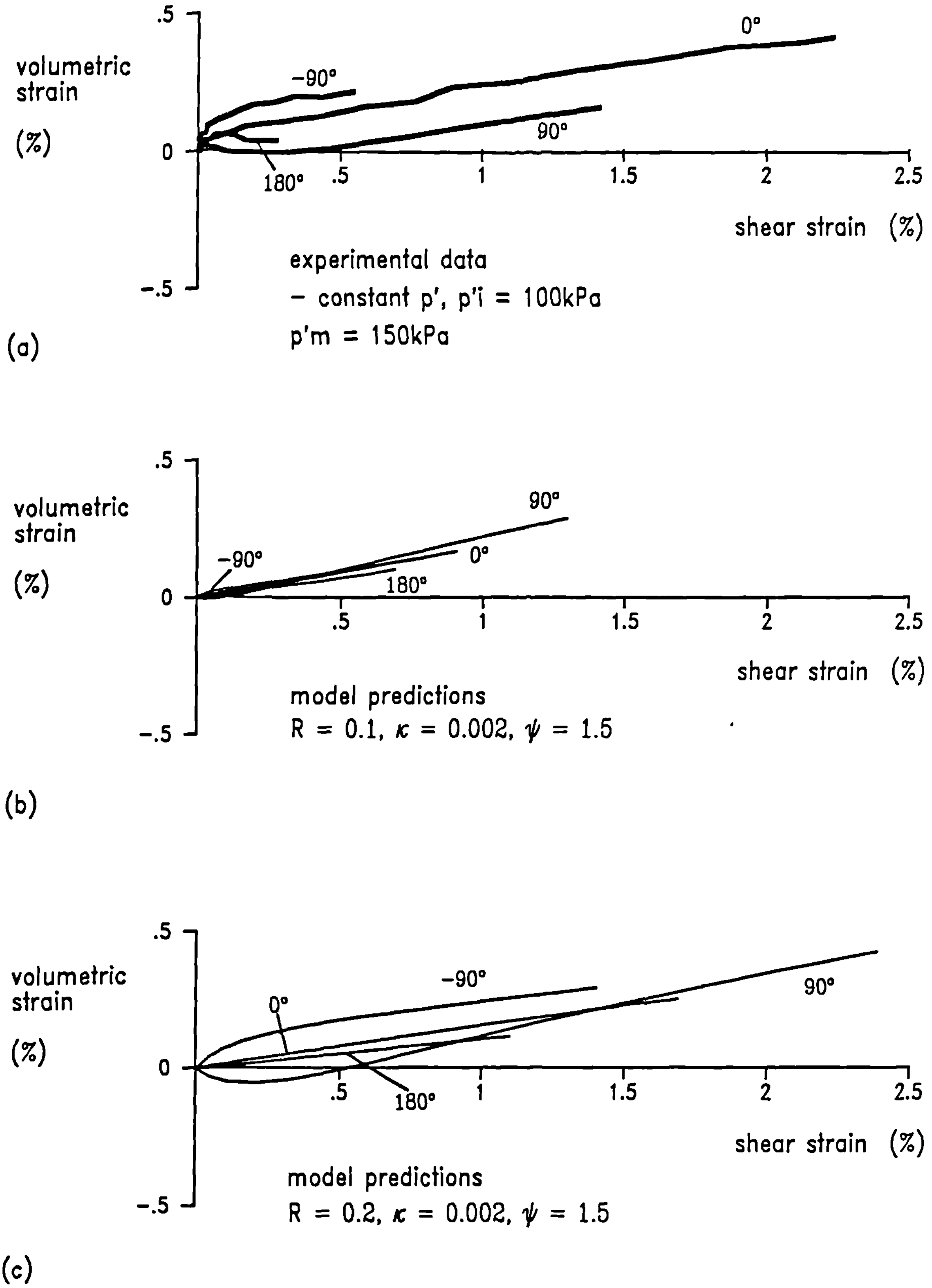

Figure 5.3.13 A comparison between predicted strain paths and experimental data for a constant p' path.

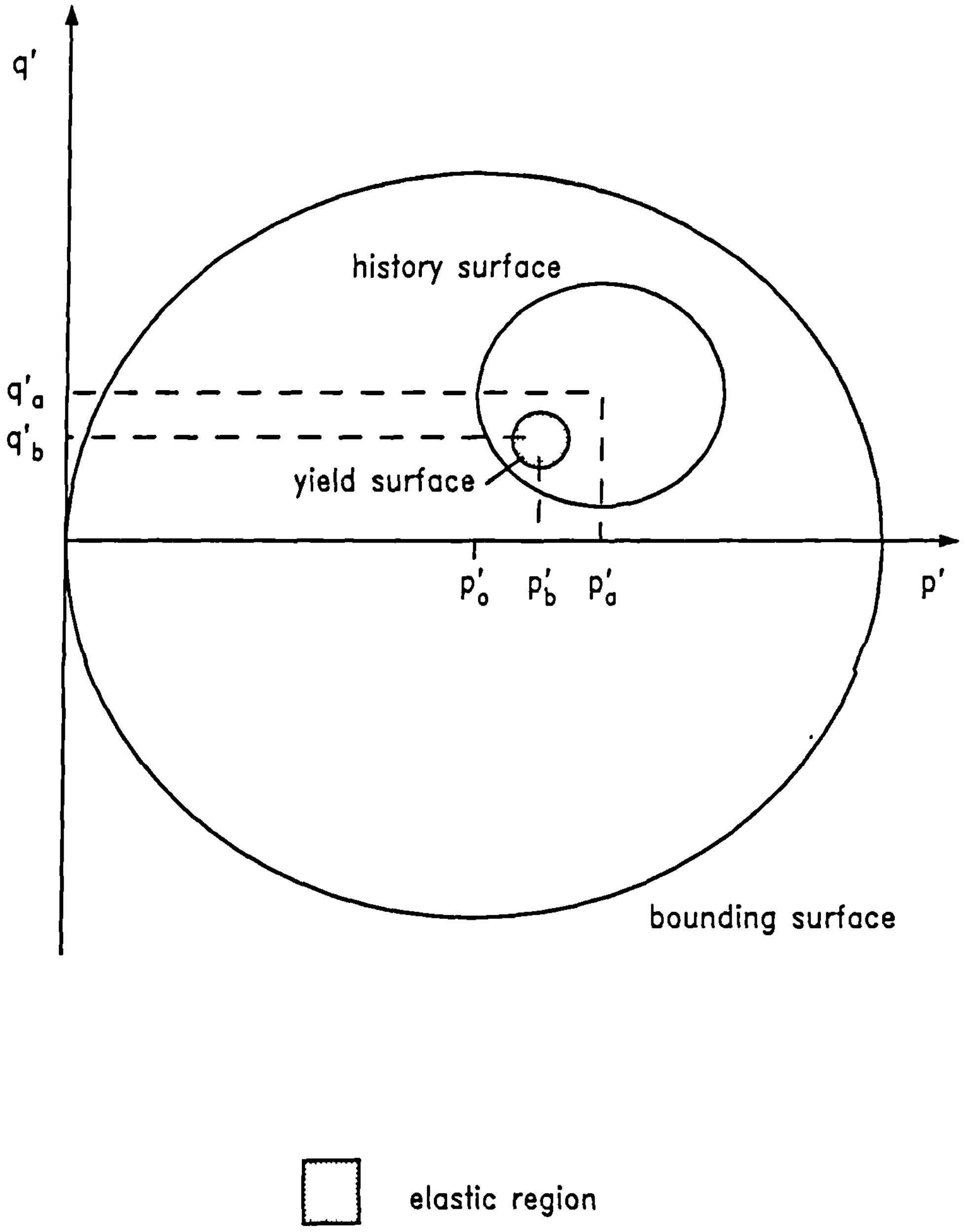

Figure 5.4.1 Diagram showing the three yield surfaces that constitute the three-surface model, defined in stress space.

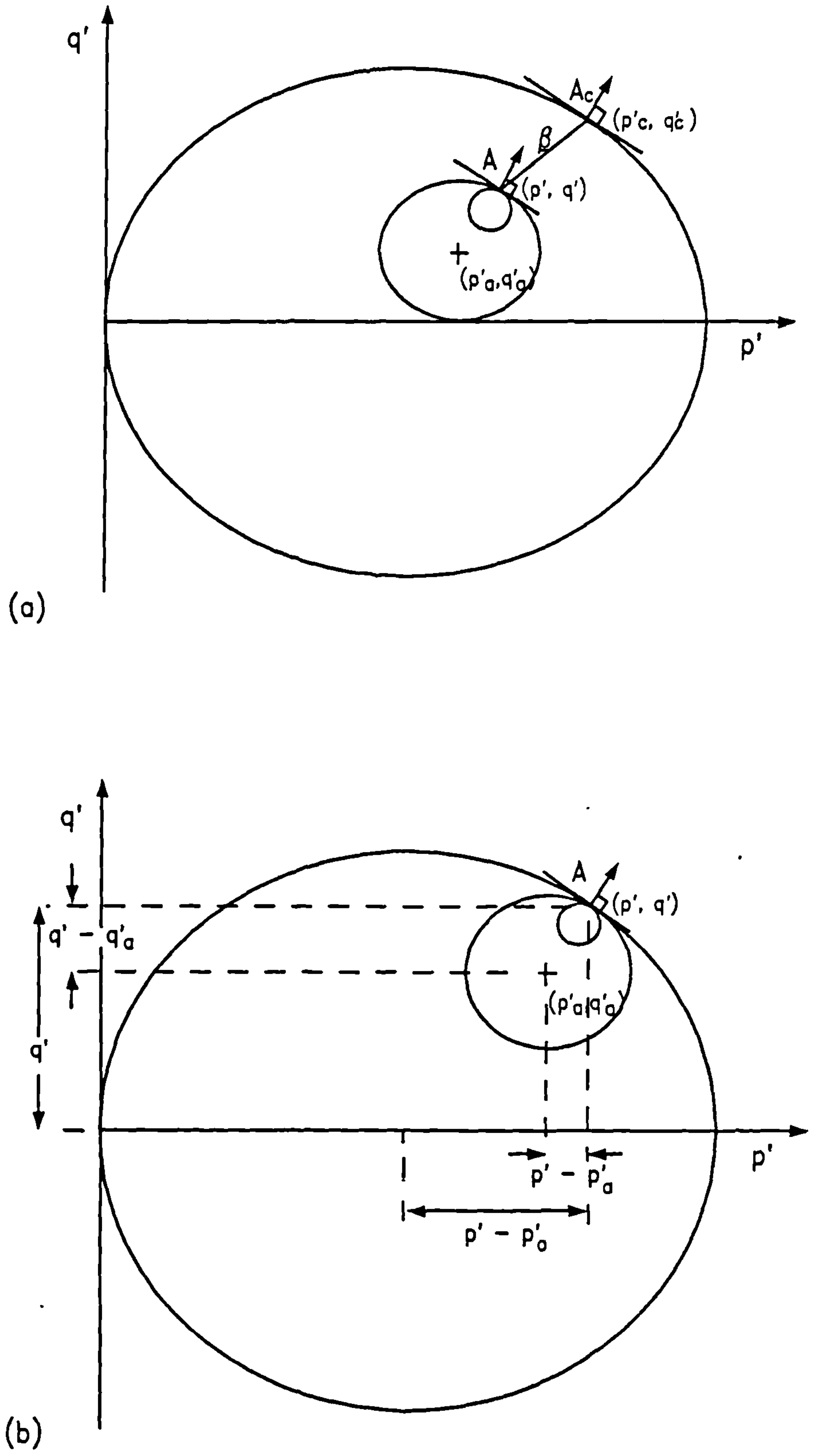

Figure 5.4.2 Diagrams illustrating (a) the definition of a conjugate point and the vector β. (b) the geometry of the surfaces when they are in contact

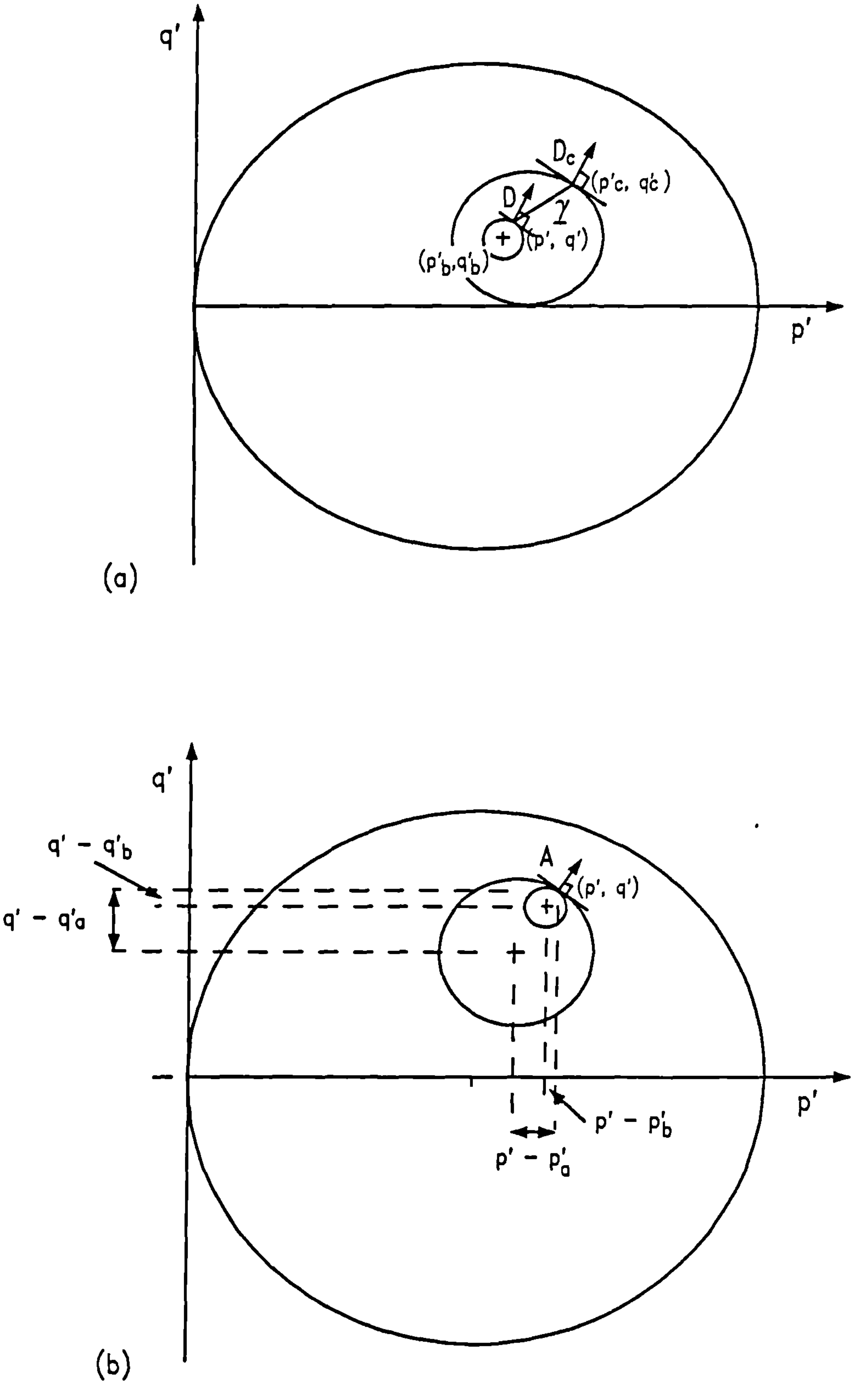

Figure 5.4.3 Diagrams illustrating (a) the definition of a conjugate point and the vector $\underline{\gamma}$. (b) the geometry of the surfaces when they are in contact

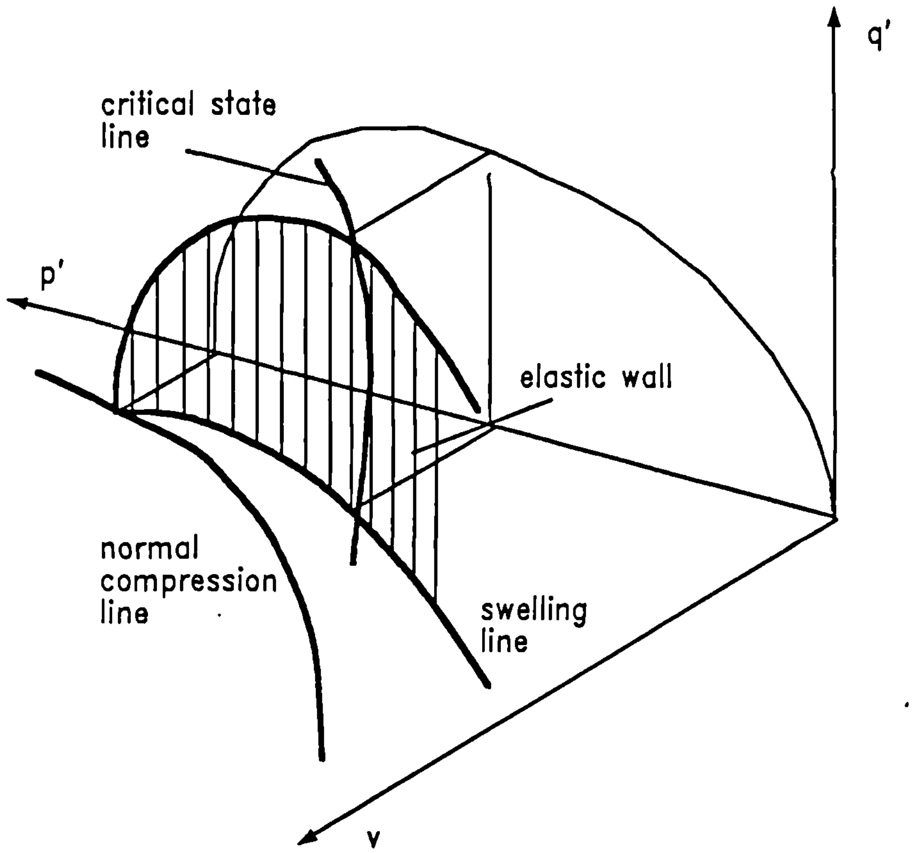

Figure 5.4.4 Diagram showing the intersection of the bounding surface or Modified Cam–clay state boundary surface with an elastic wall

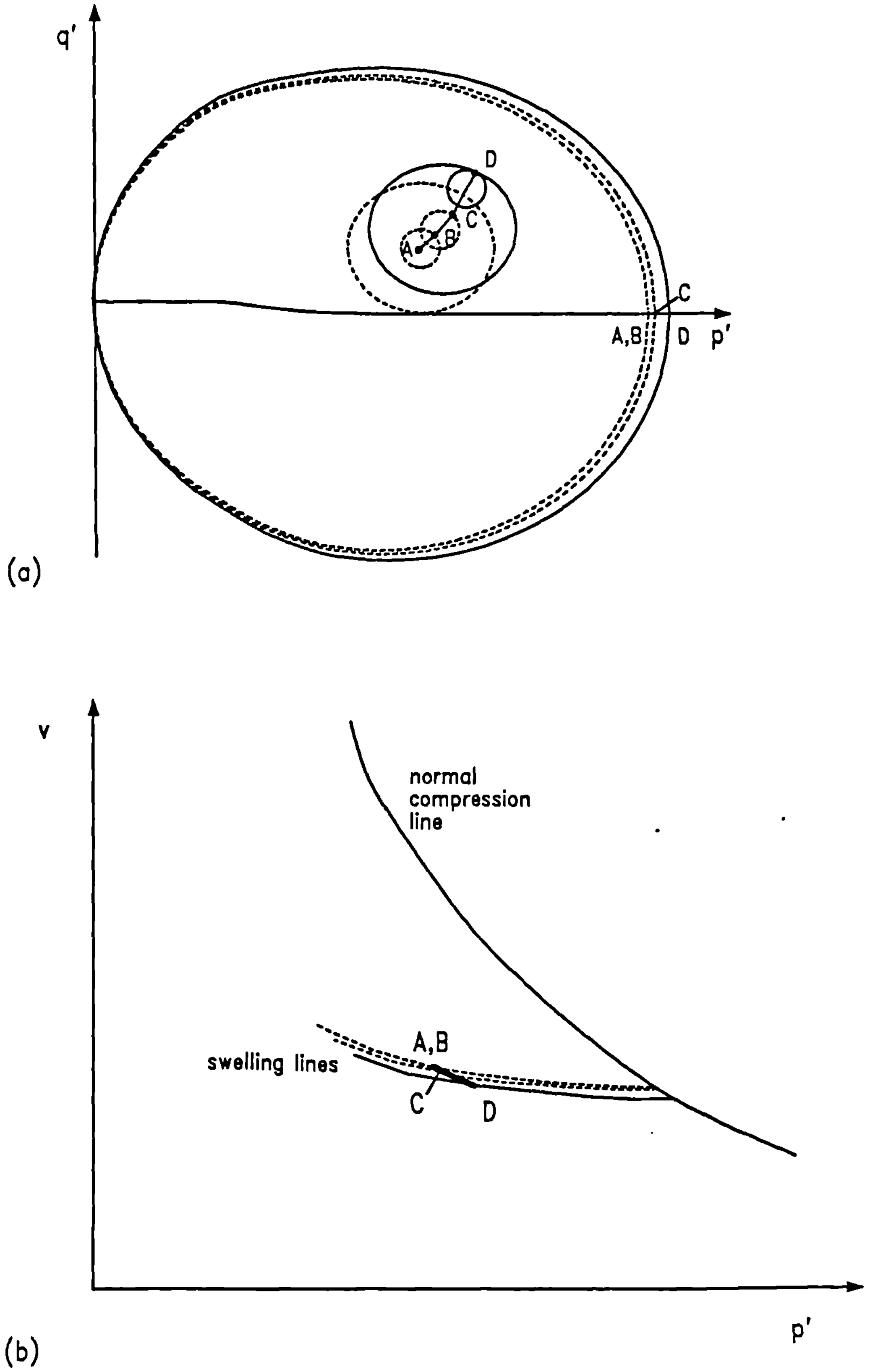

Figure 5.4.5 Diagram showing how the surfaces expand as the stress state moves to new elastic walls

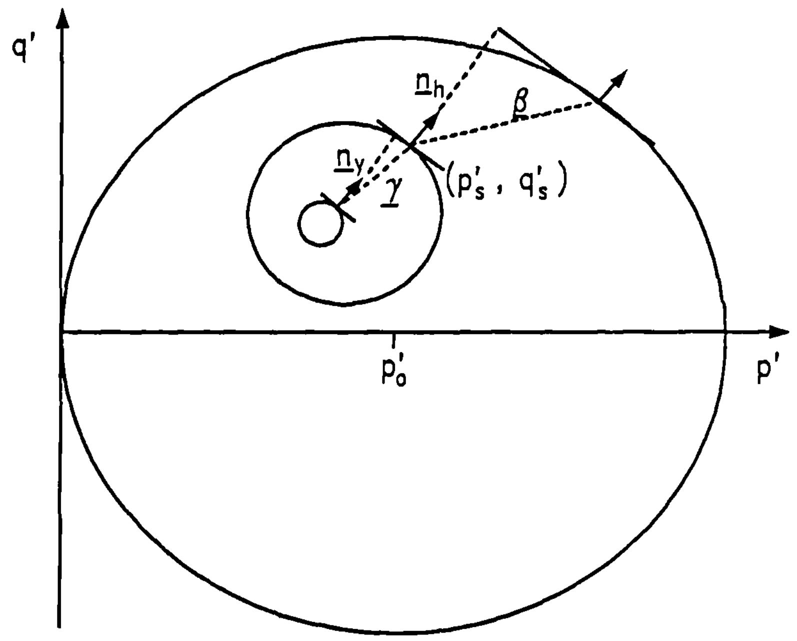

Figure 5.4.6 Diagram defining the main component of the parameters b_1 and b_2.

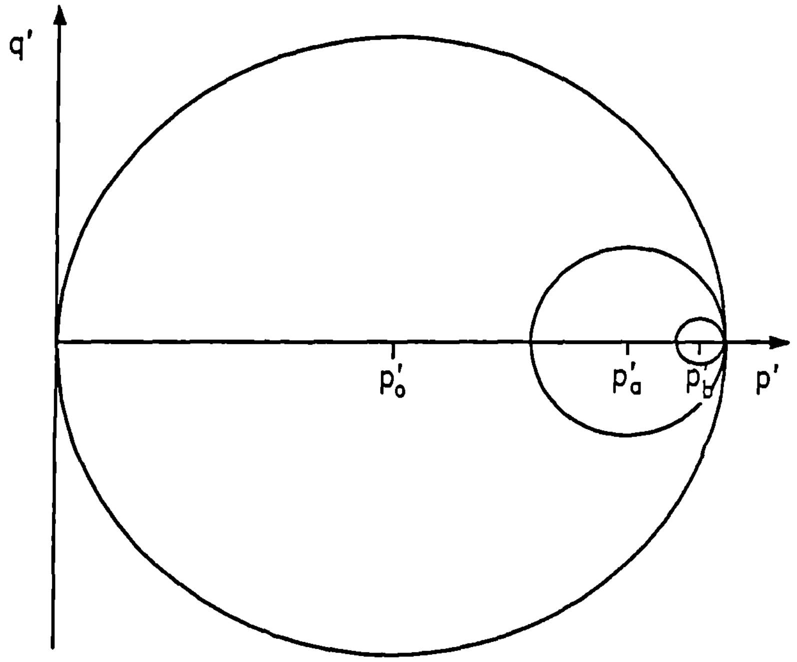

Figure 5.4.7 Diagram showing the position of the surfaces when b_1 and b_2 are at a maximum

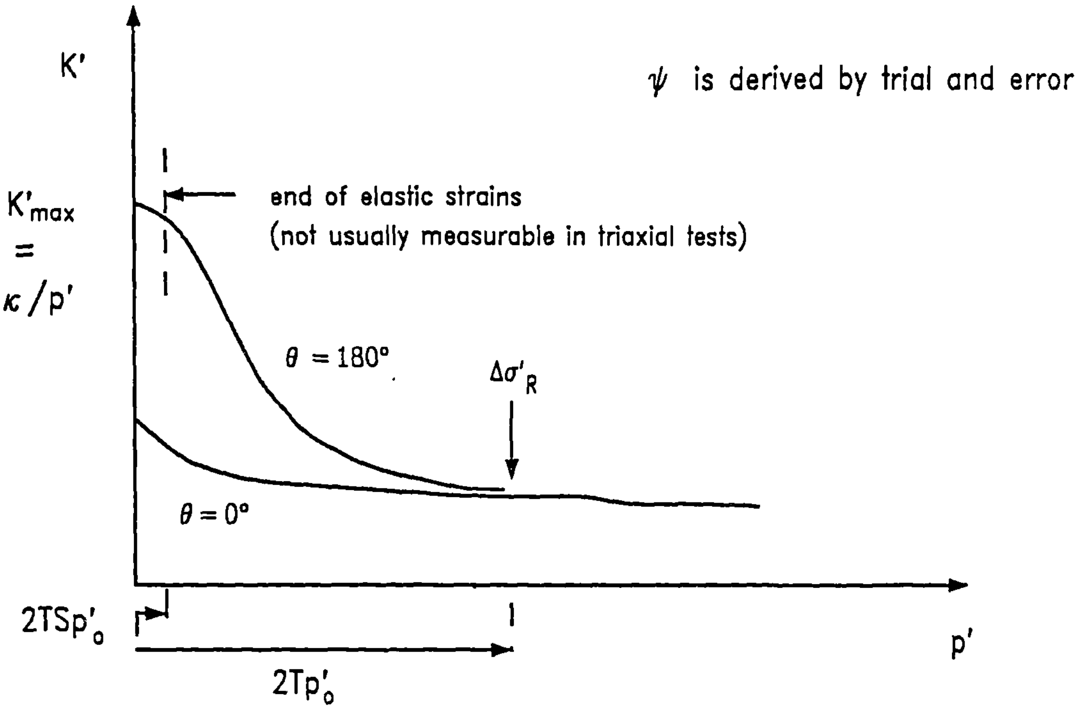

Figure 5.4.8 Diagram showing how the model parameters can be obtained fron typical stiffness curves for a constant q' compression path with two recent stress histories 0 degrees and 180 degrees.

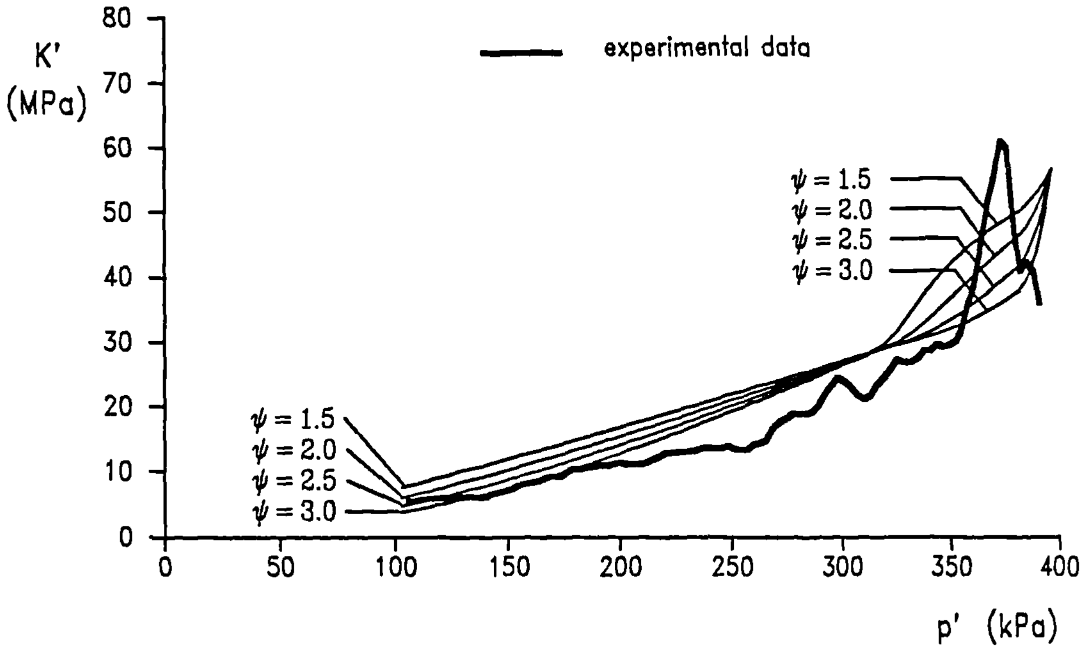

Figure 5.4.9 Model predictions for an isotropic swelling stage, showing the effect of ψ on the predicted variation in stiffness with stress change

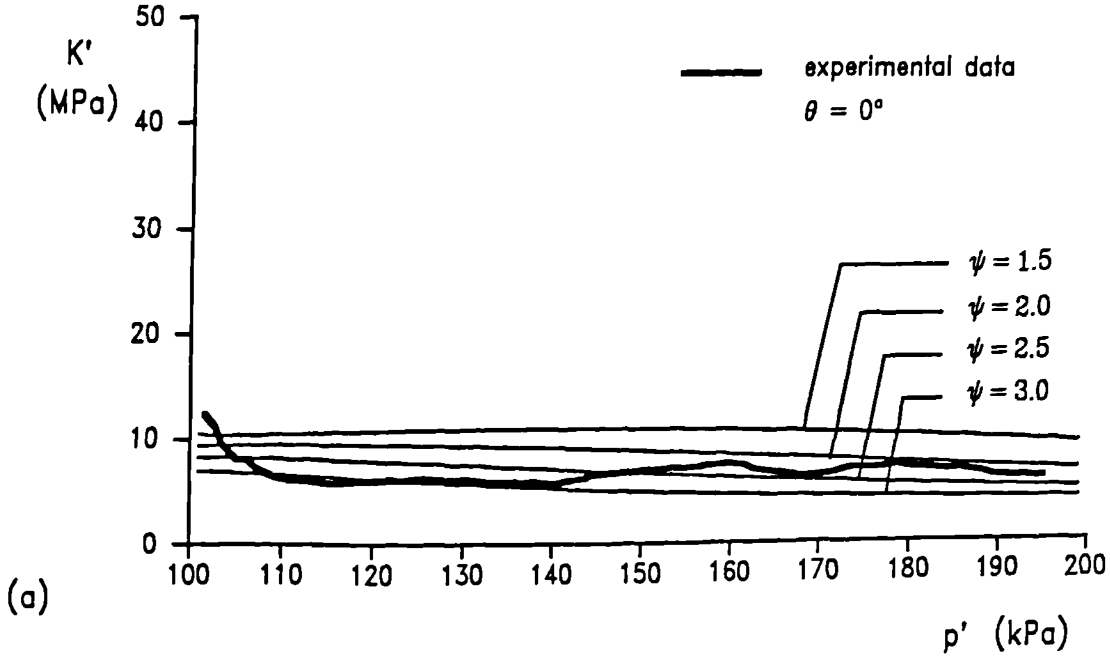

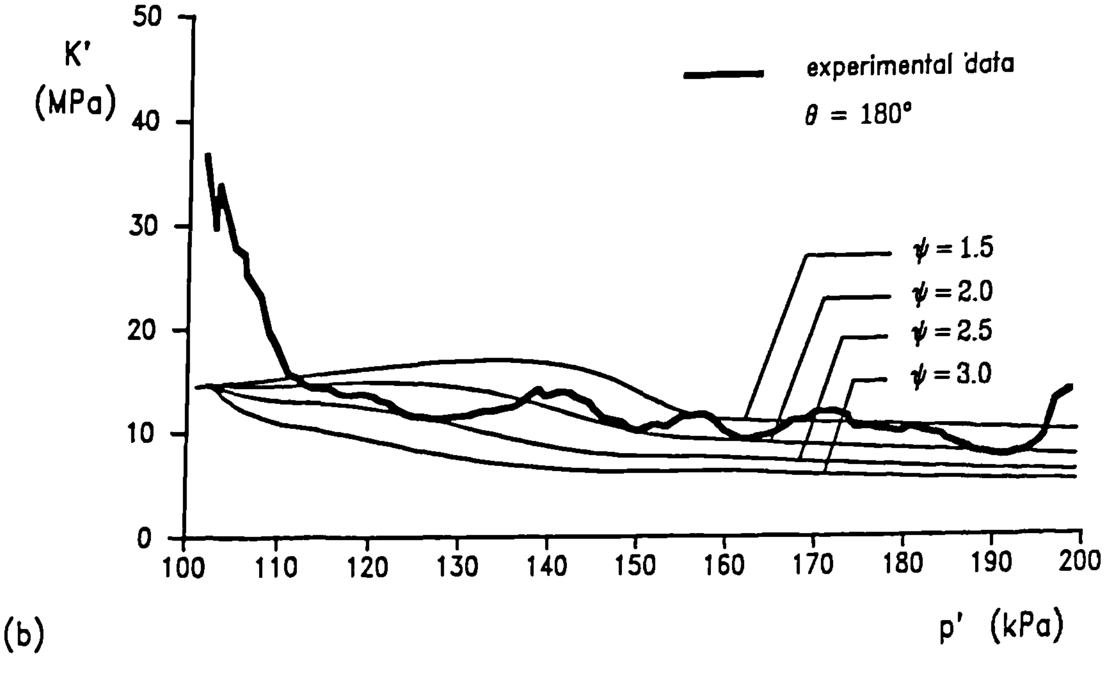

Figure 5.4.10 Model predictions for a constant q' compression path following two different stress path rotations. The sets of curves show the effect of ψ on the predicted variation in stiffness with stress change.

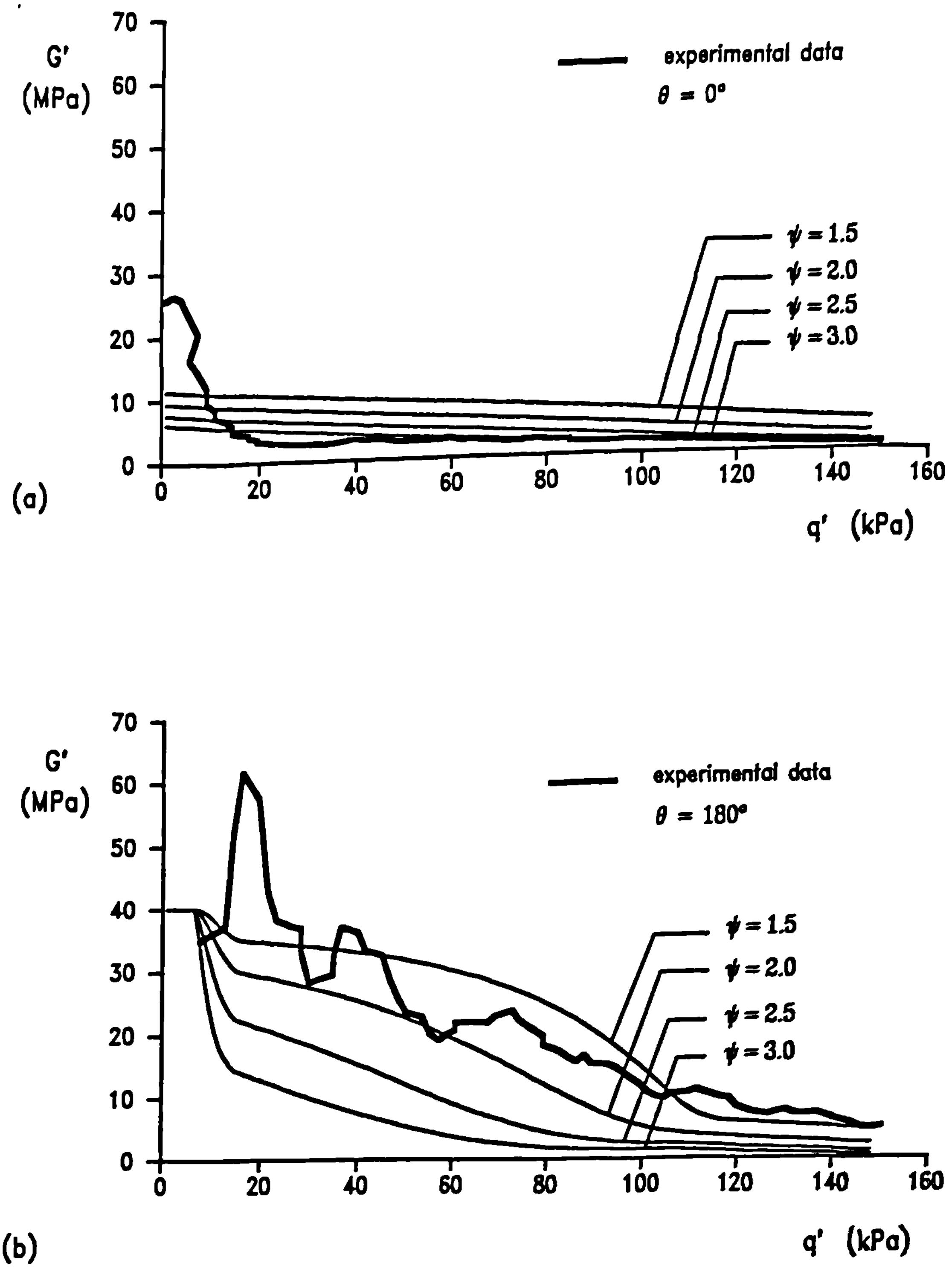

Figure 5.4.11 Model predictions for a constant p' compression path following two different stress path rotations. The sets of curves show the effect of ψ on the predicted variation in stiffness with stress change.

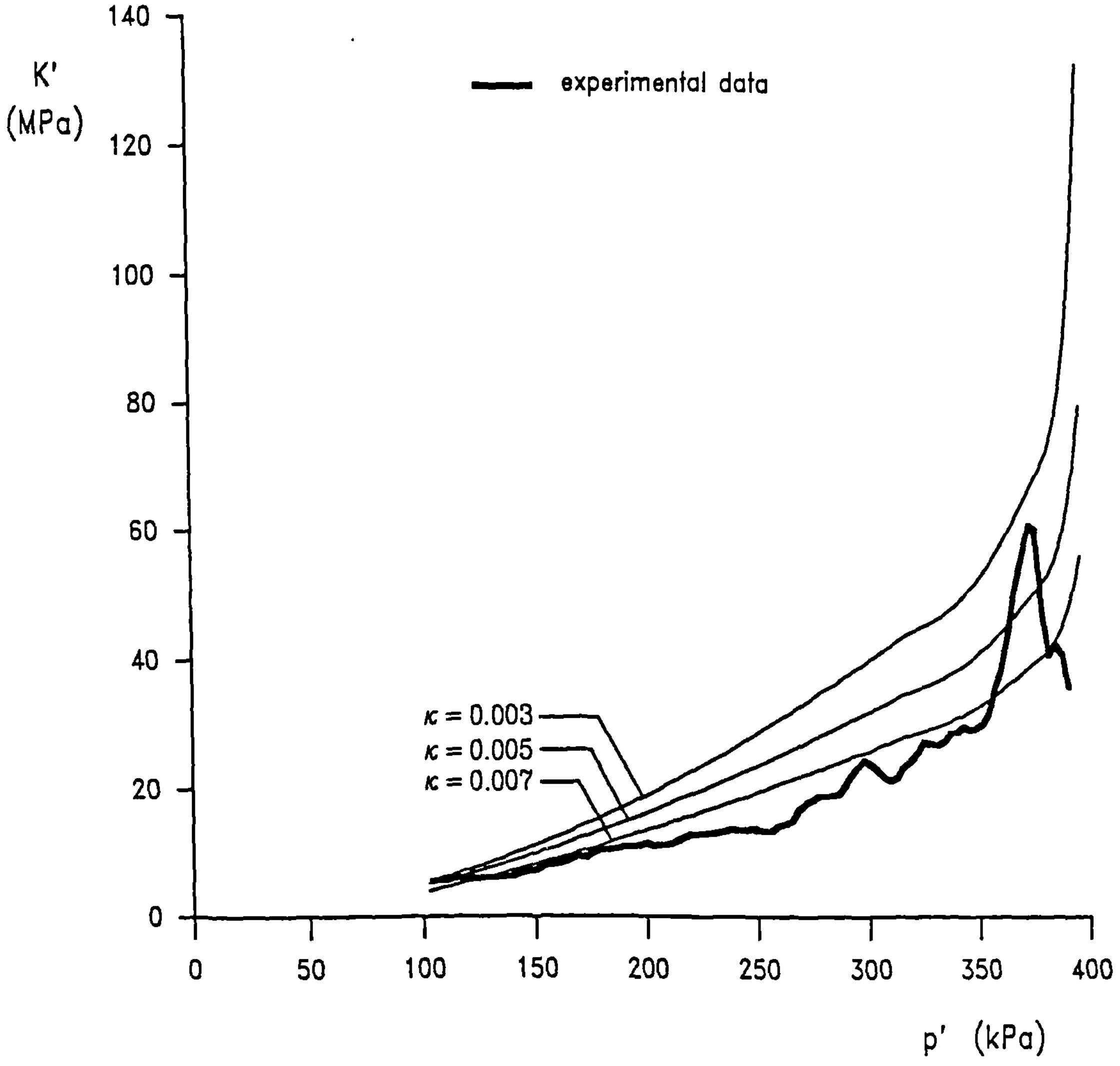

Figure 5.4.12 Model predictions for an isotropic swelling stage. The set of curves show the effect of κ on the predicted variation in stiffness with stress change

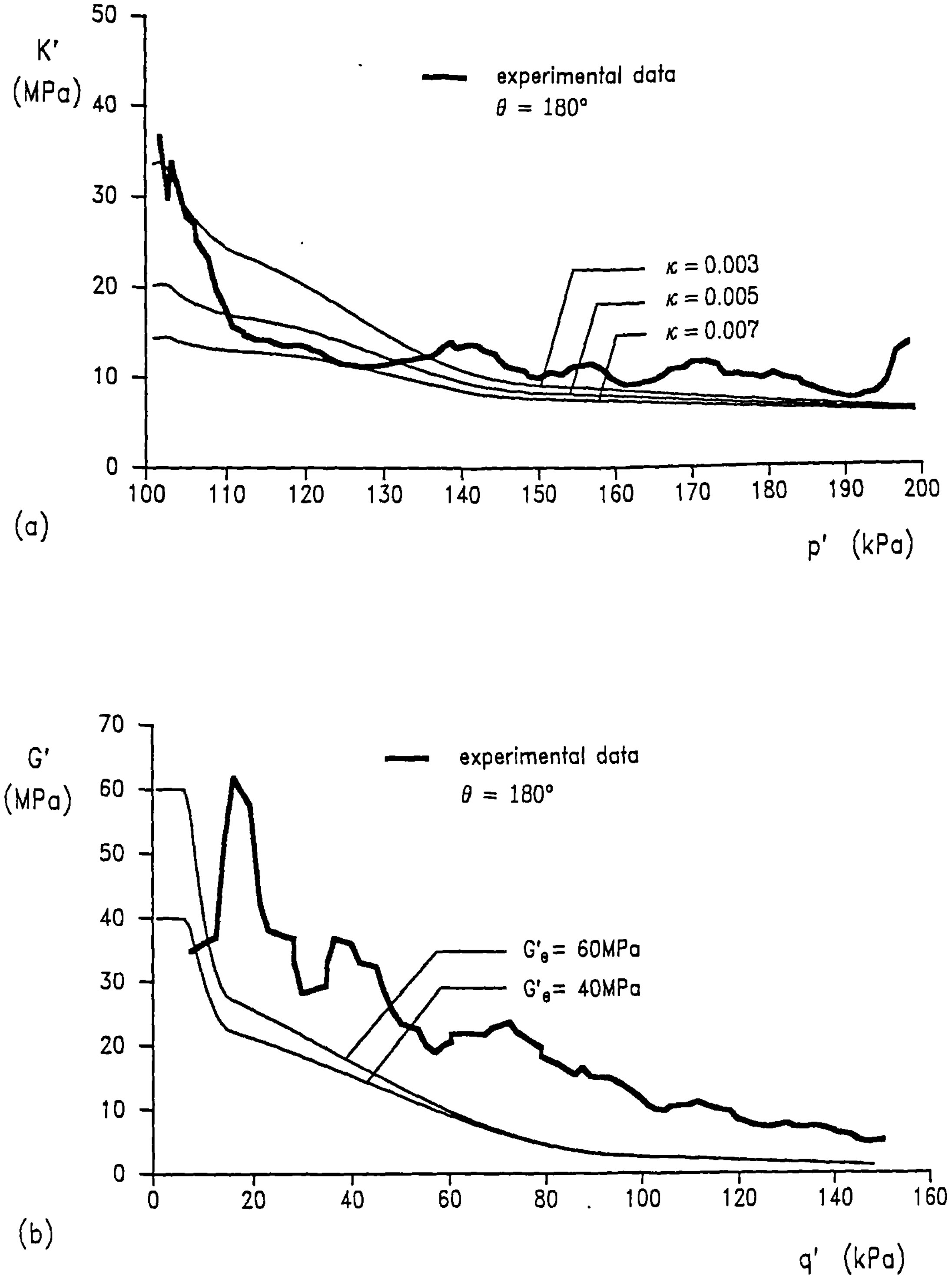

Figure 5.4.13 Graphs illustrating the effect of (a) on the variation of stiffness with stress change for constant q' compression after a stress path reversal (b) G' on the predicted stiffness during constant p' loading after a stress path reversal.

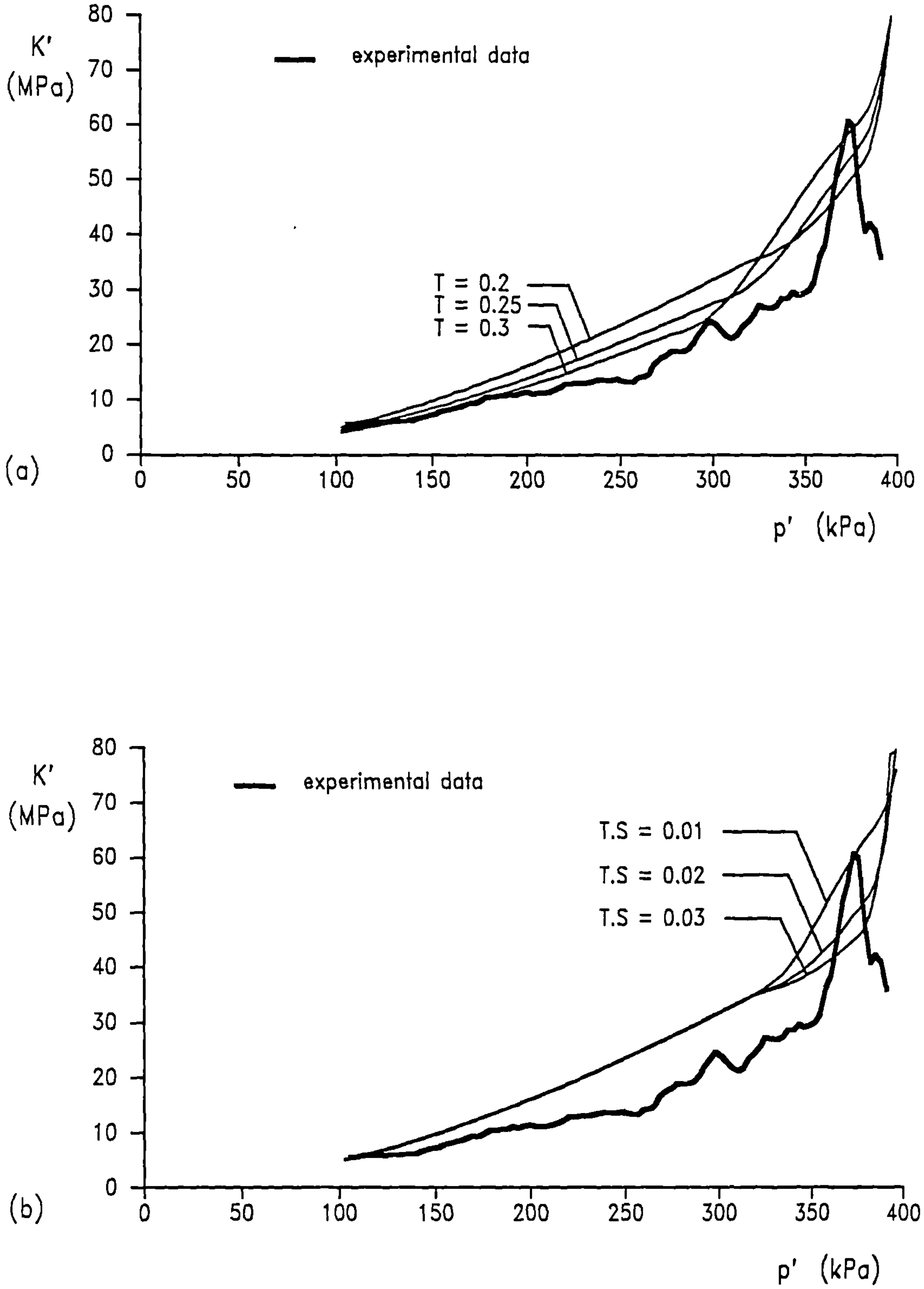

Figure 5.4.14 Model predictions for the variation of stiffness with stress change during isotropic swelling showing the effect of (a) T and (b) T.S

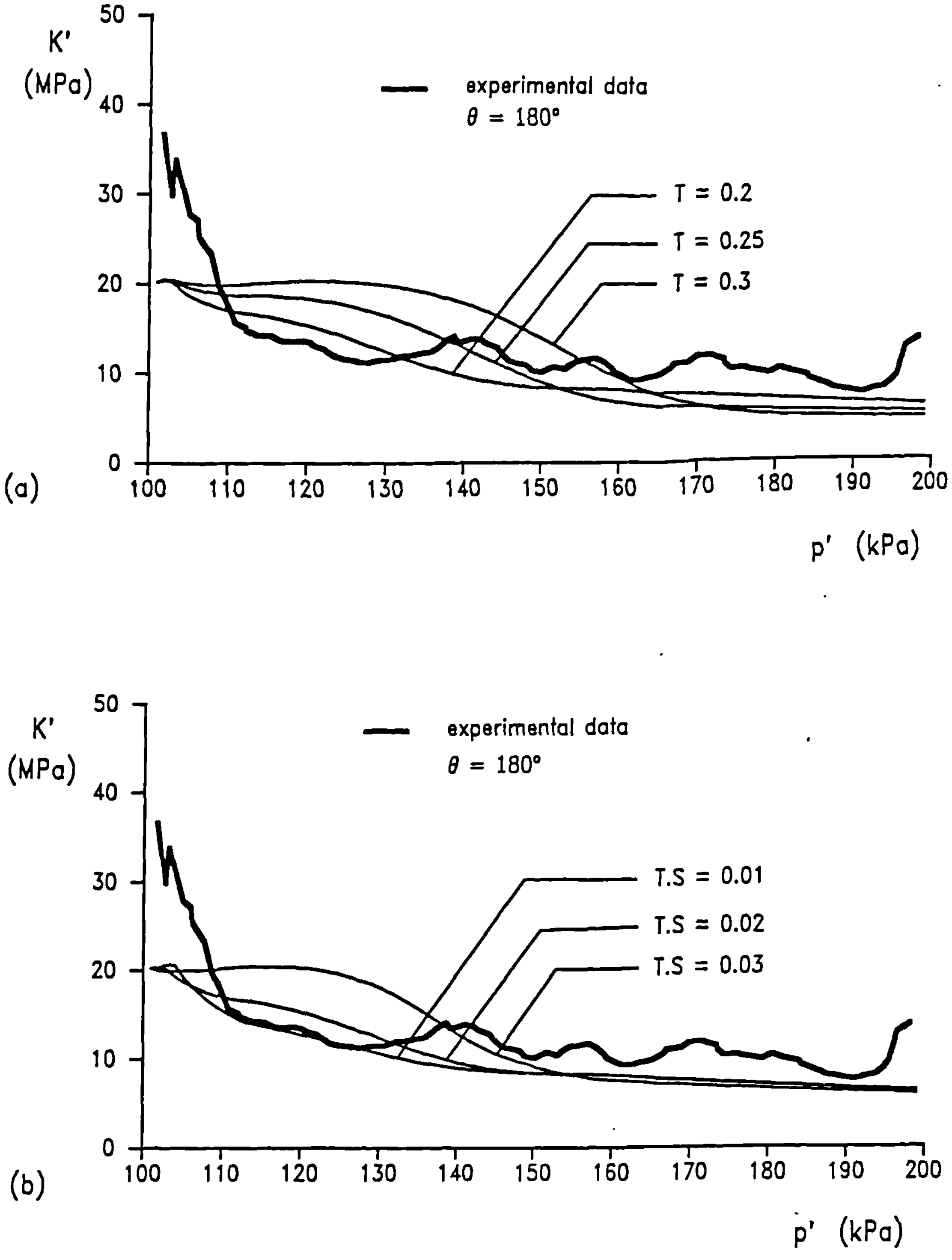

Figure 5.4.15 Model predictions for constant q' compression following a stress path reversal. The sets of curves illustrate the effect of (a) T and (b) T.S

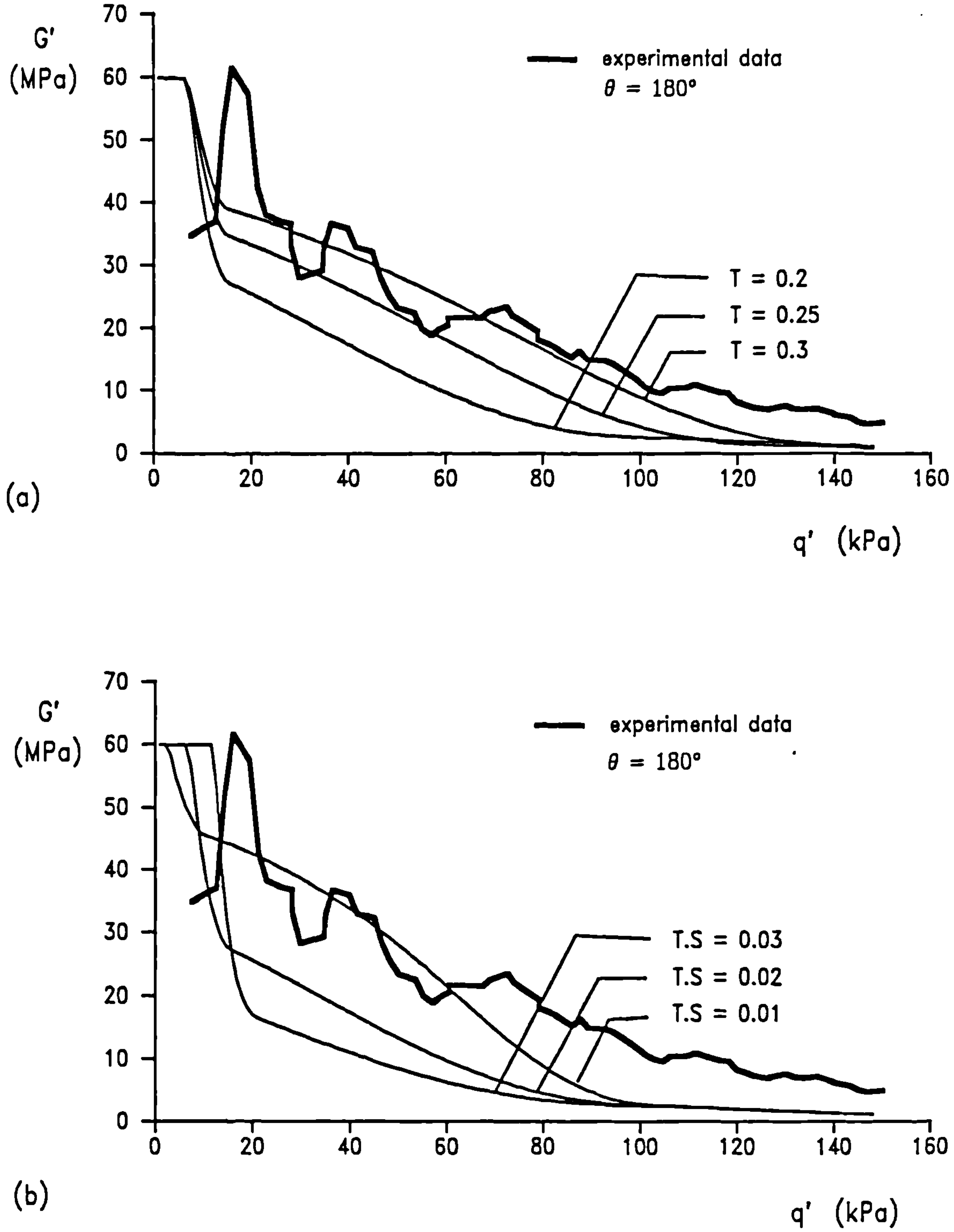

Figure 5.4.16 Model predictions for constant p' compression following a stress path reversal. The sets of data illustrate the effect of (a) T and (b) T.S

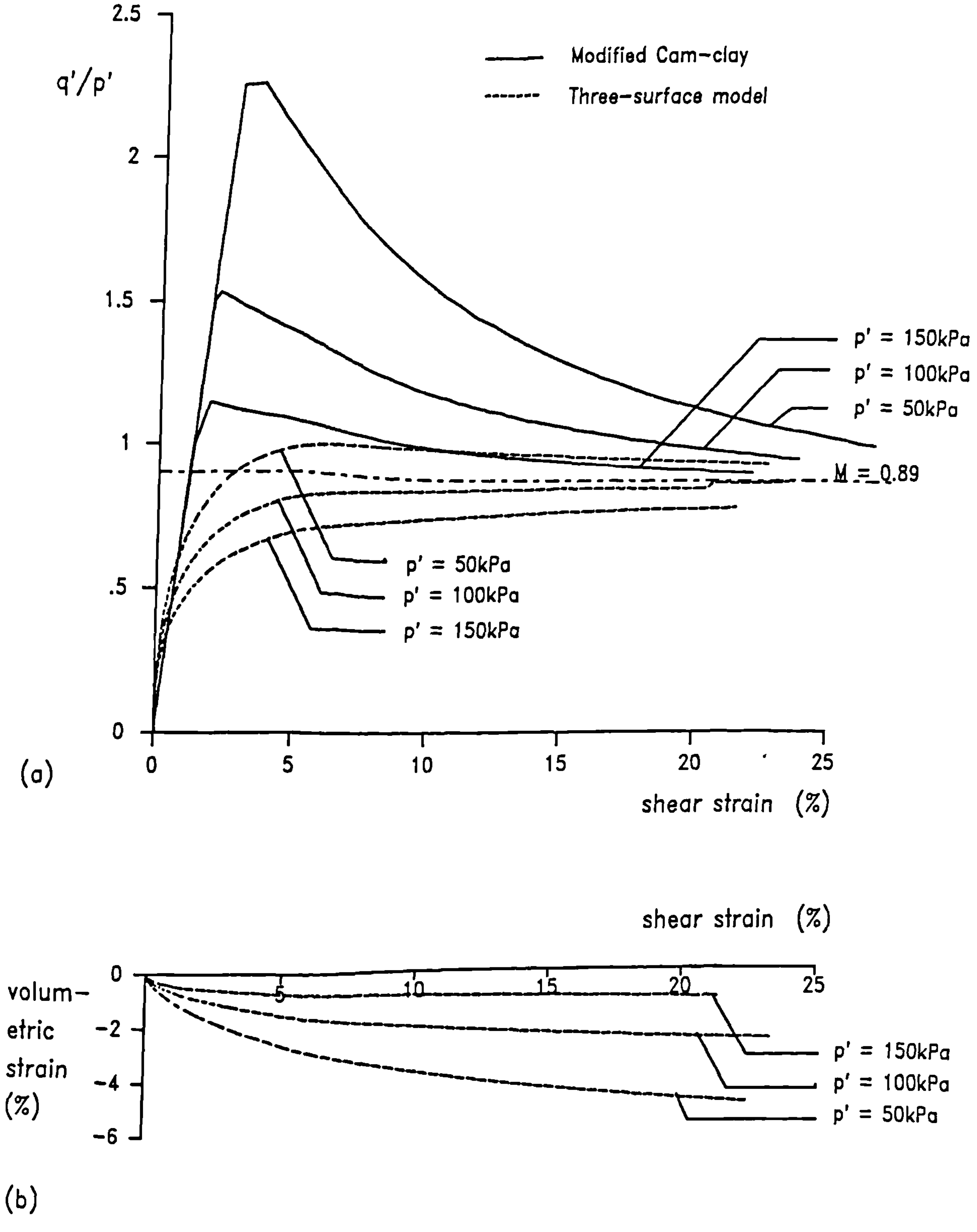

Figure 5.4.17 Comparison between stress-strain response to failure predicted by the Modified Cam-clay model and the response predicted by the three -surface model

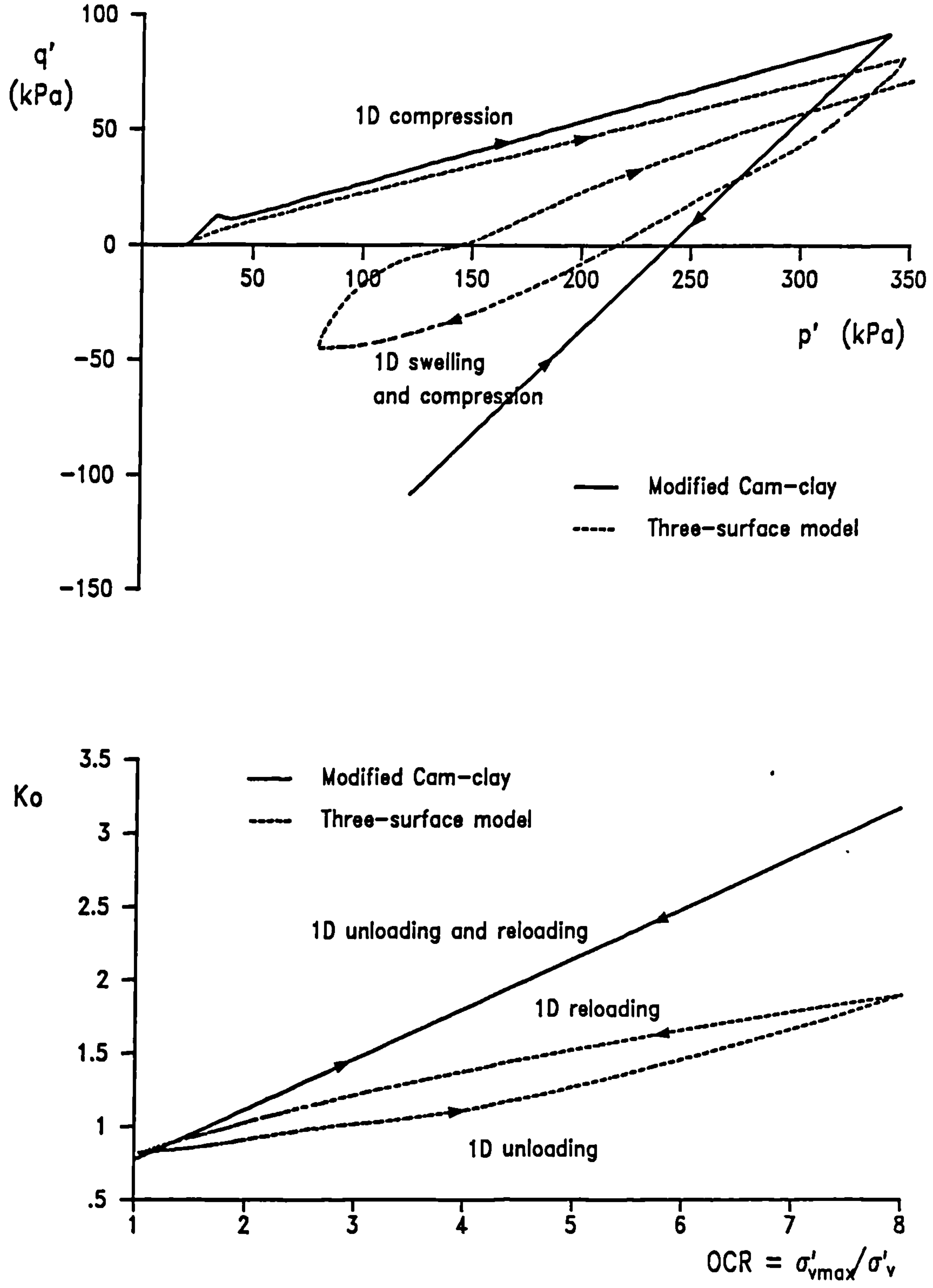

Figure 5.4.18 Comparison between stress paths for 1D compression, swelling and recompression predicted by the Modified Cam-clay model and the three-surface model

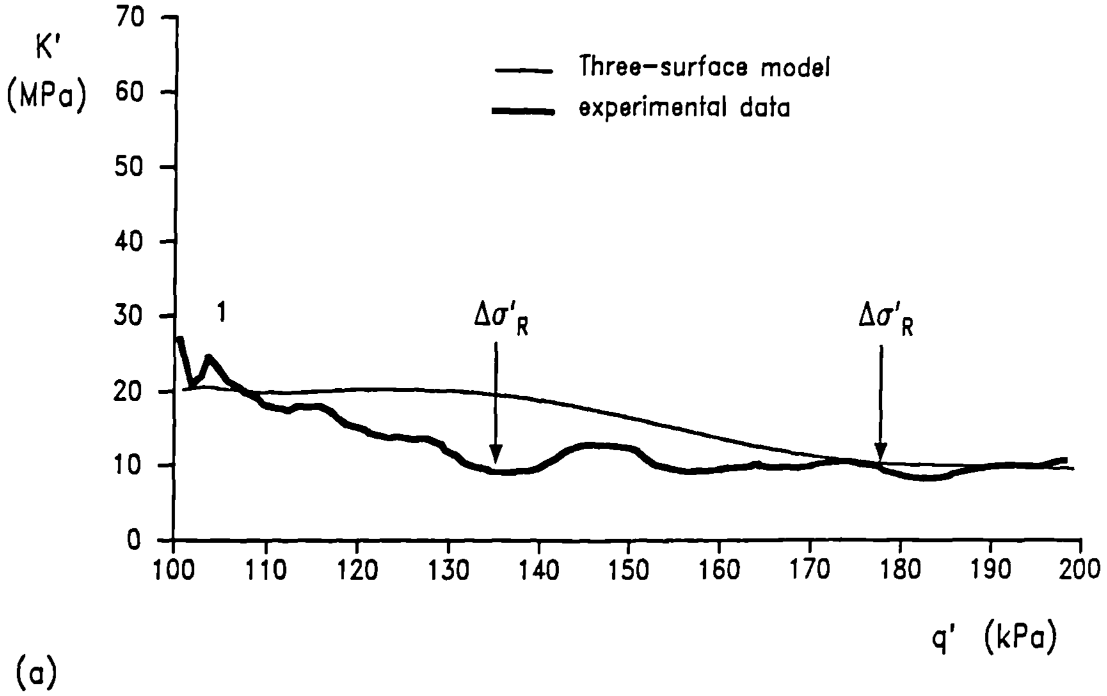

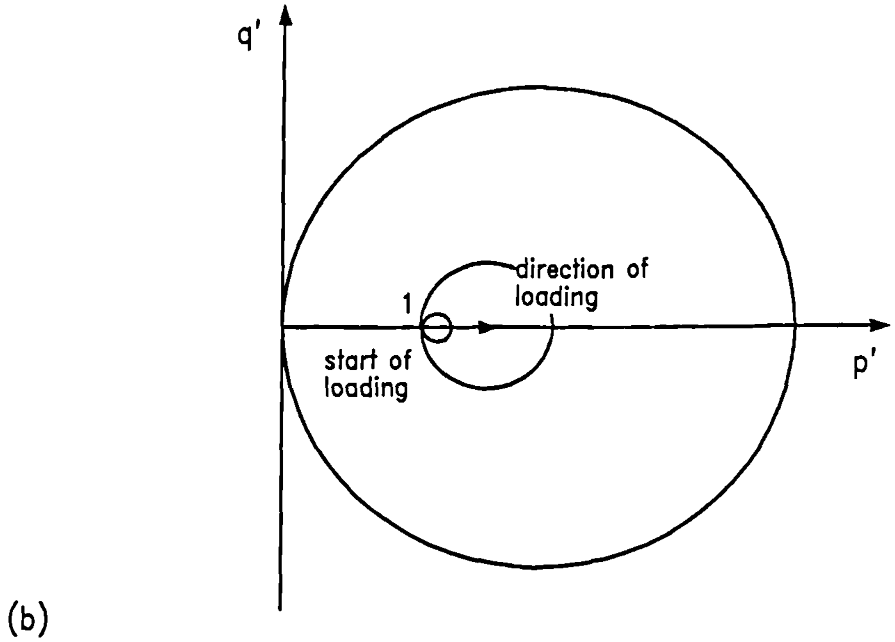

Figure 5.5.1 (a) Comparison between model predictions and experimental data for constant q' compression from p'i = 100kPa with p'm = 400kPa, θ = 180°
(b) A sketch showing the location of the three surfaces in the model at the start of loading.

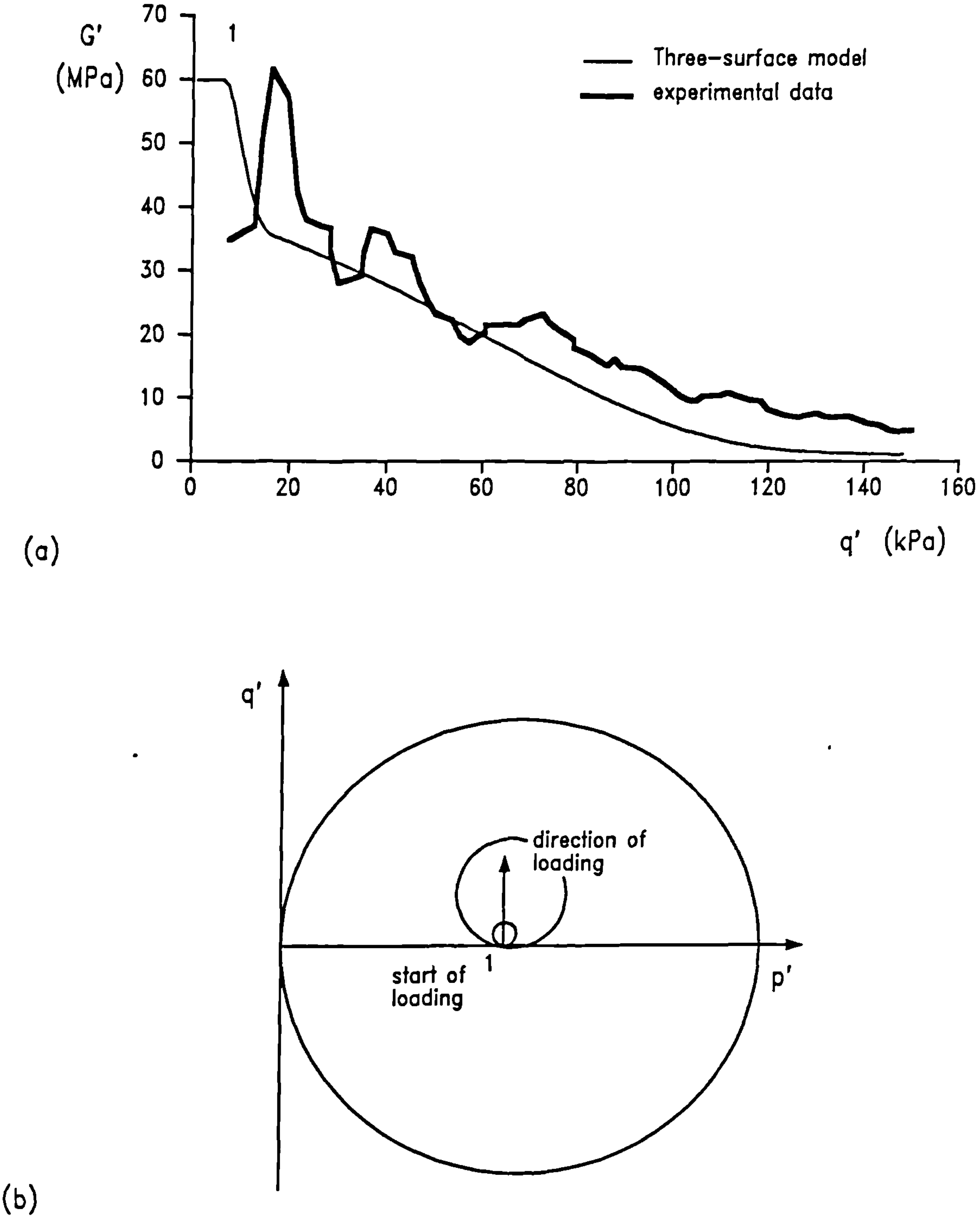

Figure 5.5.2 (a) Comparison between model predictions and experimental data for constant p' compression from p'i = 300kPa with p'm = 720kPa, θ = 180° (b) A sketch showing the location of the three surfaces in the model at the start of loading.

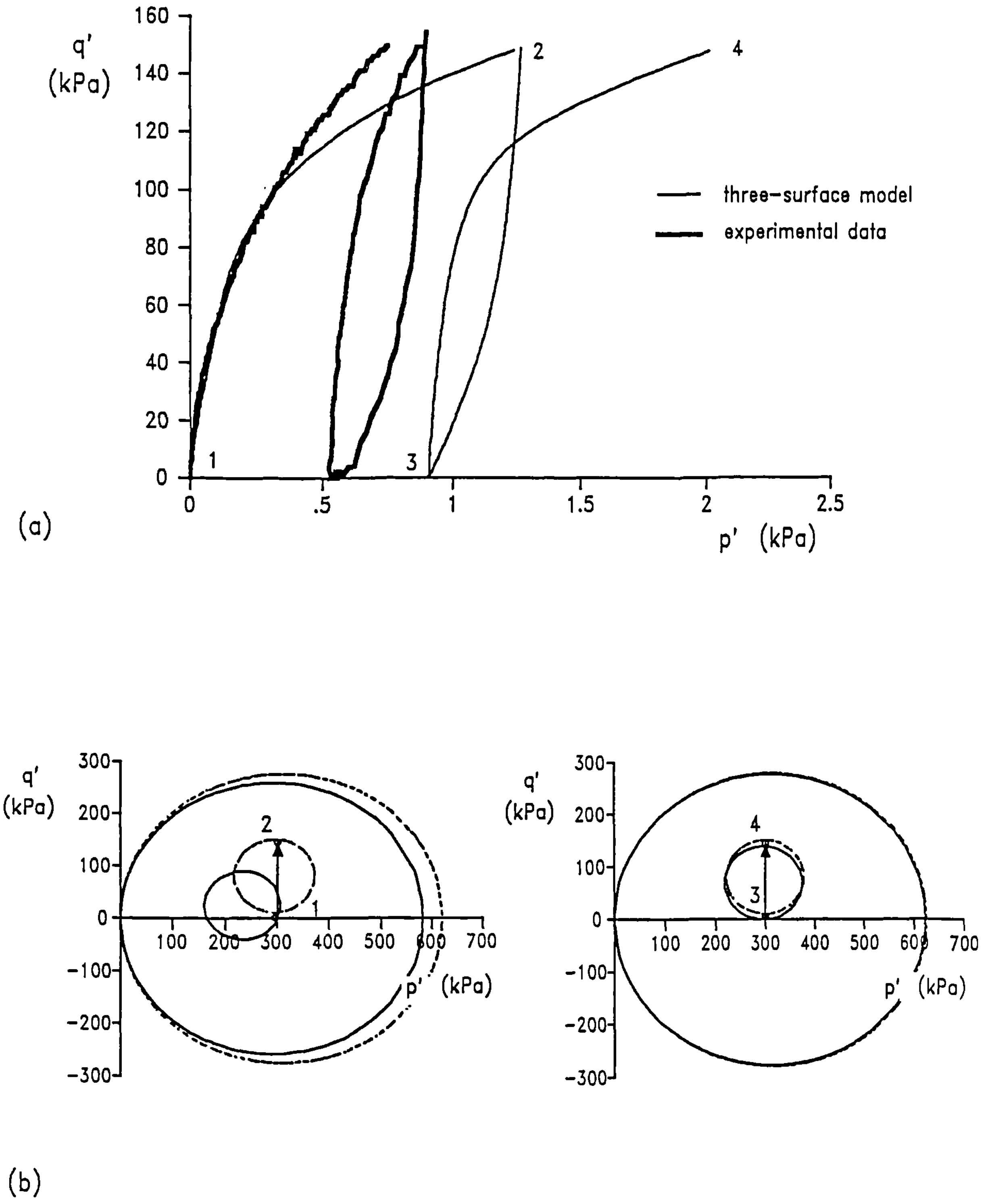

Figure 5.5.3 (a) A comparison between experimental data and model predictions for cycles of constant p' loading at p'i = 300kPa, p'm = 720kPa. (b) a sketch showing the location of the surfaces at the start and finish of each cycle

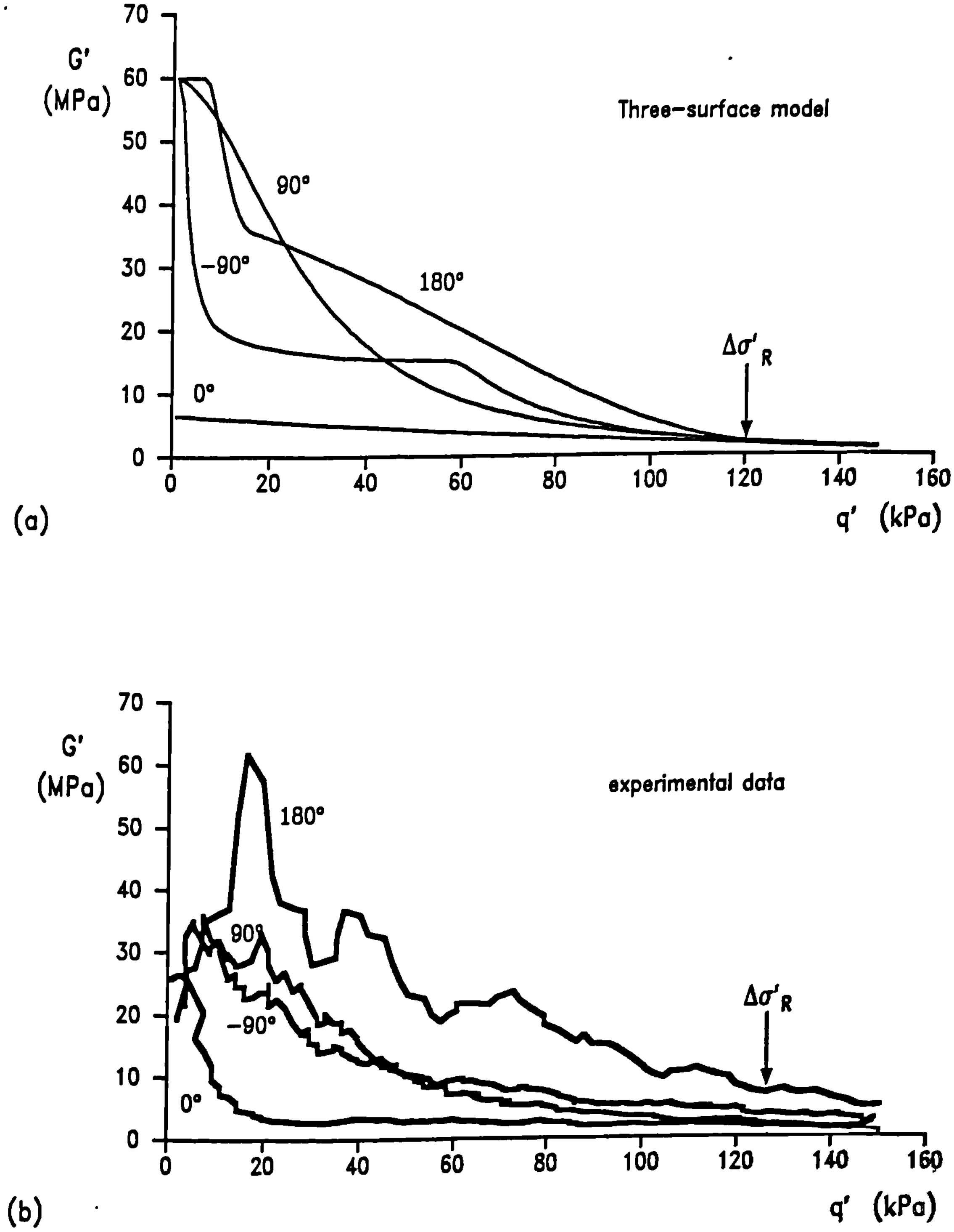

Figure 5.5.4 A comparison between experimental data and model predictions for constant p' loading at p'i = 300kPa, p'm = 720kPa after four stress path rotations.

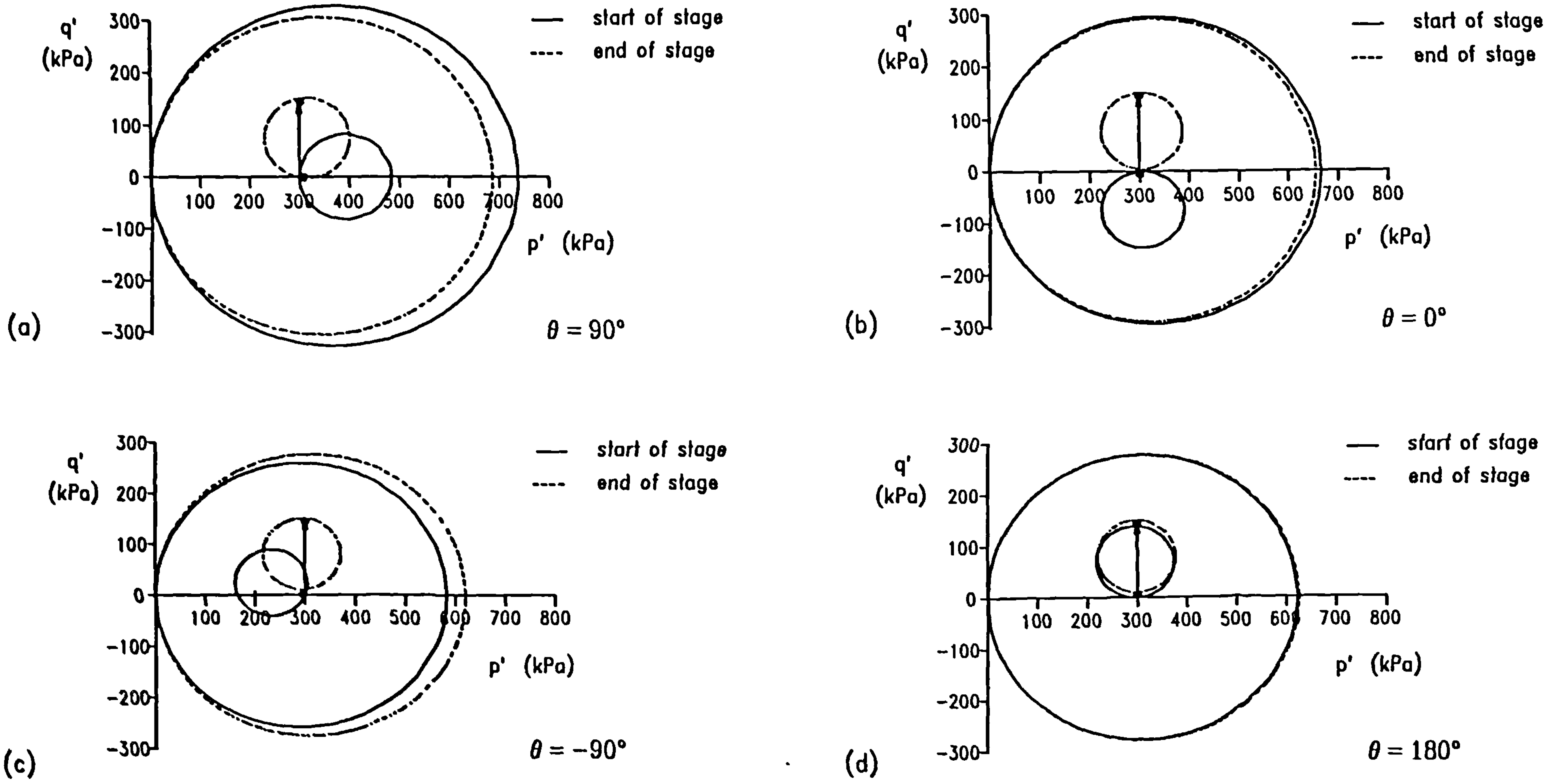

Figure 5.5.5 Plots showing the positions of the three surfaces used in the model at the start and end of each constant p' loading stage for which stiffness data are plotted in Figure 5.5.4

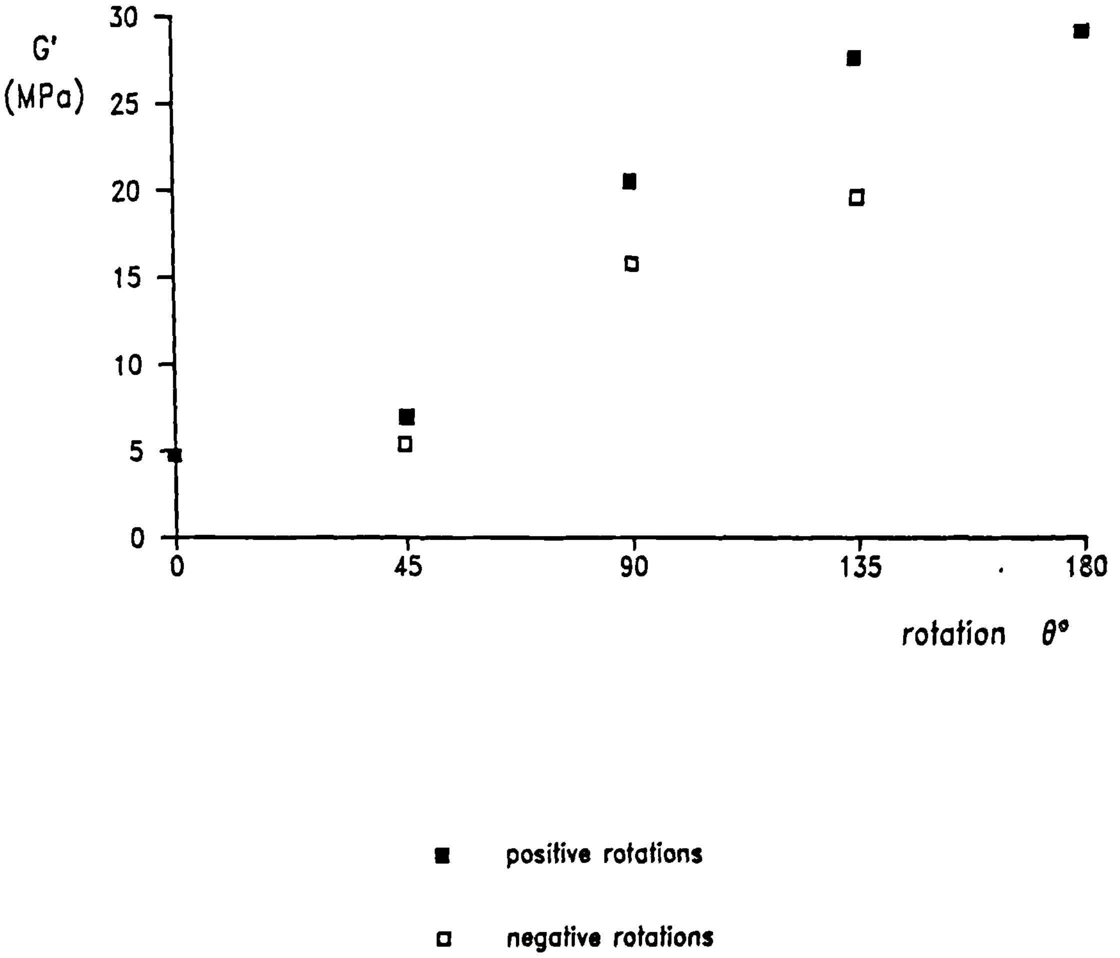

Figure 5.5.6 Model predictions of the variation in G' at $\Delta\sigma'/\Delta\sigma'_R = 0.3$ with stress path rotation. Data calculated for p'i = 300kPa, p'm = 720kPa

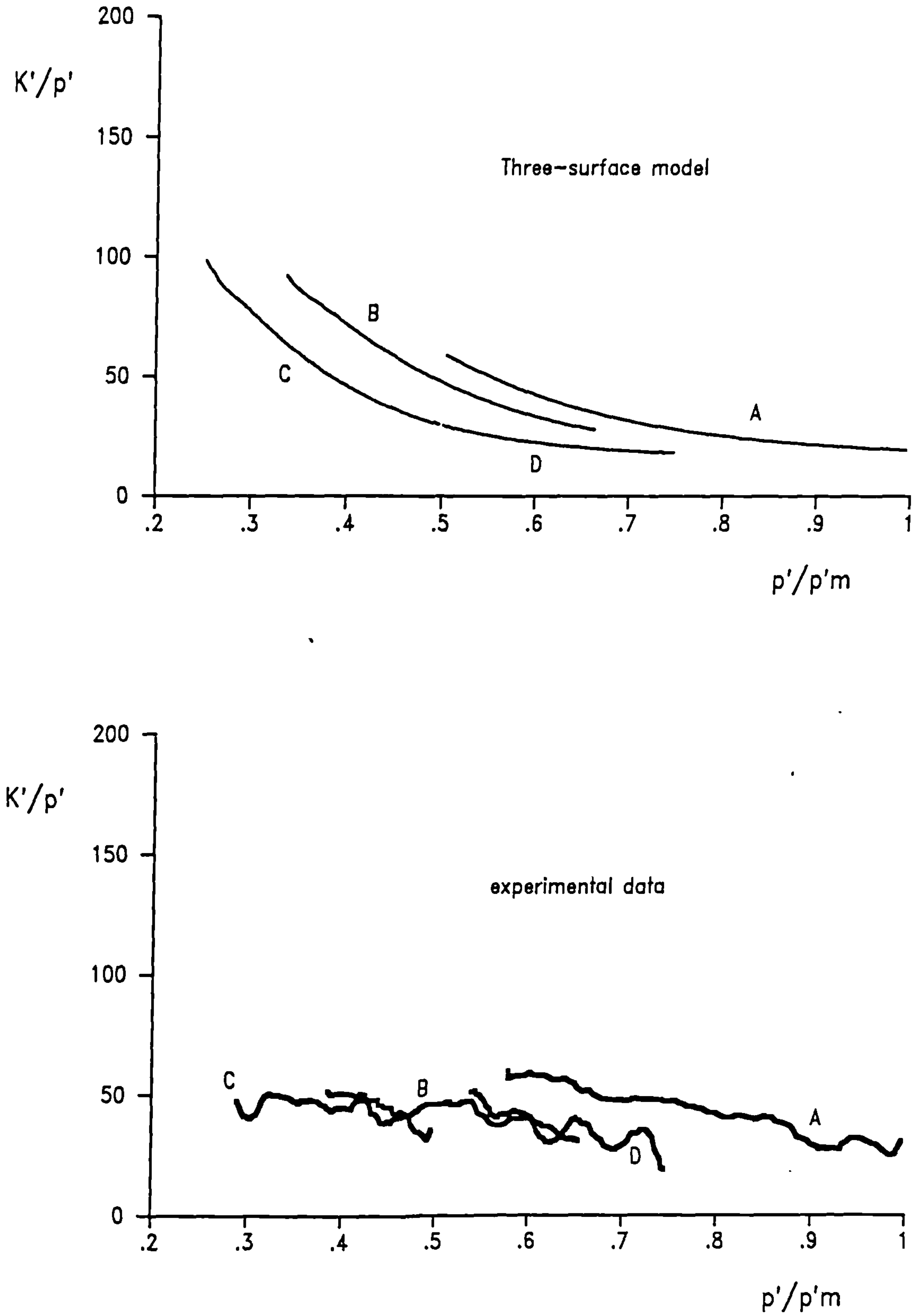

Figure 5.5.7 A comparison between experimental data and model predictions for constant q' compression paths after 0 degree stress path rotation, plotted as normalised bulk stiffness against p'/p'm.

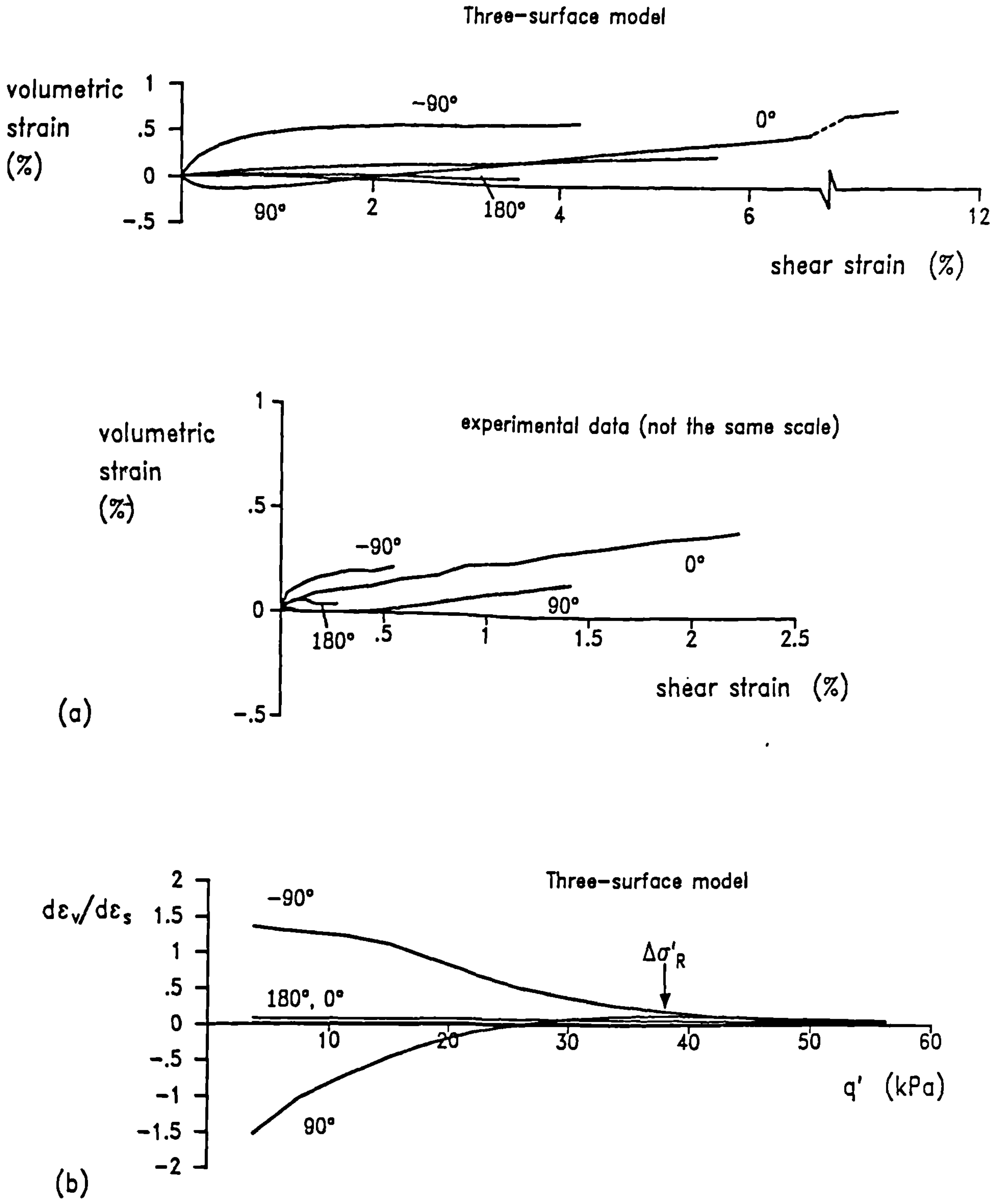

Figure 5.5.8 (a) A comparison between experimental data and model predictions for strain paths and (b) predicted curves of strain increment ratio against stress change both from constant p' loading at p'i = 100kPa, p'm = 150kPa following four different stress path rotations

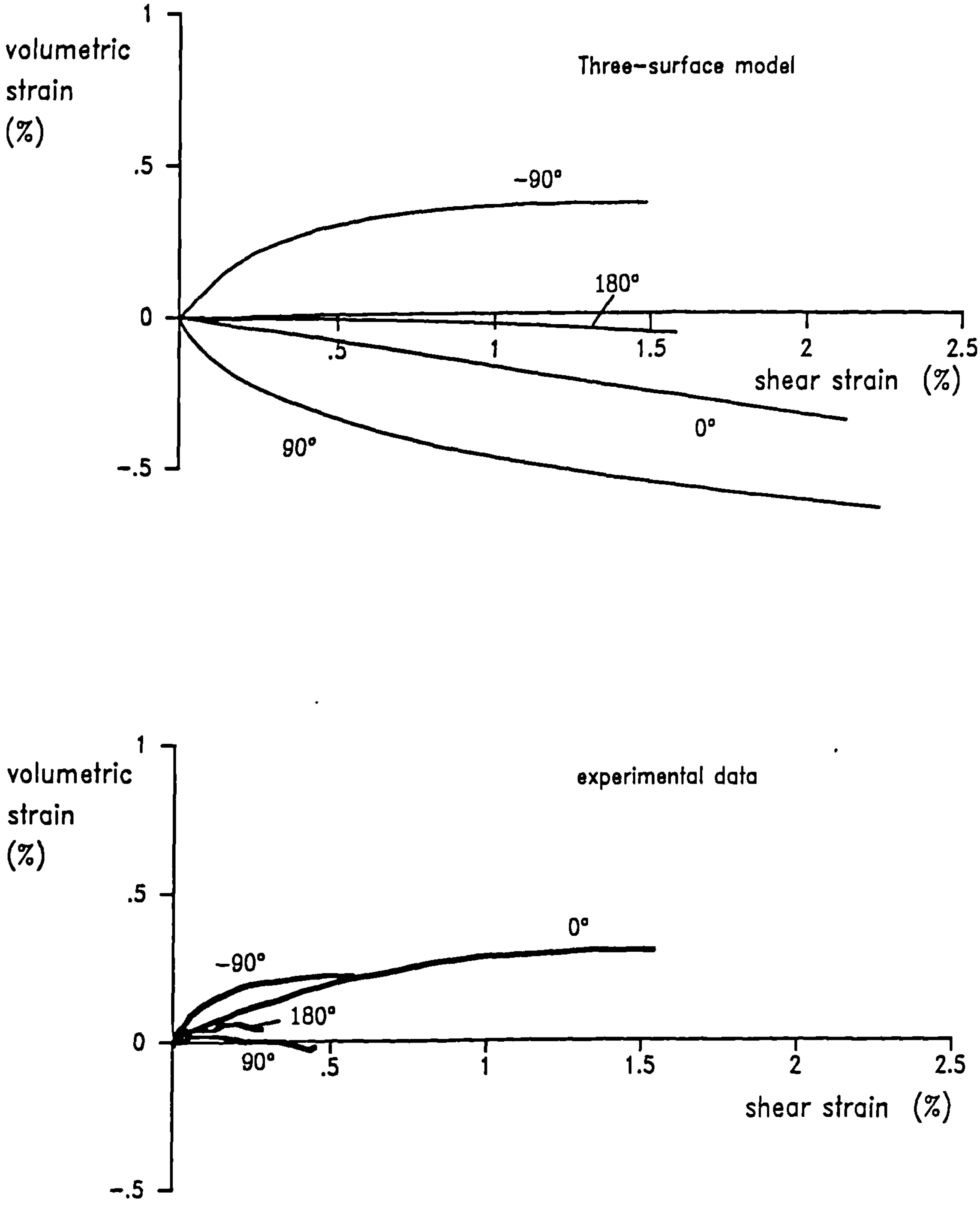

Figure 5.5.9 A comparison between experimental data and model predictions for strain paths obtained from constant p' loading at p'i = 100kPa, p'm = 400kPa, after four different stress path rotations.

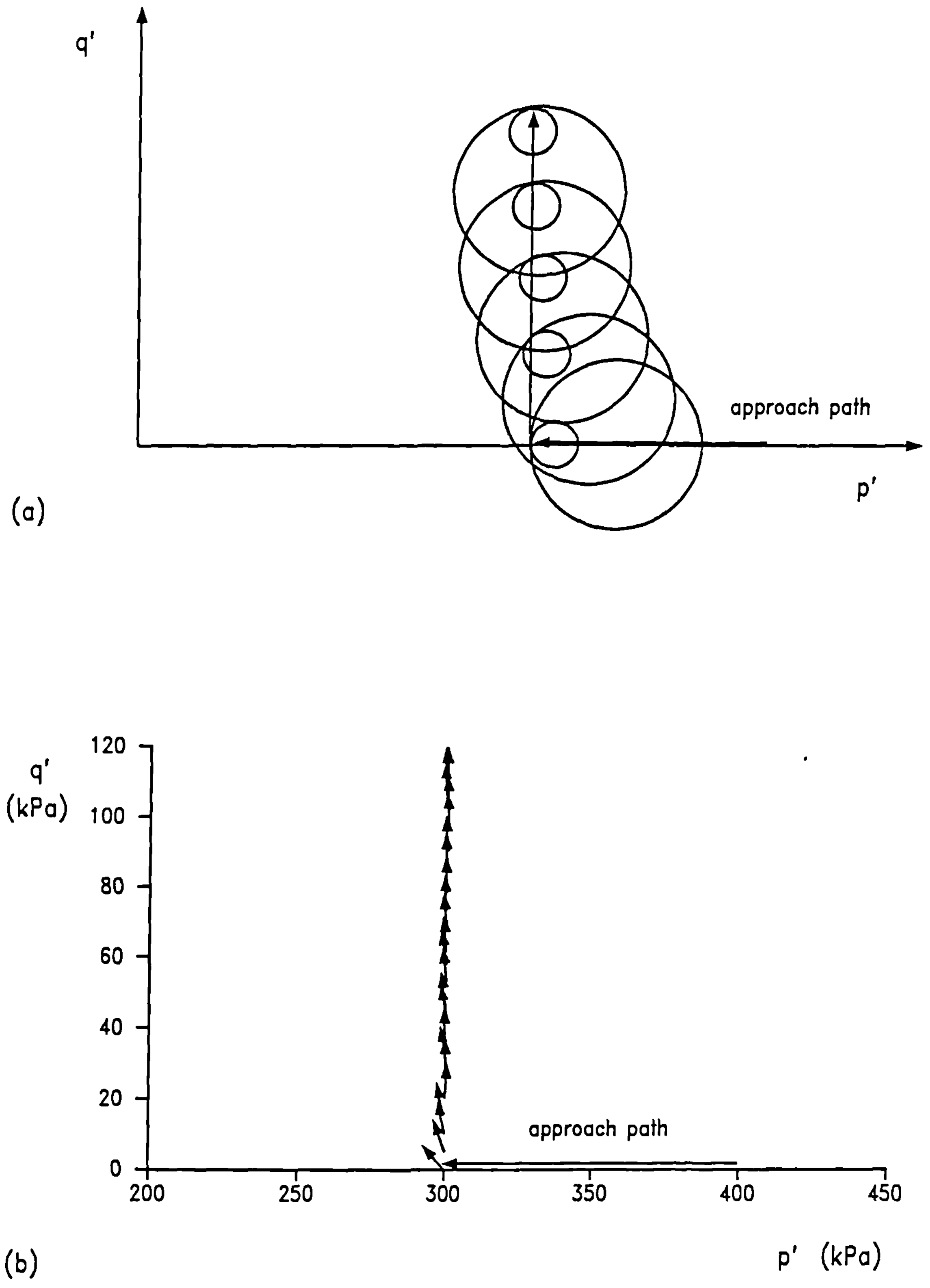

Figure 5.5.10 Diagram showing the movement of the history and yield surfaces on loading along a constant p' path following a 90 degree stress path rotation compared to experimentally derived strain increment vectors.

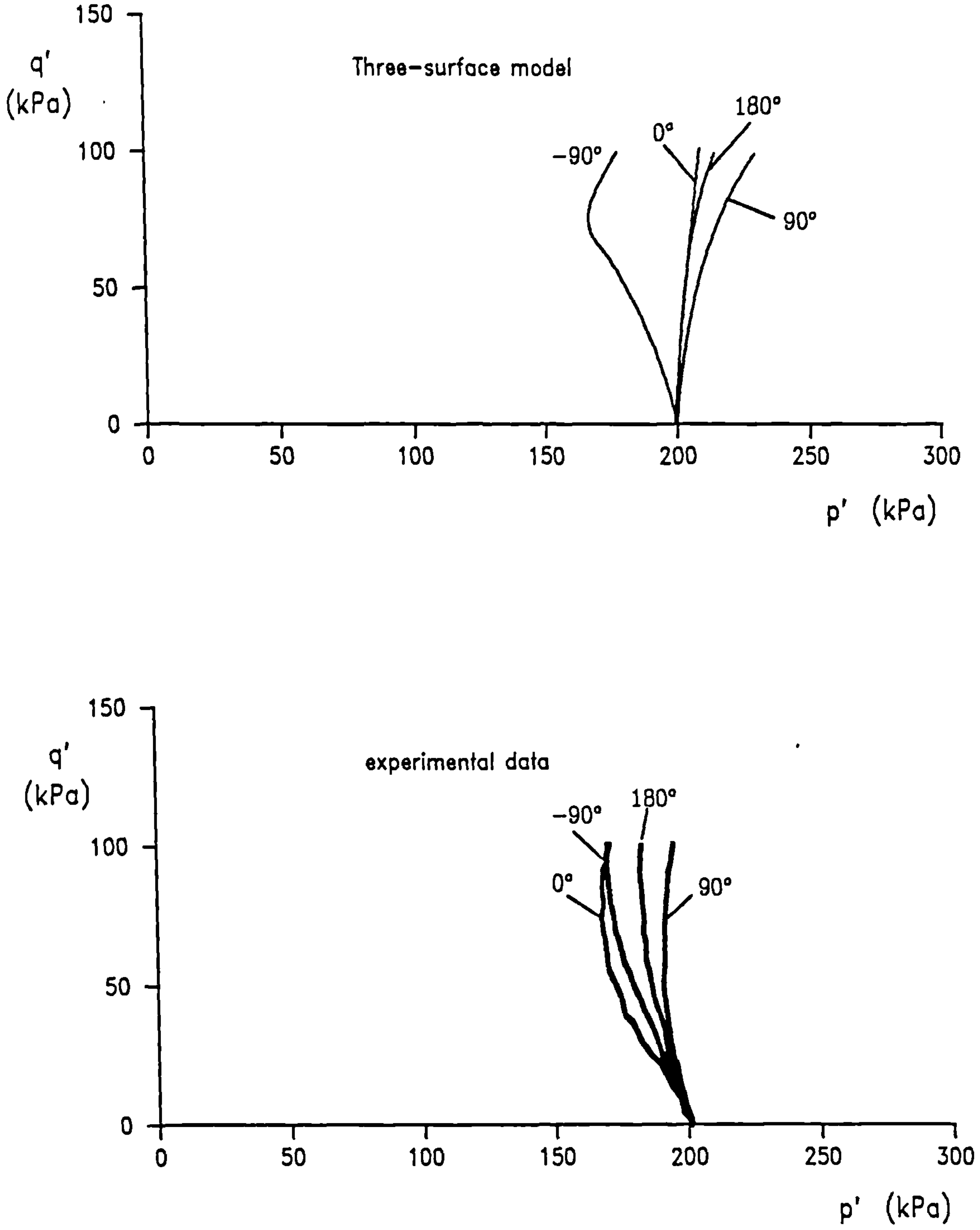

Figure 5.5.11 A comparison between effective stress paths predicted by the model and those obtained from experimental data for an undrained compression loading stage at p'i = 200kPa, Ro ~ 3 for four different stress path rotations

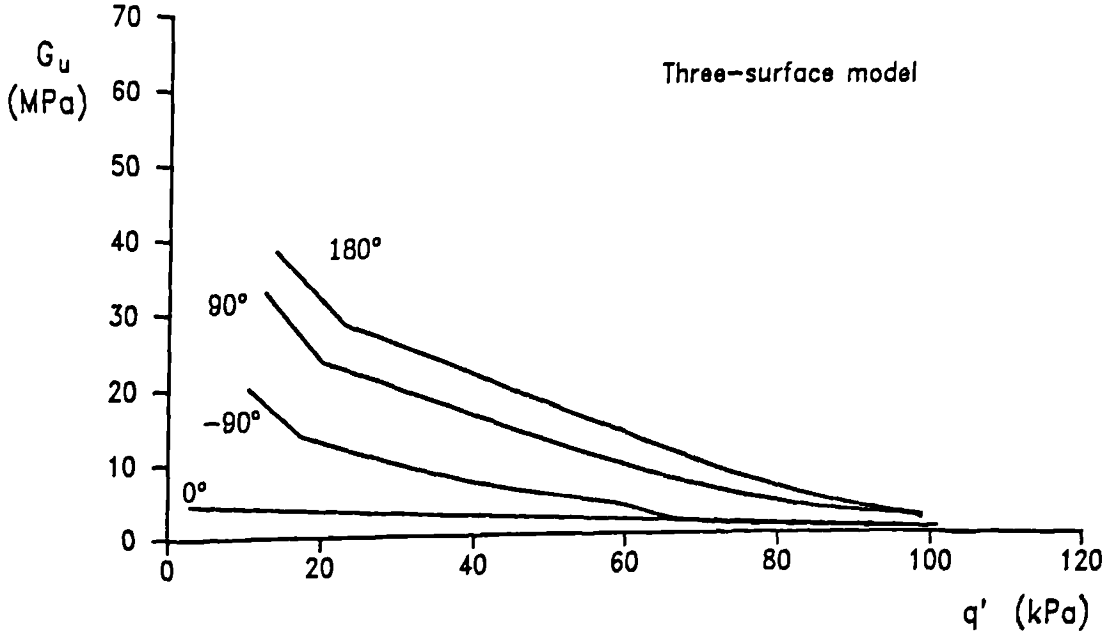

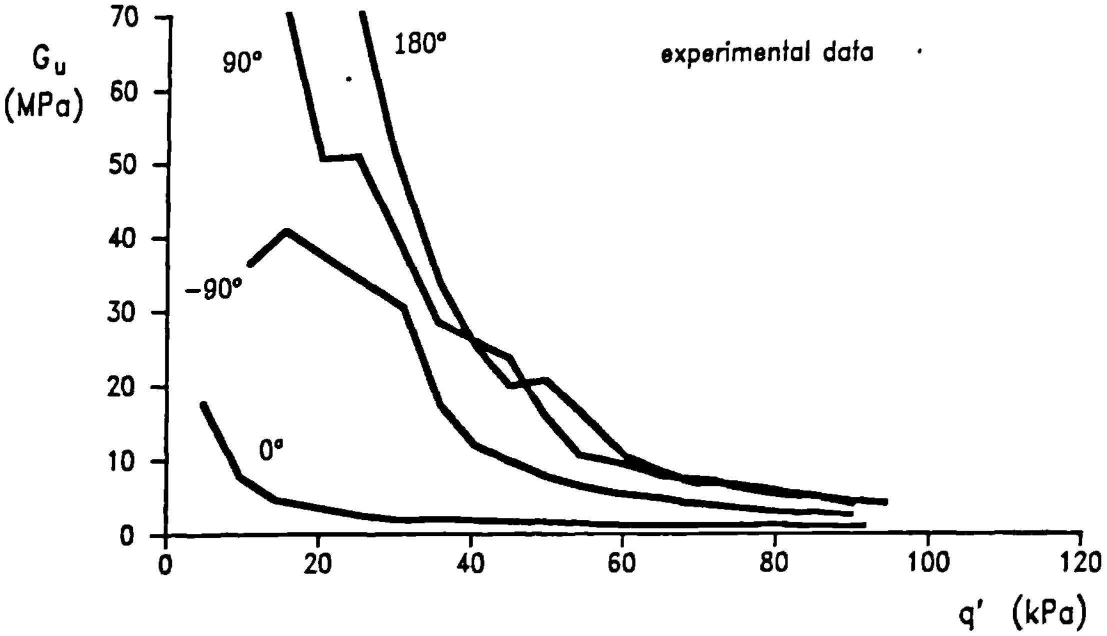

Figure 5.5.12 Comparison between variation in undrained shear stiffness, Gu, predicted by the model and experimental data, for an undrained loading stage at p'i = 200kPa, Ro ~ 3 for four different stress path rotations

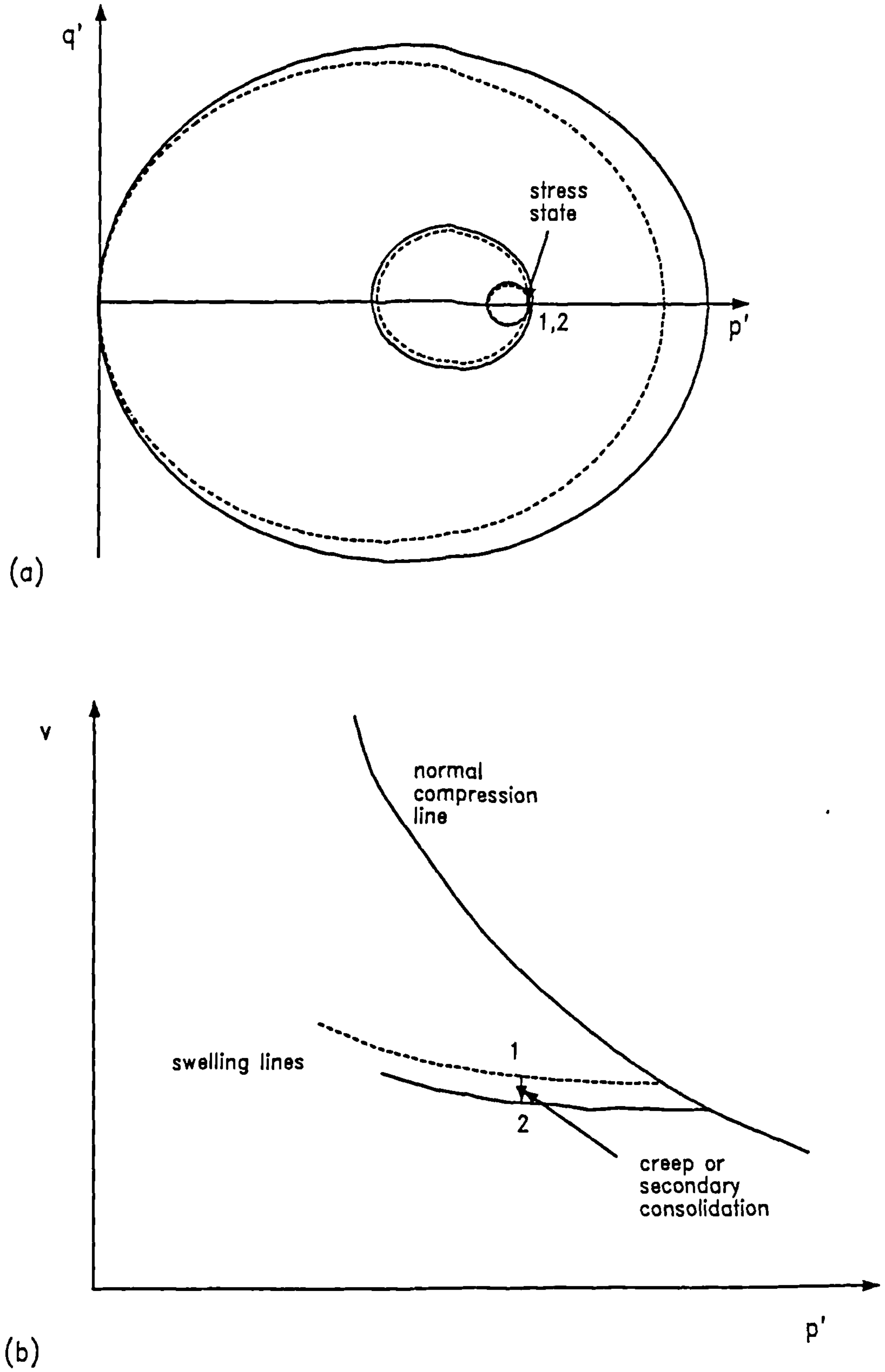

Figure 5.5.13 Diagram showing how time effects such as creep could be incorporated in the model